

# **Development of a Coupled Neutronics/Thermal-Hydraulics/Fuel Thermo-Mechanics Multiphysics Tool for Best-Estimate PWR Core Simulations**

Zur Erlangung des akademischen Grades  
**Doktor der Ingenieurwissenschaften (Dr.-Ing.)**  
von der KIT-Fakultät für Maschinenbau des  
Karlsruher Instituts für Technologie (KIT)

genehmigte

**Dissertation**

von

M.Sc.-Ing. Joaquín Rubén Basualdo Perelló  
geboren in San José de Metán, Argentinien

Tag der mündlichen Prüfung:	05.10.2020
Hauptreferent:	Prof. Dr.-Ing. Robert Stieglitz Karlsruher Institut für Technologie
Korreferent:	Prof. Dr.-Ing. Rafael Macián-Juan Technische Universität München



*Para mi mamá, Paca.  
Te amo por siempre.*

*(To my mother, Paca.  
I love you forever.)*





## *Acknowledgments*

First and foremost, I would like to express my gratitude to my advisors Prof. Dr.-Ing. Robert Stieglitz and Dr. Victor Hugo Sánchez-Espinoza for their guidance and time, and for the opportunity to pursue this doctoral research in the Institute for Neutron Physics and Reactor Technology (INR). There, a rich community of researchers on the reactor physics field has benefited my research. I also would like to thank Prof. Dr.-Ing. Rafael Macián-Juan for his feedback and support and for agreeing to be my co-supervisor.

I would like to thank all my colleagues at the INR institute with whom I have shared my time as a PhD student. Specially thanks to Dr. Uwe Imke, Dr. Valentino Di Marcello and Dr. Javier Jimenez whose technical knowledge and support were of great help for my work.

Thanks to Dr. Paul Van Uffelen and Dr. Arndt Schubert from the Joint Research Center Karlsruhe for helping me understand the inner workings of TRANSURANUS.

Special thanks to the Deutscher Akademischer Austauschdienst (DAAD) which supported me with a scholarship to pursue this doctoral work. And to the Karlsruhe House of Young Scientists for their support in the last six months of my studies.

I would like to thank my friends in Germany and my family. To the former because they have been the latter in these faraway lands and to the latter for their love and support.

Last but not least, to my parents Francisca and Ruben and to my sisters Ana and Gabriela for their unconditional love and support.



# *Abstract*

A detailed analysis of the reactor core behaviour must consider the mutual interaction of neutronics, thermal-hydraulics and fuel thermo-mechanics phenomena. In the last decade, neutronics/thermal-hydraulics coupled simulations have become a standard for the calculation of nuclear reactor systems. However, the impact that the fuel behaviour calculated by thermo-mechanics solvers, have in the reactor core simulations results, has so far not been well studied and it only started to be analyzed in recent years.

The fuel pin gap conductance and fuel conductivity can only be accurately modelled by a thermo-mechanics code. These quantities present a large range of variation during the fuel rod life in the reactor. Moreover, these properties directly influence the fuel and coolant temperature calculation and thus, their correct prediction is of importance in a best estimate simulation.

This doctoral thesis describes the development of a multiphysics tool, which couples a neutronics, a thermal-hydraulics and a fuel thermo-mechanics code. The capability of this tool to model the irradiation dependent thermo-mechanics properties, allows for a more accurate description of the physics undergoing in a reactor core.

The verification and validation work performed to demonstrate the increased prediction accuracy and performance of the new multiphysics tool will be presented. In particular, the analysis of a full PWR core reactivity-initiated accident (RIA) transient is analysed and discussed. In this design basis accident, safety criteria such as added enthalpy must be demonstrated to fulfil the regulatory requirements. This investigation has shown a significant impact in the prediction of safety-relevant parameters with the new multiphysics tool, compared to the results of traditional methods. It demonstrates also the importance of the consideration of fuel thermo-mechanics on best estimate simulations. Large local temperature deviations in the fuel centreline temperatures in a hot full power steady state simulation, and a significant increase in the prediction of the power peak in a hot zero power RIA transient, as well as an increase in the predicted fuel added enthalpy are found when using the newly developed coupled code PARCS-SUBCHANFLOW-TRANSURANUS.

Alongside the main topic of the work, a methodology for the prediction of thermal-hydraulics local safety parameters has been implemented taking advantage of the neutronics/subchannel thermal-hydraulics coupling. The implementation has been compared against

a higher order Monte Carlo/subchannel solution showing a less than 2% difference in the power prediction in most of the pins. Also, the required computational time is orders of magnitude smaller with a similar accuracy. This capability has the potential to be extended in the future by adding a coupled thermo-mechanics analysis also at subchannel level.

The performed analyses enabled by a coupled neutronics, thermal-hydraulic and fuel pin mechanics simulation, as realized by the developed package, have shown the importance of this type of holistic approach. It allows for the consideration of the irradiation dependent thermo-mechanics parameters in the core simulation. The new developed PARCS-SUB-CHANFLOW-TRANSURANUS multiphysics coupled tool paves the way for the future best estimate analysis of nuclear reactor cores.

# *Kurzfassung*

Eine detaillierte Analyse des Reaktorkernverhaltens muss die gegenseitige Wechselwirkung von neutronischen, thermohydraulischen und thermomechanischen Eigenschaften des Kerns berücksichtigen. In den letzten zehn Jahren haben sich neutronisch/thermohydraulisch gekoppelte Simulationen zu einem Standard für die Berechnung des Betriebsverhaltens von Reaktorkernen weiterentwickelt. Der Einfluss des thermomechanischen Brennstoffverhaltens auf die Ergebnisse der Reaktorkernsimulationen ist jedoch bisher noch nicht gut untersucht worden und wird erst seit einigen Jahren analysiert.

Die Leitfähigkeit des Spalts zwischen Brennstoff und Hüllrohr und die Wärmeleitfähigkeit des Brennstoffs können nur durch einen thermomechanischen Code genau modelliert werden. Diese Größen variieren in einem großen Bereich während der Lebensdauer der Brennstäbe im Reaktor. Darüber hinaus beeinflussen diese Eigenschaften direkt die Berechnung der Brennstoff- und Kühlmitteltemperatur, und daher ist ihre korrekte Vorhersage in einer Best-Estimate-Simulation von Bedeutung.

Diese Doktorarbeit beschreibt die Entwicklung eines multiphysikalischen Werkzeugs, das einen Neutronen-, einen Thermohydraulik- und einen Brennstoff-Thermomechanik-Code koppelt. Die Fähigkeit dieses Werkzeugs, die beststrahlungsabhängigen thermomechanischen Eigenschaften zu modellieren, ermöglicht eine genauere Beschreibung der Betriebs-eigenschaften eines Reaktorkerns.

Die Verifikations- und Validierungsarbeiten, die durchgeführt wurden, um die erhöhte Vorhersagegenauigkeit und Leistung des neuen Multiphysik-Tools zu demonstrieren, werden vorgestellt. Insbesondere wird die Analyse von Reaktivitätsstörfällen (RIA) für einen Vollkern-DWR diskutiert. Bei diesem Auslegungsstörfall müssen Sicherheitskriterien wie z. B. zusätzliche Enthalpie nachgewiesen werden, um die gesetzlichen Anforderungen zu erfüllen. Diese Untersuchung hat im Vergleich zu den Ergebnissen traditioneller Methoden einen signifikanten Einfluss auf die Vorhersage sicherheitsrelevanter Parameter mit dem neuen multiphysikalischen Werkzeug gezeigt. Sie zeigt auch die Bedeutung der Berücksichtigung der Thermomechanik des Brennstoffs bei Best-Estimate-Simulationen. Große lokale Temperaturabweichungen in den Brennstoffzentraltemperaturen in einer Simulation bei Volllast und ein signifikanter Anstieg in der Vorhersage der Leistungsspitze in einer heißen Nullleistungs-RIA-Transiente sowie ein Anstieg in der vorhergesagten Enthalpie des

zugesetzten Brennstoffs werden bei Verwendung des neu entwickelten gekoppelten Codes PARCS-SUBCHANFLOW-TRANSURANUS gefunden.

Neben dem Hauptthema der Arbeit wurde eine Methodik zur Vorhersage von thermohydraulischen lokalen Sicherheitsparametern unter Ausnutzung der Neutronik/Unterkanal-Thermohydraulik-Kopplung implementiert. Die Implementierung wurde mit einer Monte-Carlo/Unterkanal-Lösung höherer Ordnung verglichen, die einen Unterschied von weniger als 2% bei der Leistungsvorhersage in den meisten Bereichen zeigte. Außerdem ist die erforderliche Berechnungszeit bei ähnlicher Genauigkeit um Größenordnungen kleiner. Diese Fähigkeit hat das Potenzial, in Zukunft durch Hinzufügen einer gekoppelten thermomechanischen Analyse auch auf Subkanalebene erweitert zu werden.

Die durchgeführten Analysen, die durch die gekoppelte Simulation von Neutronik, Thermohydraulik und Brennnadelmechanik ermöglicht wurden, haben gezeigt, wie wichtig ein solcher ganzheitlicher Ansatz ist. Er ermöglicht die Berücksichtigung der bestrahlungsabhängigen thermo-mechanischen Parameter in der Kernsimulation. Das neu entwickelte Werkzeug, das gekoppelte PARCS-SUBCHANFLOW-TRANSURANUS Simulationen durchführt, ebnet den Weg für die zukünftige Best-Estimate-Analyse von Kernreaktorkernen.

## ***Publications related to this thesis***

1. J. Basualdo, V. Sánchez, R. Stieglitz, R. Macián-Juan. “Neutronic modeling of a PWR Konvoi type reactor using PARCS with few groups cross section generated with SCALE and SERPENT”, in *Proceedings of AMNT 2015*, 5-7 May 2015, Berlin
2. Joaquín R. Basualdo, Victor H. Sánchez-Espinoza, Robert Stieglitz and Rafael Macián-Juan. “PARCS-SUBCHANFLOW-TRANSURANUS MULTIPHYSICS COUPLING FOR IMPROVED PWR’S SIMULATIONS”, in *Proceedings of ICAPP 2017*, 26-28 April 2017, Kyoto
3. Joaquín R. Basualdo, Victor H. Sánchez-Espinoza, Robert Stieglitz and Rafael Macián-Juan. “PARCS-SUBCHANFLOW-TRANSURANUS Multiphysics Coupling for high fidelity PWR reactor core simulation: Preliminary results”, in *Proceedings of AMNT 2017*, 16-17 May 2017, Berlin
4. Joaquín R. Basualdo, Victor H. Sánchez-Espinoza, Robert Stieglitz and Rafael Macián-Juan. “PARCS-SUBCHANFLOW-TRANSURANUS Multiphysics Coupling for high fidelity PWR reactor core simulation: Preliminary results”, in *ATW International Journal for Nuclear Power*, Vol. 64 (2019), Pages 275-279
5. Joaquín R. Basualdo, Victor Sánchez-Espinoza, Robert Stieglitz and Rafael Macián-Juan. “Integration of the subchannel thermal-hydraulic code SubChanFlow into the reactor dynamics code PARCS: Development and testing based on a computational benchmark”, in *Progress in Nuclear Energy*, Vol. 119, January 2020. Paper ID: 103138. <https://doi.org/10.1016/j.pnucene.2019.103138>





# Table of Contents

<b>Abstract</b> .....	<b>vii</b>
<b>Kurzfassung</b> .....	<b>ix</b>
<b>Publications related to this thesis</b> .....	<b>xi</b>
<b>Glossary</b> .....	<b>xv</b>
<b>List of Acronyms</b> .....	<b>xvii</b>
<b>1 Introduction</b> .....	<b>1</b>
1.1 Motivation.....	1
1.2 Short description of a Pressurized Water Reactor (PWR) .....	2
1.3 Reactivity initiated accidents (RIA).....	6
1.4 Multiphysics reactor core calculations.....	9
1.5 Challenges for realistic PWR core simulations.....	11
1.6 Goal of the thesis.....	14
1.7 Structure of the thesis.....	15
<b>2 Fundamentals and Selected Numerical Tools for the Multiphysics Coupling</b> ..	<b>17</b>
2.1 Introduction to neutronics, thermal-hydraulics and thermo-mechanics simulations .....	17
2.2 The neutronics core simulator PARCS .....	21
2.3 The thermal-hydraulics subchannel code SubChanFlow .....	25
2.4 The fuel thermo-mechanics code TRANSURANUS.....	30
<b>3 State of the art of Multiphysics Reactor Core Simulations</b> .....	<b>39</b>
3.1 Neutronics and thermal-hydraulics coupled simulations .....	40
3.2 Neutronics, thermal-hydraulics and thermo-mechanics coupled simulations ..	42
3.3 Strategies for codes integration in multiphysics coupling .....	43
<b>4 Coupling of a Neutronics Core Simulator with a Subchannel Thermal- Hydraulics Code</b> .....	<b>50</b>
4.1 Coupling implementation description.....	50
4.2 Coupling parameters and methodology .....	51
4.3 Verification and validation of the coupled code PARCS-SCF.....	56
4.4 Automatic prediction of local safety parameters using PARCS-SCF.....	65
<b>5 Coupling of a Neutronics Core Simulator with a Subchannel Thermal- Hydraulics and a Fuel Thermo-Mechanics Code</b> .....	<b>75</b>
5.1 Introduction.....	75
5.2 Coupling parameters and methodology .....	75
5.3 Verification of the multiphysics tool .....	83
<b>6 Analysis of a UO<sub>2</sub>/MOX PWR Core with the developed Multiphysics Code</b> ....	<b>93</b>

6.1	Steady state simulation of a PWR core at HFP conditions .....	95
6.2	PWR REA simulation at HZP conditions .....	103
<b>7</b>	<b>Summary and Conclusions.....</b>	<b>115</b>
<b>8</b>	<b>Outlook.....</b>	<b>118</b>
	<b>References .....</b>	<b>121</b>
	<b>Appendices .....</b>	<b>129</b>
A.1	PARCS-SCF coupling extra results .....	129
A.2	Sensitivity analysis for selection of the time step.....	135
A.3	SERPENT/SCF 3x3 Minicore XS generation .....	136
A.4	Verification of the methodology for prediction of TH safety parameters transient capabilities .....	137
B.1	Description of TRANSURANUS restart file generation.....	140
B.2	OECD/NEA PWR RIA transient benchmark extra results.....	140
B.3	TRANSURANUS input data for the PWR model.....	150
C.1	3x3 PWR minicore description.....	151
C.2	OECD-NEA UO <sub>2</sub> /MOX PWR benchmark description .....	153

## *Glossary*

### *Nomenclature*

Symbol	Description	Physical Unit
$\beta$	delayed neutron fraction	-
$\rho$	density *	g/cm <sup>3</sup>
$\rho$	reactivity*	pcm, % $\Delta k/k$ , \$
$\vartheta$ and $T$	Temperature	K
$\nu$	average number neutron of neutrons per fission	-
$\kappa$	energy released per fission	MeV/fission
$\lambda$	thermal conductivity	W/m·K
$\lambda_i$	precursor decay constant for group $i$	-
$\Sigma$	macroscopic cross section	1/cm
$\phi$	neutron flux	neutrons/cm <sup>2</sup> sec
$\chi$	fission neutron yield	-
$\psi$	fission rate	1/cm <sup>3</sup> sec
$c_p$	specific heat capacity	J/Kg·K
$C$	precursor concentration	1/cm <sup>3</sup>
$D$	diffusion coefficient	cm
$g$	gravity acceleration	m/sec <sup>2</sup>
$h$	Specific enthalpy	J/Kg
$H$	Enthalpy	J
$h_x$	heat transfer coefficient at $x$ (e.g. $x$ =surface)	W/m <sup>2</sup> ·K
$k_{\text{eff}}$	effective multiplication factor	-

$\dot{q}$	power	W
$q'$	linear heat rate	W/m
$q''$	heat flux	W/m <sup>2</sup>
$q'''$	volumetric heat generation rate	W/m <sup>3</sup>
$p$	pressure	Pa
$P$	power	W
$t$	time	sec
$v$	velocity	m/sec

---

\* due to extended use of the  $\rho$  symbol to denote the density and the reactivity it will be used in this work as well to denote both. Whereas it represents one or the other can be easily derived from the context.

## *List of Acronyms*

<b>Acronym</b>	<b>Description</b>
ADF	Assembly Discontinuity Factor
ANM	Analytic Nodal Method
BWR	Boiling Water Reactor
CAMP	Code Assessment and Maintaining Group
CDF	Corner Discontinuity Factor
CHF	Critical Heat Flux
CR	Control Rod
CZP	Cold Zero Power
DBA	Design Basis Accident
DNB	Departure from Nucleate Boiling
EG	Energy Group
ENDF	Evaluated Nuclear Data File
FA	Fuel Assembly
HBS	High Burnup Structure
HFP	Hot Full Power
HTC	Heat Transfer Coefficient
HZP	Hot Zero Power
IAEA	International Atomic Energy Agency
LOCA	Loss of Coolant Accident
LOFA	Loss of Flow Accident
LOHSA	Loss of Heat Sink Accident
LWR	Light Water Reactor
MC	Monte Carlo
MDNB	Minimum Departure from Nucleate Boiling

MG	Multi Group
MOC	Method of Characteristics
MOX	Mixed Oxide (Uranium plus Plutonium)
MPI	Message Passage Interface
NEA	Nuclear Energy Agency
NEM	Nodal Expansion Method
NPP	Nuclear Power Plant
OECD	Organization for Economic Co-operation and Development
PCI	Pellet Clad Interaction
PDE	Partial Differential Equation
PN	Collision Probabilities Method
PPR	Pin Power Reconstruction
PRIS	Power Reactor Information System
PST	PARCS-SCF-TU
PWR	Pressurized Water Reactor
REA	Rod Ejection Accident
RIA	Reactivity Initiated Accident
RPV	Reactor Pressure Vessel
SAR	Safety Analysis Report
SCF	SubChanFlow
SN	Discrete Ordinates Method
TH	Thermal Hydraulics
TM	Thermo Mechanics
TU	TRANSURANUS
UO <sub>2</sub>	Uranium Oxide
XS	Cross Section

# ***1 Introduction***

## ***1.1 Motivation***

Today there are in the world 443 operational nuclear reactors for production of energy with an installed capacity of 391.3 GW electric power and 52 reactors are under construction (IAEA, 2019). The installed capacity generates over 10% of the world's electricity consumption. Of these reactors, 300 are of PWR type, being the most extended and producing 283.9 GW electric power, a 72.5% of the nuclear energy production.

For the design and safety assessment of a nuclear reactor, a large number of core simulations must be performed. In the past, these simulations were done with monodisciplinary codes. In this case, the interaction between the different physics fields was considered in a simplified way. For example, thermal-hydraulics system codes possessed only a point kinetics neutronics solver (zero dimensional) to represent the core behaviour under transient conditions. However, in the end of the 90's with the increasing availability of computational power, this methodology began to change and evolved to a multiphysics solution approach. The goal of a multiphysics approach is to perform best estimate simulations, describing the reactor core behaviour in a more realistic way than traditional (monodisciplinary) codes do. Thus, relaxing excessive conservative design criteria. In the early 2000's the CRISSUE project (OECD/NEA, 2004b, 2004a) devoted to the coupling of neutronics and thermal-hydraulics aimed at best estimate simulations for NPP by pursuing the coupling of 3D nodal neutronics and system thermal-hydraulics codes. The goal, was to be able to have a better description of asymmetric power feedbacks, as could be the case resulting for instance from a stuck control rod. This approach was an improvement in reactor simulations, and nowadays 3D nodal neutronics and system thermal-hydraulics coupling is a standard in reactor analysis. However, in such simulations, the fuel solvers embedded in the thermal-hydraulics codes do not describe precisely the behaviour of irradiated fuel such as fission product release, crack formation and growth, swelling, gap closing, etc.

Consequently, recent efforts in reactor core simulations are focused on the improvement of the modelling of the fuel behaviour under irradiation, as it is the case during the reactor operation. This has been pursued by coupling thermal-hydraulics codes or neutronic core simulators with fuel thermo-mechanics codes (Bielen, 2015; Magedanz *et al.*, 2015; Holt *et al.*, 2016; Targa *et al.*, 2016; Valtavirta, Leppänen and Viitanen, 2017). The goal is to be able

to consider the changes of the fuel material properties with the irradiation in the simulations in a realistic manner. This is of importance because of the range of variation of these properties during the fuel lifetime and the increasing discharge burnup of modern PWR fuel assemblies. Analysis with such tools will help to understand the impact that more accurate modeling have in the simulation results.

The fuel rod irradiation dependent phenomena calculated by fuel performance tools such as cracking, densification, swelling, etc., affect the fuel material properties, causing them to vary orders of magnitude in some cases. E.g., the gap heat transfer coefficient can vary from 5000 W/m<sup>2</sup>·K at the beginning of life up to 120000 W/(m<sup>2</sup>·K) (Lassmann and Hohlefeld, 1987) or even 200000 W/(m<sup>2</sup>·K) (Bielen, 2015) for a high burnup fuel at the end of life. Also the fuel pellet conductivity degrades with the increasing burnup (Amaya *et al.*, 2002; Ronchi *et al.*, 2004; Staicu *et al.*, 2011), which results in larger gradients between the fuel rod centreline and surface temperatures.

These effects have a direct impact on the simulation results of a rod ejection accident (REA) for a light water reactor (LWR) with highly burned fuel assemblies. This event is one of the main safety concerns for design basis accident (DBA) analysis in a nuclear reactor (OECD/NEA, 2010). The study of this transient with a coupled neutronics, thermal-hydraulics and fuel thermo-mechanics tool will shed light into the core physics.

Hence, a coupled multiphysics tool including neutronics, thermal-hydraulics, and fuel performance codes is needed to:

- perform best estimate simulations for LWR cores,
- to have more accurate description of the behaviour of the reactor core and to increase the understanding of design basis events such as the rod ejection accident (REA), and
- to better understand areas for further development in best estimate simulation tools.

## ***1.2 Short description of a Pressurized Water Reactor (PWR)***

PWRs have a primary system where the energy is generated through nuclear fission, and a secondary system which begins in the steam generators, where the steam is generated and transported to the turbines to be converted into electricity. The Reactor Coolant System (or primary system) of a PWR, consists of the reactor pressure vessel (RPV), the steam generators, the reactor coolant pumps, a pressurizer, and the piping of the primary and secondary



circuits. In Figure 1-1, a sketch of a primary system with two loops is shown. The reactor core is cooled and moderated by light water.

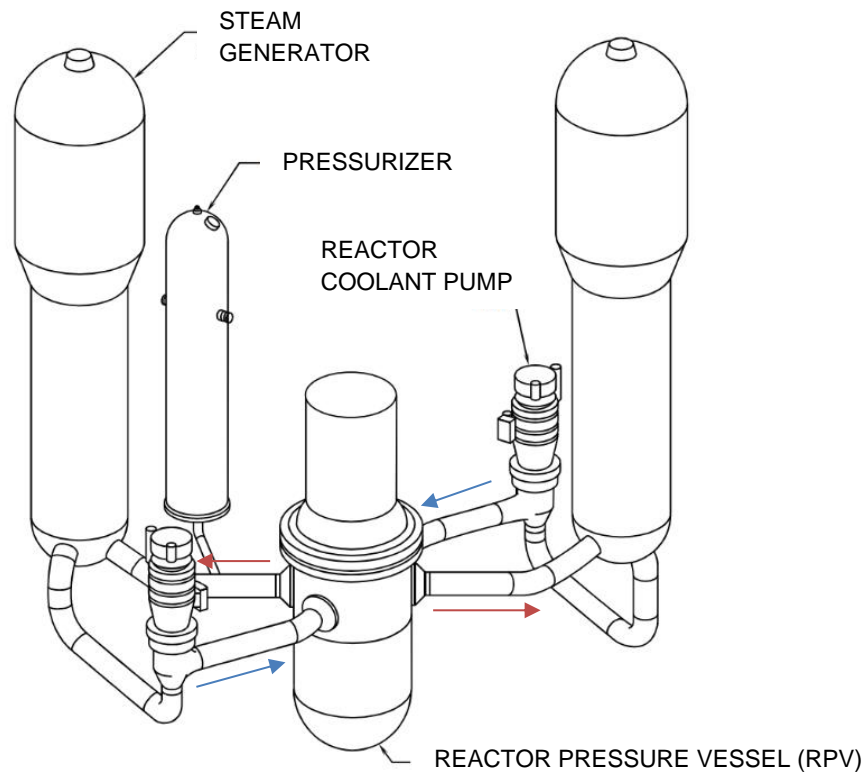


Figure 1-1. PWR components of the primary loop. The arrows represent the coolant flow direction (red=hot, blue=cold). Modified from (U.S. NRC, 2007).

The reactor core is located inside the RPV and it consists of the fuel assemblies and the control rod mechanisms. A schematic of the main parts of the RPV is depicted in Figure 1-2.

To remove the energy produced in the core, the coolant is pumped under high pressure through the reactor core where it is heated by the fission process. The heated coolant flows to a steam generator, where it transfers the heat to lower pressure secondary circuit. The steam produced in the steam generation secondary side is conducted to the turbines to produce electrical energy. The primary coolant is returned by the reactor coolant pumps from the steam generator primary side to the core to be reheated.

Thermal-hydraulic operational parameters for PWRs such as the coolant temperature and pressure are plant and design specific. Typically, the coolant enters the core at a temperature of approximate 560 K and leaves it at an average temperature of approximate 600 K. To

maintain a single phase, the working pressure of the primary system is  $\sim 15.5$  MPa, which is kept constant by the pressurizer.

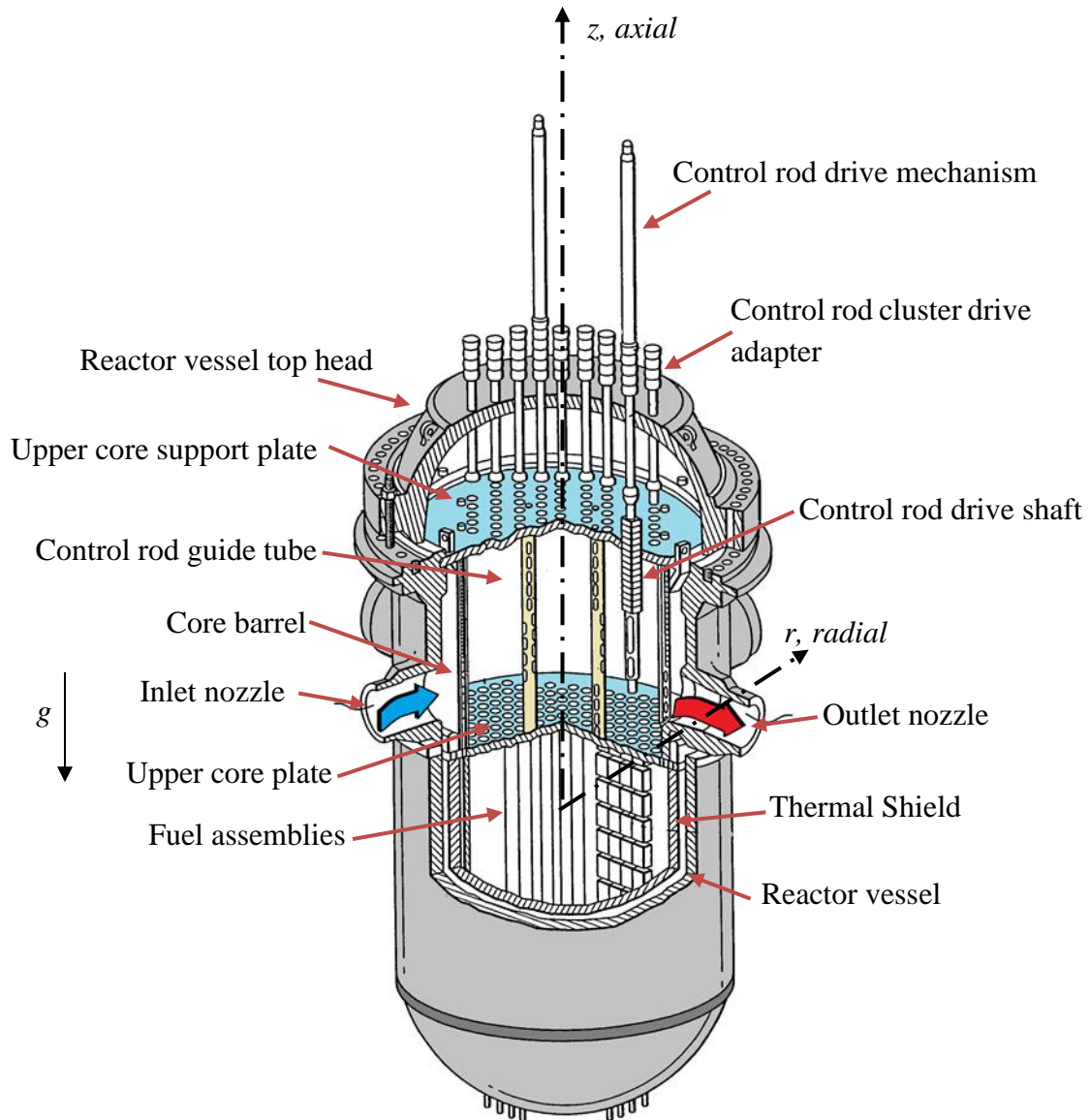


Figure 1-2. Reactor Pressure Vessel schematic showing the main components. Modified from (U.S. NRC, 2007).

The reactor core of a commercial PWR is composed of 121 to 241 fuel assemblies depending on the reactor design. The fuel is uranium oxide,  $\text{UO}_2$ , with an enrichment of typically 3 to 5 wt.% of  $\text{U}^{235}$ . Some PWRs operate also with a plutonium and uranium mixture fuels, known as mixed oxide fuels (MOX).

Fuel assemblies are approximately 4 to 5 m long and are composed of a bundle of fuel pins arranged in a rectangular shape, typically consisting of 14x14 to 18x18 pins, a typical FA scheme is shown in Figure 1-3.

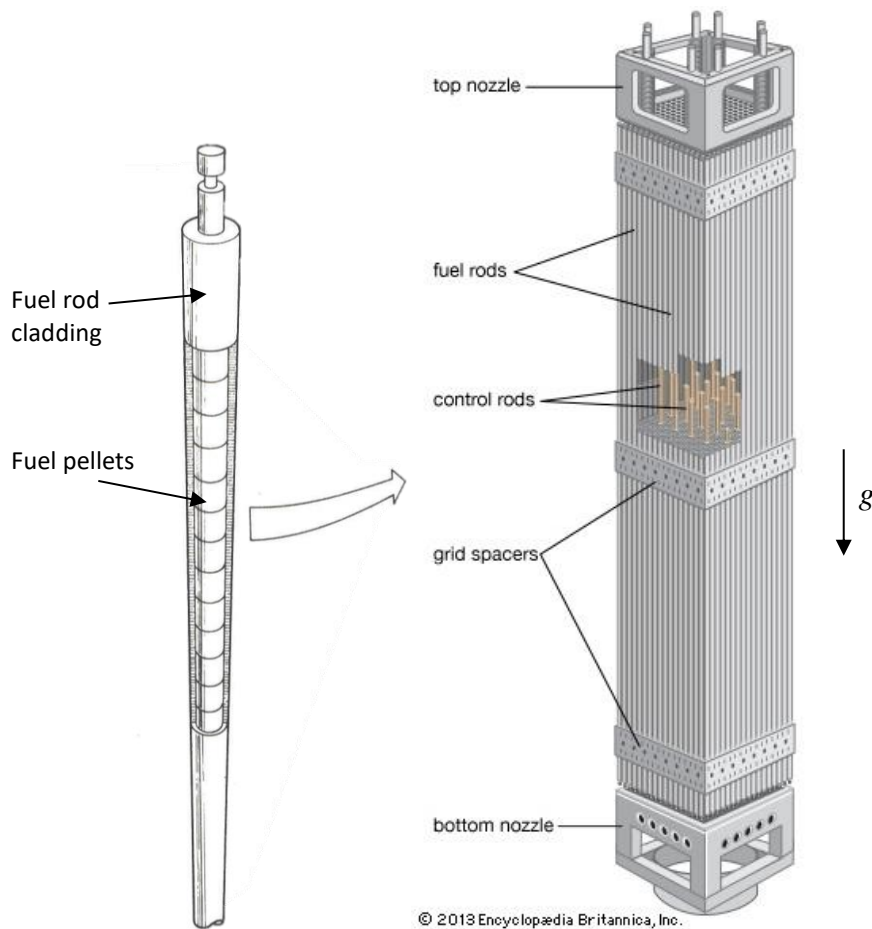


Figure 1-3. Sketch of a PWR typical fuel rod (left) and fuel assembly (right) (modified from (*nuclear reactor fuel types - Encyclopedia Britannica, 2013; Lochbaum, 2014*)).

Commercial PWRs refuelling cycle length vary typically between 12 and 24 months, and approximately one third of the fuels in the core are replaced in each refuelling. At the beginning of the cycle, the excess reactivity must be high enough to maintain the reactor operating up to the end of the cycle. To compensate for the excess of reactivity, aside from the control rod arrangement, soluble boron is added to the coolant. There are two banks of control rods, the shutdown system and the control system. The shutdown system is outside the core during normal operation, and the control system is only partially inserted in the upper part of the core. The reactivity control is achieved mainly by varying the concentration of boric acid dissolved in the coolant.

In practice, the core material composition is only exactly known at the beginning of operation. During the reactor operation there are not enough measurements zones to know the precise neutron flux distribution in the core, thus, the burnup cannot be exactly known and must be estimated with core simulations. Neutronic calculations are typically performed in order to design the optimal operation cycle (refuelling strategy) regarding the maximal amount of energy generation. Refuelling strategies, optimize the fuel utilization keeping enough safety margins, i.e., a flat as possible radial and axial power profile, avoiding hot spots within the core, etc.

The safe operation is assured by the implementation of the defence-in-depth concept, where provisions are made by design against any kind of off-normal events that may occur in all safety levels. A main concern for the core design is the core behaviour under Design Basis Accidents (DBA) such as reactivity-initiated accidents (RIAs), e.g., a rod ejection accident or boron dilution accident.

The fuel overheating can be caused either by a power increase due to a sudden reactivity insertion, denominated reactivity initiated accidents, or by a decrease in cooling which can be caused by a loss of coolant flow (LOFA), a loss of heat sink (LOHSA) or a loss of coolant (LOCA) (Snell, 2015). In this thesis the focus of the investigations is on the Rod Ejection Accident (REA). This is a fast transient delimited to the reactor core and hence can be analysed decoupled from the rest of the plant, i.e. without the need of a system code.

To analyse the reactor core behaviour and to demonstrate that the safety requirements are met, specific tools are developed dealing with neutronics, thermal-hydraulics and fuel thermo-mechanics. In the next subchapter, the RIA-phenomenology and underlying physics will be shortly described.

### **1.3 *Reactivity initiated accidents (RIA)***

Reactivity initiated accidents involve an undesired increase of power due to the sudden inadvertent insertion of positive reactivity in the reactor. The RIA events can be divided into four types: control system failures, control element ejections, events caused by coolant/moderator temperature and void effects, and events caused by dilution or removal of coolant poison.

For PWRs, the RIA accident scenario of interest is the control rod ejection accident (REA) (Rudling *et al.*, 2016). A REA can occur in PWRs by mechanical failure of the control rod

drive mechanism, resulting in the ejection of a control rod out of the core. The accident results in a rapid reactivity and power increase in a few fuel assemblies around the ejected control rod due to the local decrease of neutron absorption. The resulting power transient is much larger than for other RIA scenarios making the REA the postulated event to establish the design and operation basis for PWRs.

On normal operation the PWRs operate with only one bank of control rods positioned in the core. These control rods are, for safety reasons, only partially inserted in the top of the core, the amount of reactivity that could be added by the ejection of a control rod during normal operation is thereby limited. However, at low power PWRs can operate with control rods fully inserted. For this reason, from the added reactivity point of view, the most severe accident can occur at hot zero power (HZP) conditions (OECD/NEA, 2010). The ejection of a control rod from a position dominated by fresh or low burn-up fuel will result in a higher reactivity insertion than if the control rod is ejected from a position dominated by high burn-up fuel.

### ***1.3.1 Reactivity definition and reactivity feedbacks***

The reactivity is a fundamental quantity, expressing the departure of a nuclear reactor from criticality. The reactivity is expressed in terms of the effective multiplication factor,  $k_{eff}$ , which can be defined as:

$$k_{eff} = \frac{\text{neutron production from fission in one generation}}{\text{neutron absorption in the preceding generation} + \text{neutron leakage in the preceding generation}}, \quad \text{Equation 1-1}$$

(Duderstadt and Hamilton, 1976).

More precisely the static reactivity  $\rho$  is defined as:

$$\rho = \frac{k_{eff} - 1}{k_{eff}}. \quad \text{Equation 1-2}$$

A positive reactivity indicates that the reactor is supercritical. Since  $k_{eff} > 1$ , the neutron production is larger than the neutron leakage and absorption, whereas a negative reactivity ( $k_{eff} < 1$ ) corresponds to a subcritical reactor state.

The reactivity is a dimensionless quantity, but it can be expressed in many units, such as pcm (percent mille),  $\% \Delta k/k$ , or dollars (\$). The dollar representation is a normalization of the reactivity with respect to the delayed neutron fraction, typically named  $\beta$ . When the reactivity is one dollar, the reactor is in a super prompt critical condition. Thus, this unit is useful to express the departure of the reactor from prompt criticality conditions.

In normal operation the reactivity is controlled primarily by the addition/removal of soluble boron in the moderator, and secondarily by the partial insertion of the control rod banks. Typically, one of the control rod banks is inserted in the top of the core to fine tune the reactivity. However, the reactivity is also affected by changes in the fuel ( $T_f$ ) and moderator ( $T_m$ ) temperature (and by changes in the moderator steam void content ( $\alpha_m$ ), in case of BWRs). The rate of change of the reactivity is expressed by the equation:

$$\dot{\rho} = \dot{\rho}_{cs} + \frac{\partial \rho}{\partial T_f} \dot{T}_f + \frac{\partial \rho}{\partial T_m} \dot{T}_m + \frac{\partial \rho}{\partial \alpha_m} \dot{\alpha}_m, \quad \text{Equation 1-3}$$

where:  $\dot{\rho}_{cs}$  is the reactivity rate of change induced by the reactivity control systems. The dotted variables indicate the time derivative of the quantities.

In a REA accident, the consequence of the rod ejection is a rapid increase in the reactivity ( $\dot{\rho}_{cs}$ ), which causes a large localized power excursion in the surrounding FAs of the ejected CR. The power increase causes an increase in the fuel temperature introducing a negative reactivity  $\left( \frac{\partial \rho}{\partial T_f} \dot{T}_f \right)$ , the energy in the fuels is released to the coolant leading to a reduction of the coolant density and introducing a negative reactivity by the moderator temperature feedback  $\left( \frac{\partial \rho}{\partial T_m} \dot{T}_m \right)$ . The power and fuel temperature increase rapidly until the resulting negative reactivity introduced by the Doppler effect due to the increase in the fuel temperature, becomes large enough to counterbalance the positive reactivity introduced by the CR ejection. When this happens, the power rapidly decreases. The decrease of power ends with a tail caused by the delayed neutrons.

Under these conditions, the fuel enthalpy increases considerably, depending on the inserted reactivity. Regulators fix a maximal added fuel enthalpy rise as safety criteria for a REA event, and numerical tools are used to demonstrate that the fuel enthalpy of a core under

REA conditions is far below this safety margin. The U.S. NRC regulation sets a limit value for the fuel added enthalpy which amounts to 711 J/g (170 cal/g) for cladding differential pressure  $< 1$  MPa and decreases to 418 J/g (100 cal/g) for a differential pressure  $> 4.5$  MPa (Clifford, 2015). The cladding differential pressure is the difference between the pressures inside and outside of the fuel rod cladding. On the other hand, the RSK (Reactor Safety Commission) in Germany has set this limit to 585J/g (140 cal/g) for fresh fuels and decreases to 250 J/g (60 cal/g) for fuels with burnup higher than 50 GWd/tHM (RSK, 2005).

#### ***1.4 Multiphysics reactor core calculations***

Nuclear fuel rod thermo-mechanics is a complex phenomenon which is simulated using mechanistic codes that accurately predict the fuel properties such as fuel conductivity and gap conductance. These codes predict also the distribution of safety relevant thermo-mechanics parameters in the fuel, such as the fuel centreline temperature, the cladding temperature distribution, as well as the fission gas release, or fuel cladding failure. The fuel rod gap heat transfer coefficient and fuel conductivity values vary over a large range during the fuel lifetime, i.e. irradiation in the core, mainly due to the gap closure and fuel degradation. These properties influence the fuel and coolant temperature directly and thus, their correct prediction is of importance in a best estimate simulation.

The traditional approach to reactor core simulations, does not consider the variations of these parameters and assume a pre-defined value. Fuel vendor codes used by the industry deal in part with this problem by having special fuel properties tables, which are dependent on the thermal conditions and the fuel burnup. These tables are the result of detailed modelling and experimental data, which typically is proprietary data generated by the fuel vendors and it is not available to the research community.

On the other hand, best estimate neutronics/thermal-hydraulics coupled simulations have become a standard in the last decade. However, the impact in the core simulations due to the detailed description of the fuel behaviour and the fuel properties, calculated by thermo-mechanics codes, has started to be studied only in recent years. The increase of computational power facilitates complex calculations and the consideration of interactions between the different physics fields involved in the reactor cores simulation. This global trend of coupling calculation codes of different physics fields is referred to as multiphysics simulation approach (Mahadevan and Ragusa, 2007).

Different multiphysics coupled tools are being developed worldwide to carry out a more accurate description of the reactor core behaviour (Chanaron *et al.*, 2015; Magedanz *et al.*, 2015; Aviles *et al.*, 2017; García-Herranz *et al.*, 2017; Blakely, Zhang and Ban, 2018). The goal is to obtain a more realistic and detailed description of the core conditions through a best estimate approach during the reactor operation. Hence, the interaction between the different physics domains is implemented in multiphysics codes to better predict safety margins, by having a better description of the reactor behaviour, while keeping or improving the safe operation of the reactor.

The incorporation of fuel performance codes in the simulations will elucidate the real impact that the accurate description of fuel material properties has in the prediction of the core behaviour during the reactor operation.

The main goal of this doctoral thesis is to develop a multiphysics code system for an improved analysis of the core behaviour under realistic operating conditions by the coupling of three different solvers: neutronics, subchannel thermal-hydraulics and fuel pin thermo-mechanics.

The new multiphysics code consists of the 3D nodal neutronic diffusion core analysis solver (standard used in the industry for core calculations) PARCS, of the subchannel thermal-hydraulics code (core thermal hydraulics simulations considering crossflow among neighbour fuel assemblies or subchannels) SubChanFlow (SCF), and of the fuel thermo-mechanics solver (known also as fuel performance solver), standard used in the European industry for fuel behaviour analysis, TRANSURANUS (TU).

The inclusion of a fuel thermo-mechanics solver in addition to a neutronics and thermal-hydraulics solver, as shown in Figure 1-4, enables the addition of the prediction of the fuel rod behaviour under irradiation during operation of the nuclear power plant. This improves the simulation accuracy of design basis accidents, such as the rod ejection accidents (REA) in LWR.

Alongside with the main goal, a new automatic procedure for the neutronics/thermal-hydraulics coupling PARCS-SCF has been developed, which enables the prediction of local safety parameters via a subchannel-level thermal-hydraulics core simulation. For this purpose, the pin-power reconstruction method of PARCS is used to provide the pinwise power distribution needed by the subchannel solver. This new methodology has been verified by the comparison with a high-fidelity Monte Carlo/subchannel solution of the same problem. It is



shown that the deviations of the fast running PARCS-SCF pin power prediction differ from the ones of the Monte Carlo/subchannel predictions are less than 2% for the majority of pins, within the industrial requirements.

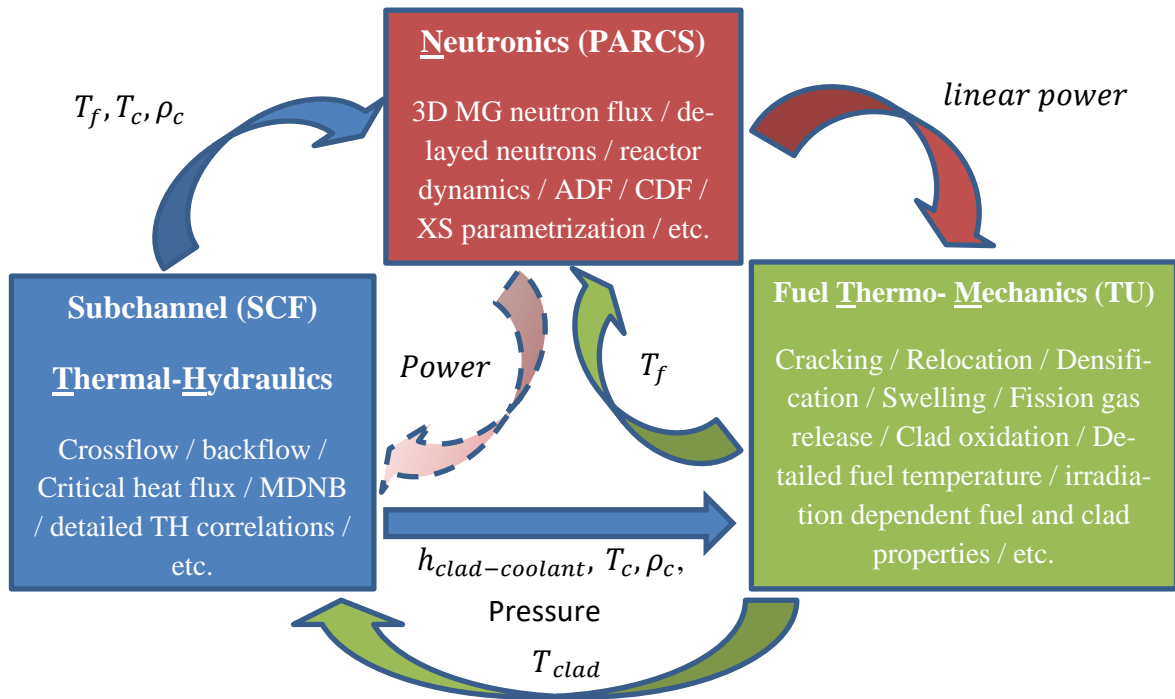


Figure 1-4. Interaction between neutronics, thermal-hydraulics, and thermo-mechanics codes and main phenomena and models of each solver. MG=Multi Group, ADF=Assembly Discontinuity Factors, CDF=Corner Discontinuity Factors, XS=Cross Sections, MDNB=Minimum Departure from Nucleate Boiling and TH=Thermal-Hydraulics.

The simulation capability of the new multiphysics code will be verified and validated using computational benchmark problems.

### 1.5 Challenges for realistic PWR core simulations

The main challenge for realistic PWR core simulations is to describe with precise physical-mathematical methods the processes occurring within the reactor which concern the accurate prediction of safety parameters. For this purpose, mechanistic models of neutronics, thermal-hydraulics and thermo-mechanics phenomena are required.

Moreover, the cheap and huge available computing power and new algorithms is fostering the development of high-fidelity multi-scale and multiphysics simulations codes. Advanced simulations tools are pursued via different approaches, either by increasing the computational

complexity of the simulations: high-fidelity/high-performance, or by increasing the complexity of the physics models in the simulation using a multi-scale/multiphysics approach.

Figure 1-5 depicts how more complex reactor core simulations are pursued. Even when the approaches cannot be fully decoupled, they focus mainly increasing the number of coupled physics (multiphysics) in the solution or increasing the description of the energy and spatial domains (high-performance):

- *Increasing the domain description* (high performance): e.g., meaning to go from the traditional description of a fuel assembly as an homogenized node in the neutronics domain or as a unique channel in the thermal hydraulics domain, to a more refined geometry where every fuel pin of the fuel assembly is treated individually in the neutronics (transport lattice calculation), and every thermal-hydraulic subchannel of the fuel channel is resolved individually (with a subchannel code). For this purpose, the number of approximations in the numerical methods must be reduced, e.g. by using a transport method instead of the diffusion method in the neutronics.
- *Increasing the description of the physics* (multiphysics): which is achieved on the other hand by using models with less simplifications, and by implementing more mechanistic models with less empirical correlations. This is achieved, e.g., by coupling firstly

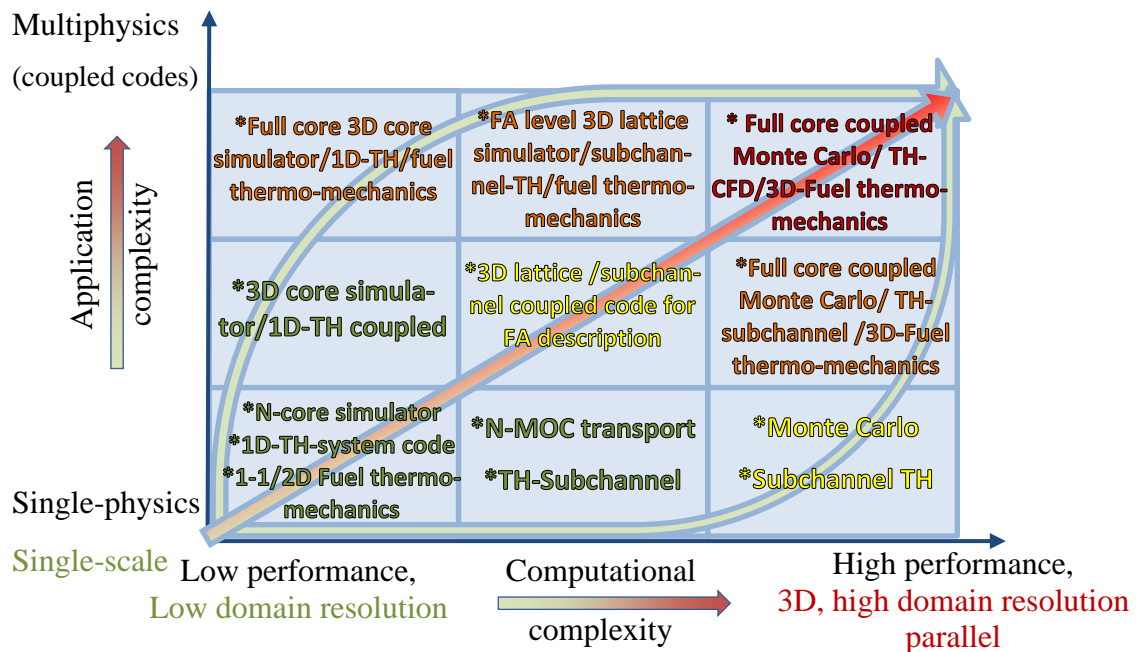


Figure 1-5. Sketch of development paths for advanced software in reactor simulations. On the multiphysics axis, a better description of the physics is pursued by coupling different physics, and on the high-performance axis a better description of the domain and along with a reduction in the numerical simplifications is pursued. N=Neutronics, TH=Thermal-Hydraulics, FA=Fuel Assembly, MOC=Method of Characteristics, CFD=Computational Fluid Dynamics.

neutronics and thermal-hydraulics, and afterwards also coupling a thermo-mechanics solver.

High performance solvers are focused on achieving better predictions by reducing the number of approximations in the equations and having a better description of the problem domain (spatial and energetic). In the recent years, neutronic Monte Carlo calculations of the nuclear reactor core on a pin level have been coupled with subchannel thermal-hydraulics (Daeubler, Ivanov, *et al.*, 2015). Also, numerous couplings of Monte Carlo tools with subchannel codes were developed (Vazquez *et al.*, 2012; Ivanov *et al.*, 2013; Kelly III *et al.*, 2017; Mylonakis, Varvayanni and Catsaros, 2017). Monte Carlo codes have been also coupled with CFD codes for static simulations (Aufiero and Fratoni, 2017; Henry, Tiselj and Snoj, 2017), and time dependent Monte Carlo methods are under development (Sjenitzer and Hoogenboom, 2011; Mylonakis, Varvayanni and Catsaros, 2016; Ferraro *et al.*, 2019).

The pursue of high-fidelity solvers is important since they are the most advanced software capable of simulating with high detail and few simplifications very complex phenomena. However, these simulations require an enormous computational power. In 2013 K. Smith (Smith and Forget, 2013) stated that *“today’s high-fidelity tools are still in the early stages of development and have a long way to go before they can be considered a replacement to well established lower order nodal calculations”*. In 2019, the most advanced high-fidelity multiphysics simulation efforts, McSAFE in Europe and CASL in the USA, have shown that the amount of computational power needed for such detailed calculations is enormous, and it will not be possible to have them as industry standards in the near future. Thus, it is foreseeable that the use of nodal neutronics and subchannel thermal-hydraulics codes will remain the standard calculation system in the industry.

Reducing the number of simplifications in the numerical models and increasing the description of the physical phenomena through multiphysics coupling is another way to increase the accuracy of simulations. In this trend, much work has been done regarding the coupling of neutronics and thermal-hydraulics from the early 2000’s to the present (OECD/NEA, 2004b, 2004a; Ivanov and Avramova, 2007). However, it is only in recent years that the coupling with fuel thermo-mechanics codes has been an emerging trend in the research in the academic community (Bielen, 2015; Hales *et al.*, 2015; Holt *et al.*, 2016; Le-Pallec, Mer-Nkongha and Crouzet, 2016; Targa *et al.*, 2016; Valtavirta, Leppänen and Viitanen, 2017).

Given the impact that parameters like the fuel pin gap thermal conductivity and the detailed fuel pin temperature may have in the prediction of the heat transfer from the fuel to the

coolant, and the Doppler feedback in the neutronics, a best estimate modelling of these fuel properties is of great importance. The changes driven by the fuel irradiation on these parameters cannot be neglected, even more with the increasing discharge burnup in modern LWR cores.

On the other hand, in the industry, there are two main driving forces for the implementation of new methodologies for reactor simulations: more precise prediction of safety margins so that over conservative margins can be relaxed (while maintaining or increasing the safety and improving the economics), and more strict requirements from the regulatory authority bodies. Consequently, to meet industry needs, and advance the industry standards, new developments must enhance the *status quo* of simulations and make possible fast running simulations in industry computer clusters.

## **1.6 Goal of the thesis**

The overall goal of this doctoral thesis is to develop a multiphysics coupled code consisting of neutronics, subchannel thermal-hydraulics and fuel thermo-mechanics solvers for more realistic, i.e. improved, simulations of the behaviour of LWR-cores. Having a more accurate description of the reactor core physics will contribute to elucidate the impact that burnup dependent fuel material properties have in the reactor core simulation. Hence, this doctoral thesis will contribute to enhance the understanding of the reactor core behaviour in operation and under transient conditions.

To achieve the overall goal the following specific goals are defined:

- Development of a multiphysics coupled code for PWR core simulations by coupling the neutronics code PARCS and the subchannel thermal-hydraulics code SubChanFlow (SCF) for improved thermal hydraulics simulation of the core.
- Development of a methodology for local safety parameters prediction by coupling PARCS with SCF and using the pin power reconstruction (PPR) capability of PARCS and a *posteriori* automatic simulation of the core thermal-hydraulics with SCF at sub-channel level using the reconstructed pin power provided by PARCS. This methodology is aligned with the goal of generating a more accurate prediction of local safety parameters of interest for the industry. The methodology is to be verified by comparison against a higher order solver solution.

- Development of a coupled Multiphysics code named PARCS-SCF-TU, where three different solvers i.e. the neutronics code PARCS, the thermal-hydraulics subchannel code SubChanFlow and fuel thermo-mechanics code TRANSURANUS (TU) are internally coupled for the improved simulation of a reactor core that takes into account the fuel thermo-mechanics as a function of the fuel burnup.
- The verification and validation of the multiphysics code PARCS-SCF-TU will be presented at each developmental step by code-to-code benchmarking to demonstrate the new code capabilities.
- Application of the verified multiphysics code for the analysis of a full PWR core at both stationary and accidental conditions, i.e. the REA scenario. This analysis, which includes the consideration of irradiation on the fuel material properties, will highlight how the inclusion of the best estimate fuel thermo-mechanics solver into the simulation will impact the prediction of safety relevant parameters.

### **1.7 *Structure of the thesis***

The workflow of the thesis is depicted in Figure 1-6. In Chapter 1, the motivation for the work, the fundamentals of a PWR and the RIA transient are described.

The Chapter 2 starts with a short description of the fundamental's aspects of PWRs core simulation. Then, the solvers selected for code coupling i.e. PARCS, SubChanFlow and TRANSURANUS are described.

In Chapter 3 the state of the art on the multiphysics core simulations is reviewed and the main strategies for the code integration into a multiphysics code are highlighted.

In Chapter 4, the description of the neutronic and thermal-hydraulic coupling developed in this doctoral thesis as well as its verification are presented. In addition, the extension of the PARCS-SCF for the prediction of thermal-hydraulics local safety parameters is discussed.

The integration of the thermo-mechanics solver into the coupled neutronics/thermal-hydraulics code PARCS-SCF and the verification of the multiphysics codes is presented in Chapter 5.

In Chapter 6, the analysis of a full core PWR by means of the developed tool is discussed. The fuel thermo-mechanics properties dependence with the irradiation is considered in the reactor core multiphysics simulation. The importance of best estimate simulation using solvers with detailed fuel thermo-mechanics is discussed in this chapter.

Finally, in Chapter 7, a summary and conclusions of the work is presented and in Chapter 8 suggestions for further developments are given.

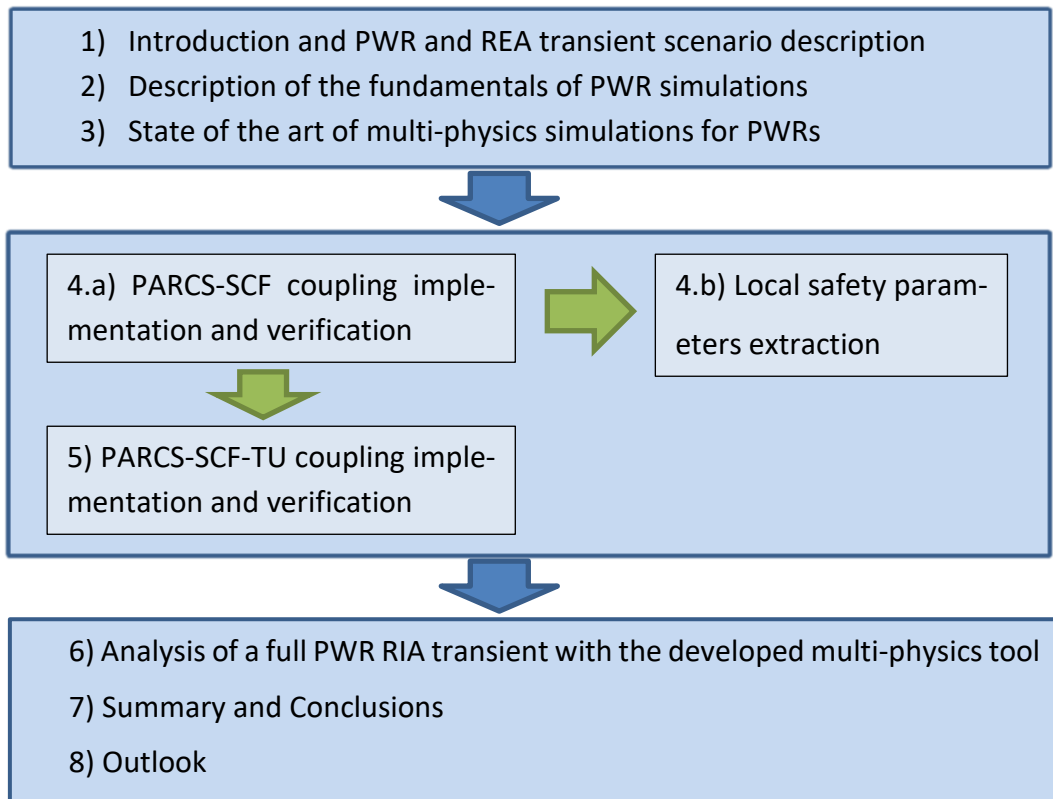


Figure 1-6. Topical structure of the doctoral thesis.

## ***2 Fundamentals and Selected Numerical Tools for the Multiphysics Coupling***

This chapter starts with an introduction to neutronics, thermal-hydraulics and thermo-mechanics core simulations. Then it is followed by the discussions of the peculiarities of the selected numerical tools to be coupled to each other in the frame of this dissertation.

### ***2.1 Introduction to neutronics, thermal-hydraulics and thermo-mechanics simulations***

The analysis of the reactor core requires a detailed knowledge on design criteria in at least three areas: the neutron-physics, the core thermal-hydraulics, and the fuel thermo-mechanics. The core designer must assure that all safety requirements imposed by the regulatory authority are met by the proposed core design to assure the safe operation of the nuclear reactor. These requirements are focus in the preservation of the fuel rod integrity and thus, limiting parameters are set to this end. Examples of these criteria are for the neutronics: the power peaking factors, maximum local linear power, reactivity coefficients and shutdown margins; for the thermal-hydraulics criteria: the minimum departure from nucleate boiling (MDNB) or maximum critical heat flux (CHF); and for the fuel thermo-mechanics: the rod structure integrity, added enthalpy in the fuel during transients and the maximum fuel temperature.

The calculation routes of the different domains, i.e. neutronics, thermal-hydraulics and thermo-mechanics, are shortly discussed hereafter.

#### ***2.1.1 The neutron physics core calculations***

Neutronics simulations are used to obtain the neutron population in the reactor core in steady state or transient conditions. Two methods exist for the neutronics simulation of the reactor core: deterministic and stochastic.

Stochastic methods or Monte Carlo methods describe a reactor core almost exactly without approximation on the spatial or energy domains. This capability to deal with complex variation in spatial and energy variables is the main advantage over deterministic transport methods. Monte Carlo calculations are also used as reference solutions to assess the accuracy of lower order deterministic methods and for the generation of nodal cross sections for neutron

diffusion codes. Monte Carlo codes are mainly used for static calculations; transient simulations are in an early development stage.

Deterministic methods solve the Boltzmann transport equation discretizing energy, time, and space by applying different degrees of simplifications. Core simulations with deterministic methods are performed in two-steps:

The first step is the generation of spatial-homogenized few-energy-group cross sections known as macroscopic cross section library. This is done via an energy domain and spatial domain homogenization. The information from the evaluated nuclear data files (ENDF) such as ENDF/B-VII, JEFF-3.2, JENDL-4.0 (IAEA-NDS, 2017), etc. are condensed from ~10000 energy groups to ~100 groups (*energy domain homogenization*). A working library is generated that is later used by transport codes – also called lattice codes. The transport codes use e.g., the methods of collision probability (PN), discrete ordinates (SN), or method of characteristics (MOC) to treat the working library and reduce further the number of energy groups (typically 2 to 8 energy groups) and to homogenize the spatial domain. The 2D neutronic flux solution of, typically, a fuel assembly is found, and a *spatial domain homogenization* is performed along the energy homogenization. A domain homogenized few-energy groups cross-section library known as *macroscopic cross-section library* is generated, which is a set of constants representing the fuel assembly. This is done for each of the different fuel assembly types loaded in the core.

In the second step, core simulators based on diffusion or SP3 methods, solve the 3D problem using the macroscopic few-group libraries. The few-energy-group neutronic flux distribution for the reactor is found. In a PWR typically 2 energy groups are used. This is done using either finite difference or nodal methods, such as the analytic nodal method (ANM) or the nodal expansion method (NEM). The process is depicted in Figure 2-1.

Both spatial and energy homogenizations are meant to simplify the calculations and some information is lost in the process. Due to the fast-computational times, this methodology is the standard for the reactor core design and safety evaluations.

For safety analysis, the condensed and homogenized nodal cross sections are generated for an appropriate range of thermal-hydraulics parameters, e.g. fuel and coolant temperature, boron concentration and control rod inserted and out of the fuel assemblies, in the frame of so-called *branch* calculations.



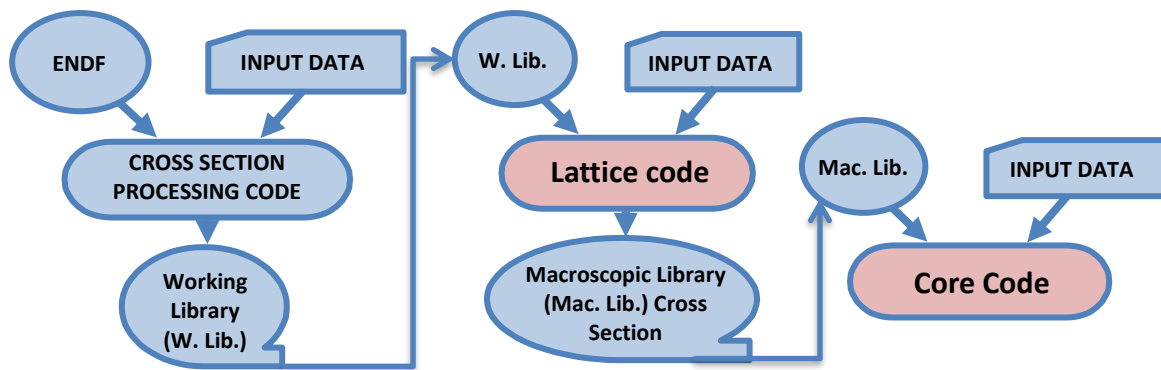


Figure 2-1. Neutronic calculation scheme. Beginning from the nuclear evaluated libraries via the lattice codes with microscopic libraries to the core codes with macroscopic nuclear cross-section libraries.

The parameters of main interest computed by reactor core simulators are the fast and thermal neutron fluxes, the axial and radial power distribution, and the  $k_{eff}$  (Equation 1-1). The 3D thermal power distribution ( $P$ ) is computed from the solution of the neutron flux as  $P = \kappa \Sigma_f \Phi$ . Where,  $\Sigma_f \Phi$  is the fission rate and  $\kappa$  (kappa not to be confused with the multiplication factor  $k$ ) is the energy released per fission.

In the core solvers,  $k_{eff}$  is the eigenvalue that solves the balance equation system  $\mathbf{M}\Phi = \frac{1}{k_{eff}} \mathbf{F}\Phi$  for a steady state calculation. Where  $\mathbf{M}$  is known as the migration matrix and it consists of all the non-fission terms in the transport equation,  $\mathbf{F}$  is the matrix consisting of the fission terms and  $\Phi$  is the neutron flux matrix.

A coarse mesh is used to discretize the spatial domain, where each radial mesh node represents one fuel assembly, and an axial discretization of the order of 20-30 cm per node is typically used in the active core domain.

The axial and radial thermal power distribution should be as flat as possible to avoid local hot spots, to minimize the neutron leakage and improve the neutron economics, and to reduce the power peaking factor. The obtained power distribution is used as an input parameter for the thermal-hydraulics codes to calculate the temperatures and safety related parameters.

More details on core neutronics simulations will be given later in this chapter when the reactor core simulator PARCS is described.

### ***2.1.2 The core thermal-hydraulics calculations***

Thermal-hydraulic simulations of the reactor core predict the temperature distribution of the coolant and the fuel rods at any operation condition. Depending on the scope, the most commonly used thermal-hydraulics simulation codes for nuclear reactors are classified into system codes and subchannel codes.

System thermal-hydraulic codes simulate the complete reactor system, i.e. the primary and secondary loop of the reactor. They are used to evaluate the plant behaviour under normal and accidental conditions, considering the feedbacks between the plant behaviour and the core by using a point kinetics model of the core, or coupled with 3D core diffusion simulators. They model the reactor core either using a 1D or 3D thermal-hydraulic description of the domain, typically with a parallel channel approach and using coarse meshes (channels representing a bundle of fuel assemblies), or single assembly description.

Subchannel codes are used to predict safety parameters such as the departure from nucleate boiling ratio (DNBR) and to calculate thermal-hydraulic conditions, such as coolant flow velocity, pressure drop, coolant temperature and fuel temperature. Subchannel codes solve the equations of mass, energy and momentum conservation for a laterally interconnected array of parallel flow channels (Vitkova, Kalchev and Stefanova, 2005) for single or two phases. To calculate the fuel temperature, the heat equation is solved for the fuel rod. A node can represent a subchannel or a larger area such as a channel equivalent to a fuel assembly.

There are many subchannel codes with different capabilities based on different solution approaches, e.g. COBRA-TF, COBRA-FLX, FLICA4, and SubChanFlow (SCF). In this dissertation, the subchannel code SCF is selected to describe the core thermal-hydraulics considering crossflow, and it will be described later in this chapter.

### ***2.1.3 The fuel thermo-mechanics calculations***

Fuel thermo-mechanics codes describe the behaviour of fuel rods under irradiation in the reactor core under quasi-stationary and transient conditions. From the knowledge of the fuel rod behaviour, operation rules can be derived to prevent fuel failure or release of fission products. A better knowledge and understanding of the fuel thermo-mechanics leads to an improved prediction of safety margins and hence improved economics.

The fuel rod behaviour is determined by thermal, mechanical and physical processes such as fuel densification, swelling, cracking, relocation, fission product gas generation and release, pellet clad interaction, etc. (Aybar and Ortego, 2005). All these phenomena influence the calculation of the fuel temperature and the heat transfer coefficient between fuel and cladding (gap conductance). Fuel thermo-mechanics codes deal with these phenomena using models or correlations specific for each fuel and reactor type. Some existing fuel thermo-mechanics codes are FRAPCON (Geelhood, Luscher and Beyer, 2011), FRAPTRAN (Cunningham *et al.*, 2001), ENIGMA (Rossiter, Palmer and Gregg, 2011), BISON (Williamson *et al.*, 2013), BACO (Harriague, Coroli and Savino, 1980), CAMPUS (Liu *et al.*, 2016), and TRANSURANUS (Lassmann, 1992). One of the most extended fuel performance codes used by many utilities and regulators in Europe, the TRANSURANUS (TU) code, is used in this work to be coupled with SubChanFlow and PARCS. A short description of this code will be given in a subsequent subchapter.

## 2.2 *The neutronics core simulator PARCS*

PARCS, is a three-dimensional (3D) core simulator which solves the steady-state and time-dependent, multi-group neutron diffusion equation and low order (SP3) transport equations in orthogonal and hexagonal geometries. The temporal discretization is performed using the theta method with an optional exponential transformation of the group fluxes (Downar *et al.*, 2012). A transient fixed source problem is solved at each time point in the transient calculations. For spatial discretization, a variety of kernels are available including the most popular for LWR two group nodal methods, ANM and NEM.

For steady state simulations, PARCS solves the multigroup diffusion equation:

$$\nabla \cdot D_g \nabla \phi_g + \Sigma_{tg} \phi_g = \sum_{g'=1}^G \Sigma_{sg \rightarrow g'} \phi_{g'} + \frac{\chi_g}{k} \sum_{g'=1}^G \nu_{g'} \Sigma_{fg'} \phi_{g'}, \quad \text{Equation 2-1}$$

where:

$D_g$  : diffusion coefficient of group g (cm),

$\phi_g$  : neutron flux of group g ( $\text{cm}^{-2}\text{sec}^{-1}$ ),

$\Sigma_{tg}$  : total macroscopic cross section of group g ( $\text{cm}^{-1}$ ),

$\Sigma_{fg}$  : macroscopic fission cross section of group  $g$  ( $\text{cm}^{-1}$ ),

$\Sigma_{sg \rightarrow g'}$  : macroscopic scattering cross section from group  $g$  to group  $g'$  ( $\text{cm}^{-1}$ ),

$\chi_g$  : fission neutron yield, and

$\nu_{g'}$  : average number of neutrons created per fission on group  $g'$ ,

$k$  : multiplication factor.

In Equation 2-1,  $\Sigma_{xg} = \Sigma_{xg}(\vec{r}, t, T_c, T_f, \rho, B, CR)$  and  $D_g = D_g(\vec{r}, t, T_c, T_f, \rho, B, CR)$ . Meaning that the cross section and diffusion coefficient for each energy group  $g$ , at each spatial location  $\vec{r}$ , at each timepoint  $t$ , are dependent on the coolant and fuel temperature  $T_c$  and  $T_f$ , coolant density  $\rho$ , boron concentration  $B$ , and control rod insertion  $CR$ . Macroscopic cross sections are constructed with the assumption of a linear superposition of partial cross section on a base reference state:

$$\Sigma(s_i) = \Sigma_{ref}(s_{i,ref}) + \sum_i^N \Delta s_i \frac{\partial \Sigma}{\partial s_i}, \quad \text{Equation 2-2}$$

where  $s_i = \{T_c, T_f, \rho, B, CR\}$ ,  $\Delta s_i$  is the variation of each parameter with respect to a reference state and  $\frac{\partial \Sigma}{\partial s_i}$  are the partial derivatives of the total XS with respect to each parameter  $s_i$ . The derivatives  $\frac{\partial \Sigma}{\partial s_i}$  are calculated from the lattice code output by the interface code GenPMAx (Ward, Xu and Downar, 2013).

The core neutronics is strongly coupled with the thermal-hydraulics through the cross sections' dependence on the thermal-hydraulic parameters. The values of the thermal-hydraulic parameters are either fixed (precomputed with a TH code and given by input) or are calculated by a simplified thermal-hydraulics solver as it is the case in PARCS. The neutron flux  $\phi$  is used to compute the thermal power that serves as an input for the thermal-hydraulics solver.

The numerical convergence of a steady state diffusion solution is checked by means of different convergence criteria:

$$\delta_{L2} = \frac{\|\psi_{n+1} - \psi_n\|_2}{\langle \psi_{n+1}, \psi_n \rangle^2},$$

$$\delta_k = |k_{eff}^{n+1} - k_{eff}^n|,$$

$$\delta_{L\infty} = \max \left| \frac{\psi_{n+1}^m - \psi_n^m}{\psi_{n+1}^m} \right|,$$

Equation 2-3

$$\delta_{Dop\infty} = \max \left| \frac{T_{D,n+1}^m - T_{D,n}^m}{T_{D,n+1}^m} \right|,$$

where:

$k_{eff}^n$   $k_{eff}$ -value at the  $n^{th}$  iteration,

$\psi_n^m$  fission rate at the  $n^{th}$  iteration at the  $m^{th}$  node, and

$T_{D,n}^m$  Doppler temperature at the  $n^{th}$  iteration at the  $m^{th}$  node.

Physically,  $\delta_{L2}$  checks the global flux convergence,  $\delta_k$  checks the convergence of the multiplication factor,  $\delta_{L\infty}$  checks the local convergence of the flux and  $\delta_{Dop\infty}$  checks the local convergence of the Doppler temperature. To reach the convergence,  $\delta_x$  must be  $< \varepsilon_x$  for all  $\delta_x$ , where  $\varepsilon_x$  are the desired convergence values set in the input by the user.

To solve the time-dependent diffusion equation, a transient fixed source problem is formulated from the two-group kinetic equation leading to:

$$\frac{1}{v_g^m} \frac{d\Phi_g^m}{dt} = \begin{cases} (1 - \beta^m)\psi^m + S_d^m - L_1^m - \Sigma_{r1}^m \Phi_1^m, \\ \Sigma_{12}^m \Phi_1^m + L_2^m - \Sigma_{r2}^m \Phi_2^m, \end{cases}$$

Equation 2-4

$$\frac{dC_k^m}{dt} = \beta_k^m \psi^m - \lambda_k C_k^m.$$

Therein  $m$  is the node number,  $\beta$  the total delayed neutron fraction,  $\psi$  the total fission source term,  $S_d$  the delayed neutron source, and  $L_g$  the leakage, which are defined as follows:

$$\beta^m = \sum_{g=1}^K \beta_k^m,$$

$$\psi^m = \frac{1}{k_{eff}} \sum_{g=1}^2 \Sigma_{fg}^m \Phi_g^m,$$

$$S_d^m = \sum_{g=1}^K \lambda_k C_k^m,$$

$$L_g^m = \sum_{u=x,y,z} L_{gu}^m,$$

Equation 2-5

and

$$L_{gu}^m = \frac{1}{h_u^m} (J_{gu}^{m+} - J_{gu}^{m-}).$$

Equation 2-6

Here  $\beta_k$  is the delayed neutron fraction,  $C_k$  is the precursor density, and  $J_{gu}^{m\pm}$  is the surface average net current.

To solve Equation 2-4, it is assumed that there is no up-scattering, that the neutrons are generated in the fast energies and that there is no dependence of the delayed neutron precursor yields on neutron energy. All these assumptions are suitable for thermal reactors, in particular for PWRs.

Since the fission cross section ( $\Sigma_f$ ), the removal cross section ( $\Sigma_r$ ) and the scattering cross sections ( $\Sigma_{12}$ ) are dependent on the fuel and coolant temperature, Equation 2-4 is also dependent on TH-parameters. It is through these constants that the feedback with the fuel thermo-mechanics and core thermal-hydraulics occurs in practice.

### ***PARCS pin power reconstruction method***

Pin power reconstruction (PPR) is a de-homogenization technique for nodal core calculations, which allows the pinwise reconstruction of the power or flux from the nodal quantities. PPR in PARCS and in almost all core simulators works on an axially averaged pin power, meaning that there is no resolution in axial levels and only one average pin power solution

per fuel assembly is calculated. The radial solution profile is then scaled with the axial power profile.

There are several approaches for the pin power reconstruction; it was first introduced by Koebke (Koebke and Wagner, 1977), with a polynomial expansion that first used 21 expansion coefficients. Years later, Rempe and Smith demonstrated that 13 coefficients were enough to achieve a good solution (Rempe, Smith and Henry, 1989). Another approach consists in an analytic expansion proposed by Böer and Finnemann (Böer and Finnemann, 1992). In the analytic approach (in contrast with the polynomial expansion approach) there is a coupling between the two energy flux expansions. It has been demonstrated that the analytic expansion method has a better accuracy. In PARCS the analytic method is used for the pin power reconstruction.

In practice, the pin power reconstruction methodology has shown good agreement with higher order solutions with an average difference of 1-5%, although local differences up to 10-15 % have been reported in interfaces where large flux variations occur, e.g. at the UO<sub>2</sub>/MOX interface (Hursin, Downar and Kochunas, 2010; Liponi, Taforeau and Hébert, 2017).

### ***2.3 The thermal-hydraulics subchannel code SubChanFlow***

The subchannel code SubChanFlow (SCF) is being developed at KIT for the analysis of fuel rod bundles and cores of rectangular and hexagonal geometries. Single and two-phase flow conditions are solved by a system of three balance equations for stationary and transient upward flow situations. The lateral flow between neighbour subchannels is described by additional equations. Version 3.0 of SCF incorporates a new solver for low flow rates, downward flow and buoyancy driven flow. Coolant properties and state functions are implemented for water using the revised IAPWS-97 (IAPWS, 2007) formulation. In addition, property functions for liquid metals (sodium and lead) and gases (helium, air, etc.) are available. For the rod heat transfer calculation, a finite volume method is used. Temperature dependent fuel UO<sub>2</sub> and UO<sub>2</sub>PuO<sub>2</sub> material properties are implemented. Cladding materials Zircaloy and stainless steel (316 SS) are available (Imke, Sanchez and Gomez-Torres, 2010) making possible the modelling of LWR in general.

Three types of subchannel are possible for the simulation: rod centred, coolant centred and triangular shape channels (Figure 2-2). For the coupling with a neutronics code, the rod centre channel is suitable since the mapping with the neutronics is in this case straight forward.

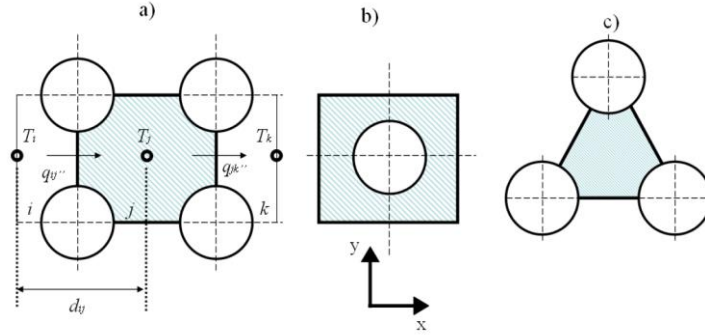


Figure 2-2. Types of possible subchannels: (a) coolant centred, (b) rod centred and (c) triangular subchannels (from (Calleja Reyna, 2013)).

### ***Fluid dynamics model***

SCF solves simplified forms of the energy, mass, and momentum conservation equations. It considers the fluid as a mixture of liquid and vapor, the two-phase flow mixture model is represented by a set of 4 equations, one for the lateral moment conservation, one for the axial moment conservation, one for the energy conservation and one for the mass conservation (Imke and Sanchez, 2012). The equations used in SCF are the following:

Mass conservation:

$$A_{i,j} \frac{\Delta X_i}{\Delta t} (\rho_{i,j} - \rho_{i,j}^{old}) + (m_{i,j} - m_{i,j-1}) + \Delta X_j \sum_k w_{k,j} = 0. \quad \text{Equation 2-7}$$

Energy conservation:

$$\begin{aligned} \frac{A_{i,j}}{\Delta t} [\rho_{i,j}'' (h_{i,j} - h_{i,j}^{old}) + h_{i,j} (\rho_{i,j} - \rho_{i,j}^{old})] + \frac{1}{\Delta X_j} (m_{i,j} h_{i,j} - m_{i,j-1} h_{i,j-1}) \\ + \sum_k w_{k,j} h_{k,j} = Q_{i,j} - \sum_k w'_{k,j} (h_{i,j} - h_{n(k),j}). \end{aligned} \quad \text{Equation 2-8}$$



Axial momentum:

$$\begin{aligned}
 \frac{\Delta X_j}{\Delta t} (m_{i,j} - m_{i,j}^{old}) + m_{i,j} U'_{i,j} + \Delta X_j \sum_k w_{k,j} U'_{k,j} &= -A_{i,j} (p_{i,j} - p_{i,j-1}) \\
 - g A_{i,j} \Delta X_j \rho_{i,j} - \frac{1}{2} \left( \frac{\Delta X f \phi^2}{D_h \rho_{liq}} + K v' \right)_{i,j} |m_{i,j}| \frac{m_{i,j}}{A_{i,j}} & \\
 - \Delta X_j \sum_k w'_{k,j} (U'_{i,j} - U'_{n(k),j}) &
 \end{aligned}
 \tag{Equation 2-9}$$

Lateral momentum:

$$\begin{aligned}
 \frac{\Delta X_j}{\Delta t} (w_{i,j} - w_{i,j}^{old}) + (\bar{U}'_{k,j} w_{k,j} - \bar{U}'_{k,j-1} w_{k,j-1}) & \\
 = \frac{s_k}{l_k} \Delta X_j \Delta p_{k,j-1} - \left( K_G \frac{\Delta X v'_k}{s_k l_k} \right)_j |w_{k,j}| w_{k,j} &
 \end{aligned}
 \tag{Equation 2-10}$$

Where

$A$	subchannel flow area (m <sup>2</sup> ),
$D_h$	hydraulic diameter (m),
$h$	specific mixture enthalpy (J/kg),
$h_{fg}$	evaporation enthalpy (J/kg),
$f$	single-phase friction coefficient (empirical correlation),
$h_{fg}$	axial pressure loss coefficient, e.g., of spacers,
$K_G$	lateral gap pressure loss coefficient (empirical constant),
$l$	distance of neighboring subchannels midpoints (m),
$m$	mass flow rate at axial cell boundary (kg/s),
$N$	number of measurements,
$p$	pressure at axial cell boundary (Pa),
$\Delta p$	pressure difference between neighboring channels (Pa),
$s$	gap width between two neighboring rods (m),
$\Delta t$	time step (s),
$w$	linear mass flow rate through the gap (kg/(m·s)),
$w'$	turbulent crossflow (kg/(m·s)),
$\Delta X$	length of axial cell (m),

$x$	steam quality,
$\alpha$	void fraction (empirical correlation, calculated from steam quality),
$\beta$	mixing coefficient (empirical constant),
$\rho$	density (kg/m <sup>3</sup> ),
$\sigma$	standard deviation,
$\phi_2$	two-phase friction multiplier (empirical correlation),
$old$	value at previous time step,
$liq$	liquid,
$vap$	vapor,
$i, j$	channel $i$ , axial cell $j$ ,
$k$	gap $k$ ,
$n(k)$	channel neighbor belonging to gap $k$ , and
$Q$	linear power released to subchannel (W/m).

### ***Rod heat conduction model***

To solve the temperature field in the fuel rod, the rod is assumed to have azimuthal symmetry, in this way the heat equation is simplified to cylindrical coordinates:

$$\rho c_p \frac{\partial T}{\partial t} = \frac{1}{r} \frac{\partial}{\partial r} \left( \lambda r \frac{\partial T}{\partial r} \right) + q''', \quad \text{Equation 2-11}$$

where

$\vec{r}$	position vector,
$t$	time,
$h = h(t, r)$	specific enthalpy,
$q''' = q'''(\vec{r}, t)$	power density dependent on position and time,
$T = T(\vec{r}, t)$	temperature dependent on position and time,
$\lambda = \lambda(\vec{r}, T)$	thermal conductivity dependent on position and temperature,
$\rho = \rho(\vec{r}, T)$	density dependent on position and temperature,

$c_p = c(\vec{r}, T)$  specific heat at constant pressure dependent on position and temperature.

The heat flux transferred from the rod to the coolant is computed as

$$q'' = h_{surf}(T_{clo} - T_{cool}) \quad \text{Equation 2-12}$$

where  $T_{clo}$  is the clad outer temperature,  $T_{cool}$  the coolant bulk temperature and  $h_{surf}$  the clad to coolant heat transfer coefficient calculated by means of empirical correlations depending on the heat transfer model.

The local power distribution  $q'''$  is required by the subchannel codes to solve the balance equations. In case of a coupled N/TH-simulation, the neutronic code predicts the 3D power distribution and transfer it to the thermal-hydraulics code.

### ***2.3.1 Thermal-hydraulics local safety parameters***

Safety analysis criteria impose limits in local parameters such as the minimum departure from nucleate boiling (MDNB), the critical heat flux (CHF) or the maximum pin power. These thermal-hydraulic local safety parameters can be computed by SCF. They are calculated for the most compromised fuel rods and it must be demonstrated that they don't exceed the core design limits. The departure from nucleate boiling (DNB) is the most limiting constraint on power for commercial PWRs. It occurs at the CHF, which is a function of the geometry and operating conditions and is characterized by a sharp decline in the heat transfer coefficient between coolant and cladding, resulting in an abrupt increase of the fuel and cladding temperature. The performance metric for the DNB is the MDNB, which is the minimum ratio of the critical to actual heat flux found in the core. The MDNB is calculated by the TH code, and given that it is a local parameter, its resolution at subchannel level is necessary for a best estimate prediction.

A typical approach used in the industry for this analysis is to perform neutronics nodal level calculation to which a pin power reconstruction is followed to reconstruct the local power distribution in each pin. With the pinwise power information, a local (subchannel) level calculation is performed for each fuel rod in the fuel assembly to obtain the local safety parameters.

## 2.4 The fuel thermo-mechanics code TRANSURANUS

The fuel thermo-mechanics code TRANSURANUS (Lassmann, 1992) used in this work, is a computer program for the thermal and mechanical analysis of fuel rods in nuclear reactors, developed at the Joint Research Centre Karlsruhe (JRC). The code has a comprehensive material data bank for oxide, mixed oxide, carbide, and nitride fuels, Zircaloy and steel claddings and several different coolants. It can solve steady state and transient problems including fuel material phase changes. All the important physical models are included, and they are thoroughly explained in TRANSURANUS' handbook (Lassmann, 2015).

Unlike PARCS or SCF, TRANSURANUS solves only one fuel rod and not a full core. The fuel rod axial discretization can be treated in two ways, slice or sectional. The slice discretization is used in this work. In it, the values are analysed in the axial centre of the node, and they represent the slice average (Figure 2-3).

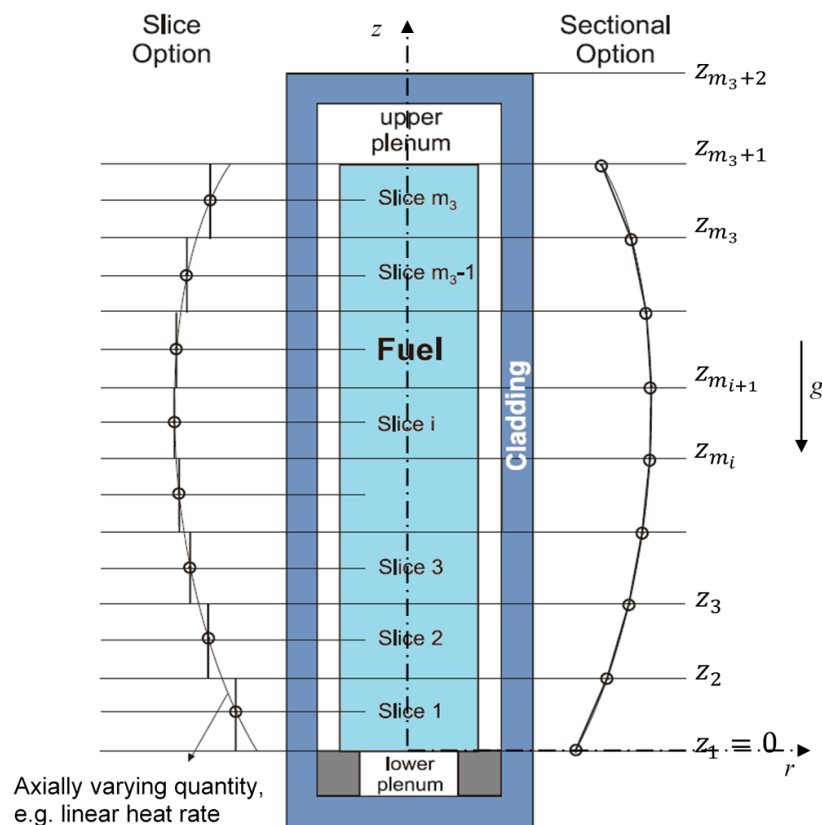


Figure 2-3. Scheme of the fuel rod discretization. The active length of the fuel rod is divided in slices (modified from (Lassmann, 2015)).

Radially, for each slice the rod is discretized as shown in Figure 2-4. Each coarse zone has a different material description. Which is one of the main characteristics of a fuel behaviour solver.

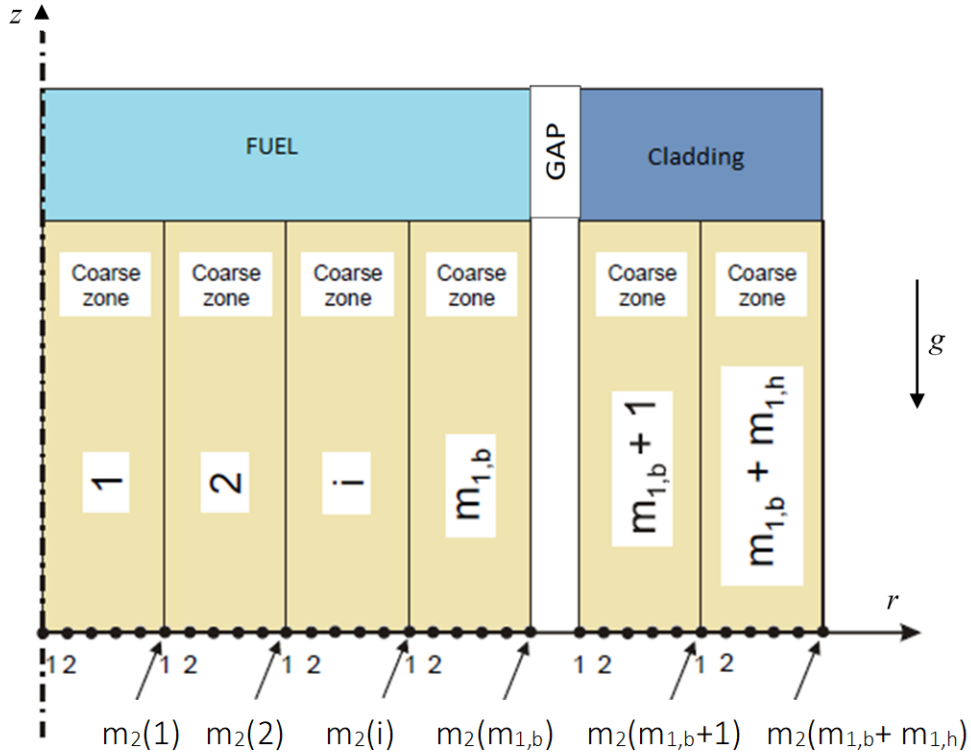


Figure 2-4. Sketch of radial discretization of a slice of a fuel pin (modified from (Lassmann, 2015)).

For the thermal analysis of the rod TU uses a superimposition of one-dimensional radial and axial energy conservation equations. For the validity of these equations, it is assumed that the temperature variation between each radial coarse zone is small, and the thermal conductivity and power density are constant within each coarse zone. The full derivation of these equations is given in (Lassmann, 1987). To obtain the radial temperature distribution for each slice:

$$\rho \frac{\partial h}{\partial t} = \frac{1}{r} \frac{\partial}{\partial r} \left( \lambda r \frac{\partial \vartheta}{\partial r} \right) + q''' \quad \text{Equation 2-13}$$

assuming  $\partial h = c \partial \vartheta$ :

$$c\rho \frac{\partial \vartheta}{\partial t} = \frac{1}{r} \frac{\partial}{\partial r} \left( \lambda r \frac{\partial \vartheta}{\partial r} \right) + q''' \quad \text{Equation 2-14}$$

where:

$c = c(t, r)$	specific heat capacity at constant pressure (J/K),
$h = h(t, r)$	enthalpy per unit mass (J/g),
$q''' = q'''(t, r)$	power density (W/m <sup>3</sup> ),
$r = r(t)$	rod radius (m),
$t$	time (s),
$\vartheta = \vartheta(t, r)$	temperature (K),
$\lambda = \lambda(t, r)$	thermal conductivity (W/(m·K)), and
$\rho = \rho(t, r)$	density (g/cm <sup>3</sup> ).

The above equation is applied to all axial sections of the rod. The parameters  $c$ ,  $\lambda$  and  $\rho$  are temperature dependent, thus, the radial discretization has to be small enough that they can be considered constant within the radial cell.

These parameters are calculated by TU as a function of the irradiation history. In this equation, the boundary condition  $\partial\vartheta(t, r) = 0$  is set in the centre, assuming radial and circumferential symmetry.

The cladding inner temperature and the fuel surface temperature are related by a simplified approach:

$$T_{fs} - T_{cli} = \frac{q''_{f,cl}}{h_{f,cl}}, \quad \text{Equation 2-15}$$

where:

$T_{fs} =$	fuel outer surface temperature,
$T_{cli} =$	clad inner temperature,
$q''_{f,cl} =$	heat flux between fuel and cladding, and
$h_{f,cl} =$	heat transfer coefficient at the fuel-cladding interface (gap conductance).

The gap conductance is dependent on the gap width or contact pressure between fuel and cladding, the gap gas pressure, the fission gas composition and the surface characteristics between fuel and clad. These properties are calculated by TU-models. In case of the coupled calculation, the coolant temperature is set as a boundary condition and the relation between the coolant temperature and the clad outer temperature defined by:

$$T_{clo} - T_{cool} = \frac{q''_{f,cl}}{h_{f,cl}}, \quad \text{Equation 2-16}$$

where,

- $T_{clo}$  = clad outer temperature,
- $T_{cool}$  = coolant bulk temperature,
- $q''_{rod}$  = heat flux density between fuel rod and coolant,
- $h_{surf}$  = heat transfer coefficient at the fuel and coolant interface.

The clad outer temperature is set then by this equation and is a boundary condition to solve Equation 2-14. From Equation 2-14 it follows that the fuel rod temperature is a function of the radial and axial position, dependent on the irradiation history, the linear power, and the thermal-hydraulics conditions. Thus, an accurate calculation of the linear power and the thermal-hydraulics conditions is a prerequisite to obtain a realistic prediction for the fuel temperature.

Given that TU solves the heat transport equation in the rod using best estimations for the material parameters and dimensions, it can be seen how replacing SCF's solver by TU would lead to a more accurate solution which also includes the dependency of the material properties with the burnup.

Next, some of the relevant phenomena considered by the fuel thermo-mechanics code are described to explain how irradiation affects the material properties.

### 2.4.1 Relevant physical phenomena considered by the fuel thermo-mechanics code

From the beginning of the irradiation until the end of life, the fuel undergoes varied and complex physical thermo-mechanical phenomena changing not only the thermophysical properties but also its geometry and the heat transfer boundary conditions. In Figure 2-5, a list of the most relevant phenomena occurring to the fuel rod since beginning of irradiation until end of irradiation is shown.

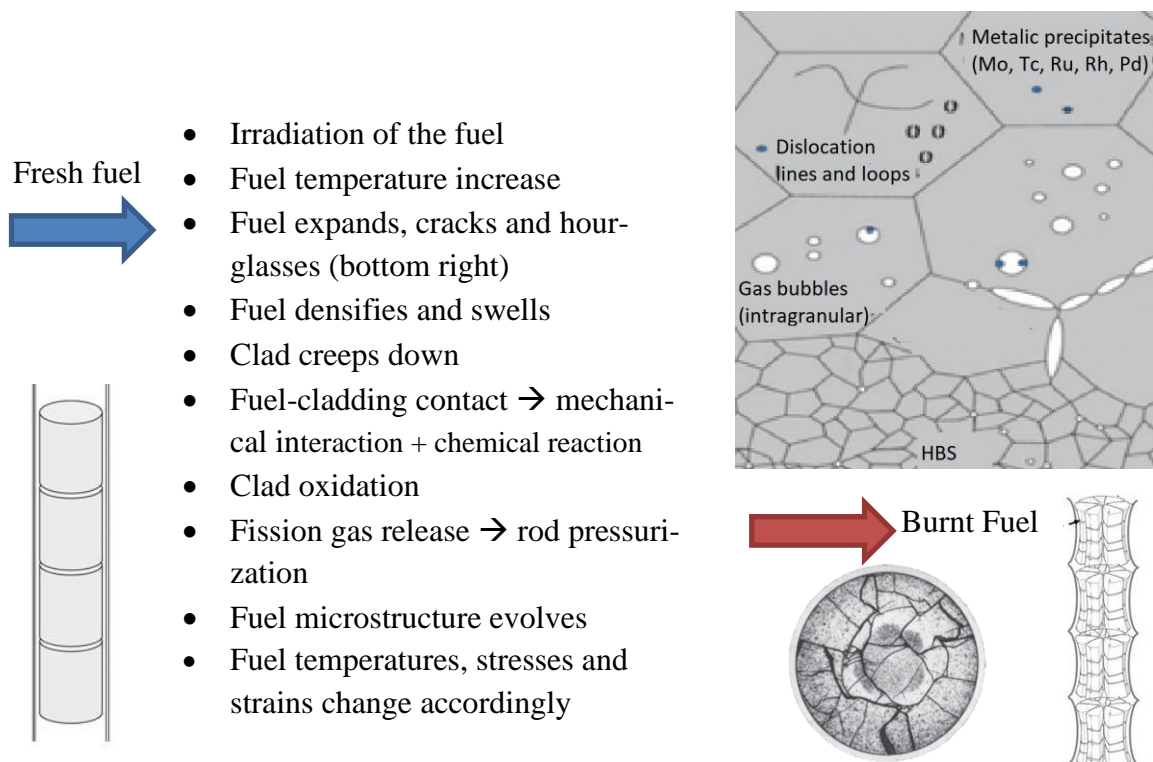


Figure 2-5. Phenomena occurring in a fuel rod from the moment its begins being irradiated until the irradiation ends (~60 GWd/tHM of burnup) (modified from (Whittle, 2016)). HBS=High Burnup Structure.

Most of these phenomena are well studied and extensive modelling and experiments to achieve accurate correlations exist, however some of these, e.g. fission gas release or the High Burnup Structure (HBS), are not yet completely understood. The most relevant of these phenomena, swelling, cracking, creep, pellet clad interaction and fission gas release will be introduced next.



## Cracking

When the fuel rod power increases, the large temperature gradients in the fuel pellet (typically 1500K at the centre, and 700K at the surface of the fuel pin at nominal power) causes a gradient in the radial expansion of the fuel matrix. This generates large thermal stresses and the ceramic fuel matrix, having a small yield strength, fractures.

Figure 2-6 depicts the cracking of a fuel with low irradiation. In TRANSURANUS, the material is modelled as a continuum and the cracks are represented by fictitious crack strains introduced in the correlations.

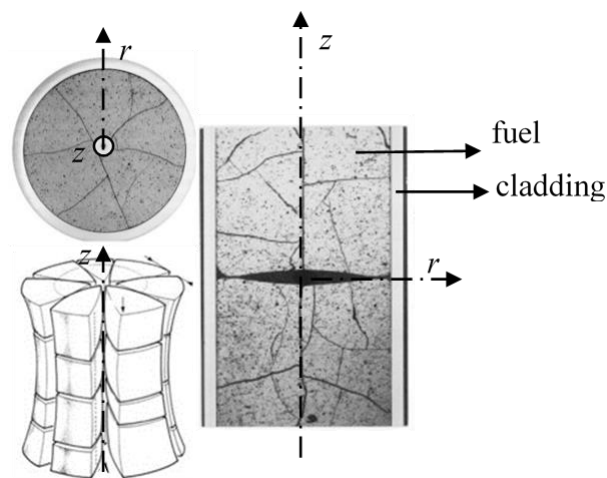


Figure 2-6. Cracked fuel pellets radial and axial slices and depiction of *hourglass* shape (bottom left) induced by the irradiation (modified from (Michel *et al.*, 2008; Olander, 2009)).

## Swelling

Irradiation induced swelling refers to the process of decrease of density in the fuel due to neutron irradiation caused by the replacement of heavy metal atoms by fission products. Most fission products are solid but also gas atoms are generated. Due to their low solubility the gas atoms coalesce into *bubbles* creating spaces into a solid fuel matrix, thus expanding the fuel. The bubbles migrate in random walk in absence of direct forces or with a given direction when forces are present (such as temperature gradients or stresses). Fission gases are released to external surfaces, such as the central void, cracks in the fuel or the fuel-cladding gap. Because of the fuel pellet growth, the gap width reduces increasing the gap heat transfer coefficient. The gap closure depends on the fuel rod geometry and materials, typically it occurs at  $\sim 10-15$  GWd/tHM of burnup.

### ***Fission gas release***

The fission gas release is one of the main phenomena affecting the fuel rod behaviour. The fission gases degrade the thermal conductivity of the gap gas, hence, increasing the fuel temperature. The modelling of fission gas release is still an area of discussion; however, it is included in the models of the fuel thermo-mechanics codes, since it affects many aspects of the fuel thermo-mechanics. The fission gases Xenon and Krypton degrade the fuel-clad thermal conductivity, increase the inner pin pressure. Swelling due to fission gas release may lead to enhanced pellet-clad interaction. The release of radioactive gases from the fuel matrix to the free volume decreases the safety margin of a power plant. Due to the lower conductivity of the fission gas released into the gap (Xenon, Krypton), the gap heat transfer conductivity decreases. This phenomenon is relevant for high burnups (~60 GWd/tHM).

### ***Creep***

Creep is defined as a slow and irreversible deformation process under the influence of stresses below the yield stress. The creep can be originated by mechanical, thermal and irradiation origins. Typically, the creep is classified into three stages, primary, secondary, and tertiary, as depicted in Figure 2-7. The primary creep presents a high amplitude deformation with a decreasing strain rate and it constitutes a small part of the total creep. The secondary creep is the part where the strain rate remains constant and is the most important part of the creep in terms of accumulated strain. The tertiary creep presents a rapid increase of the strain and in this phase the material degrades rapidly leading to failure, this phase occurs typically in a short time.

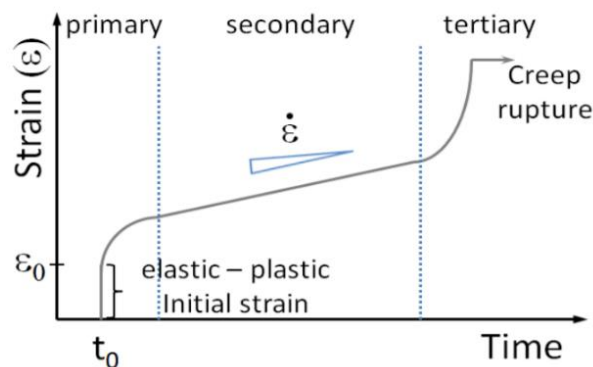


Figure 2-7. Creep stages with time during irradiation (source (Van Brutzel, Dingreville and Bartel, 2015)).

Both, clad and fuel are subjected to creep deformation. In the fuel cladding these stresses are due to the difference between the gap pressure (~2MPa for a fresh rod design pressure) and the coolant pressure (~15.5MPa for a PWR nominal conditions), this pressure difference leads to a clad creep-down, reducing the radius of the cladding.

### ***Pellet clad interaction***

At the beginning of life, the gap is reduced due to a compression caused by the coolant pressure acting from outside on the fuel pin. As the irradiation continues, the clad creeps down diminishing its radius, and the ceramic fuel matrix grows by swelling and creep mechanisms increasing its radius. When the fuel and clad enter in contact, the clad becomes loaded in tension and deforms to accommodate the fuel expansion, which is known as pellet clad interaction (PCI). The clad is then loaded with a tensile stress induced by the fuel expansion, and if there are aggressive fission products released from the pellets, it can lead to so called irradiation assisted stress corrosion cracking (IASCC), ultimately ending in fuel pin failure.

### ***Oxide crust formation***

Another phenomenon of interest to be mentioned is the oxide crust formation on the outside layer of the clad. The oxidation of Zircaloy cladding is present in LWR and is an important phenomenon to be considered because it not only affects the mechanical behaviour of the clad, but also reduces the clad thermal conductivity giving place to higher clad and fuel temperatures. Aside from this, the oxide diminishes the cladding thickness which can lead to rod failure and thus is a variable is also considered in the safety analysis. In this work however it will only be considered in such manner that it only reduces the heat transfer from the fuel to the coolant, thus increasing the fuel temperature.

## ***2.4.2 Fuel gap width, gap heat transfer coefficient and fission products dependence with the irradiation***

The physical phenomena described before have a direct impact on the gap heat transfer coefficient (HTC) and the gap width. The gap width changes due to thermal expansion, swelling, cracking, creep, etc. as well as the fission gases released to the gap affect directly the value of the gap HTC. To exemplify Figure 2-8 shows a calculation of the gap HTC and the gap width as a function of the axial height for a typical UO<sub>2</sub> fuel rod with 4.2% enrichment irradiated up to 37.5 GWd/tHM. The calculation is performed using TRANSURANUS. In

the calculation, a two cycles irradiation. A one-month stop between the cycles is considered, and a constant linear power for the irradiation is used. The axial irradiation profile used is cosine shaped and the rod is discretized in 20 equidistant axial slices.

Figure 2-8 shows that at the beginning of the irradiation the gap width value increases due to the fuel densification, and then starts to decrease mainly due to the swelling. The gap HTC varies consequently with the gap width. When the gap is almost closed the gap HTC increases exponentially. It reaches a limit when the gap is completely closed, and it remains constant until the end of the irradiation when it decreases slowly. The decrease in value of the HTC at the end of the irradiation is caused by the fission gas release triggered at higher burnups, which lowers the gas conductivity between fuel and clad.

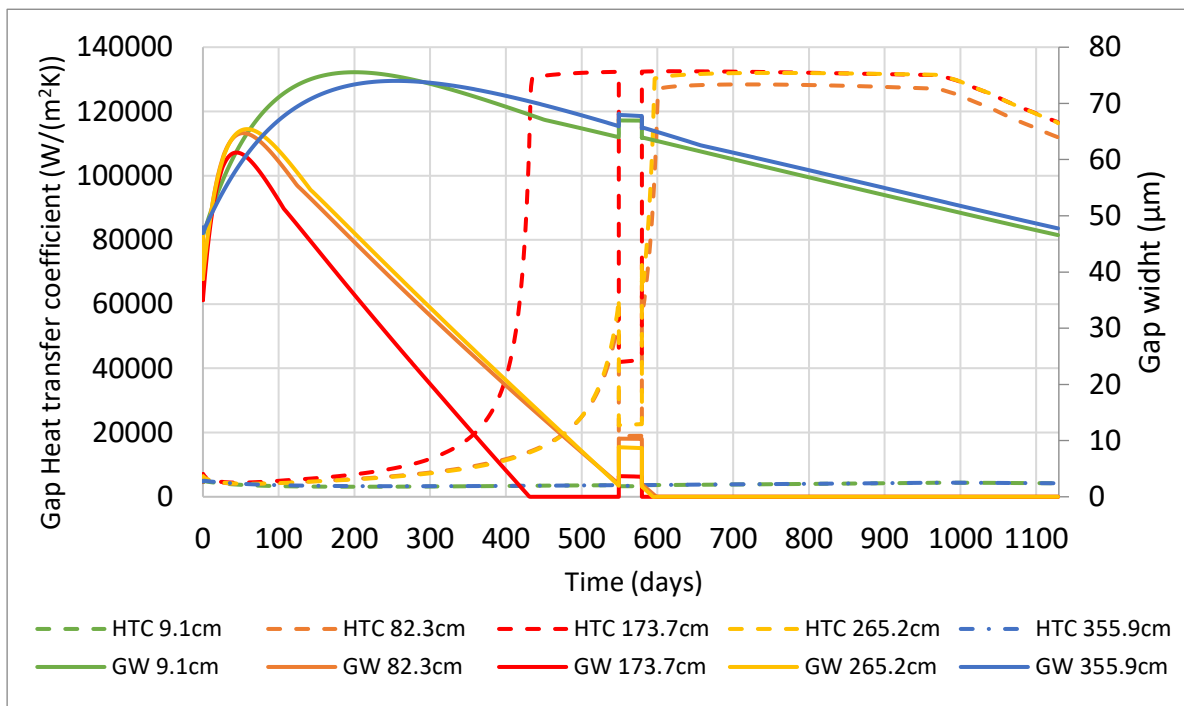


Figure 2-8. Calculated gap width (GW) and gap heat transfer coefficient (HTC) in function of the burnup. The rod is irradiated at a constant linear rate up to 37.5 GWd/tHM. During the irradiation a one-month interval is considered between irradiation cycles. The fuel rod is divided in 20 equal axial nodes of 18.25cm, the labels show the middle point axial position of the nodes.

The described behavior influences directly the prediction of the fuel temperature and thus, must be considered in the reactor core simulation.

### ***3 State of the art of Multiphysics Reactor Core Simulations***

The reactor core analysis is inherently a multiphysics problem. The thermal hydraulic, neutronics, thermo-mechanics and chemical processes taking place in the core during the operation of a nuclear power plant are strongly interrelated.

For example, any change of the thermal-hydraulics conditions, e.g. the coolant temperature will cause the fuel temperature to change, which by the Doppler effect will change the neutron absorption of the fuel and thus the neutron population and hence the power generation. In addition, a change in the coolant temperature changes the coolant density, reducing the neutron moderation and injecting a negative reactivity if the coolant temperature increases, or increasing the moderation and injecting a positive reactivity if the coolant temperature decreases. This effect is used for instance at the end of life of Convoy nuclear power plants, where the coolant inlet temperature is reduced to introduce a positive reactivity and thus operate for a longer time, which is known as *stretch out*. Another example is the radial expansion of the cladding, which reduces the flow area and hence increases the velocity of the coolant leading to an increased heat transfer, which leads to a reduced coolant temperature with an increased coolant density and power.

This interdependence between parameters of the reactor core is challenging to model for numerical simulation tools. Not all the feedbacks are equally important, and it is up to the physicists and engineers to determine which phenomena should be precisely modelled and which can be neglected or covered by an approximation.

In the past, the limitations of computer power and limitations of numerical methods and algorithms, have been overcome using a low spatial domain resolution, and the modelling of every single physics field individually.

Nowadays, the huge and cheap computational power available and the significant progress in the understanding of physical phenomena of the involved areas as well as the advances in numerical methods and algorithms, have made the development of multiphysics and multi-scale coupled simulation tools possible. Modern multiphysics core analysis aims at improving the prediction accuracy of the core physics by solving different fields simultaneously by coupling validated neutronics, thermal-hydraulics and thermo-mechanics codes to simulate the processes in the reactor core.

In the next subchapters, the state of the art of the methods for multiphysics core simulations and the relevant issues in this field are discussed.

### ***3.1 Neutronics and thermal-hydraulics coupled simulations***

The first neutronics and thermal-hydraulics coupling approaches for the core analysis were based on 3D nodal diffusion codes such as PARCS, DYN3D, CRONOS, etc. with 1D system thermal-hydraulics codes like RELAP5, ATHLET, CATHARE, etc. Before, the system codes used a point kinetics model to describe the power response of the core, based on pre-calculated reactivity coefficients.

One example of the first 3D nodal diffusion code coupling with a system TH code is the study of the PWR Main Steam Line Break (MSLB) benchmark (Ivanov, Beam and Baratta, 1999). In the MSLB scenario, the asymmetry of the power in the core required integrating a 3D description of the reactor power distribution, which was only possible with a 3D core simulator. In this simulation, the core neutronics were modelled with 241 nodes corresponding to the number of fuel assemblies in the reactor core and, due to computational constraints, only 18 parallel channels representing the thermal hydraulics of the full core. The 3D neutronics and TH system code coupling has become a standard in today's reactor core simulations and the use of one node per fuel assembly in neutronics and thermal hydraulics is no longer a constraint.

To increase the spatial resolution of the neutronics solvers to predict the power in each individual fuel pin, Pin Power Reconstruction methods based on the nodal diffusion core simulation are applied. On the other hand, in order to predict the thermal-hydraulics safety parameters in a more accurate manner, the use of more detailed thermal-hydraulics solvers such as 3D thermal-hydraulics system codes with coarse meshes (RELAP5-3D, CATHARE 3D), subchannel codes (CTF, SCF, FLICA), porous media 3D codes (CUPID, PORFLOW, TWOPORFLOW) and CFD codes gained increased interest in the research community.

Using the pin power calculated with pin power reconstruction together with subchannel codes, coupled in an offline way, reflects the industry standard e.g. for the prediction of safety parameters such as the minimum departure from nucleate boiling ratio MDNBR, which is a limiting factor in the reactor core design.

Recent multiphysics code developments worldwide are focused on the coupling of both, transport solvers (SP3, MOC) and Monte Carlo codes with subchannel codes mainly in order

to perform full core simulations at pin/subchannel level e.g. DYN-SUB5 (Daeubler, Trost, *et al.*, 2015), MPACT/CTF (Palmtag *et al.*, 2014). Such kind of advanced coupled codes can predict safety parameters considering local thermal-hydraulics feedbacks making the use of hot channel factors obsolete. In the last years, there has been an increasing development of coupling of higher order solvers, meaning subchannel and CFD for TH and lattice and Monte Carlo for neutronics. However, the computational time required for these coupled approaches, are still prohibitive for industry applications, still needing several hours or days to complete a calculation. In Table 3-1, some examples of existing code couplings are listed. There, simplified parallel channel solvers are not standalone codes per-se, but they are simplified solvers implemented into the neutronics codes to have a first approximation of the TH

Table 3-1. Examples of Neutronics/Thermal-hydraulics coupled codes.

N TH	Point- Kinetics	Nodal Diffusion	Transport MOC	Monte Carlo
Simplified parallel channel	-	PARCS DYN3D FLICA SIMULATE5	-	-
System TH	RELAP5 TRACE	PARCS/RELAP5 PARCS/TRACE DYN3D/ATHLET RELAP/PANBOX SIMTRAN/RELAP5 QUABOX/RELAP5 TRADYN	-	SERPENT/RELAP5 (Wu and Kozlowski, 2015)
Subchannel	SCF COBRA-TF	PARCS-SCF PARCS/COBRA-TF (Abarca <i>et al.</i> , 2011) CTF/DYN3D (Perin and Velkov, 2017) DYN3D/SUB- CHANFLOW (Gomez-Torres <i>et al.</i> , 2012)	MPACT/CTF (Palmtag <i>et al.</i> , 2014) CTF/TORT- TD (Yilmaz, Avramova and Andersen, 2017)	MC21/CTF (Kelly III <i>et al.</i> , 2017) OpenMC/COBRA-EN (Mylonakis, Varvayanni and Catsaros, 2017) SERPENT/SCF (Daeubler, Ivanov, <i>et al.</i> , 2015) MCNPX/COBRA-IV (Vazquez <i>et al.</i> , 2012) MCNP/SCF (Ivanov, Sanchez and Imke, 2011)
CFD	-	DYN3D/ANSYS- CFX(Grahn, Kliem and Rohde, 2015) PARCS/CFX (Peña <i>et al.</i> , 2011)	DeCART/ STAR-CD (Thomas <i>et al.</i> , 2003)	MCNP/FLUENT (Gurecky and Schneider, 2016) TRIPOLI/CFX(Henry, Tiselj and Snoj, 2017)

field. On the same way, point-kinetics solvers are simplified equations implemented in the TH codes to have an approximation of the power evolution during a transient, using pre-calculated reactivity coefficients.

Current works in neutronics-thermal hydraulics coupling are focused the coupling of transport or Monte Carlo neutronics solvers with subchannel or CFD thermal-hydraulics. The development of time dependent Monte Carlo codes like Serpent and Tripoli, allow for coupled transient subchannel codes/Monte Carlo. Solutions for a minicore with this type of coupling are works in progress e.g. in the McSAFE Project. The full reactor core steady state solution of a coupled CFD/Monte Carlo code remains a challenge for the future, and even more the transient solution.

### ***3.2 Neutronics, thermal-hydraulics and thermo-mechanics coupled simulations***

To improve the prediction of key thermal-hydraulic safety parameters of the fuel such as fuel and cladding temperatures under real operating conditions inside the core, more sophisticated fuel rod models than the implemented in the system thermal-hydraulics and subchannel codes are required. For this purpose, the coupling of fuel thermo-mechanic codes such as TRANSURANUS, FRAPCON, ENIGMA, etc. with thermal-hydraulics and neutronic codes is being pursued in the research community. This trend is also fostered by the increasing interest of the industry as well as by the new requirements from regulatory authorities.

Coupling neutronics or thermal-hydraulics codes with fuel thermo-mechanics codes started recently and can be classified into nodal or pin level. Nodal level means that the studies consider the most representative pin in the fuel assembly to represent an average pin, which represents the fuel assembly. The first coupling for a reactor core simulation for transient and steady state analysis was done by (Holt et al. 2014), with the development of a coupling interface between TU and DYN3D. Later on, (Bielen, 2015) developed a coupling for steady state simulations with PARCS-FRAPCON to study the fuel depletion during an operation cycles.

Examples of other recent studies on this topic are:

- At nodal level: transient analysis of RIA at 30% of nominal power in a VVER and boron dilution accident in a PWR with DYN3D/TRANSURANUS (Holt *et al.*, 2014, 2016), steady state burnup analysis of a PWR with PARCS/FRAPCON



(Bielen, 2015), HZP REA minicore APOLLO3-FLICA4-ALCYONE (Targa *et al.*, 2016).

- At fuel pin level: single 3D pin with DeCART/BISON (Hales *et al.*, 2015), a 4x4 pin UO<sub>2</sub>/MOX FA with TORT-TD-/CTF/FRAPTRAN (Magedanz *et al.*, 2015), and a 7x7 pins BWR fuel assembly with SERPENT2/FINIX – SERPENT2/ENIGMA (Valtavirta, Leppänen and Viitanen, 2017).

The higher order level couplings, although more accurate, are developed only for steady state calculations and for the simulation of simplified FA's geometries.

From the literature review on the coupling of neutronics/thermal-hydraulics with fuel thermo-mechanics solvers, it can be concluded that it is still in the early stages of development. Current challenges are, e.g., the full core steady state calculation of Monte Carlo/sub-channel TH/thermo-mechanics. One step further is the same calculation but with CFD TH and even more futuristic are these solutions for time dependent problems. Also, the transient solution of a full core with diffusion neutronics/subchannel TH/thermo-mechanics, as performed in the last chapter of this work is a state-of-the-art challenge.

### ***3.3 Strategies for codes integration in multiphysics coupling***

Different strategies for multiphysics code coupling are used in existing coupled codes each with their advantages and disadvantages. Hereafter, the main reasons for the selection of the coupling and methodologies are discussed.

Multiphysics coupling are categorized typically as 1-way or 2-way coupling, internal or external coupling, explicit or implicit coupling, and serial or parallel coupling. A 1-way coupling refers to the calculation by one of the codes using boundary conditions generated previously by the other code. This is used for instance to perform fuel thermo-mechanics analysis using the results of coupled N/TH as boundary conditions (Rossiter, Palmer and Gregg, 2011), or to perform subchannel level calculations using the results of nodal level neutronics simulations with pin power reconstruction as boundary conditions (Grgić, Benčik and Sadek, 2013). In this case there is no feedback between the solutions, therefore it is also known as offline calculation.

In a 2-way coupling, the codes involved in the coupling exchange information between them and iterate back and forth until a converged solution is reached. In this thesis, the coupling is performed in a 2-way manner, since the main interest is the effect of the interaction between the different physics.

In the external coupling the information between the codes is exchanged via input/output files. This approach is mostly used when there is no access to the program source code and is also used to a fast implementation of a coupling by means of scripts. An example of this is the work performed in (Vazquez *et al.*, 2012). The disadvantage of this methodology is the large overhead generated by the reading and writing from/to files, which reflects in the computational time of the simulation.

On the other hand, in the internal coupling, the source codes of the involved programs are merged together. In this way, the feedback variables are exchanged between the programs at memory level, reducing considerably the computational time of the simulation. Other advantage of this type of coupling is the increased numerical stability due to avoiding truncation errors in the variables (existing when reading/writing from/to files). In this work, the internal coupling approach is implemented.

In the coupling scheme used in this thesis, the calculated variables of one code serve as input variables to the other and vice-versa. This coupling technique is known as operator-splitting (OS), in the sense that the multiphysics variables are decomposed into each individual physics field (Ragusa and Mahadevan, 2009; Keyes *et al.*, 2013). This is also known as ‘*loose coupling*’ as opposed to a ‘*tight coupling*’ (Novascone *et al.*, 2013), where the complete set of equations describing the system is solved at the same time. The advantage of using a loose coupling is that legacy (extensively validated) codes can be adapted taking advantage of the effort put in the development and validation of existing codes.

In the implicit coupling a single system of equations must be assembled and solved for the full set of coupled physics, which requires a significant effort in the modification of the solvers of the different codes to integrate them. Hence, few implicit coupling implementations have been done and typically they are developed from scratch, e.g. (Jareteg *et al.*, 2015). The advantage of having legacy codes with decades of validation effort is lost and thus the explicit coupling is the standard in coupled calculations.

Serial or parallel refers to whether parallel programming tools are used for the coupling. The parallel approach can be used to speed up the solution or just to exchange variables between the codes. An example of parallel coupling for information exchange is PARCS/RELAP external coupling with Parallel Virtual Machine (PVM) (Abarca *et al.*, 2011), or the coupling of TORT-TD/CTF/FRAPTRAN (Magedanz *et al.*, 2015) where the coupling is used to exchange information and to speed up the solution. For the coupling of PARCS-SCF with TU the parallel programming library MPI (Message Passing Interface) has been used. The reason for the use of parallel programming is the lack of capability of TRANSURANUS to solve more than one fuel pin per calculation. More details will be discussed in Chapter 5.

To summarize, the coupling of PARCS-SCF-TU is an internal, 2-way explicit coupling with MPI parallel implementation. A description of the feedback variables exchanged in the coupling, the coupling algorithms and the spatial domain mapping between the codes will be explained.

### ***3.3.1 Feedback variables exchanged in the N-TH-TM coupling***

In the previous chapters an overview of neutronics, thermal-hydraulics and fuel thermo-mechanics codes has been presented, and the equations solved by the codes and the physical domains of their focus are presented. In Figure 3-1 there is a representation of how the codes interact with each other.

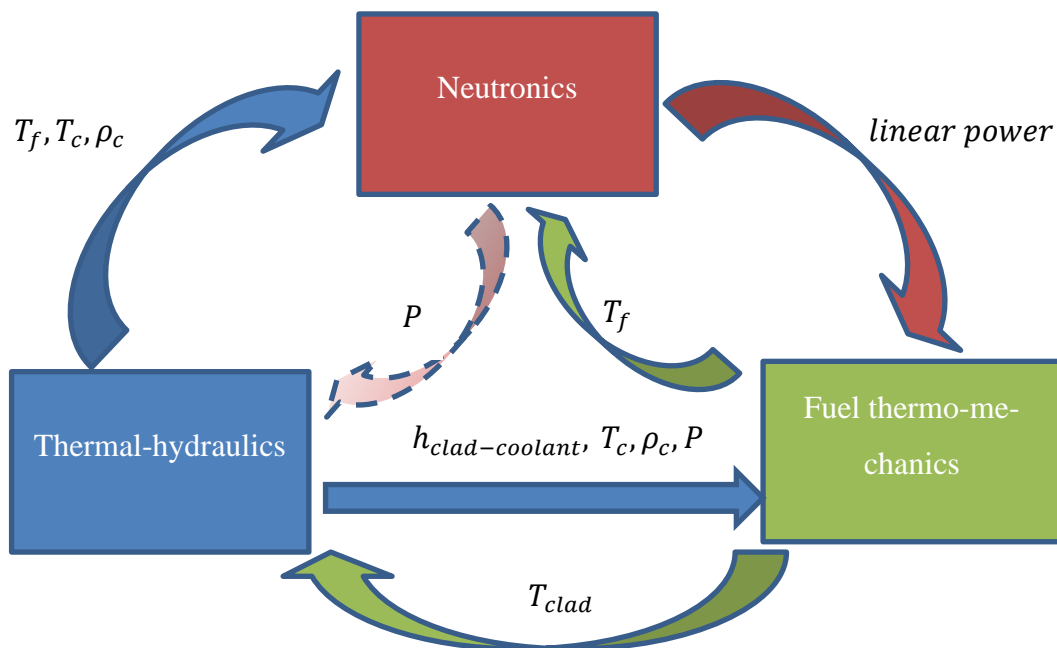


Figure 3-1. Feedback variables transferred between the codes.

There, the neutronics are coupled with the thermal-hydraulics via the coolant and fuel temperature ( $T_c, T_f$ ) and the coolant density ( $\rho_c$ ), through the dependency of the cross sections. The best estimate values for these parameters are calculated by the thermal-hydraulics ( $T_c, \rho_c$ ) and fuel thermo-mechanics code ( $T_f$ ). The fuel thermo-mechanics code needs the  $T_c$ ,  $h_{clad-coolant}$  (clad to coolant heat transfer coefficient),  $p$  (pressure) and rod linear power ( $P$ ) as boundary conditions to calculate the fuel temperature. On the other hand, the thermal-hydraulics code needs to know the energy deposited in the coolant. In a neutronics/thermal-hydraulics coupling, the power predicted by the neutronics solver is transferred to the thermal hydraulics directly. But in a full coupling of neutronics, thermal-hydraulics and fuel thermo-mechanics code, the power is transferred indirectly to the thermal-hydraulics solver through the clad temperature calculated by the fuel thermo-mechanics code.

### ***3.3.2 Algorithms for coupling implementation***

The purpose of coupling neutronics and thermal-hydraulics codes is to use the best of both codes capabilities to perform a reactor core simulation. The neutronics code solves the problem using the thermal hydraulics parameters provided by the TH solver and the TH solver solves the problem using the power distribution provided by the neutronics solver.

The neutron transport equation, heat transport equation, and momentum and energy transport equations described in the neutronics, thermal-hydraulics and fuel thermo-mechanics codes, are numerically solved by a system of partial differential equations (PDE).

In a multiphysics system on equilibrium, where two different fields are considered, the coupled equilibrium problem can be stated as

$$\begin{aligned} F_1(u_1, u_2) &= 0, \\ F_2(u_1, u_2) &= 0. \end{aligned} \tag{Equation 3-1}$$

This represents a set of equations  $F_1(u_1, u_2)$  to find a solution for  $u_1$  given  $u_2$ , and  $F_2(u_1, u_2)$  is the equation system to find the solution for  $u_2$  given  $u_1$ . Here,  $u_1$  and  $u_2$  are the set of parameters that solve both  $F_1$  and  $F_2$  simultaneously. Classic multiphysics algorithms preserve the integrity of the two mono-physics problems, solving the first equation for the first unknown, given the second unknown, and the second equation for the second unknown, given

the first. Multiphysics coupling is solved by the iteration over the pair of problems, typically in a Gauss-Seidel approach. The Gauss-Seidel algorithm to solve equilibrium multiphysics systems can be described as follows (Keyes *et al.*, 2013):

Equation 3-2. Typical Gauss-Seidel algorithm for the solution of a coupled steady state system.
Given the initiate iterate $\{u_1^0, u_2^0\}$
<b>For</b> $k=1,2, \dots$ , (until convergence) <b>do</b>
Solve for $v$ in $F_1(v, u_2^k) = 0$ ; set $u_1^k = v$
Solve for $w$ in $F_2(u_1^k, w) = 0$ ; set $u_2^k = w$
<b>end for</b>

Assuming a multiphysics problem having in the solution space a unique solution and being of hyperbolic nature, the transient problem can be described by:

$$\partial_t u_1 = f_1(u_1, u_2)$$

$$\partial_t u_2 = f_2(u_1, u_2)$$

Equation 3-3

One simple algorithm to solve the operator splitting scheme is:

Equation 3-4. Typical operator splitting algorithm for the solution of a transient coupled system.
Given the initiate iterate $\{u_1(t_0), u_2(t_0)\}$
<b>For</b> $k=1,2, \dots, N$ <b>do</b>
Evolve one timestep in $\partial_t u_1 + f_1(u_1, u_2(t_{n-1})) = 0$ to obtain $u_1(t_n)$
Evolve one timestep in $\partial_t u_2 + f_2(u_1(t_n), u_2) = 0$ to obtain $u_2(t_n)$
<b>end for</b>

In the algorithms presented here, it is assumed that only two systems are being coupled, but variations of these algorithms can be extended for the coupling of more systems.

### ***3.3.3 Spatial domain mapping***

The data exchange between codes is based on the spatial mapping being used by each code, i.e. computational domain. Hence, knowing the domain meshing, and identifying the nodes of each code with the nodes on the other and assigning them weights, allows a consistent conservation of information.

In a simulation, the reactor domain is discretized into mesh nodes (usually called *spatial meshing* in contrast to *temporal meshing*, from now on *nodes*), to represent the domain where the equations are solved. The information exchange between solvers is based on the spatial mapping, which must be defined appropriately in the inputs. In a one to one mapping, one fuel assembly is represented by one TH channel and one N node, respectively. In a flexible mapping, it can represent regions of the core; this kind of mapping is typical with system codes.

### ***3.3.4 Time step control***

For the time dependent problem of coupled simulations, in order to converge to a solution, the time step must be sufficiently small to capture the transport problem, but not too small to cause a too large computational time. The transient solution is solved by a partial differential equation (PDE) and each of the codes has implemented its own PDE solution method, some of the most popular being Crank-Nicolson, Leapfrog and Newton methods. These methods are robust and the solution is achieved with a small enough time step (Mylonakis *et al.*, 2014). Then, a necessary condition for the convergence of the solution is that the time step is small enough to capture the physical phenomena in the transient.

One option is to select one solver as a master and ensure that the other codes use the same time step as the master. In the coupling of neutronics codes and system TH codes, the thermal-hydraulic code is the master. This type of coupling is used typically to analyse problems like LOCA or MSLB, where the fastest physics occurring in the beginning is the pressure wave propagation, thus, the TH code handles the time stepping. This is the case e.g. for the couplings of TRACE/PARCS and RELAP/PARCS.

For the analysis of fast transients limited to the core such as RIA transients, the rapid power variation dominates the problem behaviour, so the neutronics solver is the driver of the solution. This is the reason why in neutronics/thermal-hydraulics couplings where fast core transients are to be analysed, the neutronics code acts as the master, e.g. such are the

cases for PARCS-COBRA-EN (Noori-Kalkhoran *et al.*, 2014), COBAYA3-SCF (Calleja *et al.*, 2012), DYN3D-SP3/SCF (Gómez Torres, 2011).

Another important aspect of time dependent calculations is the size of the time step, which can be fix or be adaptive. Adaptive time stepping is used to enhancing the efficiency of the solution. Every time step, the transient evolution is analysed, and variables such as the temperature, the global power, or local fluxes are monitored to see their rate of change and decide if a bigger time step can be used or a smaller time step is necessary (Ivanov and Avramova, 2007). In case that the variations are larger than the imposed criteria, the time step is reduced, and the solver must go back to the previous time step and recalculate the solution with the smaller time step. For this, the code must be programmed in such a way that the solution of the previous time step is available in memory, if this is not the case, considerable modifications can be necessary to implement this methodology.

If the time step is fixed, the user must decide the time step value, knowing a priori the behaviour of the solution. In practice, to know if the selected time step is appropriate and the solution is converged, a time step sensitivity analysis is done (see Appendix A.2). The time step is reduced to e.g. to one half and a new solution is calculated, when the solution is the same for a smaller time step then, it is converged. If the solution changes for a smaller time step, then the solution is not still converged and a calculation with a smaller time step must be done until the convergence is found. This sensitivity study is necessary to ensure a correct solution.

## ***Chapter summary***

In this chapter the state of the art and challenges of multiphysics simulations, the techniques used for coupled simulation as well as the fundamentals of a reactor core calculation and the computer codes used in this work are briefly discussed.

## ***4 Coupling of a Neutronics Core Simulator with a Subchannel Thermal-Hydraulics Code***

The first step of the neutronics/thermal-hydraulics/fuel thermo-mechanics multiphysics tool development is the coupling of the neutronics and thermal-hydraulics codes. The implementation methodology and verification of the tool are presented in this chapter before moving forward to the coupling with the fuel thermo-mechanics solver.

This N-TH coupled code allows to perform more detailed thermal-hydraulics simulations of the core considering the crossflow between the fuel assemblies which is not considered by the 1D system codes using parallel channels. Also, it allows the implementation of the sub-channel level methodology for extraction of TH local safety parameters. This methodology is presented at the end of the chapter, where a comparison with a high order solution is done showing the potential of this methodology.

Next, the coupling methodology is described, and verification problems are presented.

### ***4.1 Coupling implementation description***

The neutronics code PARCS and the thermal-hydraulics code SCF have been coupled by merging the codes into a single executable *PARCS-SCF*. SCF has been added as a new thermal-hydraulic solver of PARCS. SCF can be called from PARCS' input with newly implemented keywords. In this internal coupling, the exchange of information between the codes is done at memory level, thus speeding up the solution.

The coupled code PARCS-SCF needs both the PARCS input and the SCF input. The PARCS input describes the neutronics problem to be solved and the SCF input describes the thermal-hydraulic problem to be solved. Naturally, both inputs describe the same spatial domain but different physics, so there must be a consistency in the input generation and description of the problem which is partially checked by the coupled code. One of the aspects of this consistency is the spatial domain mapping (radial and axial) which will be introduced later in this chapter.

PARCS version v3.2m10r13 available at KIT through the Code Application and Maintenance Program (CAMP) of the U.S. NRC is used here. The in-house code SCF version 3.0 is used. The coupling has been performed in the Microsoft Visual Studio IDE (Integrated Development Environment) under Windows OS. The original PARCS solution is organized in



six projects. SCF has been added as a new project into the solution as well as a new project containing the coupling routines. Several code modifications and new subroutines have been modified and newly developed for the coupling.

## 4.2 Coupling parameters and methodology

The neutronics and thermal hydraulics in a PWR are tightly coupled through the fuel temperature ( $T_f$ ), the coolant temperature ( $T_c$ ) and the coolant density ( $\rho_c$ ) feedbacks. These are the variables passed from the TH solver to the N solver. On the other hand, the power distribution predicted by the neutronic solver is passed to the TH solver (Figure 4-1) to compute the TH problem. The spatial mapping implemented between PARCS and SCF for the correct transfer of information will be explained later in this chapter.

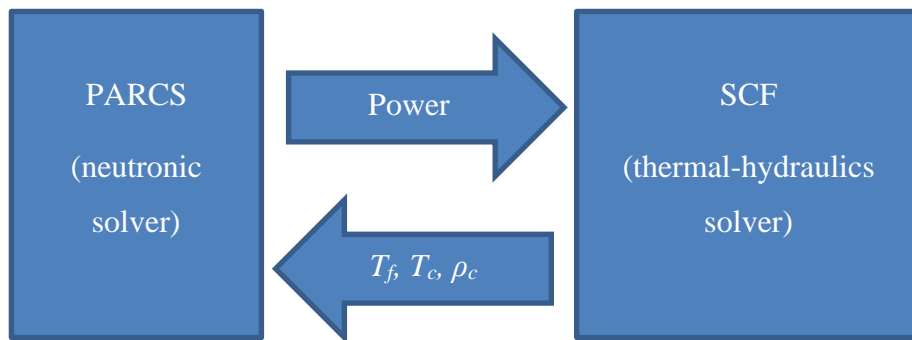


Figure 4-1. 3D node-wise variables exchanged between PARCS and SCF.  $T_f$  is the fuel temperature,  $T_c$  is the coolant temperature, and  $\rho_c$  is the coolant density.

The transient solution is implemented with an explicit coupling scheme (Figure 4-2). This scheme is used on most couplings and is known to be stable for small enough time steps (Mylonakis *et al.*, 2014). The time step advance is controlled by the neutronics code, since the goal of this work is the analysis of fast neutronic transient solutions, as is the case of a REA transient. In transients like the MSLB or the LOCA, where the pressure wave plays a major role, it is the TH code the one controlling the time step. The selection of the time step must be done by the user based on the characteristics of the problem to be solved. PARCS uses a fixed time step, so an analysis of the time step sensitivity must be done to ensure the convergence of the transient solution (Appendix A.2). This is done for every analysed transient problem presented in this work.

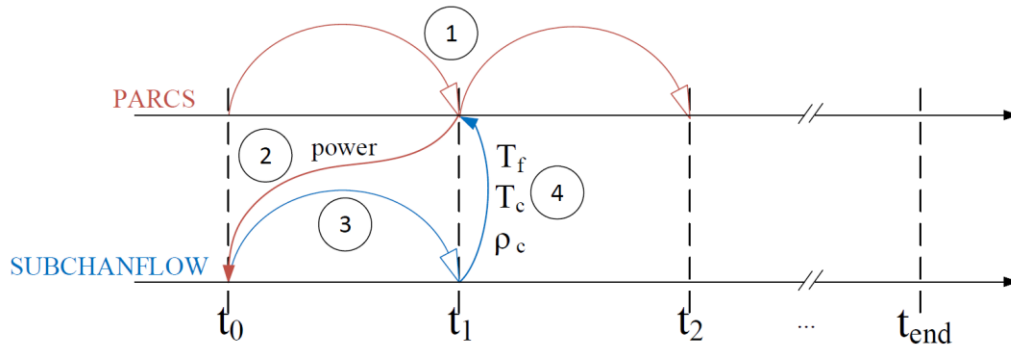


Figure 4-2. Time dependent solution scheme for PARCS-SCF coupling. At the initial time  $t_0$  the solution starts from a converged steady state solution. The transient solution advance first the neutronics until the first time-step  $t_1$ , the solution of the power is used to advance the thermal-hydraulics until  $t_1$ . At  $t_1$  the thermal-hydraulics variables are given as feedback to the neutronics to advance to  $t_2$  and the process continues until the last time step  $t_{end}$  is reached.

In Figure 4-3 the flow scheme for the coupled solution is presented, which is the implementation of the Equation 3-2 and Equation 3-4. First, the inputs of PARCS and SCF are read and a mapping between the neutronics and thermal-hydraulics domains is performed. PARCS and SCF initialize the neutronic and thermal-hydraulics fields by assuming a first guess solution for the thermal hydraulics parameters. Then the steady state iterations begin:

- 1) PARCS computes the node-wise flux and power profile,
- 2) the 3D power is passed to SCF that calculates the TH solution for the given power distribution, SCF internal convergence criteria are checked as usual by SCF. It is assumed that SCF converges, if SCF does not converge then the solution fails and the convergence criteria for SCF should be revised. This should be not an issue for a well-defined problem.
- 3) Then, the neutronics convergence criteria are checked (Equation 2-3). This checks the  $k_{eff}$  convergence, the flux convergence and fuel temperature convergence by comparing the solutions of the current iteration step with the previous iteration step. If the solution is not converged, the cross sections TH parameters are updated in PARCS with the values calculated by SCF and the iteration continues from 1). If the convergence criteria are met the steady state solution is found.

To achieve convergence of the coupled problem all convergence criteria of PARCS (Equation 2-3) and SCF must be met simultaneously. The parameter linking the convergence of both codes in a coupled manner is  $\delta_{Dop\infty}$ . By means of  $\delta_{Dop\infty}$  PARCS checks the change in the 3D temperature distribution calculated by SCF between two consecutive iteration steps,

ensuring that the maximum absolute change is less than a given criteria defined in the PARCS input, typically 0.001 K is used.

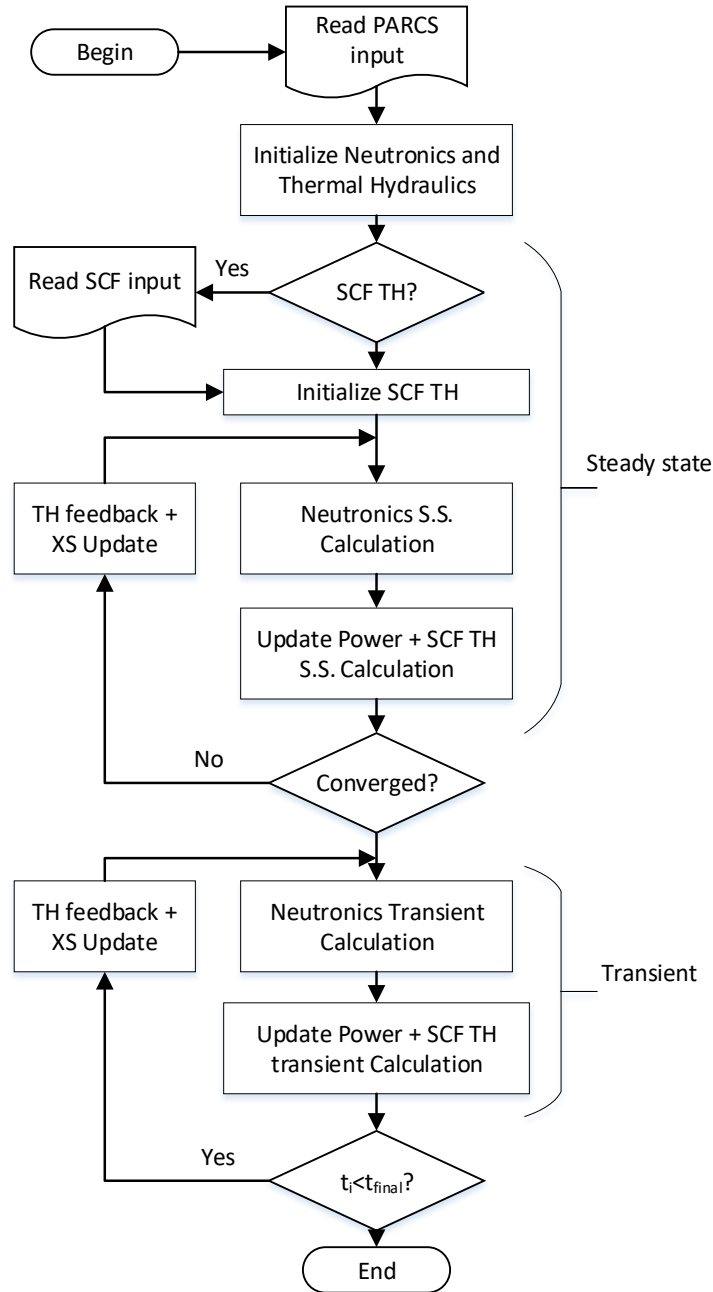


Figure 4-3. PARCS-SCF code flow scheme for the internal coupling.

To solve a transient problem, a converged steady state solution has to be evaluated serving as an initial condition at the beginning of the transient. The transient simulation is based on an explicit scheme where:

- 1) PARCS advances a time step  $\Delta t$  the neutronic solution, the calculated 3D power distribution is passed to SCF,
- 2) SCF advances  $\Delta t$  the TH-solution using the 3D power provided by PARCS Afterwards, the TH parameters are passed back to PARCS,
- 3) if  $t_i < t_{final}$ , PARCS updates the cross sections using the new TH conditions and repeats from 1) advancing a time step solving the transient diffusion equation with precursors. If  $t_i = t_{final}$ , the problem ends.

This scheme corresponds to the explicit operator scheme (Equation 3-4).

#### ***4.2.1 Neutronics thermal- hydraulics spatial mapping***

A flexible radial mapping scheme has been implemented for PARCS-SCF which includes three options for mapping. In all cases the axial nodalization of the active core zone must be the same in the neutronics and thermal-hydraulics model.

The first option is a one to one radial mapping meaning that PARCS and SCF use the same discretization (1 TH channel = 1 N node) and the internal node numbering of PARCS and SCF are the same as indicated in Figure 4-4 a). Each channel in SCF corresponds to one fuel assembly node in PARCS. In this case, a rod centre channel is used in SCF. This is done automatically, and it is the mapping used in the problems in this work.

The second option is a radial mapping where the meshing in PARCS and SCF are the same but the internal numbering of PARCS and SCF are different, see Figure 4-4 b). In this case a list of numbers indicating the node numbering order of SCF indicating the correspondence with the node numbering of PARCS must be given in PARCS' input. This option is very useful when simulating cores with hexagonal fuel assemblies where the internal node numbering of PARCS is not consecutive. This type of mapping has been tested in the simulation of a small modular reactor with hexagonal geometry.

The third option is a flexible mapping which is useful when PARCS and SCF discretization are different, Figure 4-4 c). In this case, a file with information on how the nodes of PARCS and SCF overlap is necessary. This more general is widely used in coupling of PARCS-RELAP or PARCS-TRACE. This is the most versatile way for coupling, an example of this is shown in Figure 4-5, where a 3x3 minicore is represented by nine neutronic nodes (PARCS) and two thermal-hydraulics channels (SCF).

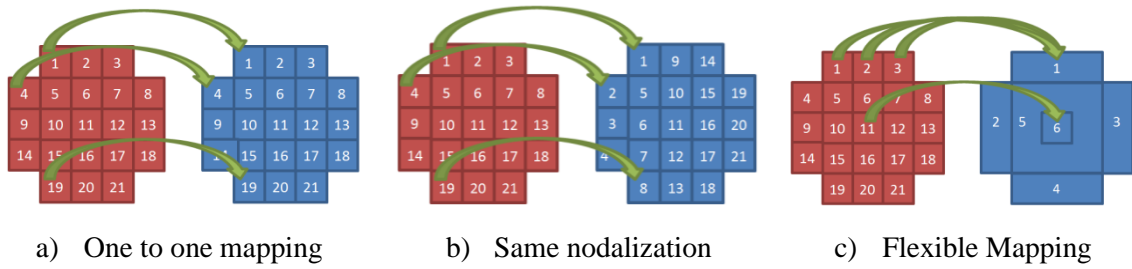
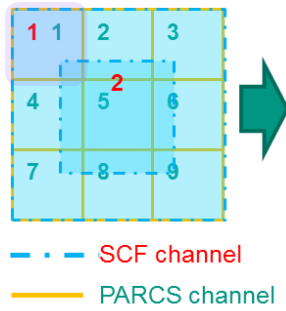


Figure 4-4. PARCS-SCF spatial domain mapping options. a) one to one mapping. b) same nodalization in PARCS and SCF but different node numbering. c) different nodalization on both codes, requires a detailed description of the superimposing areas.



9	2	17	5	2	1.0	9/25	
1	1	8/9	8/56	6	1	6/9	6/56
1	2	1/9	1/25	6	2	3/9	3/25
2	1	6/9	6/56	7	1	8/9	8/56
2	2	3/9	3/25	7	2	1/9	1/25
3	1	8/9	8/56	8	1	6/9	6/56
3	2	1/9	1/25	8	2	3/9	3/25
4	1	6/9	6/56	9	1	8/9	8/56
4	2	3/9	3/25	9	2	1/9	1/25

a) N and TH nodalization.

b) Corresponding input.

Figure 4-5. Example of a flexible mapping. a) domain meshing superposition b) 1<sup>st</sup> row: PARCS node, 2<sup>nd</sup> row: SCF channel, 3<sup>rd</sup> row: ratio of the area of PARCS node covering the SCF channel to the total area of the PARCS node, 4<sup>th</sup> row: ratio of the area of SCF channel covering PARCS node to the total area of the SCF channel.

In the flexible mapping, the weighting of the parameters is done as described by Equation 4-1. In the first two mapping options the weighting parameters are equal to one.

$$X_{PARCS,i} = \sum_j^{j \in i} W_{T-N,j} X_{SCF,j},$$

$$X_{SCF,i} = \sum_j^{j \in i} W_{N-T,j} X_{PARCS,j}.$$

Equation 4-1

Where:

$X_{PARCS}$       parameter sent or received by the neutronics code,

$X_{SCF}$       parameter sent or received by the TH code,

$W_{T-N,j}$	ratio of the area of the $j$ -th TH-channel covering the $i$ -th N-node to the area of the channel, and
$W_{N-T}$	ratio of the area of the $j$ -th N-node covering the $i$ -th TH-channel to the area of the node.

This weighting is correct for the density, power, and fuel temperature but not for the coolant temperature. Given the dependence of the  $c_p$  with the temperature and the different coolant densities in the thermal-hydraulics nodes, the of weighting the temperatures must be done based on the enthalpy (Equation 4-2) and then translated to a temperature:

$$h_{PARCS_{Tc,i}} = \sum_j^{j \in i} W_{T-N,j} h_{SCF_{Tc,j}}, \quad \text{Equation 4-2}$$

$$T_{c,i} = f(h_{Tc,i}).$$

The coolant temperature of a node to be transferred to PARCS is calculated based on the previously computed SCF enthalpy using the Equation 4-2. The flexible mapping methodology has been implemented to be able to have a direct comparison with system codes which usually use this mapping.

### ***4.3 Verification and validation of the coupled code PARCS-SCF***

First, an analysis on a 3x3 PWR minicore and for steady state case to test the coupling implementation and the crossflow impact in the model is presented. Then, a PWR full core transient is presented to show the correct implementation of PARCS-SCF transient capabilities. The verifications presented in this chapter are important to build further into the solution of the safety parameters and the coupling with the thermo-mechanics code. The PWR minicore and PWR benchmark full core are described in Appendix C.1 and C.2.

#### ***4.3.1 Peculiarities of the SCF models development***

For the verification of the developed coupled code, a PWR minicore consisting of 3x3 fuel assemblies and a PWR full core is analysed and the advantages of using a subchannel code for the core thermal hydraulics are discussed.

Special attention is given to the simulation of the cross flow between the fuel assemblies using SCF, where the mixing coefficient which is necessary for the calculation of the turbulent inter subchannel mixing, and the crossflow resistance coefficients which is an axial pressure loss coefficient (e.g. of spacers), are scaled from subchannel to channel level. The turbulent mixing coefficient between two neighbouring subchannels is defined by:

$$Mix_{coef\ subchannel} = \frac{S}{\dot{m}}, \quad \text{Equation 4-3}$$

where  $\dot{m}$  is the average axial mass flow rate in the subchannels that exchange the turbulence and  $S$  is the surface area per unit length through which the eddies flow.

According to the COBRA-FLX methodology developed by AREVA (AREVA, 2010), for a fuel assembly with rectangular arrangement (as used in this work), the turbulent mixing coefficient between two fuel assemblies is inversely proportional to the number of fuel pins in a row:

$$Mix_{coef\ channel} = \frac{Mix_{coef\ subchannel}}{\text{number of pins in a row}}, \quad \text{Equation 4-4}$$

and the crossflow resistance coefficient, for a channel is directly proportional to the number of pins in a rod row:

$$CF_{res\ channel} = CF_{res\ subchannel} \cdot \text{number of pins in a row}. \quad \text{Equation 4-5}$$

### ***4.3.2 Steady state simulation of a 3x3 PWR minicore considering the cross-flow model***

First, for the verification of the coupling, the results obtained with PARCS-SCF are compared to the results of the PARCS standalone that uses a simplified internal parallel channel thermal-hydraulics solver.

Then, to show the advantages of using a subchannel code able to simulate cross flow between the fuel assemblies a comparison of the behaviour of PARCS-SCF modelling of the

crossflow vs. without modelling of the crossflow is presented. The 3x3 PWR minicore description is found in Appendix C.1.

***Comparison of PARCS standalone vs PARCS-SCF simulations without crossflow***

Figure 4-6 shows the axially integrated power distribution, normalized by the mean FA power, for the minicore obtained with PARCS standalone (a) and the relative difference with the results obtained with PARCS-SCF without crossflow. Due to the insertion of the control rod, the power is depressed in the corner and a large power gradient exists between the FA B2 and the FA A1. The nodal power predicted by PARCS-SCF is in good agreement with the ones calculated by PARCS standalone, i.e. they deviate from each other as much as 0.21%. These small differences may originate from the different thermal-hydraulics solvers.

	A	B	C
1	0.35	1.03	0.84
2	1.03	1.54	1.23
3	0.84	1.23	0.9

a) Normalized axially integrated power distribution predicted by PARCS standalone.

	A	B	C
1	0.17	0.03	0.12
2	0.03	-0.21	-0.03
3	0.12	-0.03	0.09

b) Relative power difference (%).

Figure 4-6. Predicted PARCS standalone axially integrated radial power distribution (a) and relative percental differences between PARCS standalone and PARCS-SCF without crossflow (b). The relative difference is calculated as  $\frac{(P_{PARCS-SCF} - P_{PARCS\ standalone}) \cdot 100}{P_{PARCS\ standalone}}\%$

The outlet coolant temperature for PARCS standalone is shown in Figure 4-7 a) as well as the difference between the predicted temperature by PARCS standalone and PARCS-SCF without crossflow Figure 4-7 b).

The predicted heat up is almost identical in both solutions with a maximum difference in the outlet temperature smaller than 0.05K. These results show the correct implementation of the coupling of SCF with PARCS. This verification procedure is a key step to proceed further with the analysis.



	A	B	C
1	296	312	308
2	312	324	317
3	308	317	309

a) Outlet Coolant Temperature (°C) predicted by PARCS standalone.

	A	B	C
1	-0.01	-0.01	0.00
2	-0.01	-0.04	-0.02
3	0.00	-0.02	-0.01

b) Outlet coolant temperature absolute differences (K).

Figure 4-7. Outlet Coolant Temperature (°C) predicted by PARCS standalone (a) and absolute temperature difference between PARCS standalone and PARCS-SCF without crossflow (b). The difference is calculated as  $(T_{PARCS-SCF} - T_{standalone})$ .

### Assessment of the influence of the crossflow in the calculations

To assess the influence of the crossflow, the SCF models used for the coupled simulations consider two cases: a) cross flow activated using a mixing coefficient of 0.0035 as recommend for PWR FA channels (Imke and Sanchez, 2012) and b) deactivated cross flow between the FAs.

The axially integrated power distribution obtained with PARCS-SCF without crossflow is shown in Figure 4-8 a), and the difference when comparing with the case without crossflow in (b). In the previous case, the differences were due to the different TH solvers and steam tables of the codes (SCF uses the revised IAPWS-97 (IAPWS, 2007) tables whereas PARCS has implemented a simplified correlation). In this case the same solver is used in both codes, but in one case the crossflow is considered.

	A	B	C
1	0.35	1.03	0.83
2	1.03	1.58	1.23
3	0.83	1.23	0.89

a) Computed normalized PARCS-SCF power distribution.

	A	B	C
1	-0.37	0.00	-0.28
2	0.00	0.49	0.03
3	-0.28	0.03	-0.29

b) Relative power difference (%).

Figure 4-8. Computed PARCS-SCF without crossflow normalized axially integrated radial power distribution (a) and relative percental differences between PARCS-SCF with and without crossflow (b). The relative difference is calculated as  $\frac{(P_{with CF} - P_{without CF}) \cdot 100}{P_{without CF}}\%$

The difference in the power distribution presents a maximum of ~0.5% in channel B2, this is considerable larger than in the previous case. The reason for the observed differences, is the different coolant temperatures predicted in both cases due to the crossflow influence and thermal mixing. Even though the impact in the power was found not to be large, the coolant temperature is impacted significantly, as will be shown next,

Figure 4-9 shows the outlet coolant temperature distribution for the case of PARCS-SCF without crossflow (a) and the absolute difference with the case with crossflow (b). Differences up to 5.1 K are found in the coolant outlet temperatures, caused by the modelling of the crossflow. The different power releases in the FAs yield a displacement of the fluid from the central channel towards the side channels in form of a pressure driven flow.

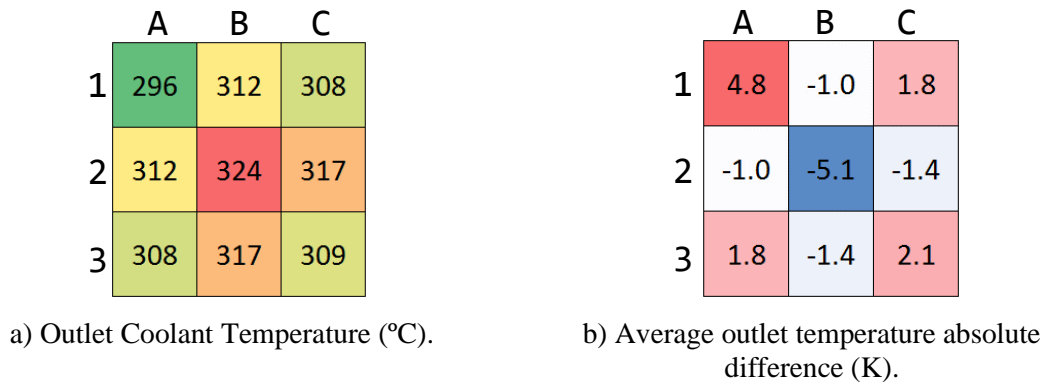


Figure 4-9. Outlet Coolant Temperature (°C) predicted by PARCS-SCF without crossflow (a) and absolute temperature difference between PARCS-SCF with and without crossflow (b). The difference is calculated as  $(T_{with\ CF} - T_{without\ CF})$ .

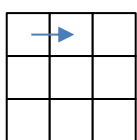
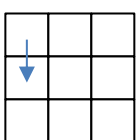
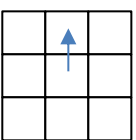
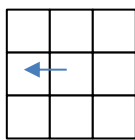
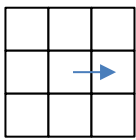
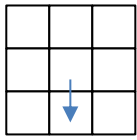
The crossflow in each of the faces of the central (B2) and the top left corner (A1) channel, where the maximum temperature differences occur, are shown in Table 4-1. In the central channel the net crossflow through the faces is leaving the channel, due to the high power in the central channel which causes the coolant to heat up and expand (lower density).

The magnitude of the crossflow is higher on the faces with a larger power gradient (e.g. A1 to B1, A1 to A2, B2 to B1 and B2 to A2). The higher enthalpy coolant leaving channel B2, causes this channel to transfer thermal energy to the neighbours, explaining the predicted lower temperature when compared to a non-crossflow solution.

In channel A1 the net crossflow is entering the channel from the neighbours. The fluid entering comes from the neighbours with higher temperature due to the higher power in the

neighbours, meaning that the corner channel is *gaining* energy from its neighbours through the flow mixing. This is only possible in the model with crossflow, which explains the higher temperature predicted in the corner channel when comparing to a non-crossflow solution. A difference of 5.1 K in the outlet temperature is of considerable magnitude and could only be modelled thanks to the crossflow capability of PARCS-SCF.

Table 4-1. PARCS-SCF with Crossflow model: neighbor pressure driven cross flow (Kg/s/m) as predicted by SCF. The values corresponds to the average crossflow through the face of two neighboring channels. In the header figures, the arrows indicate from which channel to which channel the crossflow goes. The arrows point to the positive direction of the crossflow.

Axial node mid height (cm)						
	A1 to B1	A1 to A2	B2 to B1	B2 to A2	B2 to C2	B2 to B3
356.6 (top)	-7.38E-02	-7.38E-02	5.94E-02	5.94E-02	7.22E-03	7.22E-03
338.3	-1.26E-01	-1.26E-01	9.70E-02	9.70E-02	5.11E-03	5.11E-03
320.0	-1.66E-01	-1.66E-01	1.24E-01	1.24E-01	1.88E-03	1.88E-03
301.8	-1.95E-01	-1.95E-01	1.43E-01	1.43E-01	-2.19E-03	-2.19E-03
283.5	-2.15E-01	-2.15E-01	1.57E-01	1.57E-01	-5.54E-03	-5.54E-03
265.2	-2.29E-01	-2.29E-01	1.68E-01	1.68E-01	-6.75E-03	-6.75E-03
246.9	-2.36E-01	-2.36E-01	1.78E-01	1.78E-01	-5.22E-03	-5.22E-03
228.6	-2.36E-01	-2.36E-01	1.86E-01	1.86E-01	-1.47E-03	-1.47E-03
210.3	-2.31E-01	-2.31E-01	1.90E-01	1.90E-01	3.11E-03	3.11E-03
192.0	-2.19E-01	-2.19E-01	1.89E-01	1.89E-01	7.08E-03	7.08E-03
173.7	-2.01E-01	-2.01E-01	1.81E-01	1.81E-01	9.49E-03	9.49E-03
155.4	-1.80E-01	-1.80E-01	1.67E-01	1.67E-01	1.00E-02	1.00E-02
137.2	-1.56E-01	-1.56E-01	1.49E-01	1.49E-01	8.82E-03	8.82E-03
118.9	-1.30E-01	-1.30E-01	1.28E-01	1.28E-01	6.29E-03	6.29E-03
100.6	-1.04E-01	-1.04E-01	1.05E-01	1.05E-01	2.87E-03	2.87E-03
82.3	-7.82E-02	-7.82E-02	8.19E-02	8.19E-02	-9.98E-04	-9.98E-04
64.0	-5.33E-02	-5.33E-02	5.86E-02	5.86E-02	-5.03E-03	-5.03E-03
45.7	-2.96E-02	-2.96E-02	3.59E-02	3.59E-02	-9.00E-03	-9.00E-03
27.4	-7.51E-03	-7.51E-03	1.47E-02	1.47E-02	-1.28E-02	-1.28E-02
9.1 (bottom)	9.90E-03	9.90E-03	-1.73E-03	-1.73E-03	-1.57E-02	-1.57E-02

The core axial average coolant temperature predicted by PARCS-SCF with and without cross-flow as well as the absolute difference between them is shown in Figure 4-10, where a maximal difference of less than 0.22 K is observed. The difference is calculated as  $(T_{with\ CF} - T_{without\ CF})$ .

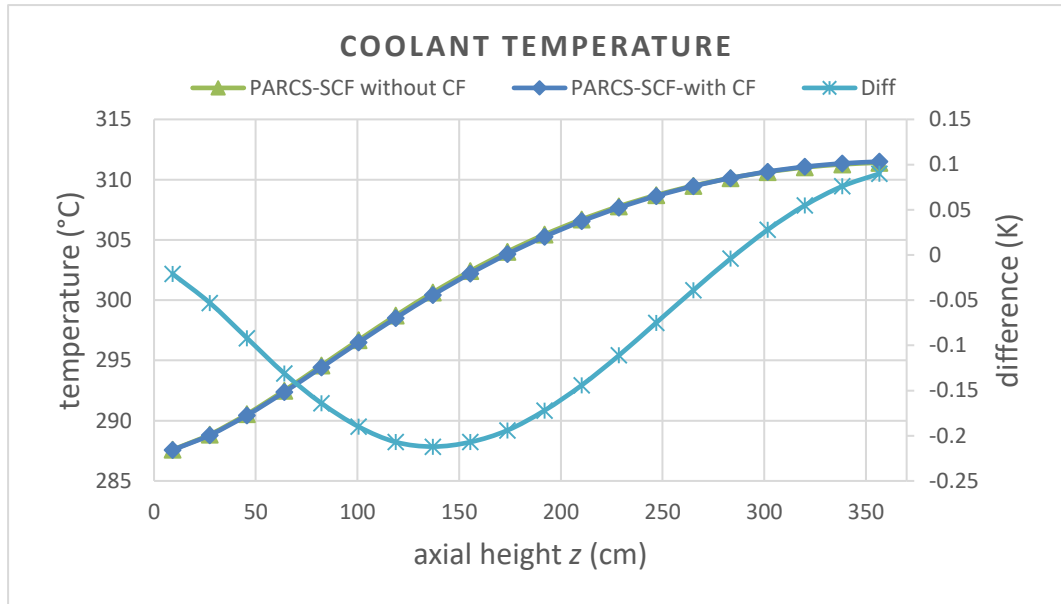


Figure 4-10. Core axial coolant temperature as a function of the active core length predicted by PARCS-SCF without and with cross-flow and the absolute difference between them.

In Figure 4-11 and Figure 4-12 a comparison of the axial coolant temperature of channel A1 (corner) and B2 (central) where the a maximal differences occur (see Figure 4-9) is performed.

The coolant temperature of the central channel (B2) is reduced when cross-flow is considered due to the lateral exchange with the four lower temperature neighbour fuel assemblies. Analogously, the temperature in the corner assembly (A1) is higher for the simulation with cross-flow. This behaviour underlines the importance of the use of subchannel codes for a more realistic description of the thermal-hydraulics phenomena within the reactor core.

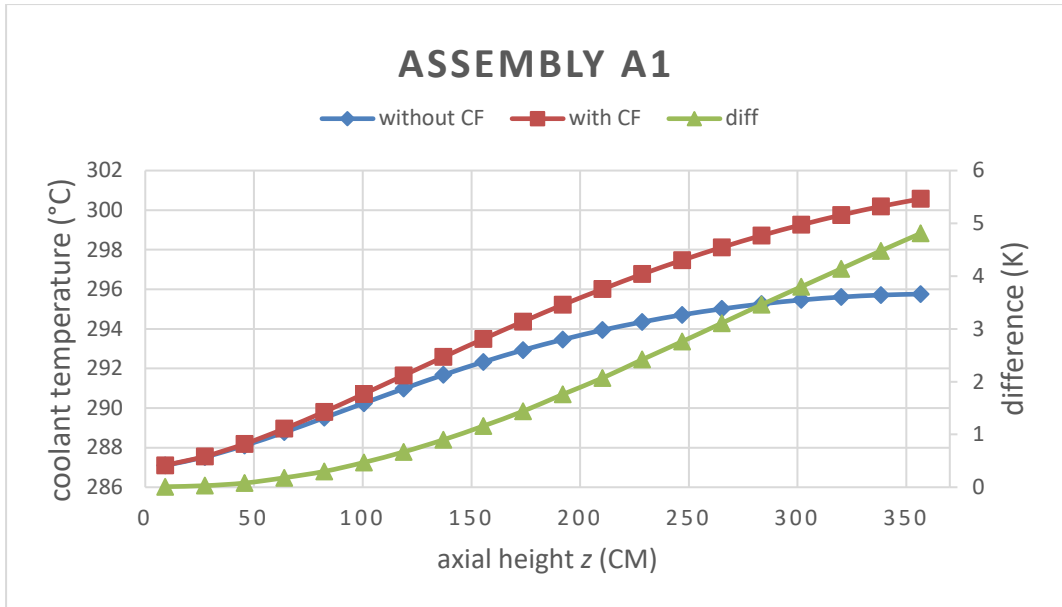


Figure 4-11. Mean axial coolant temperature as a function of the active core length in assembly A1 predicted by PARCS-SCF without and with cross-flow and the absolute difference between them.

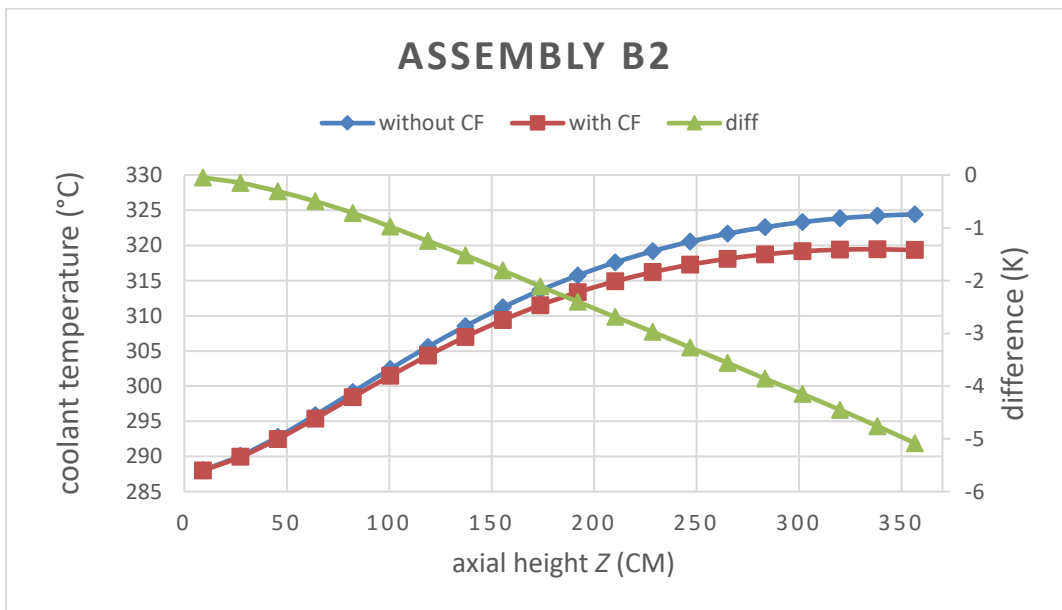


Figure 4-12. Mean axial coolant temperature as a function of the active core length in assembly B2 predicted by PARCS-SCF without and with cross-flow and the absolute difference between them.

Finally, it is worth to mention that using the cross-flow model a multiplication factor of 0.99956 is obtained, while without cross-flow a value of 0.99916 is predicted by PARCS-

SCF meaning a 40 pcm difference higher in the model with cross-flow, showing a small impact in the  $k_{\text{eff}}$ . This is caused by the lower mean coolant temperature in the core, which yields a higher neutron flux, meaning a positive reactivity contribution.

The results obtained with the coupled code and the comparison with the stand-alone one demonstrates the correct code coupling and emphasizes the importance of the simulation of the cross flow thanks to the coupling of PARCS with a subchannel code.

Next a computational benchmark case for PARCS-SCF is presented where the implementation of the transient solution is demonstrated.

### ***4.3.3 Validation using the UO<sub>2</sub>/MOX PWR REA benchmark***

The OECD/NEA U.S. NRC UO<sub>2</sub>/MOX transient benchmark (Kozlowski and Downar, 2007) is used for the validation of PARCS-SCF capability to simulate safety-relevant transients such as a REA. The description of the core and benchmark conditions are in Appendix C.2. Models for the core have been developed for PARCS and SCF using the data provided by the benchmark. Each FA is represented by a radial neutronic node in PARCS and by a TH channel in SCF. As in the minicore case previously presented, the same fuel thermo-physical properties are used in both PARCS-SCF and in the PARCS TH internal model.

### ***Discussion of the results for the REA transient simulation***

The presented REA transient is a response to a control rod ejection at HZP conditions. As explained in Chapter 1.3, these are the conditions where the largest reactivity insertion occur. The power for the HZP condition is defined as  $10^{-4}$  % of the nominal power. The CR with the highest worth (rod L12) is ejected in 0.1 seconds causing a large reactivity injection and a sudden increase of power.

In Figure 4-13, the power evolution predicted with PARCS-SCF and PARCS standalone are shown. The time step used in the solution is 0.001s, and a sensitivity analysis has been done for the timestep selection as explained in Appendix A.2. Both models use the same parameters for the fuel material properties, and gap HTC. The solutions of both cases present a very good agreement, observing a difference in the power peak of less than 2% and the peak occurring at the same time. This shows the correct implementation of the coupling for the transient implementation.

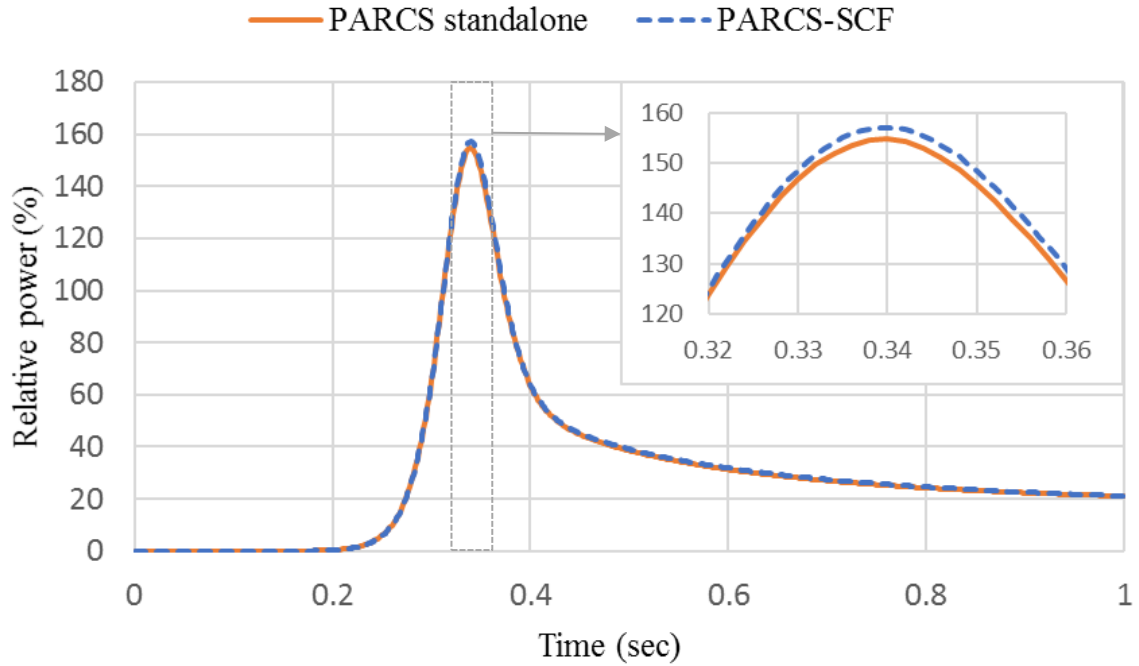


Figure 4-13. Relative power evolution (percent of nominal power) during the RIA transient predicted by PARCS standalone and PARCS-SCF. PARCS-SCF simulation performed using benchmark properties for the fuel material (conductivity) and a fixed HTC of 10000 (W/(m<sup>2</sup>K)).

Is important to notice that a fixed HTC is used in the benchmark conditions for the simulation for all fuel assemblies knowing that they have different burnup. The HTC depends on the irradiation of the fuel and the temperature. The modelling of the material properties and gap HTC by a best estimate code will be presented with the coupling of TU, and the results obtained with the best estimate solutions will be further analysed from a physical point of view in Chapter 6.

#### 4.4 Automatic prediction of local safety parameters using PARCS-SCF

In order to automatically predict the local safety parameters using the Pin Power Reconstruction (PPR) capability of PARCS, the PARCS-SCF coupling has been extended. The automatic calculation is performed by PARCS-SCF according to the scheme shown in Figure 4-14. A major advantage is the fact that it can be done for the full core or for a selected number of fuel assemblies inside the core in which the highest pin power is expected to occur. For example, the fuel assembly where the control rod is ejected, and its neighbour fuel assemblies can be considered for the local safety parameters calculation.

This is essentially a one-way coupling, where the pinwise power distribution is used as boundary condition by the thermal-hydraulic solver. For the pin power reconstruction, the

FA form function parametrized with the fuel temperature and coolant temperature and density are necessary. These values must be given for each type of fuel assembly and for each energy group and are generated in the lattice level calculation along with the cross sections.

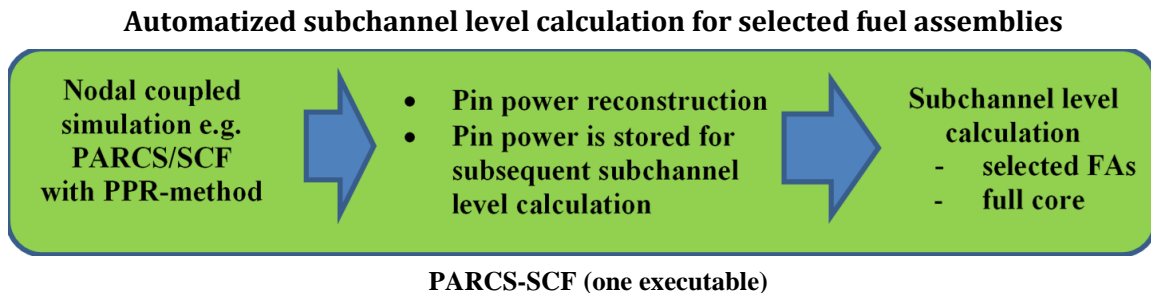


Figure 4-14. Scheme of the automatic PPR + subchannel level calculation. A Nodal level calculation is done, the pin power reconstruction is performed from the nodal calculation, the necessary tables are generated, and subchannel level calculation with pinwise power information is performed to obtain subchannel level information on TH parameters.

#### ***4.4.1 PPR + subchannel level methodology implementation description***

The flow scheme for the subchannel level calculation is shown in Figure 4-15. First, a PARCS-SCF nodal calculation with a pin power reconstruction is performed. The pinwise information for the steady state and transient conditions is stored in memory. After the nodal calculation ends, the pinwise information is used to create a subchannel level model. For it, SCF automatically generates the geometry and local power distribution tables. With the subchannel level model and using the pin power SCF predicts the local safety parameters. For the automatic generation of the tables a pre-processor developed at KIT-INR has been adapted into PARCS-SCF.

The implemented domain mapping is flexible. The fuel assemblies can be solved at channel or subchannel level in a hybrid manner. The logics for the mapping are chosen in the PARCS input via newly introduced key cards. Since the concern of safety analysis is usually focused in the most compromised fuel assemblies, the most recommended discretization is to choose a subchannel mesh for the most compromised FAs and a channel discretization for the surrounding FAs as indicated schematically in Figure 4-16 b).



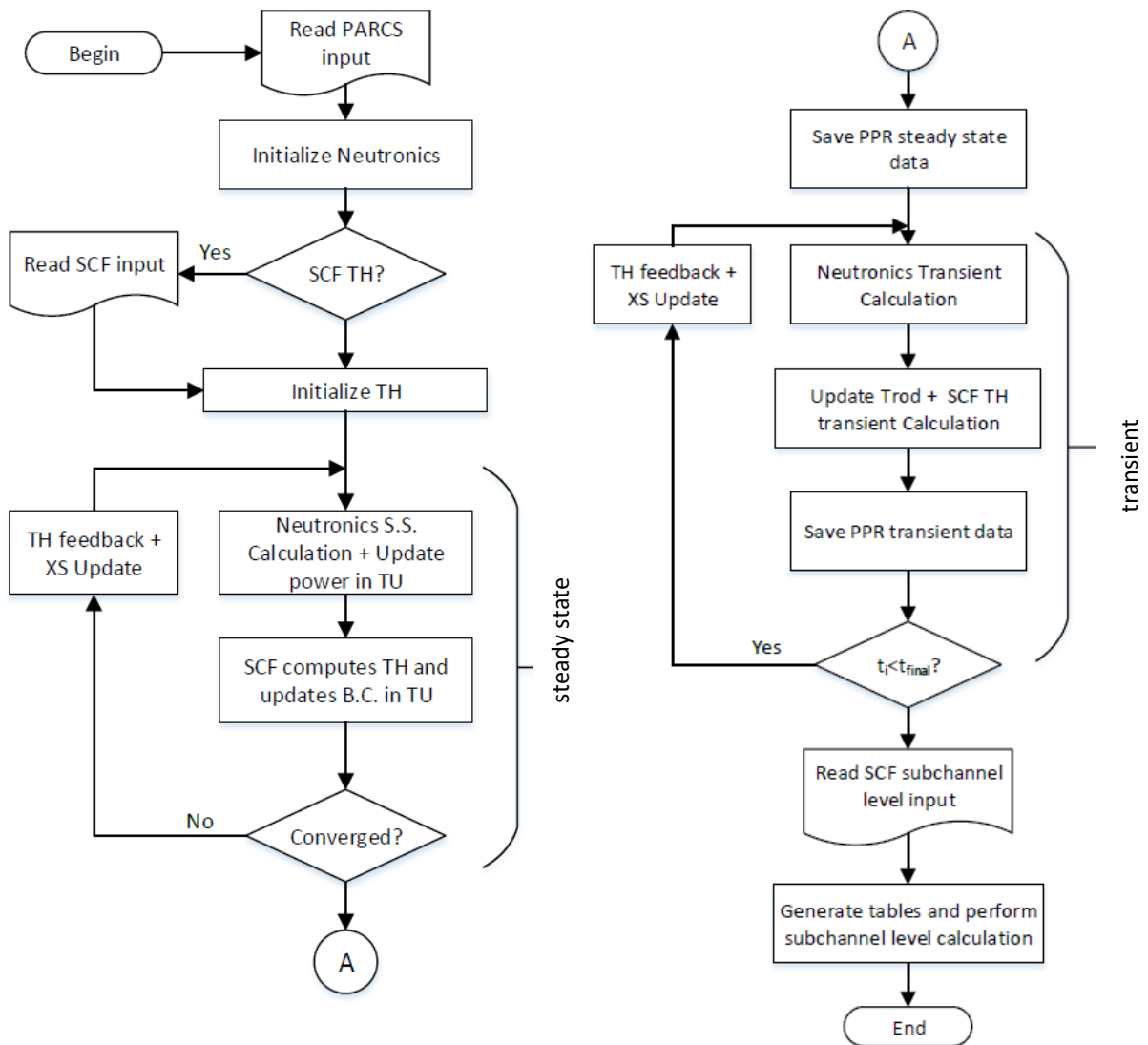


Figure 4-15. PARCS-SCF execution scheme for the steady state (left) and transient (right) calculation of local safety parameters.

The number of surrounding FAs (to the FAs of interest where the subchannel-level simulation will be performed) is chosen by the user. To exemplify this, Figure 4-16 shows different possible discretizations for a 3x3 minicore, examples of the discretization for a nodal solution (a), a hybrid solution (b, c) or a full subchannel solution (d) are shown.

If the most compromised FA is in the centre, a nodalization like Figure 4-16b can be chosen. If the compromised channel is in a corner and a better description of the surrounding channels is required, a nodalization like Figure 4-16c could be used. If the mixing is important the nodalization in Figure 4-16d is most suitable.

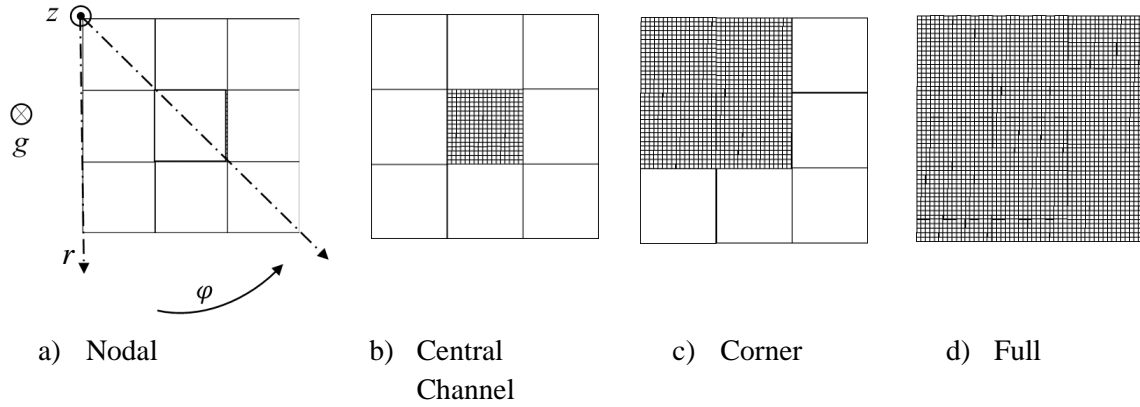


Figure 4-16. Examples of different types of possible nodalization for the PARCS-SCF subchannel-level calculation.

For the subchannel calculation a correct normalization of the power is important. The power for a subchannel of SCF is computed as:

$$P_{SCF}(i_{SCF}, i_{SCF}, k, t) = P_{nom} \cdot P_{level}(t) \cdot P_{PPR}(i_{FA}, j_{FA}, t) \cdot P_{Nodal}(i, j, k, t), \quad \text{Equation 4-6}$$

where,

$P_{SCF}(i_{SCF}, i_{SCF}, k, t)$  is the local pinwise absolute power for SCF for a pin radially positioned at  $(i_{scf}, i_{scf})$ , for the  $k$ -th axial node at time  $t$  [W],

$P_{nom}$  is the nominal power [W],

$P_{level}(t)$  is the power level at time  $t$  ( $0=0\%$ ,  $1=100\%$ ,  $1.5=150\%$ , etc.) [%],

$P_{PPR}(i_{FA}, i_{FA}, t)$  is PARCS' local pinwise relative power for the fuel rod positioned radially at  $(i_{FA}, j_{FA})$ , for the fuel assembly FA at time  $t$  (the FA power is normalized to one), and

$P_{Nodal}(i, j, k, t)$  is PARCS' local relative power for a FA positioned radially at  $(i, j)$ , for the  $k$ -th axial node at a time  $t$ . The total core power is normalized to one.

#### 4.4.2 Verification of the methodology

To verify the implementation and assure the conservation of energy, comparisons between subchannel level calculations and channel level calculations have been performed confirming the correctness of the implementation.

A key aspect of the validation is the assessment of the accuracy of the solver. This is demonstrated next with a comparison against higher order solution results from the Monte Carlo/Subchannel code SERPENT-SCF (Daeubler, Ivanov, *et al.*, 2015). Some extra results for the verification process can be found in Appendix A.1. The verification of the transient implementation can be found in Appendix A.4.

#### Comparison with a higher order solution

A 3x3 PWR minicore is used to assess the accuracy of the PARCS-SCF subchannel level calculations. The used minicore consists of nine UO<sub>2</sub> and MOX fuel assemblies, with an active length of 365.76 cm divided into 20 axial equidistant nodes, the core configuration is shown in Figure 4-17. The boundary conditions are reflective on the sides and black on top and bottom. This minicore has been used in the comparison of SERPENT-SCF with MCNP-SCF (Daeubler, Ivanov, *et al.*, 2015).

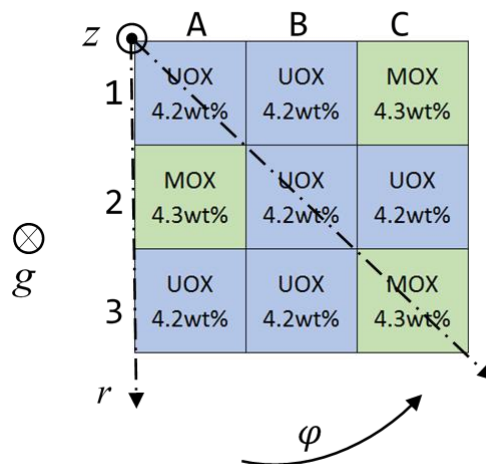


Figure 4-17. Sketch of the 3x3 PWR UO<sub>2</sub>/MOX minicore configuration and its fuel composition. Reflective neutronic boundary conditions are used on the laterals whereas zero incoming current are used top and bottom.

The cross sections and form functions for the calculation were generated with SERPENT-2 using the JEFF library and converted to the PMAXS format using an adapted version of GenPMAXS able to convert SERPENT-2 form functions to the PMAXS format. The range

of variation for the cross section branching to account for the dependence on  $T_f$  and  $T_c$  has been selected based on the range of variation of SERPENT-SCF solution. A description of the XS generation methodology is given in Appendix A.3.

Figure 4-18 shows the results for the pinwise normalized power distribution obtained with PARCS-SCF and the relative normalized differences when compared with the results obtained with SERPENT-SCF. The fuel assembly geometry is shown in Figure C-4 in Appendix C.2.

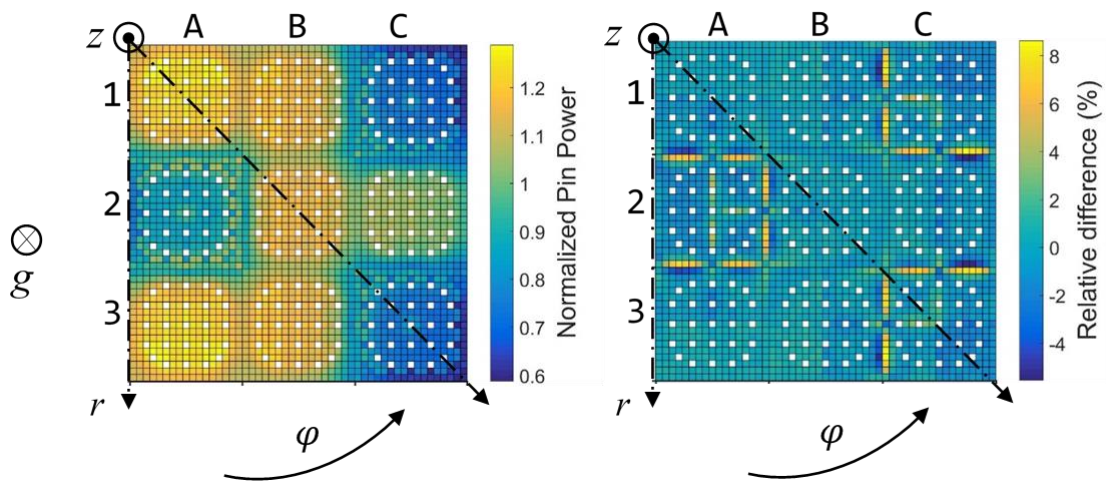


Figure 4-18. PARCS-SCF pinwise normalized power distribution for a 3x3 UO<sub>2</sub>-MOX PWR minicore (left). Pinwise relative power difference between PARCS-SCF vs SERPENT-SCF calculated as  $\frac{SERPENT-SCF-PARCS-SCF}{SERPENT-SCF} \cdot 100$ .

The power distribution is normalized to the average fuel pin power. In most of the pins the differences are within  $\pm 2\%$ . The largest differences are localized in the interface between UO<sub>2</sub> and MOX fuel assemblies. This is a known issue caused by the large flux gradient between the different types of FAs. PARCS solves the diffusion equation using the NEM method which integrates the flux over the node. When large gradients are present, the diffusion equation, which assumes an isotropic behaviour of the flux, loses accuracy. To overcome this problem, discontinuity factors are used (Smith, 1986). However, the solution can only be improved partially. In general, PARCS-SCF PPR presents a good agreement with the higher order solution, and the found differences are within what is found in the literature for PPR compared against higher order solutions (Hursin, Downar and Kochunas, 2010; Liponi, Taforeau and Hébert, 2017)

In Figure 4-19 the coolant outlet temperature distributed calculated with PARCS-SCF subchannel level and a comparison with the distribution calculated with SERPENT-SCF are presented. The major differences are in the interfaces of the fuel assemblies, where the maximum pin power differences are located. The calculated core heat up is 44.7 K in both cases and the maximum subchannel difference in the outlet coolant temperature is 1.4K which is ~3% of the heat up. The absolute average difference calculated as

$$d = \frac{1}{n} \sum_{i=1}^n |T_{PARCS-SCF,i} - T_{SERPENT-SCF,i}|, \quad \text{Equation 4-7}$$

with  $n$  the total number of subchannels, is 0.22 K, showing a good agreement of the solutions.

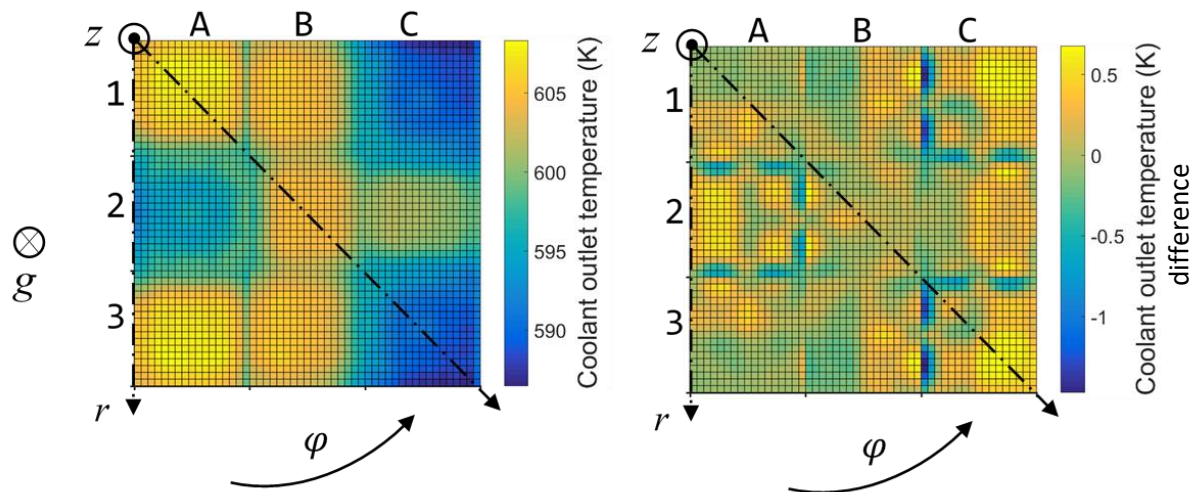


Figure 4-19. PARCS-SCF pinwise coolant outlet temperature distribution for a 3x3 UO<sub>2</sub>-MOX PWR minicore (left). Outlet coolant temperature difference between PARCS-SCF vs SERPENT-SCF  $PARCS - SCF - SERPENT - SCF$  (K) (right). The average outlet temperature difference is 0.22 K and the maximum absolute difference is 1.4K showing a good agreement between the solutions.

The maximum coolant temperature is located in the fuel assembly A3. In Figure 4-20 the axial average coolant temperature for subchannel-level and channel-level calculated with PARCS-SCF, are shown for channel A3. The result labelled 'subchannel avg', corresponds to the averaged coolant temperature calculated from the subchannel solution using the enthalpies. Its value overlaps with the nodal solution showing the correct energy balance. The average outlet coolant temperature is 604.7 K. In channel A3 the hottest subchannel outlet coolant temperature is 608.27 K, and the lowest subchannel outlet coolant temperature is

596.74 K. A difference of 11.5 K exists between the lowest and the higher coolant temperature in channel A3.

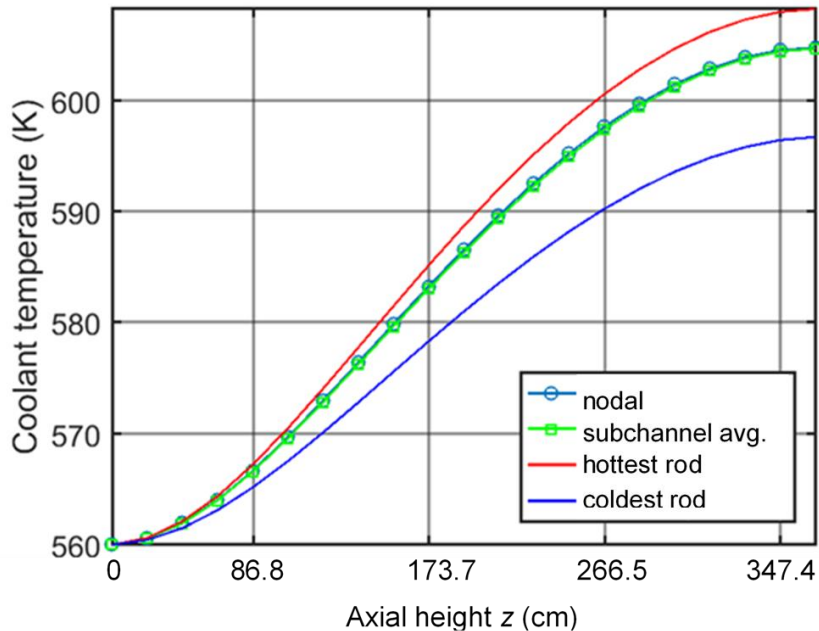


Figure 4-20. Computed axial coolant temperature (K) for the hottest subchannel, coolest subchannel, the nodal and bundle average solution for channel A3, and the nodal solution for the channel A3. The subchannel average corresponds to the average coolant temperature of channel A3 calculated with the enthalpies.

Figure 4-21 shows the predicted local and nodal average cladding temperatures. There is a large difference between the hottest and coldest cladding temperatures, amounting to 24K in the central location.

For SERPENT-SCF the found  $k_{\text{eff}}$  is 1.22197 and for PARCS-SCF 1.22121 finding a difference of 60 pcm which is a very good agreement.

Since one of the main goals of this methodology is the extraction of local safety parameters a comparison for the solutions for the MDNB is presented in Table 4-2, where a comparison with the values obtained at nodal level is also presented. The W-3 correlation (Tong, 1967) for DNB has been used in all cases. The subchannel level solutions of both PARCS-SCF and SERPENT-SCF present a considerably lower MDNB with respect to the nodal solution. This is due to the local resolution of the pin powers, which present higher local heat fluxes leading to a lower MDNB.

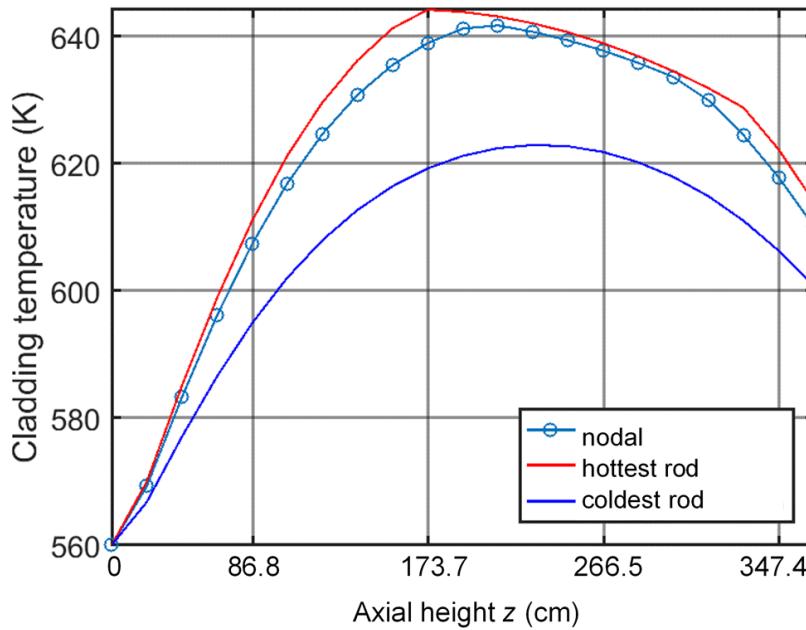


Figure 4-21. Axial cladding temperature for the hottest rod and the coldest rod in channel A3, and nodal value for channel A3).

Table 4-2. MDNB value and location for the nodal, hybrid and full subchannel solutions (see Figure C-2 in Appendix for pin position reference).

	Nodalization		
	Nodal PARCS-SCF	Subchannel PARCS-SCF	Subchannel SERPENT-SCF
rod position, (channel)	(A1)	E14, (A3)	E14, (A3)
mid axial height of node from bottom (cm)	209.9	173.4	194.6
MDNB	3.161	2.552	2.538

For the channel level solution, the MDNB is in channel A1, whereas for the subchannel level solutions of PARCS-SCF and SERPENT-SCF is in the symmetrical channel A3. In the subchannel level solutions the MDNB occurs at the local position at the pin E14 of the channel A3 for both subchannel level solutions of PARCS-SCF and SERPENT-SCF, although axially it occurs with one node of difference. The agreement in the MDNB for PARCS-SCF and the higher order solution SERPENT-SCF is very good, with a total difference of 0.5%.

The good agreement in the solutions highlights the accuracy of the PARCS-SCF subchannel level methodology. The computational running times required for the SERPENT-SCF solution is 29 hours and 2 minutes using 24 threads, equivalent to 587 CPU hours and for



PARCS-SCF, 2 minutes and 7 seconds in a single CPU which is considerably lower, making the methodology suitable for industrial requirements.

## ***Chapter summary***

The implementation of PARCS-SCF has been developed and verified showing a correct implementation of the coupling by performing code to code comparisons. The cross-flow capability of SCF has been demonstrated on a minicore coupled calculation showing the effect of considering the crossflow in the solution. The configuration for the calculation was set to present a large power gradient between the central and the corner channel causing a significant crossflow, which led to an outlet coolant temperature difference of 5.1 K between the models.

An automatic subchannel level calculation for the extraction of local safety parameters has been implemented in PARCS-SCF. The capability has been tested showing the conservation of energy and the prediction of pin-level parameters. To check the accuracy of the methodology, PARCS-SCF solution has been contrasted with a higher order solution showing a good agreement also for the calculation of the MDNB, a safety relevant parameter. Moreover, the computational time required by the PARCS-SCF methodology is considerably lower than for the higher order solution.



## ***5 Coupling of a Neutronics Core Simulator with a Subchannel Thermal-Hydraulics and a Fuel Thermo-Mechanics Code***

### ***5.1 Introduction***

The inclusion of a fuel performance (thermo-mechanics) solver such as TRANSURANUS (TU) within the coupled neutronics/thermal-hydraulics code PARCS-SCF is necessary for an accurate simulation of the reactor core at operation conditions. The capability of TU to predict complex thermo-mechanics phenomena occurring in the fuel allows a realistic fuel rod modelling, taking into account the changes of the thermo-physical properties with the temperature, burn-up, pressure, etc.

The consideration of such phenomena in the simulations directly affect the prediction of important feedback parameters such as the fuel rod temperature and the gap heat conductance, as it is shown in this and the next chapter.

TU has been added as a module to the PARCS-SCF coupling in a similar way that SCF was added to PARCS.

### ***5.2 Coupling parameters and methodology***

In the neutronics, thermal-hydraulics and fuel thermo-mechanics coupling, the role of the fuel thermo-mechanics code is the prediction of the fuel temperature distribution in the fuel rod, considering the changes in the fuel rod dimensions and material composition due to irradiation in the core. For TU to be able to compute this parameter, boundary conditions such as the linear heat rate calculated by PARCS, plus the pressure, the clad-to-coolant heat transfer coefficient and coolant temperature calculated by SCF must be provided.

Figure 5-1 shows a scheme of how the codes are linked together. As shown here, TU replaces the fuel rod temperature solver of SCF. TU and SCF are coupled through the clad outer surface temperature calculated by TU and the coolant conditions (clad-to-coolant HTC, pressure, and coolant temperature) calculated by SCF. In contrast to the PARCS-SCF coupling, the power (energy deposited in the fuel and coolant) is not transferred directly from PARCS to SCF, but it is transferred from PARCS to TU. Then, SCF uses the clad outer surface temperature calculated by TU to compute the heat transferred to the coolant (Equation

2-12). Both, SCF and TU can solve the heat conduction equation (Equation 2-11, Equation 2-14) for the fuel rod, the difference between them is that TU has better models and correlations which are dependent on the irradiation and fuel history, thus, predicting a more accurate temperature distribution within the fuel rod.

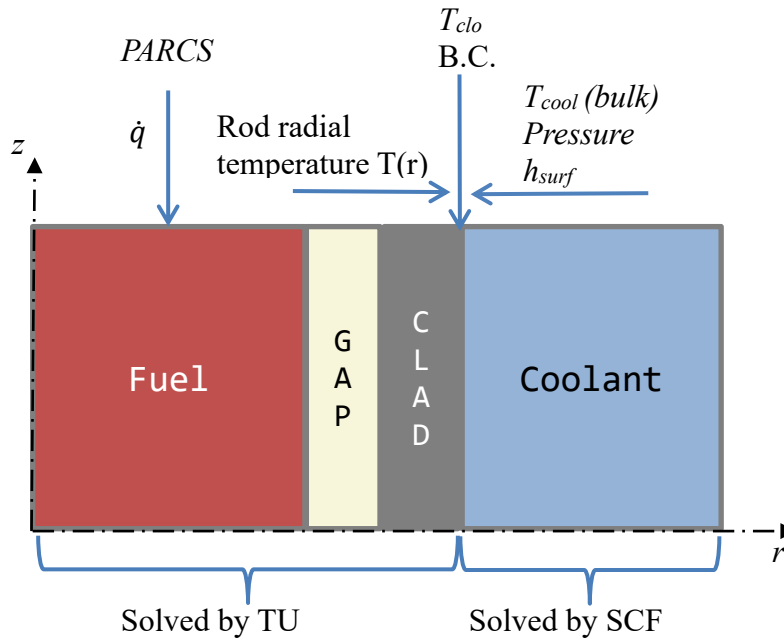


Figure 5-1. The clad outer surface is the thermal boundary between TU and SCF. TU uses the power provided by PARCS ( $\dot{q}$ ) and the parameters provided by SCF ( $T_{cool}$ , pressure,  $h_{surf}$ ) to find the temperature distribution in the fuel rod. Then, the clad outer temperature is used by SCF to find the solution for the thermal-hydraulics.

Whereas both PARCS and SCF are designed to solve a full reactor core, TU can only solve one fuel rod (in our case an average fuel rod) at a time. To be able to solve a full core with the coupled PARCS-SCF-TU, the information for all the fuel assemblies must be made available on memory simultaneously for the neutronics and thermal-hydraulics and thermo-mechanics solvers. To achieve this, a parallel coupling approach has been developed based on MPI (Message Passage Interface) libraries.

### ***5.2.1 MPI parallel implementation***

Using a parallel programming approach, all the fuel assemblies can be resolved simultaneously with TU. Each fuel assembly is represented by an average fuel rod in the TU model. Adopting this approach, a full PWR core model consists of, e.g., 193 representative fuel rods and needs the same number of TU-calculations to be performed simultaneously.

A *master* process handles the distribution and collection of data to/from all other processes and synchronizes them. A scheme showing how this approach works is exhibited in Figure 5-2. When the program is executed, it launches  $N+1$  processes, where  $N$  is the number of fuel assemblies in the core. The main process (master) is identified with a task identification number equal to zero ( $taskID=0$ ) as used per convention in MPI.

The processes  $1$  to  $N$  correspond to TU processes, each one linked to one fuel assembly through a one-to-one mapping. These processes receive the boundary conditions for the average fuel rod from PARCS and SCF and then compute the temperature distribution and send it back to PARCS and SCF. Each process must ‘know’ when to send and receive information, and the stage of the calculation flow, e.g. if an inner loop iteration is converged or not before moving forward to an external loop.

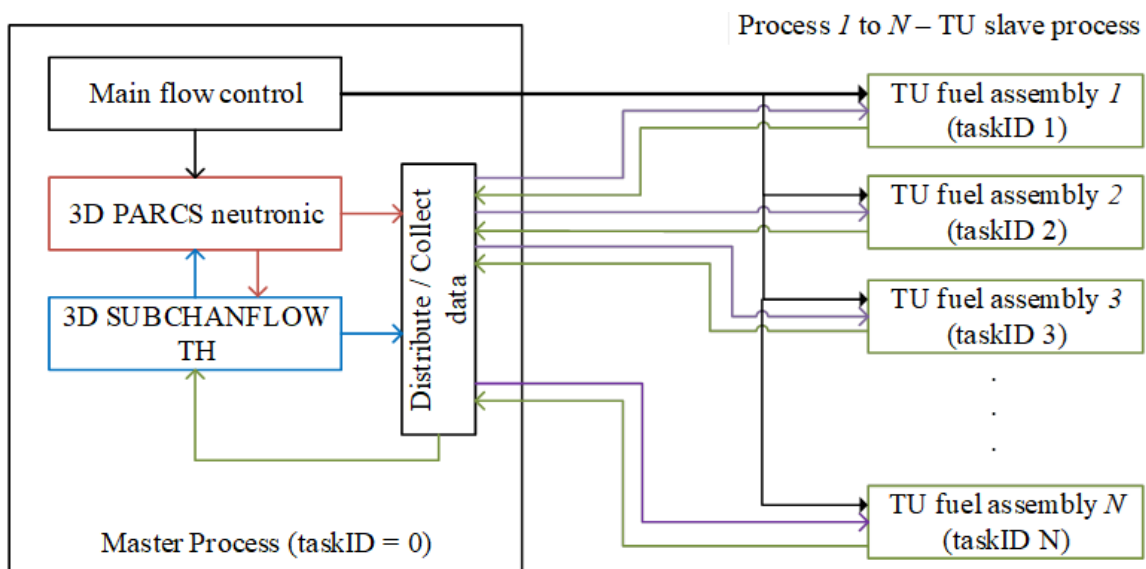


Figure 5-2. MPI coupling scheme. A master process containing PARCS and SCF distributes and collects the data between the master and slave processes and set flags to synchronize them. A total number of  $N+1$  processes are launched in a simulation ( $N =$  number of FAs in the reactor core).

A synchronization of the simulation is important for the correct execution. Information transferred in the incorrect moment leads to a failure in the overall simulation. A correct execution is achieved having the master process setting flags which inform each process of the stage on the global simulation. Barriers are used to hold a process on standby at a given flow point until it is allowed to advance forward to the next iteration step or time step. The

time advancement scheme for the transient coupled simulation is shown in Figure 5-3. It corresponds to an explicit scheme, as it is in the case of PARCS-SCF.

The transient simulation begins from the converged PARCS-SCF-TU steady state solution. First, the neutronics solver advances from  $t_0$  to  $t_1$  using the TH conditions of the converged steady state solution to predict the power at time  $t_1$  (1). The calculated power is given from PARCS to TU along with the TH conditions of the converged SCF steady state solution (2). Then, the TU solver advances from  $t_0$  to  $t_1$  to predict the new fuel rod temperature at  $t_1$  (3). Finally, the new fuel rod temperatures are passed to SCF (4), which uses the clad outer temperature to calculate the heat flux and uses it to advance the TH-problem predicting the TH-parameters at time  $t_1$  (5). This is the end of one timestep and at this point the new TH conditions, e.g. the fuel and coolant temperature and coolant density, are transferred to PARCS (6) which uses them to update the nodal cross-sections before solving the neutron diffusion equation for the new time step  $t_2$  (7).

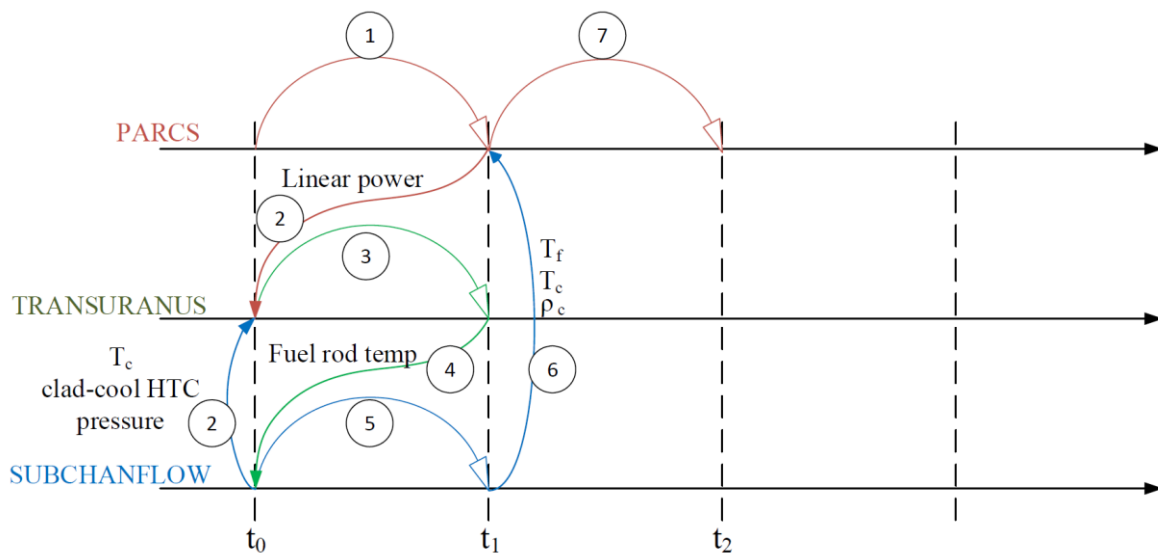


Figure 5-3. Time dependent PARCS-SCF-TU time step advancement, explicit coupling scheme.

If necessary, TU can automatically use smaller time steps to achieve convergence. However, the information exchange is conducted only at the time step interval set by the master process. All the processes must advance simultaneously, and each time step must finish for all processes before advancing to the next one. This is achieved by setting barriers, which are freed when all other processes reach the time step and the information is transferred.

Figure 5-4 shows how a barrier works. On each time step, each TU process (*Task1* to *Task193*) advance its solution, e.g. *Task1*, and then remains on stand-by until all other processes, *Task2* to *Task193*, reach the same predefined point. At this point, the information from all tasks, i.e. fuel assemblies' temperatures distribution, is transferred back to SCF, which can advance its solution and send the TH-feedback to PARCS to advance to the next time step. When this happens, the TU processes receives the information for the next time step and can continue the simulation.

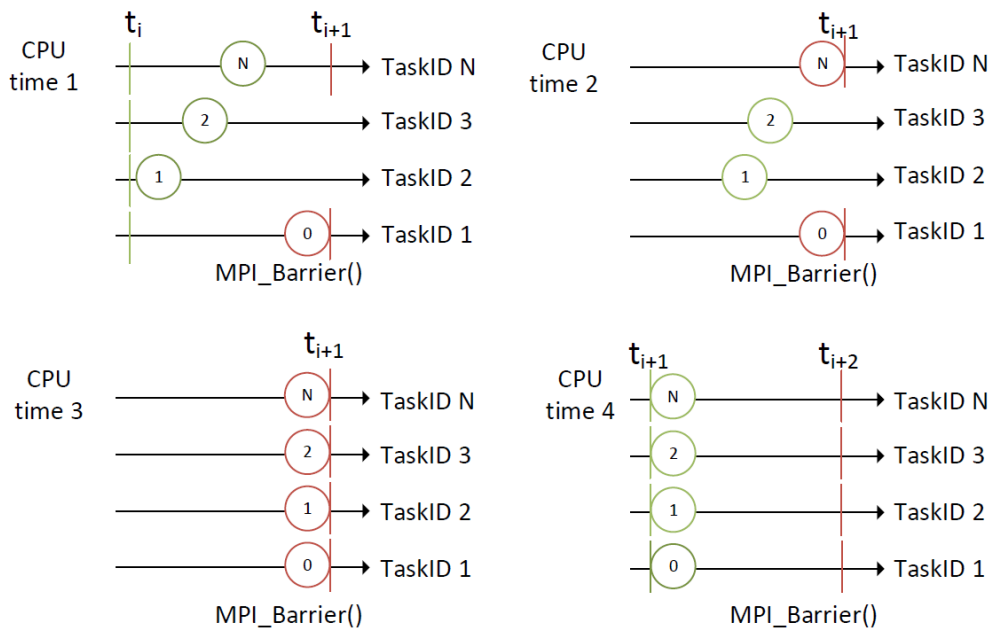


Figure 5-4. Example of how an MPI barrier works. The barrier defines a point that all the processes must reach to continue the execution. When all the processes reach a certain time and share the solutions among them, the barrier is lifted and the processes advance to the next time step. At CPU time 1 only the task 0 reached the solution point at  $t_{i+1}$  and it is put on stand by with the MPI barrier, at CPU time 2, e.g. task N reached the time  $t_{i+1}$  and is put on stand by too, at CPU time 3 all the tasks reached the time  $t_{i+1}$  and the barrier is released and finally at CPU time 4 all the processes start the calculation for the new time step  $t_{i+2}$ .

### 5.2.2 Coupling scheme flowchart

A scheme of the steady state simulation flow is presented in Figure 5-5. The code begins by reading the PARCS input, in which the simulation parameters are given as well as the mapping information for SCF and TU with PARCS. Then, SCF and TU inputs (e.g. 193 input files) are read and the codes are initialized.

The flowchart differs from the one of PARCS-SCF in how the feedback parameters are transferred. In this case, the power is now given from PARCS to TU, and TU replaces the

fuel rod solver of SCF. Because of this, there is an inner iteration between SCF and TU to find a converged solution for the TH parameters. In this inner iteration the cladding temperature must be such that the deposited power in the coolant equals the power generated by PARCS in the steady state case.

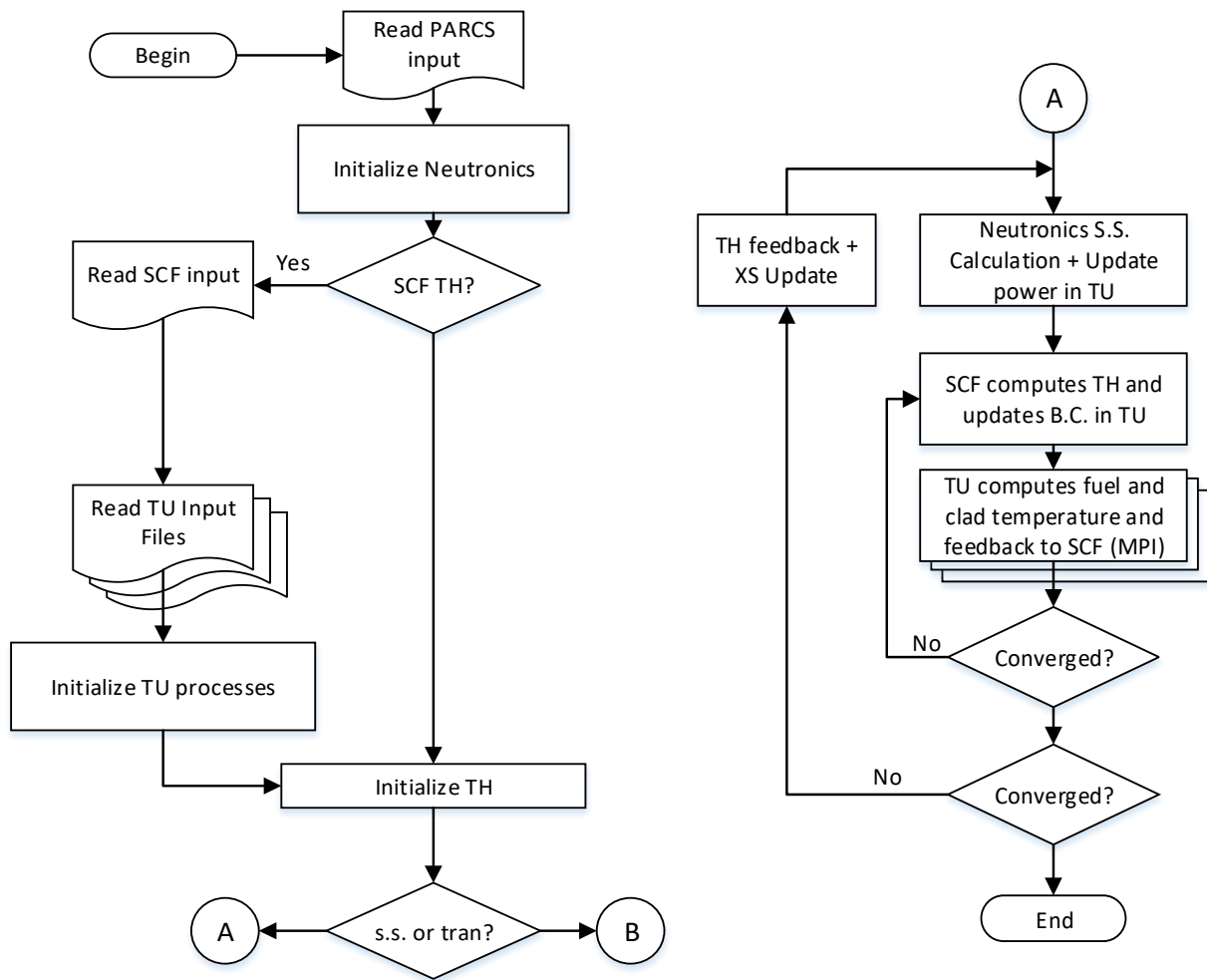


Figure 5-5 PARCS-SCF-TU coupling flow scheme for initialization (left), and steady state simulation (right).

In principle, for the steady state case the power calculated by PARCS can be passed directly from PARCS to SCF and no iteration between TU and SCF is needed. This scheme is for instance being used in the coupling of SERPENT-SCF-TU currently being performed within the European McSAFE Project. However, such scheme is not useful in the case of a transient problem where not all of the generated power is immediately deposited in the coolant, but some energy is stored in the fuel. For the transient case the coupling through the clad temperature is mandatory.

The convergence between SCF and TU is tested by the coolant temperature, which is directly linked to the clad temperature via the following relation (see Equation 2-12):

$$T_{cool} = T_{clo} - \frac{q''}{h_{surf}}. \quad \text{Equation 5-1}$$

The convergence criterion for the SCF-TU nested loop is:

$$\delta_{Tc} = \max \left| \frac{T_{c_{n+1}}^m - T_{c_n}^m}{T_{c_{n+1}}^m} \right| < \varepsilon. \quad \text{Equation 5-2}$$

Where,  $T_{c_n}^m$  is the local mean coolant temperature at the  $n^{th}$  iteration at the  $m^{th}$  node. This means that the maximum allowed variation between two successive TU and SCF iterations in any node (e.g. 193 FA x 20 axial nodes = 3860 nodes) does not exceed a prescribed given value ( $\varepsilon$ ), typically set to 0.001 K.

When the iteration between SCF and TU ends, another iteration loop starts for PARCS and SCF-TU (see Figure 5-5 right). The convergence criteria for PARCS are checked as described in the previous chapter (in this case the fuel temperature is calculated by TU). If the solution is not converged, the TH variables are transferred back to PARCS, the cross sections are updated with the new TH values, and PARCS solves again the time dependent diffusion equation and a new iteration step continues.

In Figure 5-6 the flow for the transient coupling scheme is shown. After the initialization (see Figure 5-5), the first part is a steady state calculation. When the steady state is converged, the solution continues with the transient. This is simply an extended implementation of the algorithm in Equation 3-4 and described in Figure 5-3.

An important remark is that the large overhead present in the steady state simulation needed for the inner iteration between SCF and TU, and for the TU files reading at each SCF-TU-iteration, is eliminated in the transient part of the solution, leading to a reduced computational time. This is because, in the transient part, all TU processes run in parallel from  $t_0$  to  $t_{end}$  and the boundary conditions are updated in each time step without reinitializing the calculation.

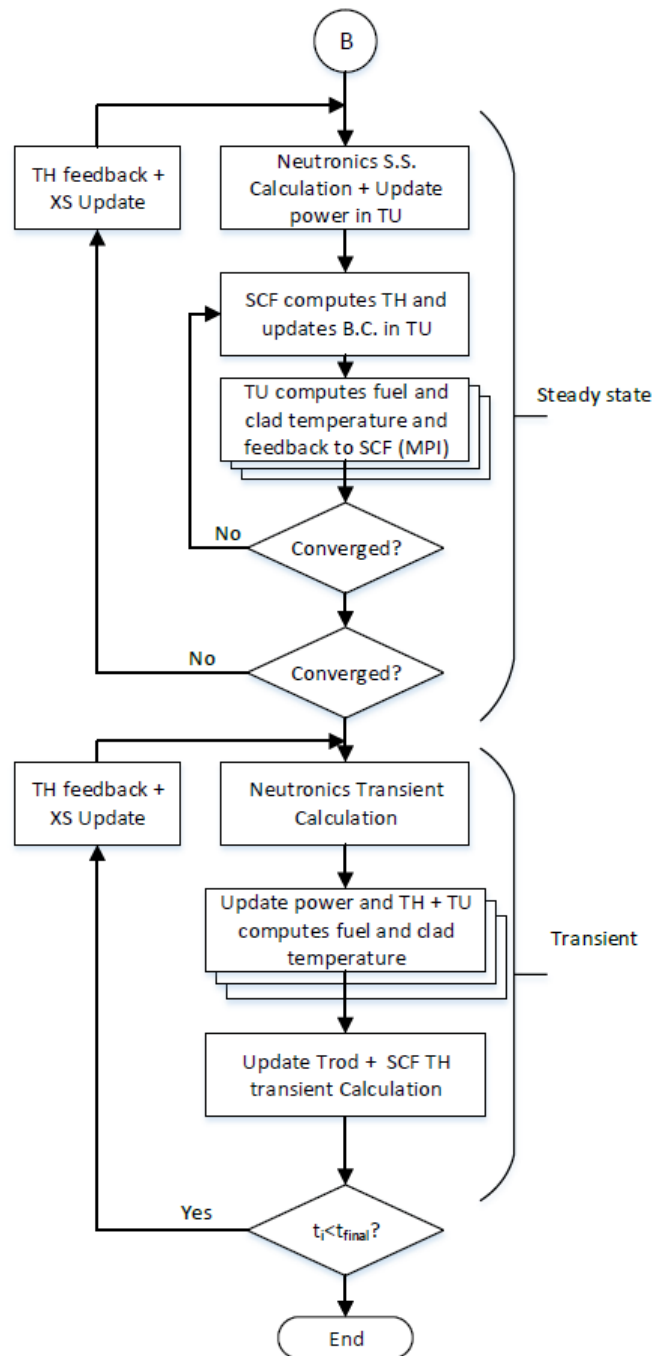


Figure 5-6. PARCS-SCF-TU coupling flow scheme for transient simulation.

### ***5.2.3 Restart capability for TRANSURANUS Pre-Irradiated models and core simulation***

One of the main goals of this thesis is the simulation of pre-irradiated fuel. To achieve this, the irradiation history of each fuel assembly must be considered in order to predict the fuel assembly properties corresponding to the actual reactor operation conditions. This is very



important in the simulation, because as shown in Subchapter 2.4.2 the thermo-mechanical properties of a fuel pin greatly depend on the fuel irradiation. For this purpose, a precomputation of the whole irradiation history of a fuel assembly must be carried out *a priori* with TU standalone code.

In the coupled N/TH/TM calculations, all the information about each fuel assembly along with the irradiation history is needed. Hence, the restart capability of TU is required in the coupled calculation. For this purpose, the TU source code has been modified. Additional modifications are necessary to make sure that a thermal equilibrium is achieved before starting the transient problem. This means that in the initialization of the calculation (in the steady state part of the problem), TRANSURANUS runs for a fixed time keeping the thermal hydraulics B.C. constant, to ensure that a thermal equilibrium is achieved. This is necessary because the TH condition of the last point of the restart are not the same as the ones at the start of the simulation, which cannot be known *a priori*. Exploring studies have shown that 2000 seconds is enough to achieve this equilibrium.

One restart calculation file must be given for each fuel assembly, each file containing the history of the fuel assembly. This implies the generation of large amounts of input information, which needs to be consistently prepared and organized for the simulation. Because the correctness of the simulation depends on this step of the process, a script has been developed to automatically prepare and organize the data. The script written in MATLAB prepares the TU input for each of the FA, e.g. 193 input cases and a script to run all the cases and organize the output files automatically. Each input case contains information about the fuel type and burnup information. This will be presented in Chapter 6 where the simulation of the benchmark is discussed.

### ***5.3 Verification of the multiphysics tool***

The OECD/NEA U.S. NRC UO<sub>2</sub>/MOX transient benchmark described in Appendix C.2 is used for the verification of the new coupled code PARCS-SCF-TU. The verification of the implementation is a necessary step in the validation process. It demonstrates the correct implementation of the coupling by comparing e.g. with the solution of another already verified code, in this case PARCS-SCF. In this code-to-code comparison, similar numerical models, boundary and initial condition are used. In particular, in TU the gap heat transfer coefficient is predicted by the URGAP model (Lassmann and Hohlefeld, 1987). In SCF also this URGAP

model is implemented for fresh fuel conditions and is used in this comparison. The URGAP model requires the input of the gap width, which depends on many factors, like densification, cracking, relocation, and burnup among others. These parameters are calculated in different ways in SCF and in TU and thus, it is expected that even when both codes use the same URGAP model the solution will not be identical. To reduce the sources for differences, a fresh core is considered for the verification purpose.

### ***5.3.1 Steady state simulation of a PWR fresh core***

#### ***Short description of the benchmark conditions***

As described in Appendix C.2, the core consists of fuel assemblies with a 17x17 geometry containing 264 fuel pins and 25 guide tube positions (Figure C-4). There are 2 types of FAs each with 2 different enrichments. In the coupling each fuel assembly is represented by an average fuel pin. The most representative pin in the fuel assembly is used as the average fuel pin in TU. In Table 5-1 the material composition of the most representative fuel pins of the core loading under investigation are shown.

Table 5-1. Benchmark fuel assembly types and most representative pin for each case according to (Kozlowski and Downar, 2007).

<b>Fuel Assembly Type and enrichment</b>	<b>Most representative fuel pin</b>
UO <sub>2</sub> 4.2%	235U: 4.2 wt. %, 238U: 95.8 wt. %
UO <sub>2</sub> 4.5%	235U: 4.5 wt. %, 238U: 95.5 wt. %
MOX 4.0%	4.5 wt.% Pu-fissile; vector: 234/235/236/238 = 0.002/0.2/0.001/99.797 wt.%
MOX 4.3%	5.0 wt.% Pu-fissile; vector: 239/240/241/242 = 93.6/5.9/0.4/0.1 wt.%

Figure 5-7 shows the sketch of a fuel rod and its main components. Information on the design of the fuel rod such as the upper plenum volume and dish geometry, necessary to compute the total free volume, plus the fill gas pressure, surface roughness for the clad and fuel, etc., must be provided to the fuel thermo-mechanics code.

The data of the fuel pins model is not fully given in the benchmark specifications and has been completed from fuel vendor data sheets and reports on fuel thermo-mechanics models (O'Donnell, Scott and Meyer, 2001) to properly model the fuel pin. The most relevant fuel rod data is summarized in Table 5-2, a complete list is given in Table B-1 in Appendix B.2.

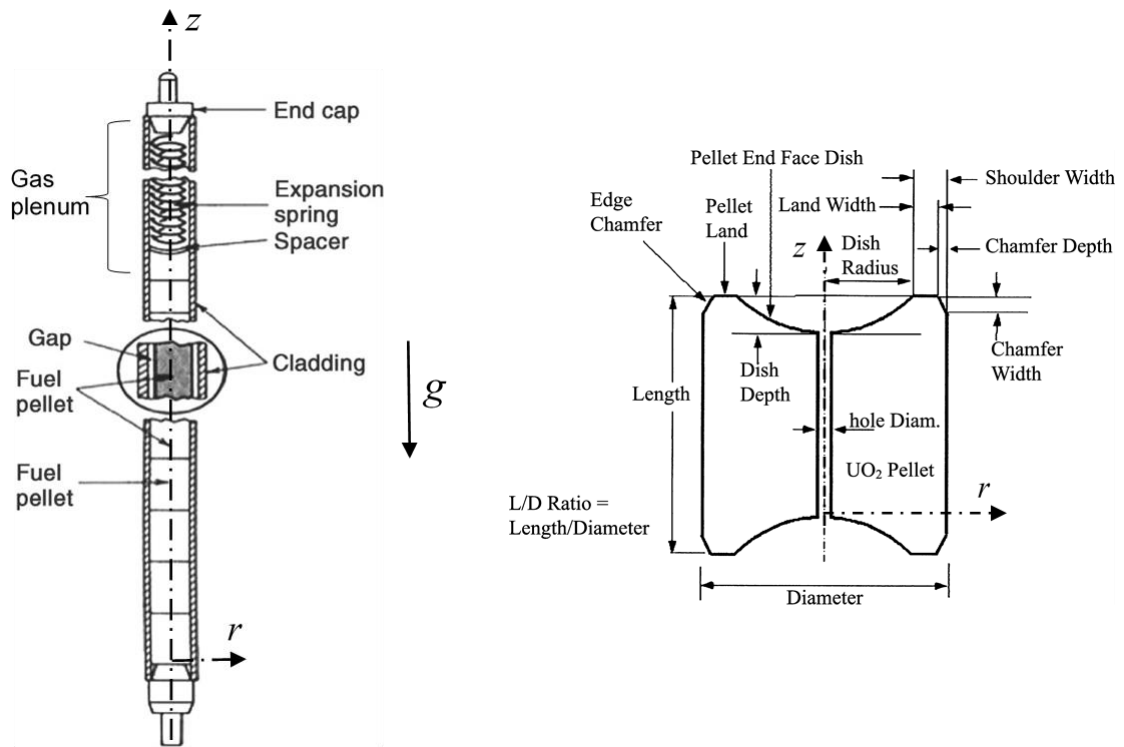


Figure 5-7. Vertical cut through a fuel rod (left). The fuel rod is a sealed cladding containing the fuel pellets (from (Allen *et al.*, 2010)). And fuel pellet sketch (right) (from (Philip *et al.*, 2015)).

Table 5-2. Typical fuel design parameters for a 17x17 PWR FA (see Figure 5-7).

Dish diameter (mm)	4.01
Dish depths (mm)	0.287
Gas plenum length (m)	0.188
Helium fill gas pressure (MPa)	2.41
Fuel surface roughness (mm)	$7.6 \cdot 10^{-4}$
Cladding surface roughness (mm)	$5.1 \cdot 10^{-4}$

### ***PARCS, SCF and TU models***

The input models used for PARCS and SCF are the same as the ones used in Chapter 4.3.1, except that in SCF the URGAP model is used instead of having a fixed value for the HTC. Reference parameters for the HFP conditions of the core are shown in Table C-2 in Appendix C.2. In Appendix B.3 a listing of the parameter's values used in the TU model of the fuel rods can be found.

A coupled PARCS-SCF-TU stationary simulation of the fresh PWR UO<sub>2</sub>/MOX core has been performed for the conditions given in Table C-2 and using the core models described above. A converged solution has been found after 12 outer iterations for which 34 minutes CPU-time are needed. In addition, a PARCS-SCF steady-state simulation of the same core under the same conditions has been performed, converged in 1 minute 48 seconds CPU-time.

### ***Main results of the steady state simulation***

The maximum fuel centreline temperature of each fuel assembly predicted with PARCS-SCF-TU is shown in Figure 5-8 (top), as well as the differences between PARCS-SCF-TU and PARCS-SCF (bottom). There is a good agreement between the simulations. The maximum differences are between -57 K and 84.3 K. The reasons for the observed differences will be explained later in this chapter.

In Figure 5-9 the map of the different fuel types of the fuel assemblies is shown. Comparing the results of the centreline temperatures with the fuel type indicates that that differences are linked directly to the fuel type. It is observed that MOX fuel exhibit a negative difference and UO<sub>2</sub> fuels show a positive difference.

It is important to understand and explain the origin of these differences to assure that the implementation of the coupling is correct. There are two main reasons for the observed results:

- 1) The SCF and TU models predict different gap widths due to the different models for relocation, cracking, and thermal expansion. In general, it has been observed in studies on single fuels that SCF predicts a smaller gap for both UO<sub>2</sub> and MOX fuels. E.g., Figure 5-10 shows the gap width predicted by SCF and TU for different UO<sub>2</sub> and MOX fuel assemblies as a function of the axial height. The nominal gap width is 59 µm. At the top and bottom of the assembly the predictions are similar in both cases, but they grow apart in the centre up to 10 µm of difference. The difference between the gap widths predicted by TU and SCF increases with the temperature. The predicted gap is always smaller in the case of SCF, which leads to the prediction of a lower centreline temperature by SCF with respect to TU.
- 2) The second reason are the correlations for the fuel thermal conductivity. Figure 5-11 shows the thermal conductivity as a function of the temperature used by the models in SCF and TU, for fresh UO<sub>2</sub> and MOX fuels. For both fuel types, the values are lower for the SCF correlation which in turn yields to the prediction of a higher centreline

temperature by SCF. In TU this correlation is dependent on the burnup. However, the problem considered is at zero burnup, since fresh fuel is assumed.

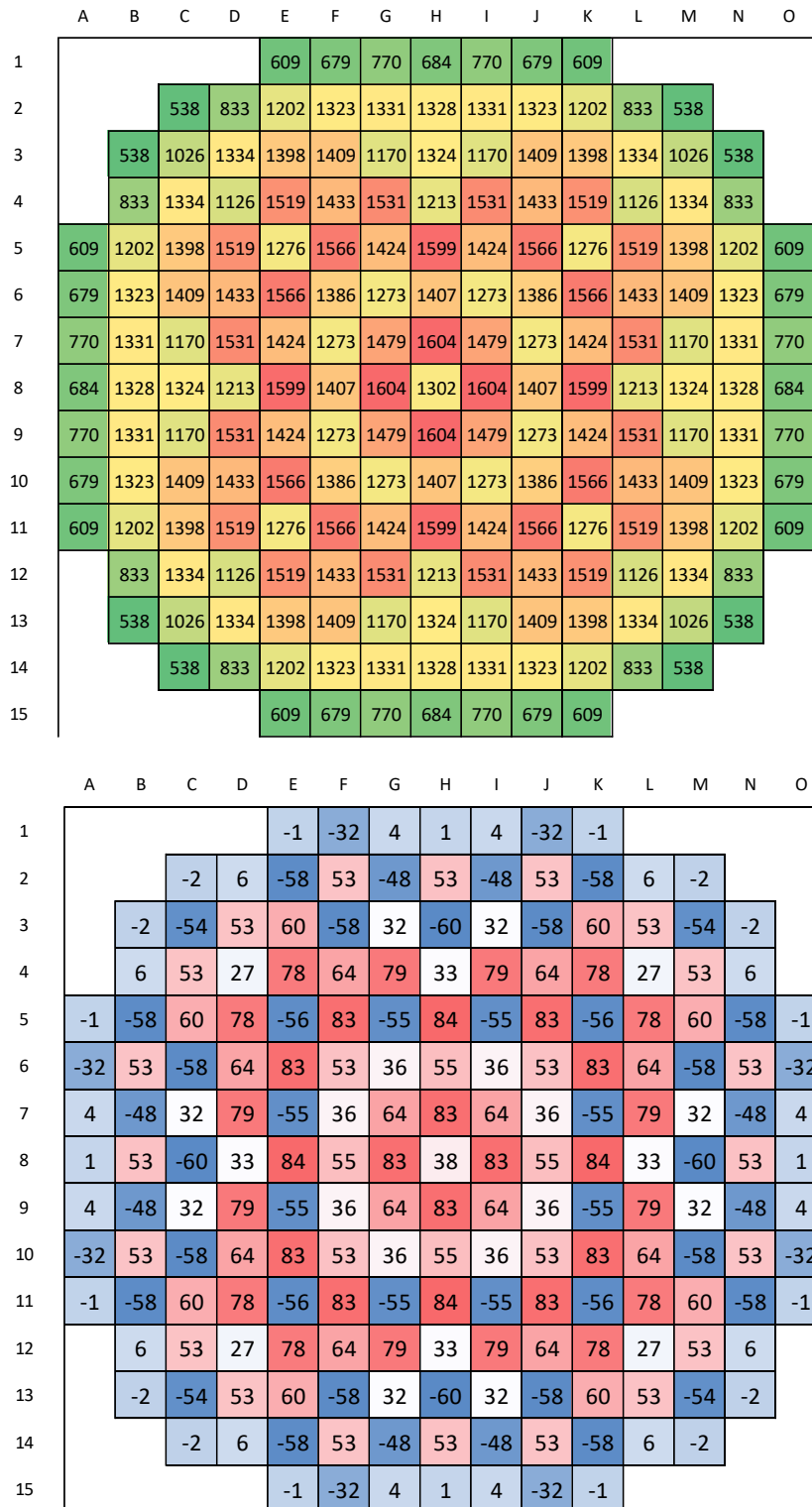


Figure 5-8. Simulated PARCS-SCF-TU maximum fuel centreline temperature (K) (top) and difference with PARCS-SCF  $P_{PARCS-SCF-TU} - P_{PARCS-SCF}$  (K) (bottom) for the steady state solution of the OECD/NEA Benchmark (Kozłowski and Downar, 2007).

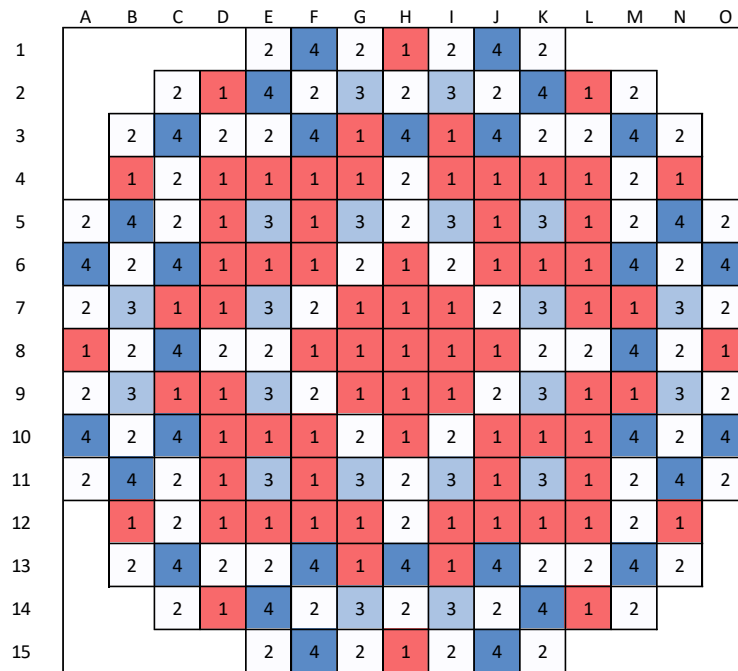


Figure 5-9. Fuels types: 1 =  $\text{UO}_2$  4.2%, 2=  $\text{UO}_2$  4.5%, 3 = MOX 4.0%, 4 = MOX 4.3%.

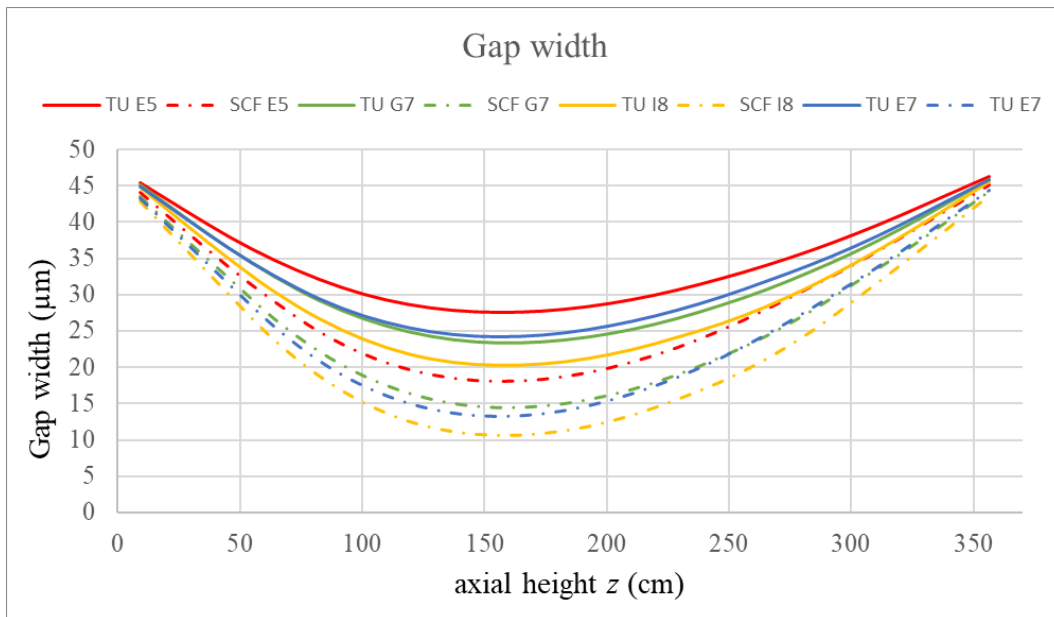


Figure 5-10. Gap width predicted by SCF (dashed lines) and TU (full lines) for FAs E5, E7 (MOX) and G7 and I8 ( $\text{UO}_2$ ).

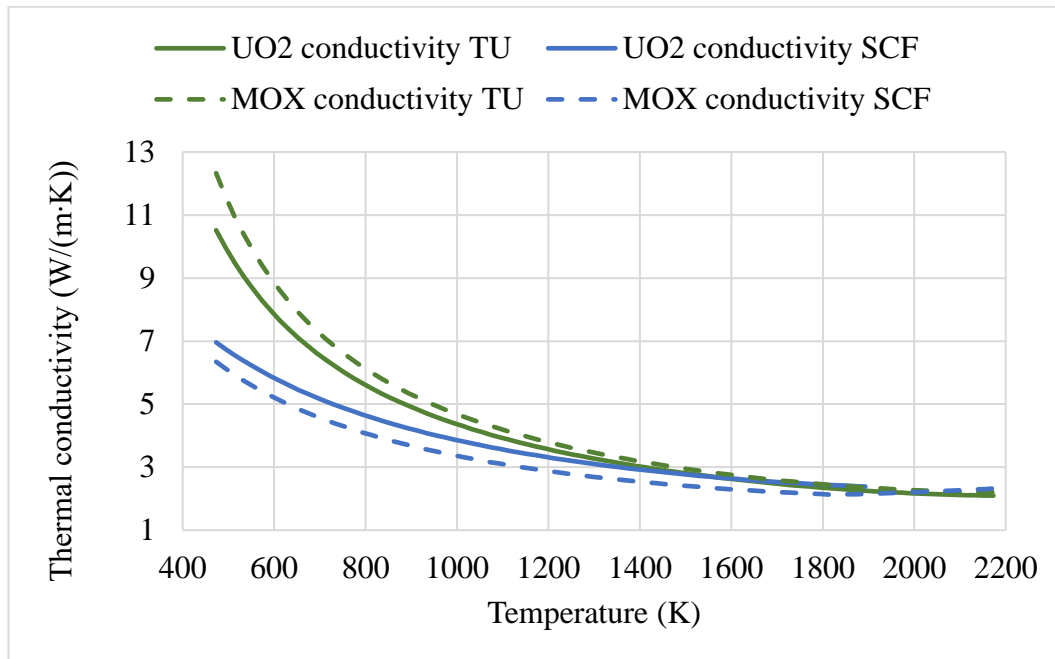


Figure 5-11. Modelled thermal fuel conductivity correlation as a function of temperature for UO<sub>2</sub> and MOX fuel used in SCF and in TU.

Observing the conductivity curves and the predicted fuel temperature distribution in the core, a qualitative analysis can be made by grouping the fuel assemblies into UO<sub>2</sub> or MOX types and into lower and higher temperatures. E.g., lower temperature UO<sub>2</sub> FAs are in the range of 500 to 800 K which are located in the periphery of the core and higher temperature UO<sub>2</sub> FAs are in the range of 1000 to 1600 K located in the inner area of the core (Figure 5-8). In the lower temperature range the difference in the conductivity correlation is considerable, whereas in the higher temperature range is not.

Table 5-3 shows a qualitative analysis of the influence of the gap width predicted by SCF models and TU models and the fuel conductivity for the correlations used in SCF and TU in the centreline temperature prediction, and the observed overall effect. The gap width predicted by TU is bigger than the one predicted by SCF in every case.

The following statements can be made:

- UO<sub>2</sub> low temperature range: for the UO<sub>2</sub> FAs in the periphery of the core, the fuel temperatures are in the range of 500-800 K where the conductivity correlation is lower for SCF with respect to TU. This leads to the prediction of higher centreline temperature by SCF. On the other hand, the effect of the gap width in the opposite direction, compensates for this leading to the prediction similar temperatures by SCF and TU.

Table 5-3. Qualitative effects of the influence of the fuel conductivity and gap width on the centreline temperature prediction for UO<sub>2</sub> and MOX fuel types.

UO <sub>2</sub> fuel				
Temperature range	Parameter	Values for TU and SCF	Effect on $T_{centerline}$ prediction	Net effect on $T_{centerline}$
500-800K	Fuel Conductivity	TU > SCF	$T_{cent,TU} < T_{cent,SCF}$	$T_{cent,TU} \approx T_{cent,SCF}$
	Gap width	TU > SCF	$T_{cent,TU} > T_{cent,SCF}$	
1300-1600 K	Fuel Conductivity	TU $\approx$ SCF	$T_{cent,TU} \approx T_{cent,SCF}$	$T_{cent,TU} > T_{cent,SCF}$
	Gap width	TU > SCF	$T_{cent,TU} > T_{cent,SCF}$	
MOX fuel				
Temperature range	Parameter	Values for TU and SCF	Effect on T <sub>centre</sub> prediction	Net effect on $T_{centerline}$
500-800K	Fuel Conductivity	TU > SCF	$T_{cent,TU} < T_{cent,SCF}$	$T_{cent,TU} < T_{cent,SCF}$
	Gap width	TU > SCF	$T_{cent,TU} > T_{cent,SCF}$	
1000-1400 K	Fuel Conductivity	TU > SCF	$T_{cent,TU} < T_{cent,SCF}$	$T_{cent,TU} < T_{cent,SCF}$
	Gap width	TU > SCF	$T_{cent,TU} > T_{cent,SCF}$	

- UO<sub>2</sub> high temperature range: values for the fuel conductivity are similar for SCF and TU suggesting that this does not influence considerably the differences in the centreline temperature. The temperature difference is mostly influenced by the lower gap width prediction by SCF, which causes an overall lower temperature prediction by SCF.
- MOX fuels in the low temperature range: the difference in the conductivity between SCF and TU is larger for MOX FA, leading to higher temperature differences. In this case, although the gap width effect acts in the opposite direction, it does not compensate completely, and the overall result is larger fuel temperature predicted by SCF.
- MOX fuels in the high temperature range: there is still a small difference in the conductivity between TU and SCF. At the lower range of temperatures (500-800K), the gradient between surface and centreline temperatures is in the order of 300 K, whereas in the higher range of temperature this gradient is in the order of 900 K. The larger gradient means that the fuel thermal conductivity difference between has a higher absolute impact. This leads to the net effect of SCF predicting higher temperatures than TU.

As a conclusion, it can be said that the observed differences in the centreline temperature can be explained and are consistent with the models of the gap width and the correlations for the fuel conductivity.



Another important parameter to be discussed is the coolant temperature. This variable is computed by using the power transferred directly from PARCS to SCF in the case of PARCS-SCF, and by equalizing the cladding temperature of TU and SCF in the case of PARCS-SCF-TU. In Figure 5-12 the core average axial coolant temperature obtained by PARCS-SCF and PARCS-SCF-TU is presented as well as the difference between them.

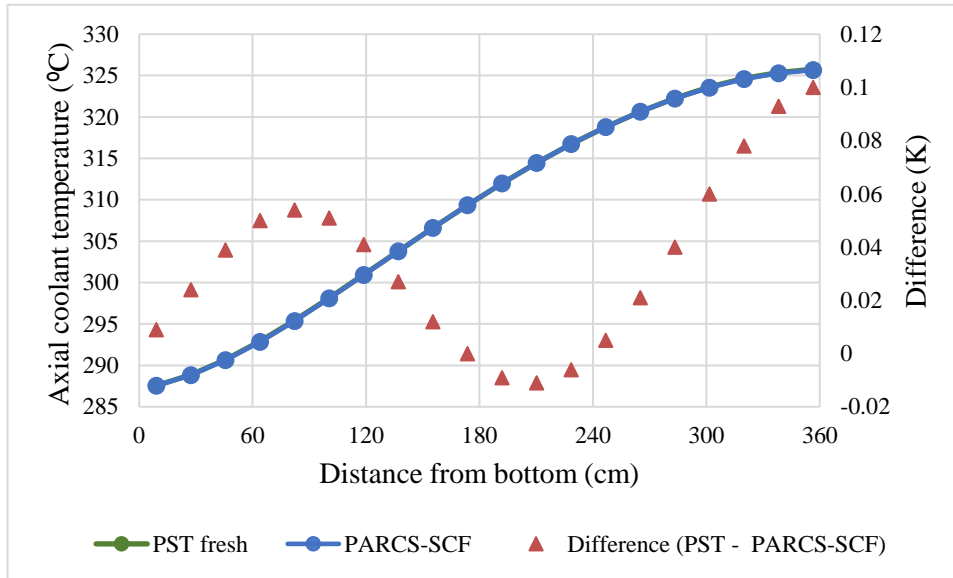


Figure 5-12. Axial moderator temperature distribution obtained with PARCS-SCF and PARCS-SCF-TU (PST). The values are given at calculated at the centre of each mesh node. The almost exact agreement between the solutions is a proof of the correct energy balance.

There is a good agreement in the axial temperature distribution with differences  $< 0.11\text{K}$ , between PARCS-SCF and PARCS-SCF-TU showing a correct energy balance in the PARCS-SCF-TU coupling.

Finally, the results for the  $k_{\text{eff}}$  are shown in Table 5-4. There is a good agreement in the solutions observing a difference of only 89 pcm. The fuel temperatures predicted by PARCS-SCF-TU are in average higher than the ones predicted by PARCS-SCF. Hence, more neutrons are absorbed due to the Doppler effect leading to a slightly lower  $k_{\text{eff}}$ .

Table 5-4.  $k_{\text{eff}}$  results for the coupled simulations.

	$k_{\text{eff}}$
PARCS-SCF	0.999947
PARCS-SCF-TU	0.999115

In general, a good agreement of the solutions of PARCS-SCF-TU for the model of fresh fuel and the simulation with PARCS-SCF with the URGAP model has been found demonstrating the correct implementation of the coupling of PARCS-SCF with TU.

## 6 Analysis of a UO<sub>2</sub>/MOX PWR Core with the developed Multiphysics Code

In this chapter, the simulations of a full PWR core operating at HFP conditions for steady state and at HZP conditions for a REA transient is analysed with PARCS-SCF-TU. By including TU in the simulation, the model takes into account the irradiation dependent thermal-physical properties of the fuel rods to study its impact in the global simulation. The selected core for the analysis is the one defined in the OECD/NEA UO<sub>2</sub>/MOX PWR benchmark. The main characteristics and simulation parameters as well as the development of the models for PARCS and SCF has been described in chapters 4 and 5.

In the PWR benchmark core loading, four different fuel types and seven burnup points with three fuel cycles are considered. A TU model for each fuel must be developed according to the fuel type, enrichment, burnup and number fuel cycles in the core, to consider the pre-irradiation, i.e. the fuel history. The fuel burnup distribution is shown in Figure 6-1.

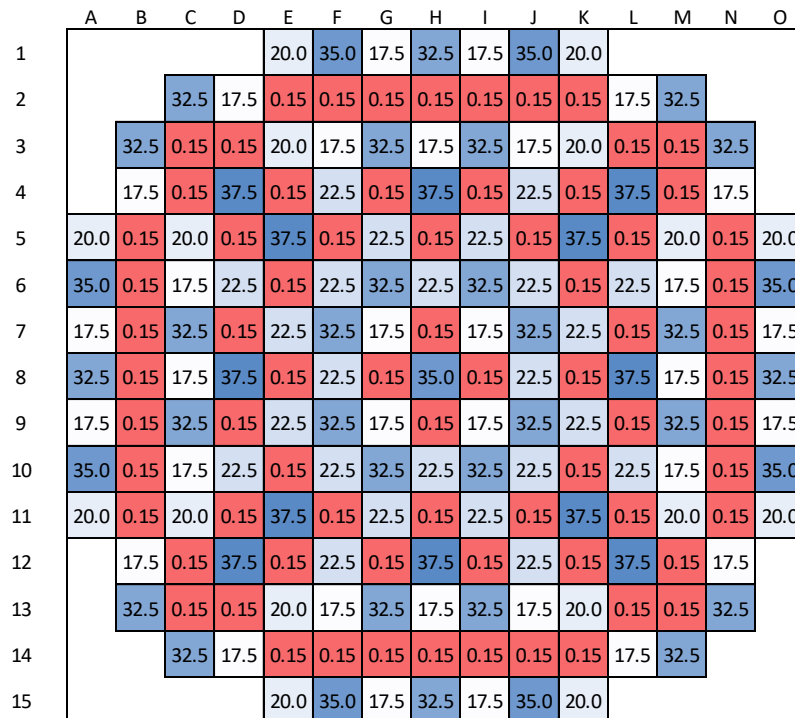


Figure 6-1. PWR assembly average burnup distribution (GWd/tHM).

The 193 inputs (restart files) describing the conditions of each fuel rod at the given burnup are generated automatically with a MATLAB script. The script requires information regarding the core (3D) distribution:

- map of the fuel types in the core (4 fuel types),
- map of the fuel burnup distribution (7 average burnups),
- number of cycles for each fuel (0, 1 or 2 cycles),
- and core axial power profile.

An interval of one month is considered between the cycles and a constant power is assumed within each cycle. The fuel assembly average power distribution obtained with a PARCS-SCF simulation is given to set the last point of the restart to speed up the convergence. It has been tested that using a core average power distribution increase only marginally the calculation time. An average axial power and flux profile are also required. The core average axial distribution is assumed to model the fuel irradiation in TU. With the target average burnup for each FA, the script estimates the average power and flux necessary to achieve the desired burnup in the desired time. Finally, the FA history is estimated from the given data. In Figure 6-2 for instance, the linear power used as input to generate the restart of a FA with two cycles are depicted for the different equidistant axial slices.

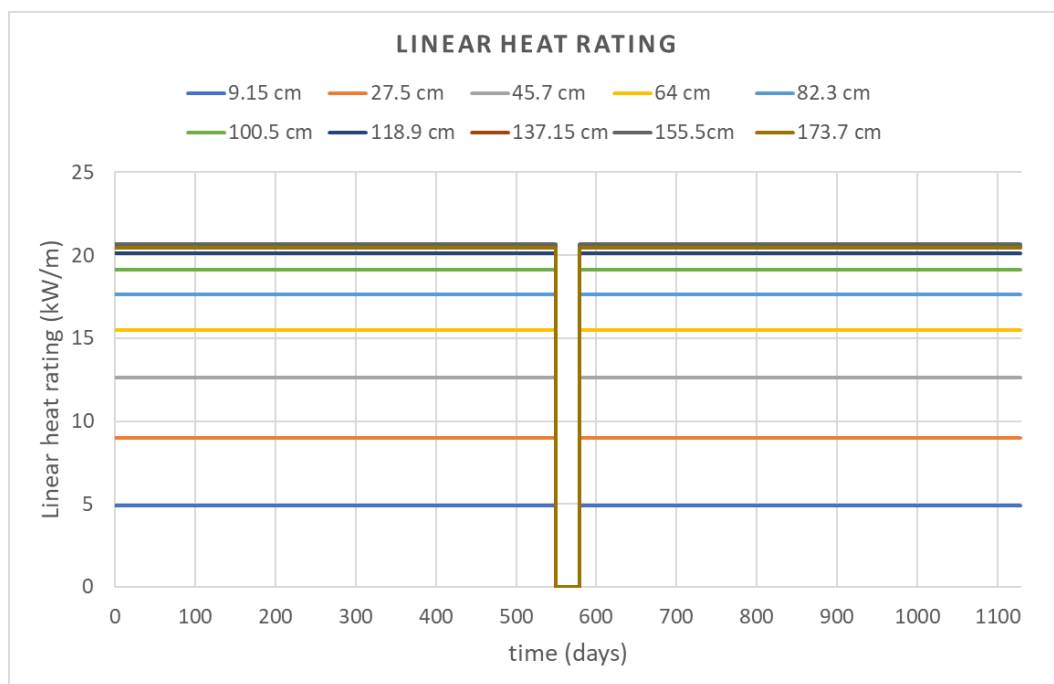


Figure 6-2. Linear heat rating for the UO<sub>2</sub> 4.2% - 37.5 GWd/tHM BU – 2 cycles of 18 month with 1-month interval between cycles. The bottom ten nodes are shown in the figure. The mid axial height of each node is shown in the labels.

The methodology for the generation of the TU restart files with MATLAB is further described in Appendix B.1.

The final burnup cannot be exactly predicted in a first iteration but a very good approximation (< 1% error) can be achieved. The power level can be corrected in a second iteration using the information of the burnup achieved in the first iteration so that the target burnup is reached. For this, the power level must be corrected by a factor  $\gamma = \frac{Bu_{desired}}{Bu_{achieved\ in\ first\ iteration}}$ .

## ***6.1 Steady state simulation of a PWR core at HFP conditions***

First, a characterization of the different representative fuel assemblies is presented. Then, a steady state simulation with PARCS-SCF-TU using pre-irradiated conditions is performed and the obtained results are compared against the ones of the simulation with fresh irradiation conditions. This will show the impact of the burnup on the fuel properties and the importance of the detailed thermo-mechanics models in the coupled simulation. Selected results are presented and discussed. The HFP thermal-hydraulics conditions and the geometry data for the steady state simulation are those of Table C-2 in Appendix C.2.

### ***6.1.1 Characterization of the core loading based on TU simulations***

In an equilibrium core, the burnup of the fuel assemblies (FA) varies between FAs and presents an axial burnup distribution. Thus, there is the need to model the fuel-thermo-mechanics for all FAs and consider the axial dependency. To exemplify how the fuel properties can change with the irradiation time, the irradiation dependent gap width, fission gas release and gap HTC are shown in Figure 6-3 to Figure 6-5 as predicted by TU. These figures correspond to the case of a two-cycles, UO<sub>2</sub> 4.2% FA with 37.5 GWd/tHM of average burnup. In these figures the top 10 (out of 20) axial nodes of a FA (representative pin) are plotted.

In Figure 6-3, it can be seen that the gap width at zero days has a fast decrease due to the thermal expansion. As it was shown in Figure 5-10, the gap width closes more in the central part due to the higher fuel temperatures. The axial fuel temperature distribution remains similar during the irradiation and thus also does the thermal component for the gap width. Later on, the gap width begins to grow, due to the fuel densification. Following this, after some months, the gap begins to close mainly due to the fuel swelling and the cladding creep-in. It closes first at the central part of the fuel. This is due to the axial cosine flux profile, meaning that the local burnup is higher at the centre and thus also are the swelling and creep components.

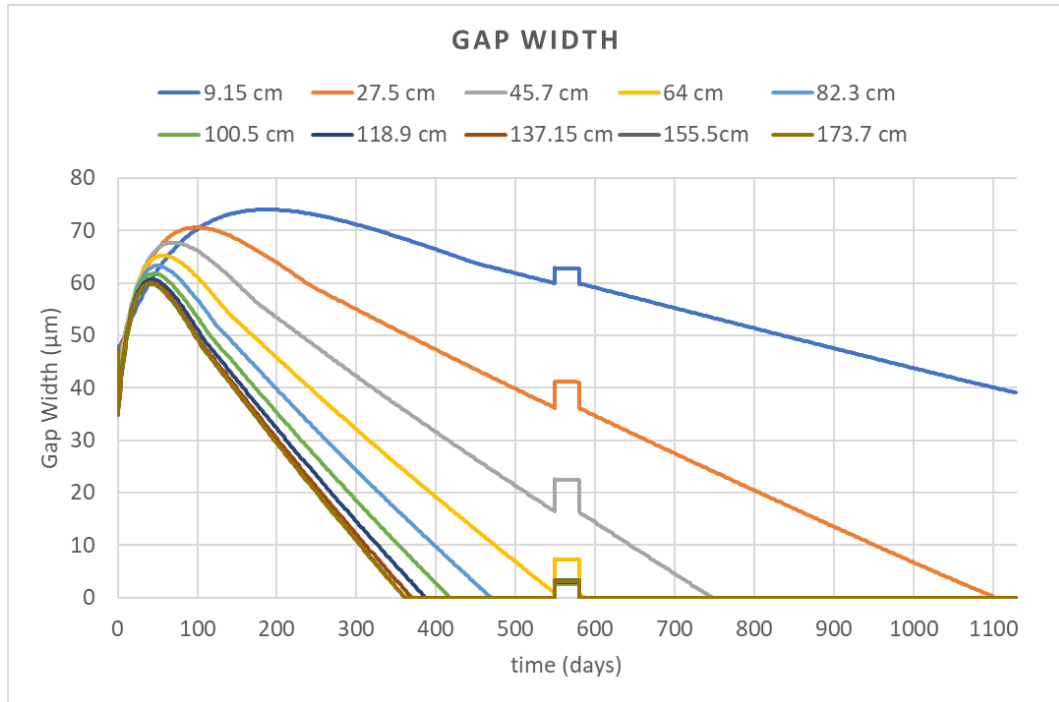


Figure 6-3. Gap width ( $\mu\text{m}$ ) evolution during the irradiation for a UO<sub>2</sub> 4.2% FA with 37.5 GWd/tHM. The mid axial height of each node is shown in the labels.

The large variation of the gap width caused by the creep, cracking, swelling and thermal expansion processes, have consequently a large variation in the heat transfer coefficient, as shown in Figure 6-4.

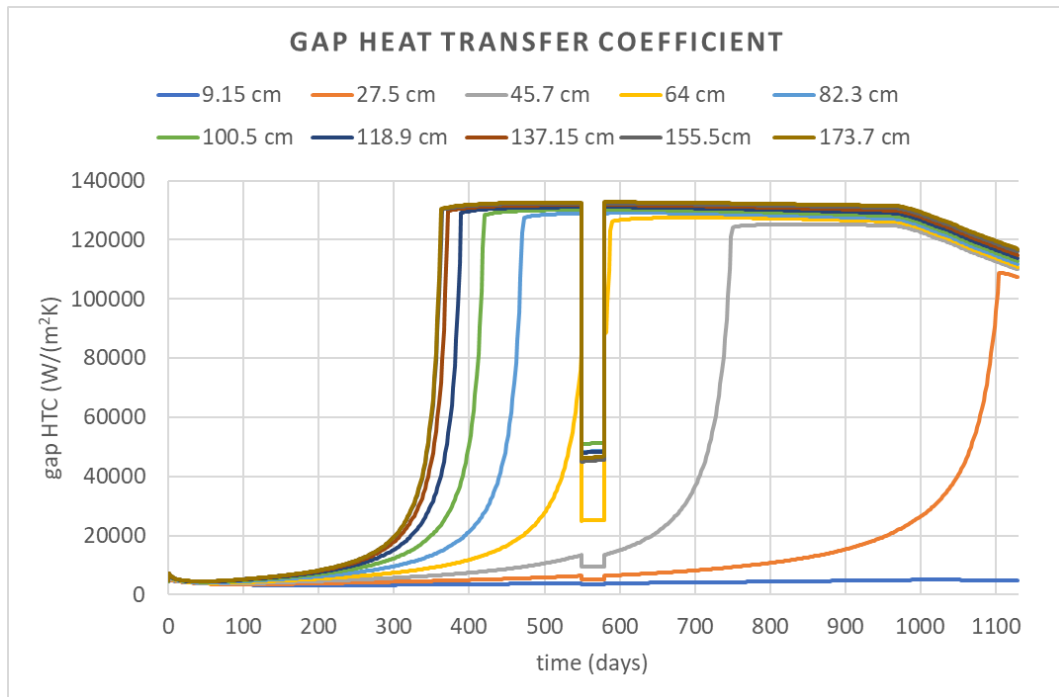


Figure 6-4. Gap heat transfer coefficient ( $\text{W}/(\text{m}^2\text{K})$ ) evolution during the irradiation for a UO<sub>2</sub> 4.2% FA with 37.5 GWd/tHM. The mid axial height of each node is shown in the labels.

In the first year of irradiation of the fuel in the core, there is a very large variation in the gap HTC until the gap is closed. Once the gap is closed the gap HTC remains constant until higher irradiations are reached, when the fission gas release becomes significant, at ~1000 days as shown in Figure 6-5. When this happens the gas release causes a drop in the value of the gap HTC due to an accumulation of gases in between the pellet and clad, which lowers the gap conductivity. However, this only occurs for high burnups.

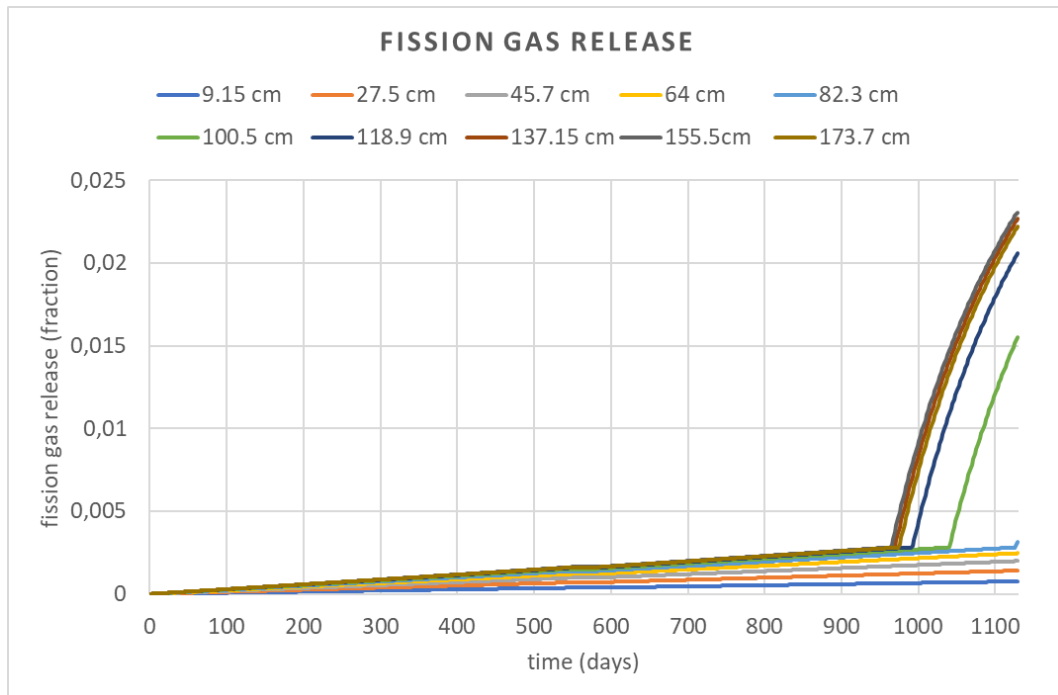


Figure 6-5. Fission gas release (fraction) evolution during the irradiation for a UO<sub>2</sub> 4.2% FA with 37.5 GWd/tHM. The mid axial height of each node is shown in the labels.

### ***6.1.2 Discussion of the main results for the HFP steady state simulation***

Figure 6-6 shows the maximum centreline temperature prediction by PARCS-SCF-TU with irradiated fuel models and the differences with the case using fresh fuel model. Differences up to -110 K are found for low burnup fuels and up to 172 K for high burnup fuels. In this comparison all the codes and models are the same in both simulations. The consideration of the fuel irradiation in the thermo-mechanics is the only difference between the two models. Hence, the differences in the results are due to the difference in the thermal-physical properties changes due to the fuel irradiation and in general due to the improved capabilities of TU to describe the behaviour of the irradiated fuel.

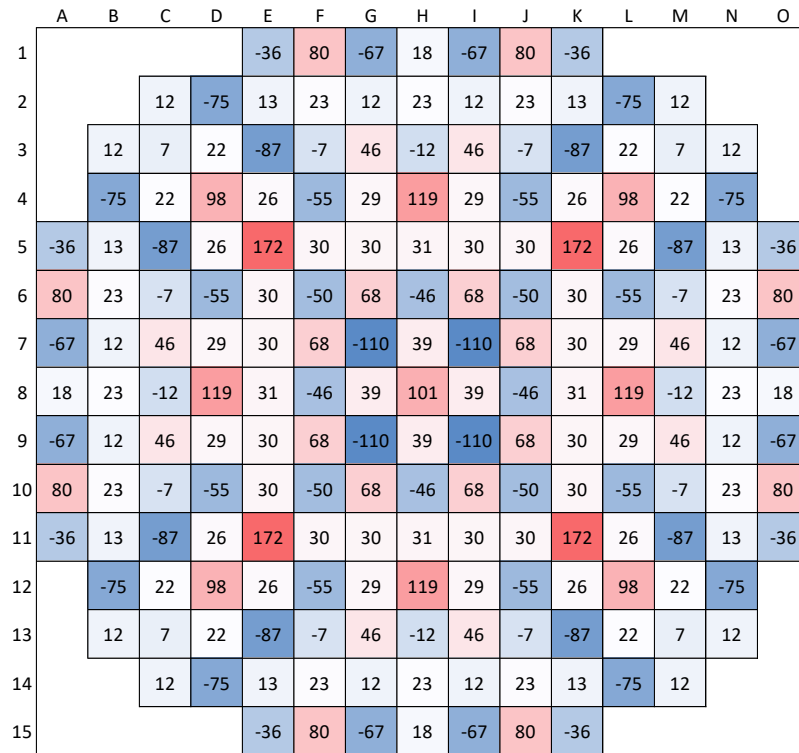
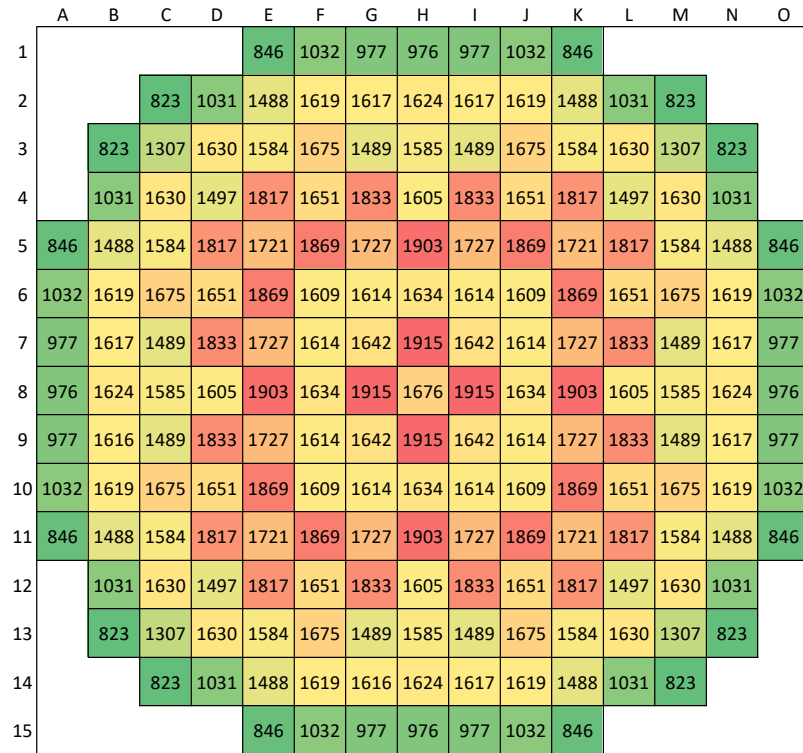


Figure 6-6. Fuel assembly maximum centreline temperature distribution [K] calculated with PARCS-SCF-TU for pre-irradiated conditions (top). Difference of the fuel centerline temperature [K] predicted by PARCS-SCF-TU with burnup and for fresh fuel conditions (bottom). This shows that the consideration of burnup in the calculations have a significant influence on the centreline temperature prediction.



There are two main reasons for the difference in the results:

- the gap closing lowers the surface temperature and consequently the centreline temperature and,
- the fuel conductivity degradation increases the centreline and surface temperature difference, hence increasing the centreline temperature.

The behaviour of three fuels with different burnups (highlighted in Figure 6-6), a low (0.15 GWd/tHM, FA I8), medium (17.5 GWd/tHM, FA G7), and high burnup (37.5 GWd/tHM, FA E5) are discussed hereafter.

For a detailed discussion and interpretation of the results, the axial temperature distribution at different radial points, fuel centreline and surface, clad average, and coolant temperature (Figure 6-7) will be studied.

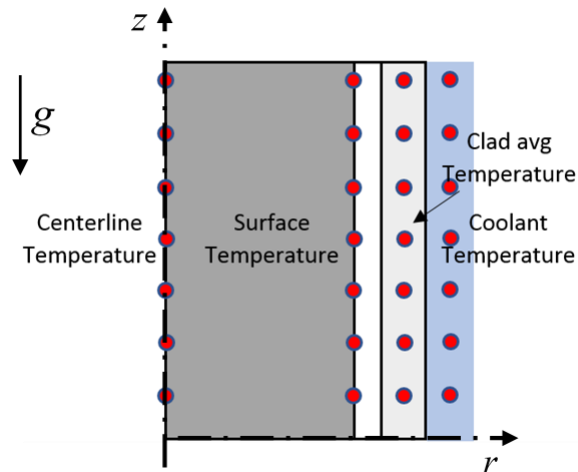


Figure 6-7. Axial temperatures presented in the temperature analysis.

For low burnup fuel, e.g. FA I8 (yellow) corresponding to UO<sub>2</sub> fuel with 4.2% of enrichment and 0.15 GWd/tHM, the gap width is bigger for the irradiated fuel (Figure 6-8) since at this lower burnup the densification process is dominant and the fuel pellet decreases its radius. The higher gap width leads to a smaller gap conductance and this results in a higher surface temperature of the pre-irradiated fuel. The fuel conductivity is similar for both fresh and burnt cases. Hence, the temperature difference between centreline and surface fuel temperature follows the same behaviour in both cases leading to a higher centreline temperature prediction for the burnt fuel.

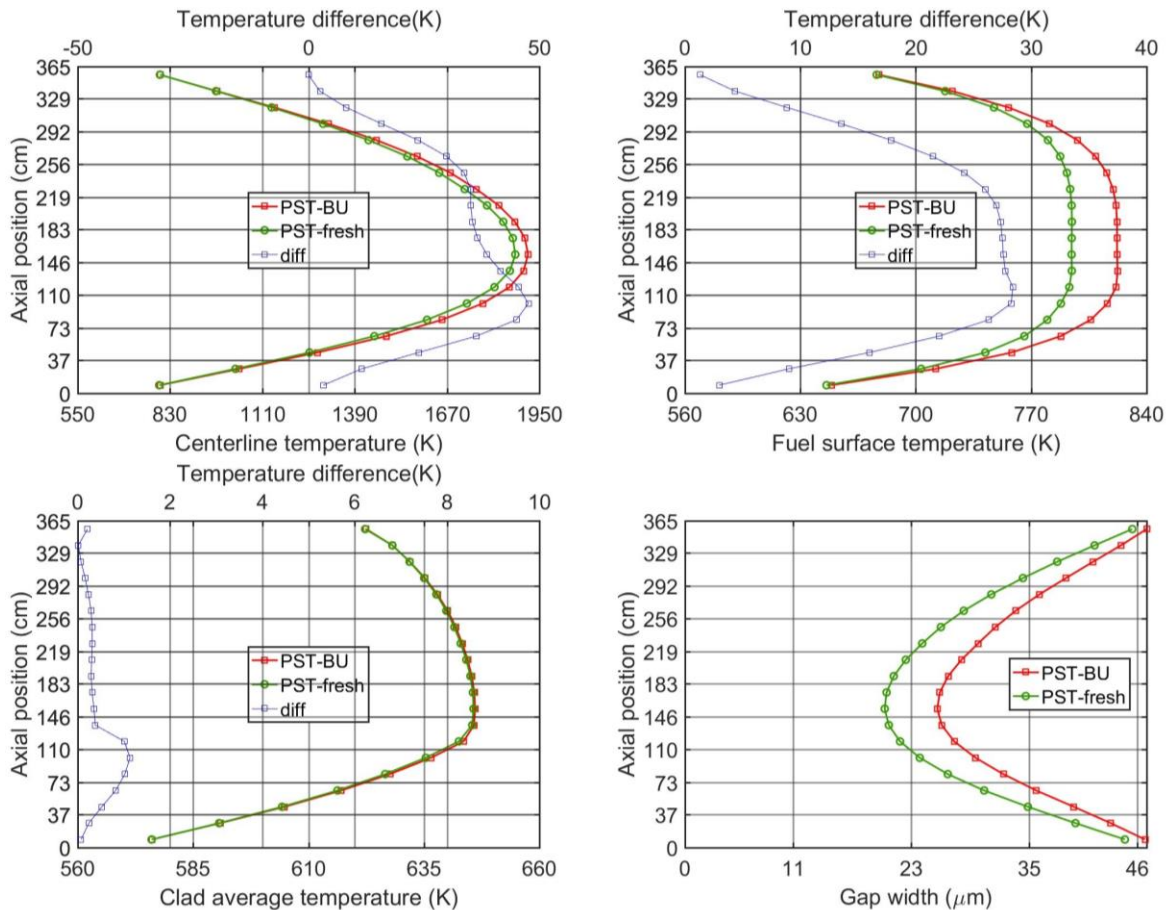


Figure 6-8. Fuel centreline, fuel surface and clad average temperatures axial distribution and gap width for FA I8 UO<sub>2</sub> 4.2 – 0.15 GWd/tHM.

For high burnup fuel, e.g. FA E5 (red), corresponding to a MOX with 4.0% enrichment and 37.5 GWd/tHM burnup, the gap is closed almost completely except at the top and bottom of the fuel (Figure 6-9). The gap closure causes a higher gap conductance and thus, the surface temperature to be lower ( $\sim 70$ K at the maximum temperature, and  $\sim 110$ K at the bottom of the rod). A higher clad average temperature of  $\sim 27$ K is observed for the burnt case due to the gap closure and to the oxide corrosion layer, which increases with the burnup and it decreases the conductivity in the clad. Whereas the surface temperature difference is  $\sim 70$ K the centreline temperature difference is  $\sim 170$ K. This is due to the degradation of the fuel conductivity, shown Figure 6-10, which generates larger temperature gradients ( $\sim 240$ K) in the burnt fuel when compared to the fresh case.

At an intermediate burnup, e.g. FA G7 (green) corresponding to a UO<sub>2</sub> fuel with 4.2% enrichment and 17.5 GWd/tHM of burnup. In this case (Figure 6-11) the surface temperature is  $\sim 110$  K lower for the burnt case due to the gap closing, and the centreline temperature is  $\sim 120$  K lower for the case of the burnt fuel.

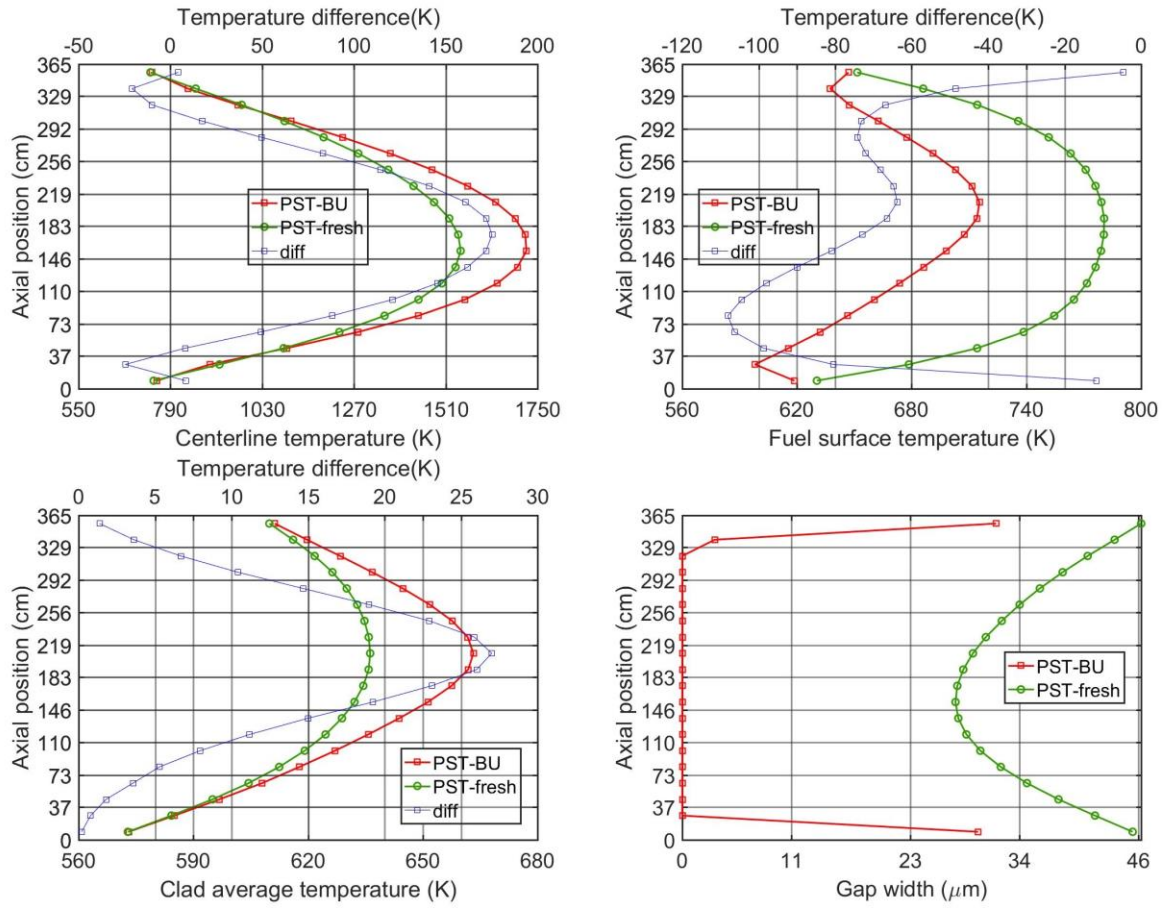


Figure 6-9. Fuel centreline, fuel surface and clad average temperatures axial distribution and gap width for FA E5 MOX 4.0 – 37.5 GWd/tHM.

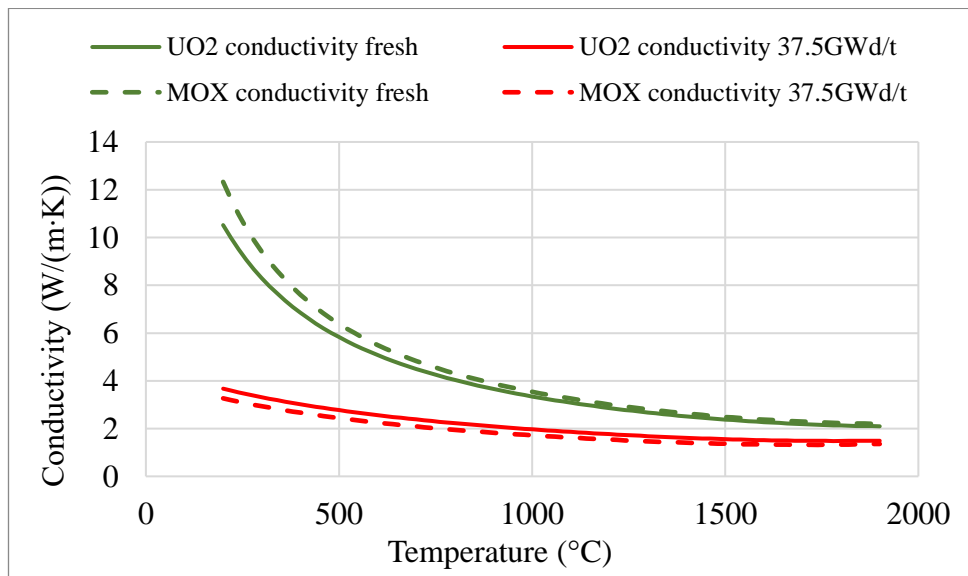


Figure 6-10. Values for the fuel conductivity correlation for UO<sub>2</sub> and MOX for TU for fresh fuel conditions and 37.5 GWd/tHM of burnup.

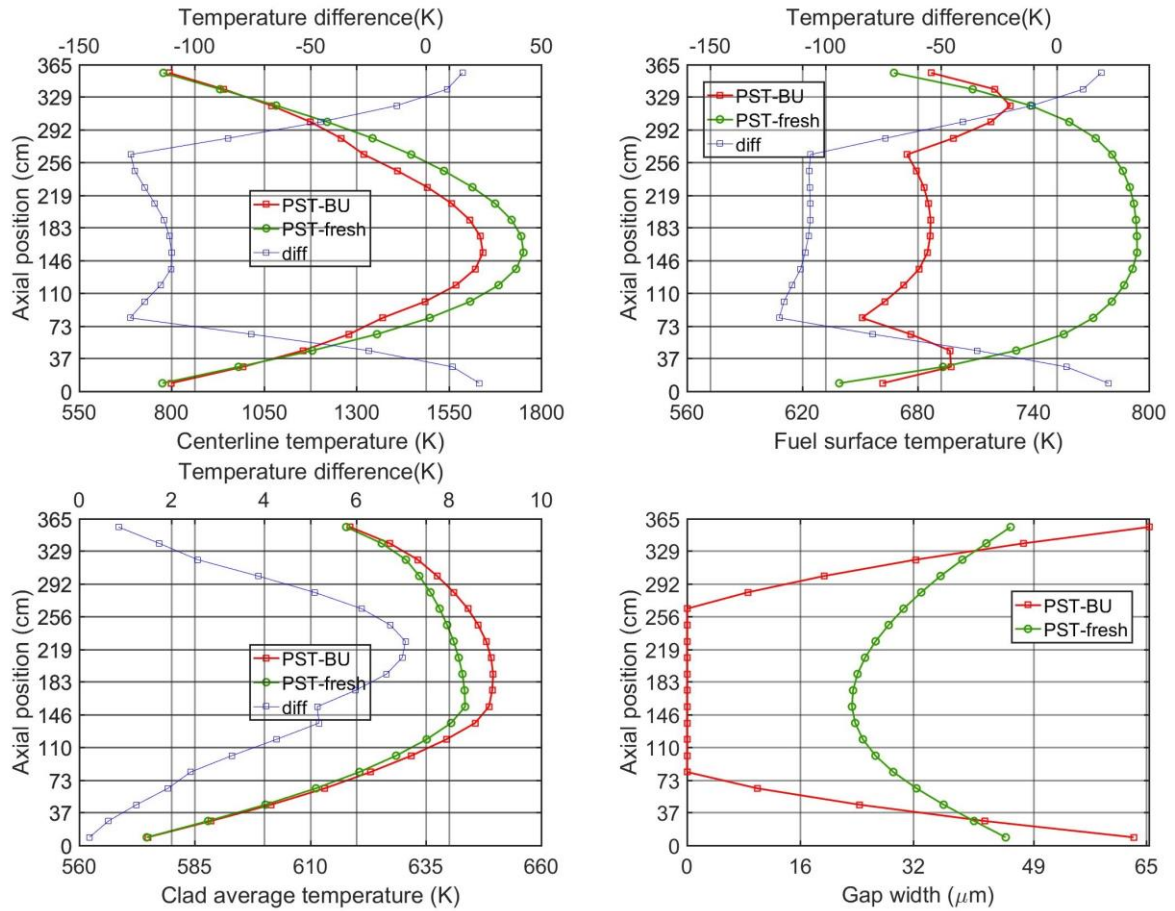


Figure 6-11. Fuel centreline, fuel surface and clad average temperatures axial distribution and gap width for FA G7, UO<sub>2</sub> 4.2% – 17.5 GWd/tHM.

On the contrary of what is observed for higher burnups, at this middle burnup the fuel conductivity is not yet degraded enough to cause a larger centreline-surface temperature gradient, and the centreline temperature difference follows the surface temperature difference.

Regarding the  $k_{eff}$ , the results obtained for the simulation are shown in Table 6-1. The observed difference between PARCS-SCF-TU simulation done for a fresh and a burnt core amount to 50 pcm only.

Table 6-1.  $k_{eff}$  results for PARCS-SCF-TU burnt and fresh cases.

Case	$k_{eff}$
PARCS-SCF-TU burnt	0.99965
PARCS-SCF-TU fresh	0.99912

The  $k_{eff}$  difference is mainly due to the fuel temperatures, i.e., the Doppler feedback. Figure 6-12 shows the axially averaged fuel Doppler temperature difference between the values

predicted by PARCS-SCF-TU for the core loading fresh and burnt fuel. The core average fuel temperature difference is -22 K meaning that the burnt case predicts globally a lower Doppler temperature, thus there is less absorption which leads a slightly higher  $k_{eff}$ .

	A	B	C	D	E	F	G	H	I	J	K	L	M	N	O
1					-35.4	-25.7	-46.1	-36.2	-46.1	-25.7	-35.4				
2			-26.1	-50.4	8.23	15.8	8.72	15.9	8.72	15.7	8.21	-50.4	-26.1		
3		-26.1	6.24	15.6	-71.7	-64.8	-51.5	-64.3	-51.5	-64.8	-71.7	15.6	6.24	-26.1	
4		-50.4	15.6	-38.2	18	-69.3	19.1	-35.7	19.1	-69.3	18	-38.2	15.6	-50.4	
5	-35.4	8.22	-71.7	18	-26.7	19.9	-59.5	20.4	-59.5	19.9	-26.7	18	-71.7	8.22	-35.4
6	-25.7	15.7	-64.8	-69.3	19.9	-67.7	-49.1	-67.2	-49.1	-67.7	19.9	-69.3	-64.8	15.7	-25.7
7	-46.1	8.72	-51.5	19.1	-59.5	-49.1	-71.1	21.8	-71.2	-49.1	-59.5	19.1	-51.5	8.72	-46.1
8	-36.2	15.9	-64.3	-35.7	20.4	-67.2	21.8	-42.3	21.8	-67.2	20.4	-35.7	-64.3	15.9	-36.2
9	-46.1	8.72	-51.5	19.1	-59.5	-49.1	-71.2	21.8	-71.2	-49.1	-59.5	19.1	-51.5	8.72	-46.1
10	-25.7	15.7	-64.8	-69.3	19.9	-67.7	-49.1	-67.2	-49.1	-67.7	19.9	-69.3	-64.8	15.7	-25.7
11	-35.4	8.22	-71.7	18	-26.7	19.9	-59.5	20.4	-59.5	19.9	-26.7	18	-71.7	8.22	-35.4
12		-50.4	15.6	-38.2	18	-69.3	19.1	-35.7	19.1	-69.3	18	-38.2	15.6	-50.4	
13		-26.1	6.24	15.6	-71.7	-64.8	-51.5	-64.3	-51.5	-64.8	-71.7	15.6	6.24	-26.1	
14		-26.1	-50.4	8.22	15.8	8.72	15.9	8.72	15.8	8.21	-50.4	-26.1			
15					-35.4	-25.7	-46.1	-36.2	-46.1	-25.7	-35.4				

Figure 6-12. Difference between PARCS-SCF-TU with burnup – PARCS-SCF-TU fresh for the axially averaged fuel Doppler temperature (K).

The closure of the gap causes a decrease in the surface temperature, and the degradation of the fuel properties leads to an increase in the centreline temperature. As a result, the change on the Doppler temperature is not of major importance and the net effect on the  $k_{eff}$  is small. However, the impact on the centreline temperatures prediction is very important: it varies from - 110 K to 172 K for the investigated core. Due to the corrosion layer formation on the cladding there is an increase of the cladding average temperature up to 30 K. However these temperatures are well below the safety limits (IAEA - Safety Assessment Section, 2003).

## 6.2 PWR REA simulation at HZP conditions

The rod ejection accident in a PWR with UO<sub>2</sub>/MOX core loading, described in Chapter 2 is analysed with PARCS-SCF-TU (PST) starting with a core loaded with burnt fuel as de-

scribed previously. The inclusion of a thermo-mechanics solver, i.e. TU in the coupled simulation, represents a more realistic simulation of the behaviour of irradiated fuel under accidental conditions than the one without pin-mechanics solver.

For this analysis, the same TU models developed for the steady-state simulation of the PWR UO<sub>2</sub>/MOX core at hot full power conditions (explained in Chapter 6.1) are used. The power and the thermal-hydraulics initial conditions for the restart files are set to the HZP conditions at the end of the irradiation (beginning of the transient simulation). This means that the TU models for all the FAs at the end of the irradiation, go from HFP to HZP condition. As consequence of removing the power generation (HZP conditions are 10<sup>-6</sup> of the nominal power), the fuel temperature diminishes and a thermal contraction of the fuel and clad takes place. However, in the centre of the rod, an elastic cladding deformation persists causing the gap to reopen, as is shown later on.

### ***6.2.1 Initial conditions for the fuel at HZP***

The HZP conditions refer to a condition with the coolant at normal operating inlet temperature and pressure but with nearly zero reactor power. The thermal hydraulics conditions for HZP are given in Table C-2 in Appendix C.2, with the difference that at HZP conditions the power is 10<sup>-4</sup>% of the nominal power.

Because of the zero power conditions, the core is initially in a thermal equilibrium with the coolant inlet temperature, i.e., the fuel temperature is equal to the coolant temperature. The decrease of the fuel temperature with respect to HFP nominal conditions causes a change of volume of the fuel and clad. Only plastic deformation induced by creep and swelling remains, and the gap reopens producing a decrease in the gap conductance as showed in Figure 6-13. Here, it can be seen that the gap reopens at the centre of the fuel rod, but at positions near the top and bottom it remains closed for the case of a UO<sub>2</sub> 4.2% with 37.5 GWd/tHM FA. The reason for this, is the behaviour of the clad inner radius deformation and the fuel outer radius deformation when going from nominal power to zero power conditions.

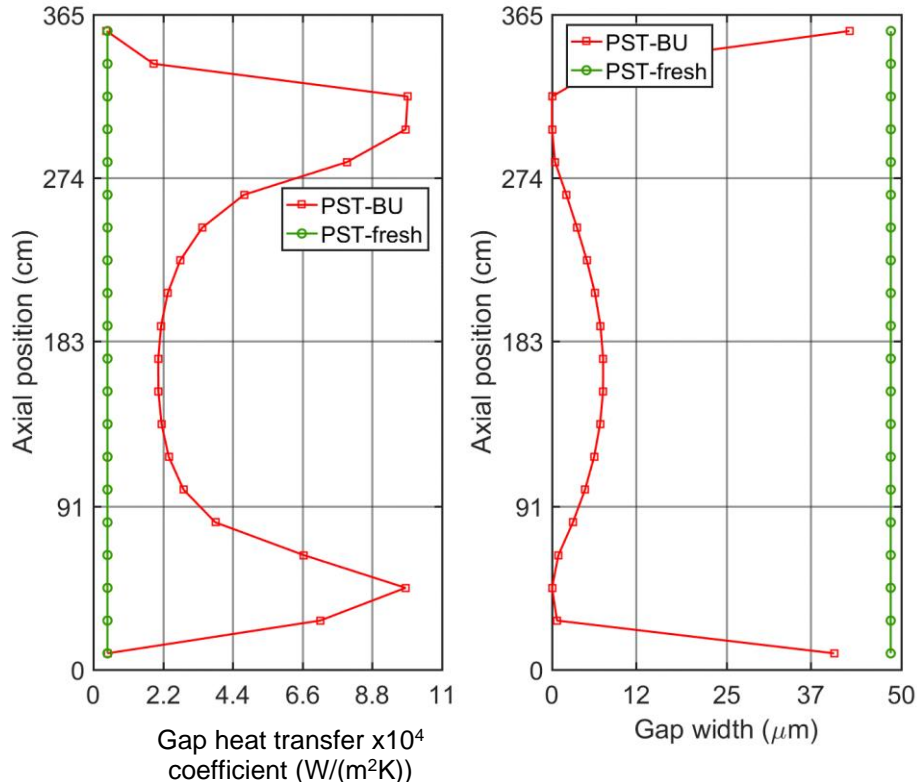


Figure 6-13. Gap with and gap heat transfer coefficient for the fuel rod corresponding to the FA L12, UO<sub>2</sub> 4.2% enrichment with 37.5 GWd/tHM BU at the beginning and end of the transient. Even when it is a short transient, the values for the gap width and HTC change considerably.

In Figure 6-14 the change in deformation of the fuel outer radius and clad inner radius when changing the power conditions from HFP to HZP for a fuel rod with 37.5 GWd/tHM of burnup are shown. The deformations are calculated from the reference design values.

The fuel outer radius deformation due to swelling, creep and thermal expansion is positive (pellet expansion). When the fuel temperature decreases, the change in deformation is more pronounced at the fuel centre height where there are higher temperatures at HFP nominal operating conditions.

The deformation in the inner clad is negative due to the creep induced by the irradiation and the higher outer coolant pressure. At the fuel rod axial centre, there is contact between fuel and clad at nominal conditions. This induces a plastic creep deformation and a deformation due to the strain caused by the fuel-clad contact.



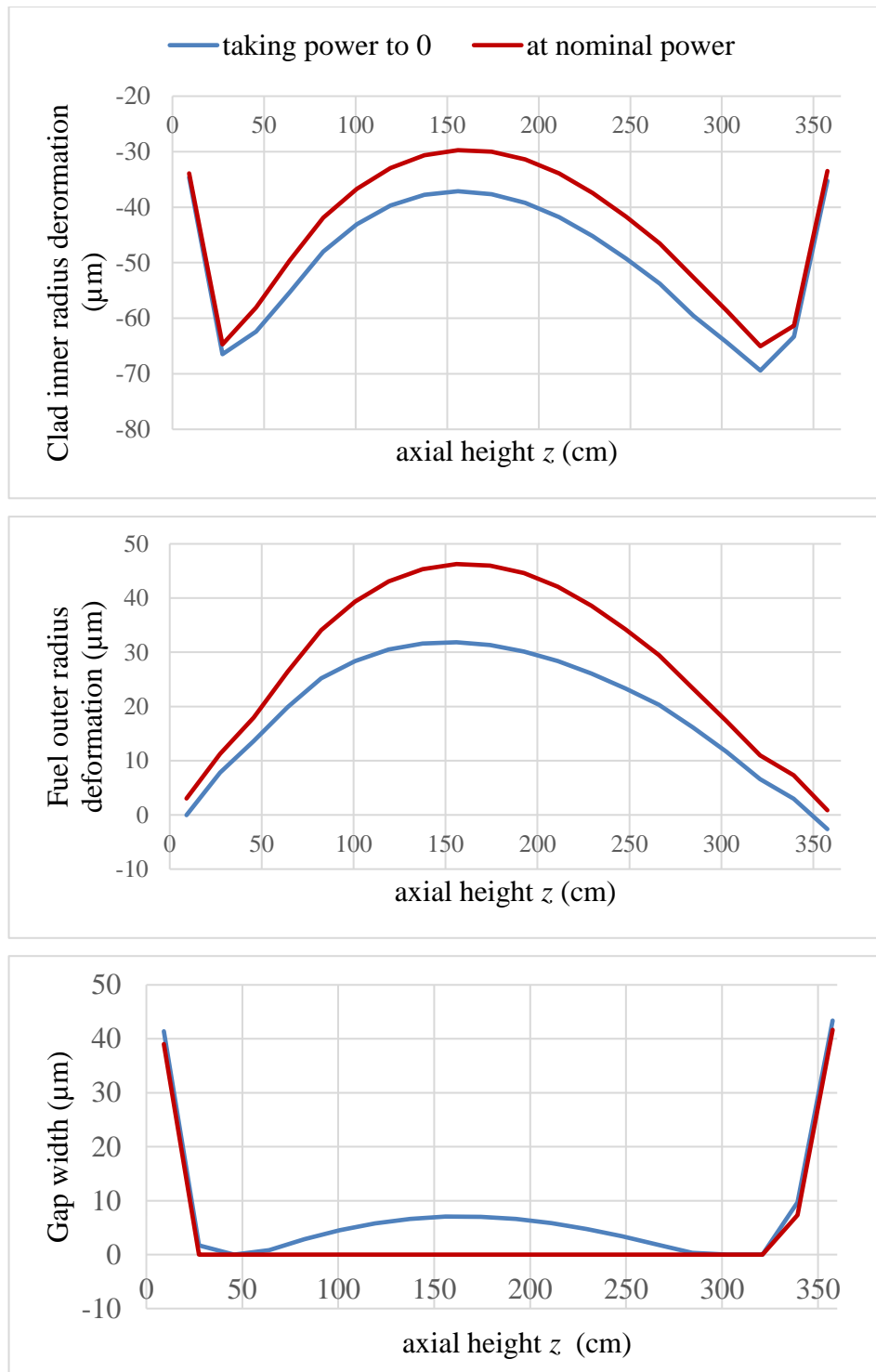


Figure 6-14. Calculated deformation of the outer fuel radius and inner clad radius during the transition from nominal power conditions to hot zero power conditions for a fuel with 37.5 GWd/tHM.

Going from HFP to HZP conditions the fuel temperature decreases, thus, the fuel pellet radius decreases and releases the strain off the clad causing the clad radius to diminish. However, the plastic deformation of the clad remains, which causes the gap reopening.



The reopening is higher in the centre of the rod height due to the higher change in temperature and fuel thermal expansion. And it goes to zero near top and bottom, where the contact between fuel and clad has just started and hence there is no clad plastic deformation.

This effect changes considerably the gap conductance, which plays a major role during the RIA transient and hence its accurate modelling is necessary.

### ***6.2.2 Discussion of the main results for the REA transient***

The RIA transient of the PWR UO<sub>2</sub>/MOX core loaded with fresh and burnt fuel is analysed with the developed coupled code PARCS-SCF-TU. Selected results of the two analysed REA cases (fresh/burnt) are compared and the importance of the inclusion of a fuel thermo-mechanics solver in the coupled system is analysed and discussed.

The total power evolution of the PWR core during the REA transient, predicted by PARCS-SCF-TU (PST) considering a core loading with fresh and burnt fuel as well as the results of PARCS-SCF using the URGAP model obtained for the benchmark are presented in Figure 6-15. It should be noted that the solution of PARCS-SCF URGAP model conditions are fresh conditions.

The peak predicted with the pre-irradiated fuel is 15% higher than that of the fresh (non-irradiated) fuel and 12% higher than the PARCS-SCF solution. This shows the impact that the more realistic modelling of the fuel properties by means of a coupled calculation with a fuel thermo-mechanics code has on the simulation. The solution for PARCS-SCF and PARCS-SCF-TU differ less than 3% in the power peak, verifying the correct implementation of the coupling. It must be noted that the obtained results with the more realistic solution using burnt conditions for the fuel, find themselves in a non-conservative side, since the predicted energy deposited in the fuel is higher as the one predicted without the fuel thermo-mechanics irradiation conditions.

The predicted higher power peak obtained in this work is consistent with other analysis found in the literature where other thermo-mechanics codes coupled to neutronics and thermo-hydraulics codes for REA analysis (Holt *et al.*, 2016; Le-Pallec, Mer-Nkongha and Crouzet, 2016; Nawaz *et al.*, 2016).

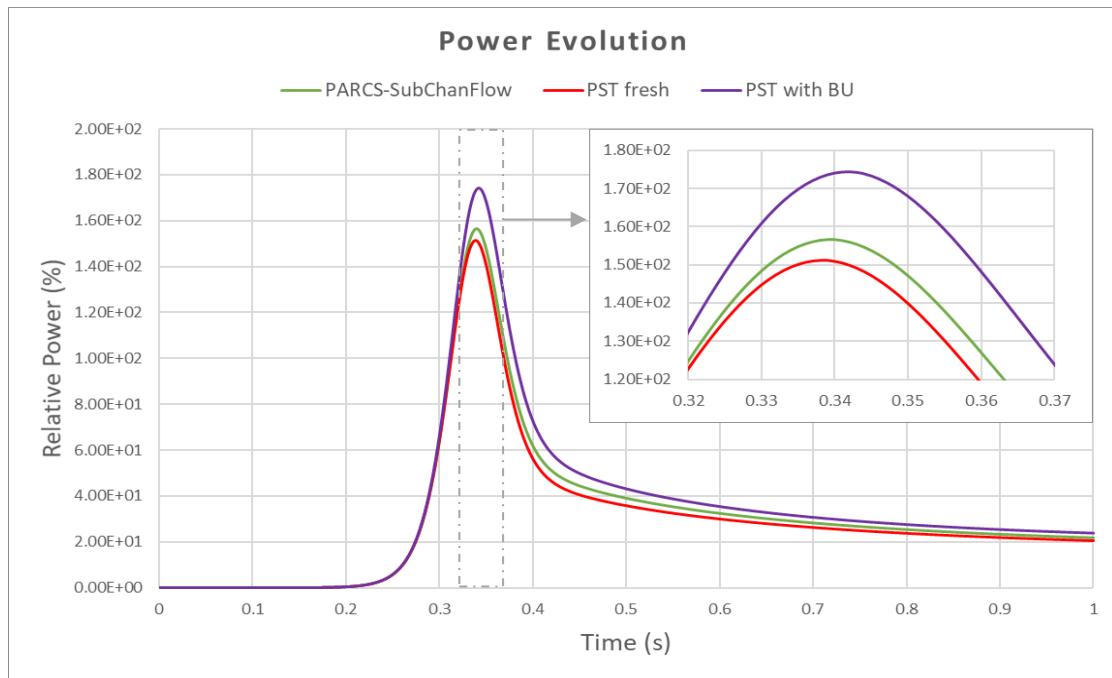


Figure 6-15. Power evolution during the RIA transient predicted by PARCS-SCF-TU (PST) fresh and with burn-up and by PARCS-SCF with the URGAP model with fresh fuel conditions. The case with burnup considers the fuel pre-irradiation with a more realistic modelling of the gap width, gap HTC and fuel material conductivity.

In order to understand the cause for the differences in the predicted results, a qualitative analysis for selected local parameters are discussed hereafter. The temperatures evolution for the fuel assembly L12 (UO<sub>2</sub> 4.2% enrichment, 37.5 GWd/tHM burn-up) where the CR is ejected is shown at different times in Figure 6-16 and Figure 6-17. In Figure 6-16, at time 0.34 sec (~peak time) the fuel centreline and fuel surface temperatures predicted by PARCS-SCF-TU burnt and fresh cases are shown.

The fuel centreline and surface temperature predicted by the coupled code PST considering the burnt core are lower than the ones of the fresh core. However, the cladding temperature predicted by PST with burnup is higher than the one for the fresh core. The reason for it is the fact that TU predicts more accurately the fuel rod behaviour including the gap width change and hence a larger heat transfer coefficient over the gap which leads to a higher cladding temperature and consequently a lower surface and centreline temperature for the case with burnup.

At this time, a large energy deposition in the fuel has occurred causing the rapid increase in the fuel temperature, but the energy is not yet released to the coolant, so the coolant temperature change is negligible.

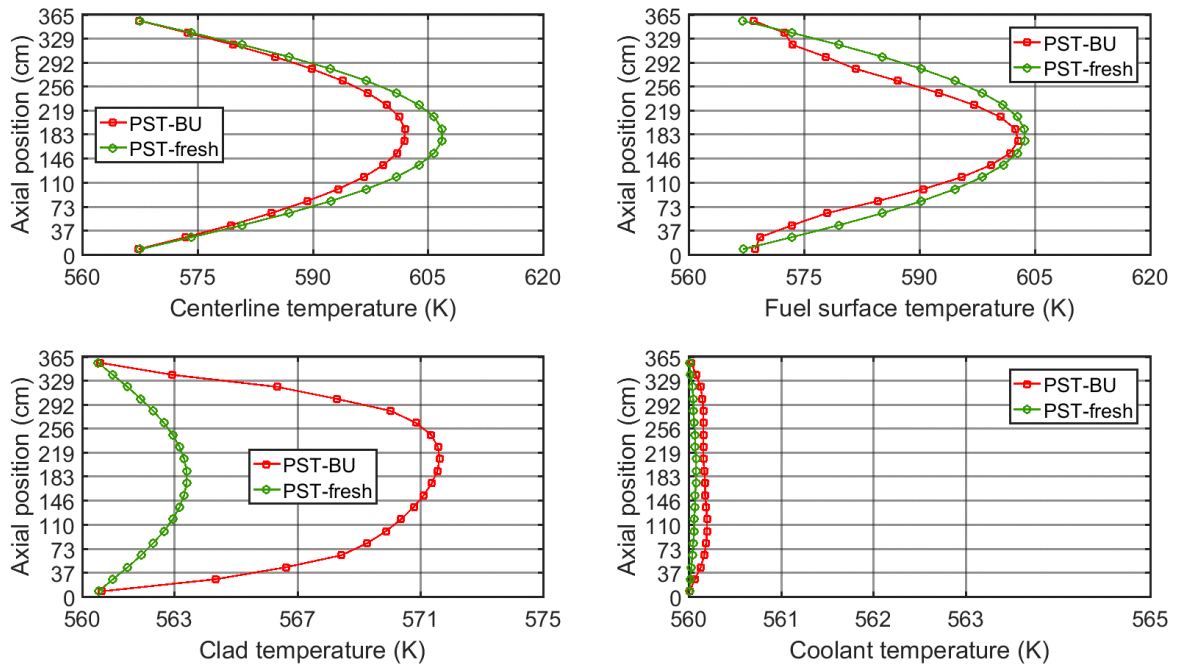


Figure 6-16. Centreline, fuel and clad average and coolant axial temperatures distribution for fuel assembly L12 (UO<sub>2</sub> 4.2% enrichment, 37.5 GWd/tHM burn-up) at time 0.34 sec.

At the end of the simulation in 1 sec (Figure 6-17), the centreline and surface temperatures predicted for the burnt case remains lower than for the fresh case. In addition, it can be observed that the cladding temperature and the coolant temperature increases due to the higher gap conductance, since TU is predicting in a more realistic manner the fuel behaviour of the burnt core.

This is also explaining why a higher power peak is reached. In both cases, the reactivity introduced by the control rod is the same, since the neutronics parameters at time zero are the same (this includes the cross sections and dynamic parameters like the delayed neutron fractions and neutron inverse velocity) and also the TH conditions at the beginning of the transient. For the power to stop increasing, the CR reactivity must be balanced by the Doppler negative reactivity which acts fast due to the rapid increase on the fuel temperature. To achieve similar temperatures, the power level of the model with burnup must be higher for two reasons:

- First, for a given power level, in the case with burnup the predicted surface and centreline temperature will be lower than the fresh case at the same power level due to the higher gap conductance. The higher gap conductance lowers the surface temperature and thus the Doppler temperature. Meaning, that to have a same temperature than in the fresh case, the power must be higher.

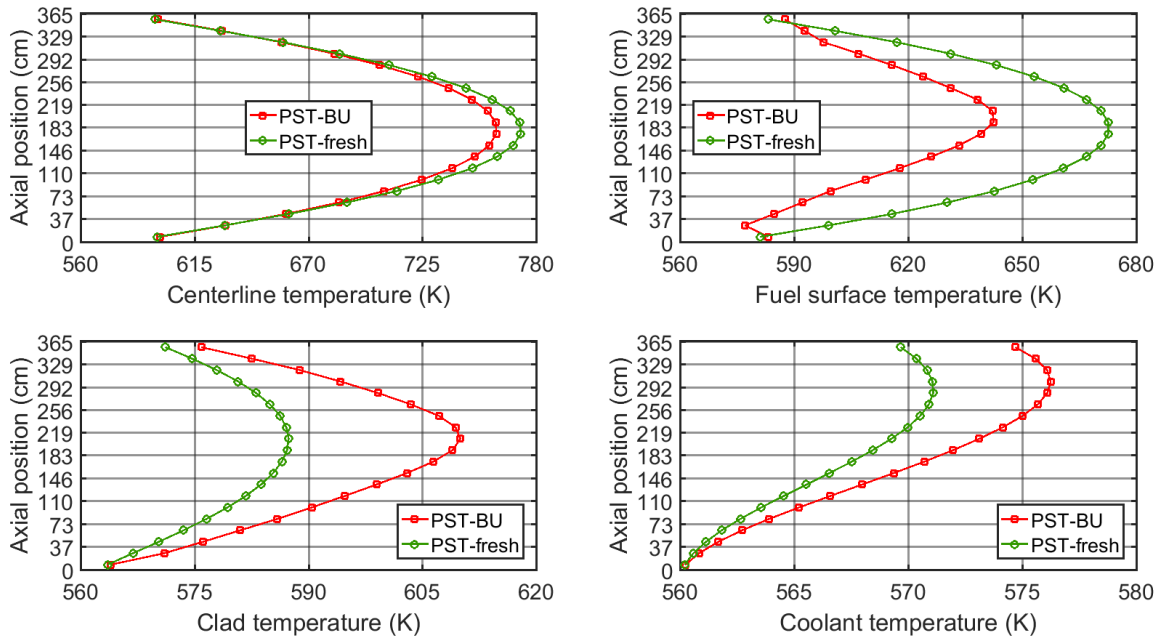


Figure 6-17. Centreline, fuel, clad average and coolant axial temperatures distribution for FA L12 (UO<sub>2</sub> 4.2% enrichment, 37.5 GWd/tHM burn-up) at time 1.00 sec.

- And second, in the burnt case there is a higher heat flux to the coolant due to a higher heat transfer coefficient, which lowers the fuel temperature and increases the coolant temperature. This effect is, however, of minor importance given that the transient is almost adiabatic up to the peak time.

As a result, the power must be higher in the burnt case to counteract the reactivity inserted by the control rod ejection. The analysis at other discrete times and fuel rod types can be found in Appendix B.2.

The calculated reactivity due to Doppler and coolant temperature feedbacks are shown in Figure 6-18. There, it can be seen how the Doppler feedback for the burnt fuel case is slightly lower than for the fresh case. In addition, the moderator density negative feedback is higher for the core with burnt fuel when compared to the one of the fresh core due to the enhanced gap conductance.

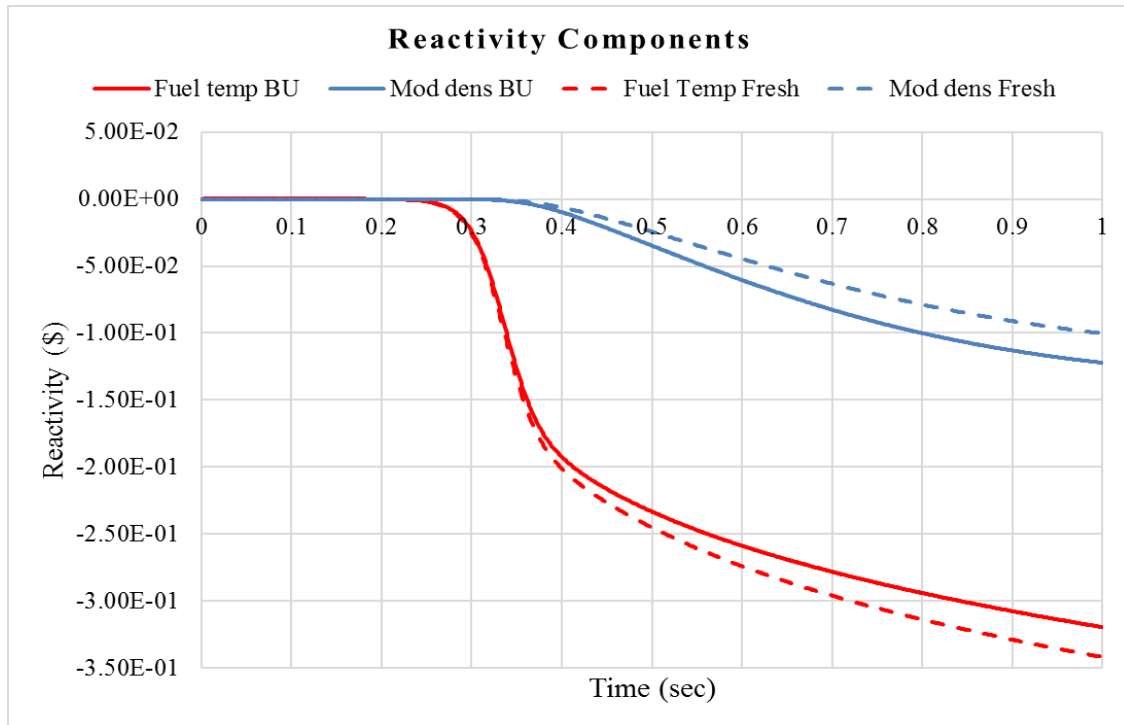


Figure 6-18. Moderator density and doppler temperature reactivity components predicted by PARCS-SCF-TU fresh and burnt during the REA evolution. The doppler temperature feedback predicted by PARCS-SCF-TU fresh is larger due to the smaller gap HTC which causes larger fuel temperatures. For the same reason, the energy deposited in the coolant is higher in the case of PARCS-SCF-TU with BU which causes higher coolant temperatures and a higher (negative) moderator density feedback.

During the REA transient, from  $t=0$  to  $t=1$  sec, a considerable change of the gap width and conductance along the core height can be observed, as illustrated in Figure 6-19 and Figure 6-20. The variation of these parameters can only be modelled by the integration of TRANURANUS in the coupled code PARCS-SCF and it emphasizes the importance of a thermo-mechanics solver in multiphysics simulations.

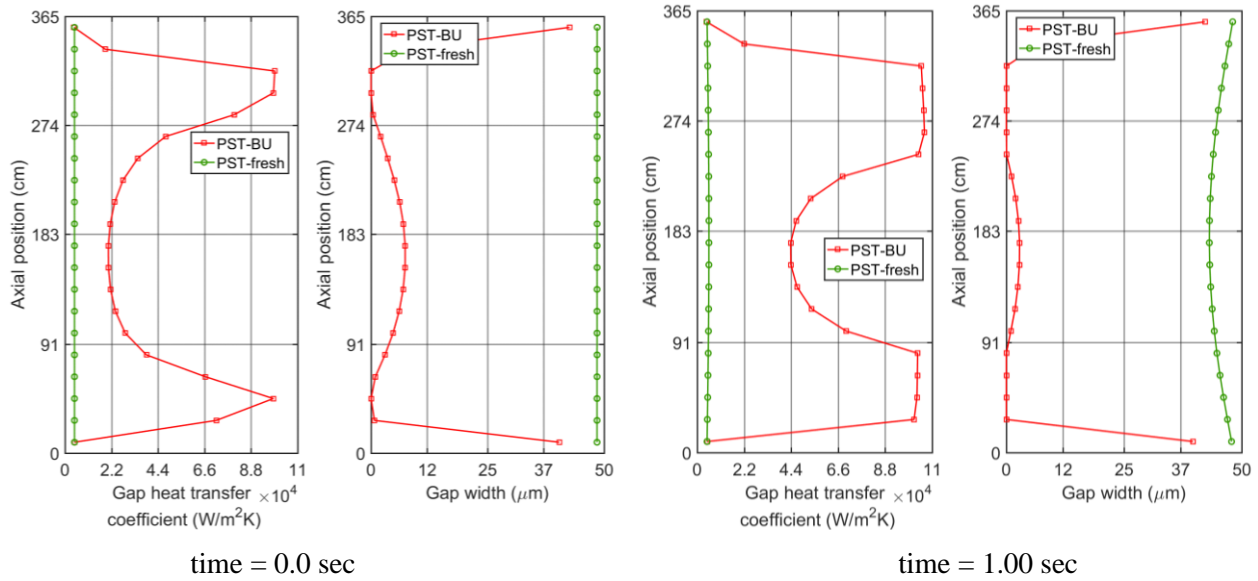


Figure 6-19. Gap width and gap heat transfer coefficient for the fuel rod corresponding to the FA L12, UO<sub>2</sub> 4.2% enrichment with 37.5 GWd/tHM BU at the beginning and end of the transient.

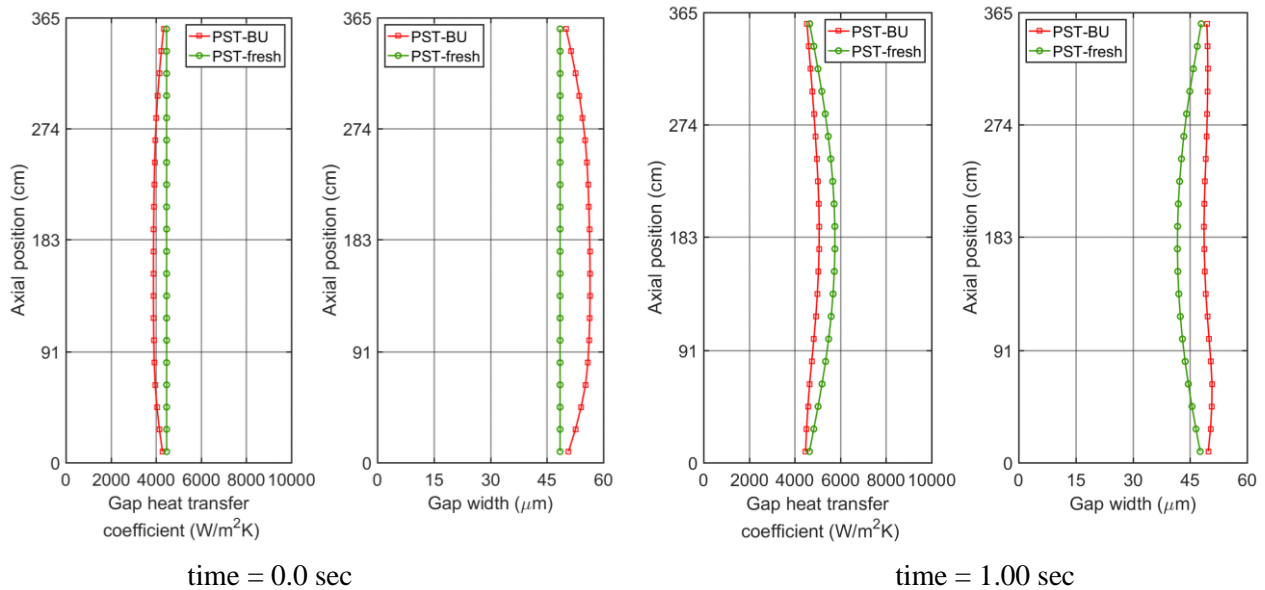


Figure 6-20. Gap width and gap heat transfer coefficient for the fuel rod corresponding to the FA L12, UO<sub>2</sub> 4.2% enrichment with 0.15 GWd/tHM BU at the beginning and end of the transient. The gap width is higher for the burnt rod due to the densification at low burnup, causing a lower HTC.

The accurate prediction of the energy deposited in the fuel is of safety relevance in the REA transient, since it determines the stress level on the fuel and clad (failure mode). In Figure 6-21, the fuel enthalpy added during the REA as predicted by PARCS-SCF-TU considering the burnup is exhibited (top).

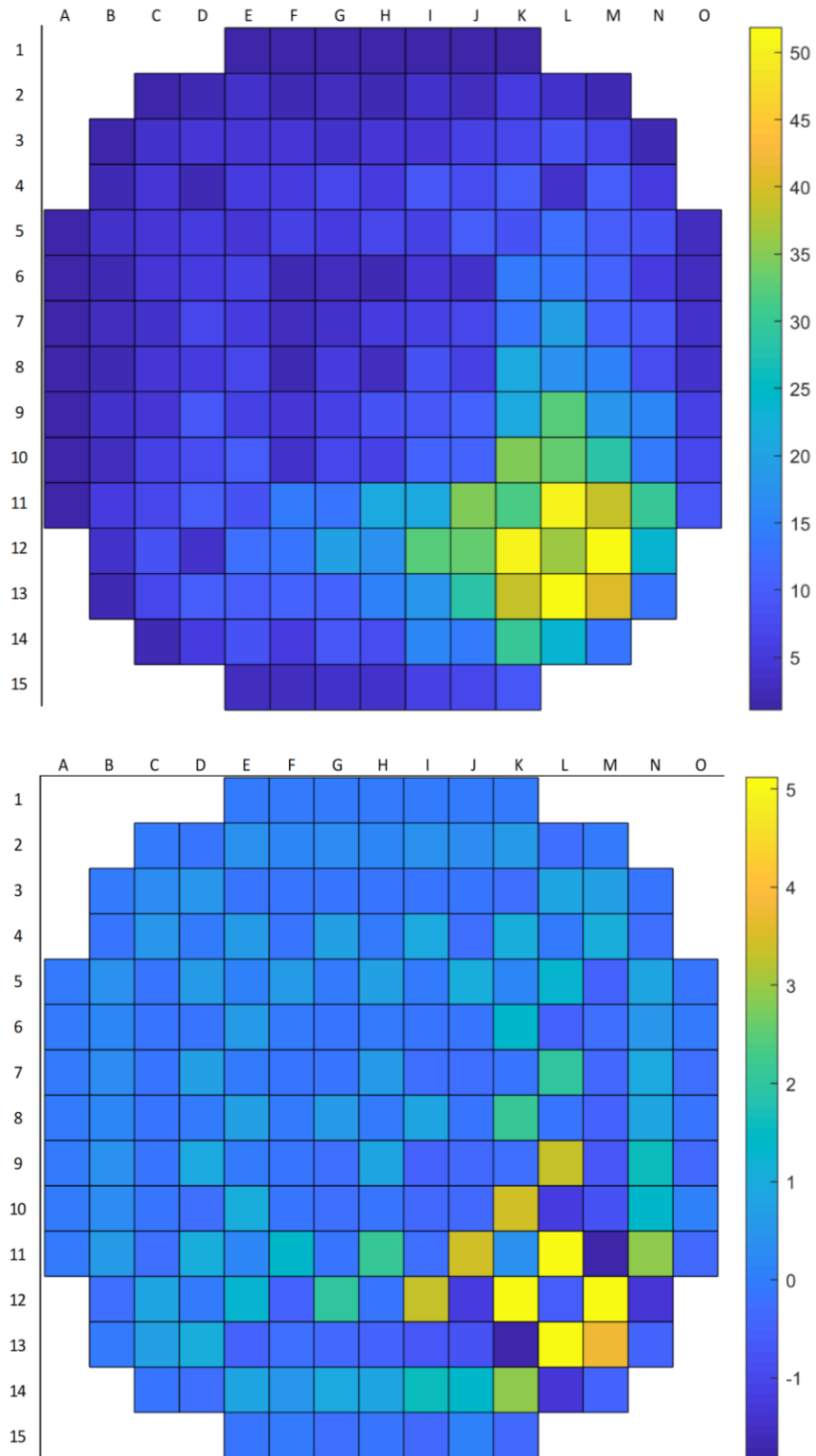


Figure 6-21. Fuel added enthalpy per fuel [J/g](BU) in REA transient at 1.0 sec. Left: results for burnt case, right: difference burnt-fresh case [J/g]. The higher power peak in the pre-irradiated simulation has therefore a higher the enthalpy difference. The biggest enthalpy difference occurs on the low burnup fuels surrounding the ejected control rod.

A maximal value of 51.8 J/g has been calculated with PARCS-SCF-TU with BU for the REA at position M12. This value is far below the safety limit fixed by the U.S. NRC regulation which sets a minimum of 418 J/g (100 cal/g) (Clifford, 2015) and the RSK (Reactor Safety Commission) in Germany which sets a minimum of 250 J/g (60 cal/g) (RSK, 2005). The enthalpy difference between the two PARCS-SCF-TU calculations for fresh and burnt cases is shown in Figure 6-21 (bottom). The obtained results are consistent with results found in the literature for HZP REA transients in PWR cores (Rudling *et al.*, 2016).

In general, the enthalpy deposited in the fuels is higher for the burnt case, with a maximum enthalpy difference between the simulations with and without burnup in a fuel with 0.15 GWd/tHM and it amounts to 5.1 J/g (10% higher) at position M12. It means that the not consideration of the real material composition and fuel rod state (burnt fuel), i.e. local gap width size and local heat transfer coefficient, at each fuel assembly along the core height prevailing before the REA-transient, leads to an under-prediction of this safety relevant parameter. Hence, showing that fixed parameters approach is not conservative with the current values.

These results underline the importance of the inclusion of a thermo-mechanics solver in addition to a neutronic and thermal-hydraulics one for a more realistic simulation of the behaviour of pre-irradiated fuel i.e. real core loadings of nuclear power plants.

Consequently, it can be concluded that the traditional approach of selecting a fixed HTC coefficient must be questioned given the significant impact of this parameter in the simulation results obtained in this study.



## ***7 Summary and Conclusions***

The goal of this thesis is to develop a coupled multiphysics code which allows a best estimate simulation of a nuclear reactor core by considering detailed physical phenomena such as crossflow in the thermal-hydraulics, and the detailed evolution of the fuel behaviour properties modelled by a fuel performance solver. Furthermore, by applying the developed coupled code, to assess the impact of a more detailed/realistic modelling in the reactor core calculations.

Thus, a new multiphysics coupled code consisting of a neutronics, a thermal-hydraulics, and a fuel thermo-mechanics solver has been developed by coupling the validated codes PARCS, SubChanFlow and TRANSURANUS.

In the first step, PARCS and SubChanFlow are internally coupled for static and transient simulations at fuel assembly level. The new PARCS-SCF code capabilities are demonstrated by applying it to a mini core and a full PWR core static behaviour, and by analysing a rod ejection accident. Emphasis has been put to analyse the advantages of having a subchannel code coupled to a 3D neutron kinetics code. Hence, the crossflow model of SubChanFlow is studied by simulating a PWR minicore, where a large power gradient is considered to observe the impact of the crossflow. The simulations with crossflow show a significant difference in the prediction of the outlet channel coolant temperature of up to 5.1 K, demonstrating the added crossflow capabilities and its impact in the simulation.

Moreover, an automatic methodology for the prediction of thermal hydraulics local safety parameters has been developed. By performing a nodal coupled simulation using PARCS-SCF plus the Pin Power Reconstruction (PPR) followed-up by a SubChanFlow standalone simulation at subchannel level. In this approach, the pin power predicted by PARCS/PPR is stored in memory to be used in an automatic way by SubChanFlow at subchannel level. Doing so, the local thermal-hydraulics safety parameters such as DNBR, maximal fuel and cladding temperatures can be predicted. This methodology is validated by a comparison of the solution with a fuel-pin/subchannel-level solution obtained with the high fidelity coupled code SERPENT-SubChanFlow, requiring orders of magnitude lower CPU-time than high the order solution at similar accuracies. The code-to-code comparison showed a very good agreement between the PARCS-SCF and the SERPENT-SCF solutions demonstrating the accuracy of the methodology.

In the following, the thermo-mechanics code TRASNURANUS has been coupled with PARCS-SCF. The coupling by means of an MPI-based parallel approach has been tested and verified by simulating the stationary plant conditions of a PWR UO<sub>2</sub>/MOX core at full power conditions considering the core loading with fresh and burnt fuel. The comparison of the obtained results for both cases has shown that the inclusion of TU in the coupled system PARCS-SCF allows a more realistic simulation of an irradiated fuel behaviour, especially in the REA transient simulation.

For the HFP steady state conditions, a large difference in the prediction of fuel centreline temperatures is found when comparing the best estimate with the traditional approach (up to 180 K of difference). In general, a decrease in the surface temperature is found in the best estimate approach, as consequence of the gap closure modelling, and a larger gradient between surface and centreline temperature is obtained due to the degradation of the pellet conductivity. The impact on the Doppler feedback for the steady state conditions is small, and hence the impact in the  $k_{\text{eff}}$  is not significant in the steady state simulation. However, the impact in the prediction of the fuel centreline temperatures is considerable.

A REA scenario for a PWR (UO<sub>2</sub>/MOX) with a fresh and burn core loading is investigated considering Hot Zero Power (HZP) conditions. The simulation of the HZP REA transient demonstrates the importance of the more realistic modelling of the gap conductance, the thermo-mechanical behaviour of the fuel and cladding, the fission gas release, etc. For higher burnup fuel rods, the increased gap conductance causes a higher energy transfer to the coolant, which leads to a faster increase of the coolant temperature and a consequently faster decrease of the fuel temperature in the transient. An increase on the cladding temperature is observed which is due to the gap closure and the modelling of a corrosion layer which decreases the clad to coolant transfer coefficient.

The REA power peak for the burnt case increases by 15% compared to the fresh case. This increase in the power peak translates directly in an increase of the added fuel enthalpy, which is about ~10% higher for case of the burnt core.

The selection of an HTC by expert judgement is a common practice in the RIA transient simulation. The results show that the use of the fixed HTC purposed in the benchmark is non-conservative and should be revised. If a fixed HTC is used in the calculations, its value should be further increased to obtain conservative results.

The studies performed in this work allow a better insight in the physics taking place in the reactor core and help to understand where a special effort should be put to improve the traditional simulation approach. In particular, the result obtained in the REA simulation elucidate the importance of the correct modelling of the fuel properties by means of a fuel performance code.

The developed code and the analysed problems pave the way for a better understanding of the core behaviour and a best estimate simulation of PWR cores.

## 8 Outlook

Based on the performed investigations, the following issues have been identified as an outlook to this work, to be tackled in the near to mid-term:

- **Extend the coupled code PARS-SCF-TU from a nodal level solution to a pin/sub-channel level solution in order to directly predict the fuel local safety parameters.**

This effort implies three important steps for its realization. First, the feedback at neutronic level must be possible. For this purpose, it is important to use the PARCS SP3-transport solver instead of the diffusion one since it allows a solution at pin level. Second, a coupling of SubChanFlow with PARCS at subchannel level considering a pin level thermal hydraulics feedback must be performed. In this sense it must be noticed that the problem size will increase by a factor of  $\sim 250$  (depending on the fuel geometry, e.g. 16x16, 18x18, etc.). Cross sections must be generated and stored in memory not only for a fuel type but for a fuel pin type. This increases the memory requirements considerably and generates another problem that must be tackled. And third, TRANSURANUS should be coupled at pin level. The same coupling approach used in this thesis could be directly transferred for the pin level simulation. The mapping methodology should be able to handle a pin by pin description. This implies a large demand of available memory to keep the TU calculation data, which would increase also a factor of  $\sim 250$ . The solution in a Linux server is necessary to be able to compute the solution with a larger number of parallel processes.

- **Improve the time step control of the coupled code by, e.g., applying an adaptive time stepping.**

This improvement requires the modification of the PARCS algorithms for time stepping. The adaptive time stepping requires retrieving the solution of the previous time point, meaning that the problem variables must be stored in memory. PARCS has already the capability of performing a restart, which can be adapted to be used in such algorithm. SubChanFlow does not have a restart capability and should be modified to be able to restart from a previous time point which demands a significant programming effort.

- **Consider the axial deformation of the fuel rods.**

Currently, the mechanical clad deformation calculated by TRANSURANUS is not taken into account explicitly as a feedback neither by the neutronics, nor the thermal hydraulics. This task implies modifications on the neutronics and thermal-hydraulics solvers to be able

to handle a deformation of the axial and radial geometry. The modifications in SubChanFlow could be implemented for instance as a change in the channel flow area. In the neutronics the deformation could be considered for instance by adding a new parameter in the XS parametrization which has into account the XS variation dependent with the rod diameter. In principle an increase in the rod diameter means a smaller moderator volume which implies a lower  $k_{inf}$ .

- **Look for appropriate data in order to validate the new coupled code.**

The full validation of the developed code should be done by comparing its predictions with plant measurements data. A PWR core model must be developed, considering the operation history of the reactor. An operating condition of the reactor must be selected, and the core configuration, the nodal burnup map distribution, as well as the CR position history, and reactor operation history is needed. To generate the cross sections the geometry and material composition for the fuel elements is needed. To generate the TRANSURANUS restarts the fuel characteristics and cycle history for all the fuels is necessary. As a first step the model development, an uncoupled HZP conditions should be modelled with PARCS to have a base case. Once such a working model is settled, the full coupled calculation can be developed. To validate the results, the boron concentration and power distribution should be calculated and compared against plant measured data.

- **Replace the internal coupling of PARCS-SCF-TU by a new general coupling approach.**

A general coupling approach implies generating a general interface between the codes which allow them to communicate between each other. In a sense, this interface exists already in the current coupling, however not in an explicit way. The task here is to define a protocol for communication between the codes which standardizes the variables to be sent and received, the domain nodalization, and the routines to calculate a steady state or advance a time step. This is for instance done in the Salome platform and could be done for instance using the ICoCo general interface, which is flexible and general purpose.

- **Apply uncertainty methods for the quantification of the uncertainties in the coupled simulations:**

Uncertainty propagation and sensitivity studies are nowadays a relevant topic in the reactor's simulations. There is an active research ongoing to develop methodologies which allow to quantify uncertainties in multiphysics simulations. This work is pursued for instance

in the best estimate plus uncertainty international conference (BEPU). This task is challenging because of the interdependence of the different codes. In this context, methods (such as statistical, Bayesian, and hybrid methods) must be developed to propagate uncertainties in a coupled simulation. Also, sensitivity methods should be developed and applied as supporting tools for the uncertainty analysis. Existing methodologies like SUSANIE or URANIE could be applied.

## References

Abarca, A., R. Miró, T. Barrachina, and G. Verdú. 2011. 'A procedure for coupled thermal-hydraulic subchannel and neutronics codes using COBRA-TF and PARCS', *International Nuclear Atlantic Conference*, ISBN: 978-85-99141-04-5. INIS report number: INIS-BR--11236. Available at: [http://www.iaea.org/inis/collection/NCLCollectionStore/\\_Public/43/056/43056350.pdf](http://www.iaea.org/inis/collection/NCLCollectionStore/_Public/43/056/43056350.pdf) (Accessed: 21 October 2019).

Allen, Todd, Jeremy Busby, Mitch Meyer, and David Petti. 2010. 'Materials challenges for nuclear systems', *Materials Today*, Vol. 13 (12), pp. 14–23. doi: 10.1016/S1369-7021(10)70220-0.

Amaya, Masaki, Mutsumi Hirai, Hiroshi Sakurai, Kenichi Ito, Masana Sasaki, Terumitsu Nomata, Katsuichiro Kamimura, and Ryo Iwasaki. 2002. 'Thermal conductivities of irradiated UO<sub>2</sub> and (U, Gd)O<sub>2</sub> pellets', *Journal of Nuclear Materials*, Vol. 300, pp. 57–64. doi: 10.1016/S0022-3115(01)00704-8.

AREVA. 2010. *COBRA-FLX: A Core Thermal-Hydraulic Analysis Code Topical Report, ANP-10311NP*. Available at: <https://www.nrc.gov/docs/ML1015/ML101550179.pdf> (Accessed: 21 October 2019).

Aufiero, Manuele, and Massimiliano Fratoni. 2017. 'A new approach to the stabilization and convergence acceleration in coupled Monte Carlo/CFD calculations: The Newton method via Monte Carlo perturbation theory', *Nuclear Engineering and Technology*, Vol. 49, pp. 1181–1188. doi: 10.1016/j.net.2017.08.005.

Aviles, Brian N., Daniel J. Kelly, David L. Aumiller, Daniel F. Gill, Brett W. Siebert, Andrew T. Godfrey, Benjamin S. Collins, and Robert K. Salko. 2017. 'MC21/COBRA-IE and VERA-CS multiphysics solutions to VERA core physics benchmark problem #6', *Progress in Nuclear Energy*, Vol. 101, pp. 338–351. doi: 10.1016/j.pnucene.2017.05.017.

Aybar, Hikmet S., and Pedro Ortego. 2005. 'A review of nuclear fuel performance codes', *Progress in Nuclear Energy*, Vol. 46(2), pp. 127–141. doi: 10.1016/j.pnucene.2005.01.004.

Bielen, Andrew Scott. 2015. *Sensitivity and Uncertainty Analysis of Multiphysics Nuclear Reactor Core Depletion (Doctoral Thesis)*. University of Michigan. Nuclear Engineering and Radiological Sciences Department. Ann Arbor, Michigan, USA. Available at: [https://deepblue.lib.umich.edu/bitstream/handle/2027.42/111444/asbiele\\_1.pdf?sequence=1&isAllowed=y](https://deepblue.lib.umich.edu/bitstream/handle/2027.42/111444/asbiele_1.pdf?sequence=1&isAllowed=y).

Blakely, Cole, Hongbin Zhang, and Heng Ban. 2018. 'Sensitivity analysis of VERA-CS and FRAPCON coupling in a multiphysics environment', *Annals of Nuclear Energy*, Vol. 111, pp. 683–701. doi: 10.1016/J.ANUCENE.2017.09.029.

Böer, R., and H. Finnemann. 1992. 'Fast analytical flux reconstruction method for nodal space time nuclear reactor analysis', *Annals of Nuclear Energy*, Vol. 19, pp. 617–628. doi: 10.1016/0306-4549(92)90006-W.

Calleja, M., J. Jiménez, U. Imke, and V. Sanchez. 2012. 'Extension of the Coupling between COBAYA3 and SUBCHANFLOW for the Simulation of Boron Dilution Transients', in *Annual Meeting of the Spanish Nuclear Society 2012*. INIS ref. number: 44113256, Cáceres (Spain), Oct 17-19, 2012.

Calleja Reyna, Manuel. 2013. *Improvements in Multi-physics and Multi-scale Methodologies for Safety-related Investigations of Pressurized Water Reactors within the NURESIM Platform*. INR-KIT, Fakultät für Maschinenbau, Karlsruhe. doi: 10.5445/IR/1000040466.

Chanaron, Bruno, Carol Ahnert, Nicolas Crouzet, Victor Sanchez, Nikola Kolev, Olivier Marchand, Soeren Kliem, and Angel Papukchiev. 2015. 'Advanced multi-physics simulation for reactor safety in the framework of the NURES SAFE project', *Annals of Nuclear Energy*, Vol. 84, pp. 166–177. doi: 10.1016/j.anucene.2014.12.013.

Clifford, Paul M. 2015. *Technical and Regulatory Basis for the Reactivity-Initiated Accident Acceptance Criteria and Guidance*. U.S. NRC. Report: ML14188C423. Available at: <https://www.nrc.gov/docs/ML1418/ML14188C423.pdf> (Accessed: 13 October 2019).

Cunningham, M. E., C. E. Beyer, P. G. Medvedev, and G. A. Berna. 2001. *FRAPTRAN: A Computer Code for the Transient Analysis of Oxide Fuel Rods*. U.S. NRC, NUREG/CR-6739, Vol. 1, PNNL-13576. Available at: <https://www.nrc.gov/docs/ML0125/ML012530260.pdf>. (Accessed: 20 September 2020)

Daebler, Miriam, Aleksandar Ivanov, Bart L. Sjenitzer, Victor Sanchez, Robert Stieglitz, and Rafael Macian-Juan. 2015. 'High-fidelity coupled Monte Carlo neutron transport and thermal-hydraulic simulations using Serpent 2/SUBCHANFLOW', *Annals of Nuclear Energy*, Vol. 83, pp. 352–375. doi: 10.1016/j.anucene.2015.03.040.

Daebler, Miriam, Nico Trost, Javier Jimenez, Victor Sanchez, Robert Stieglitz, and Rafael Macian-Juan. 2015. 'Static and transient pin-by-pin simulations of a full PWR core with the extended coupled code system DYN SUB', *Annals of Nuclear Energy*, Vol. 84, pp. 31–44. doi: 10.1016/J.ANUCENE.2014.09.057.

Downar, Thomas, Yunlin Xu, Volkan Seker, and Nathan Hudson. 2012. *PARCS v3.0 U.S. NRC Core Neutronics Simulator: Theory Manual*. Nuclear Engineering and Radiological Sciences Department, University of Michigan Ann Arbor, MI, USA.

Duderstadt, James J., and Louis J. Hamilton. 1976. *Nuclear Reactor Analysis*. Ann Arbor, ISBN:978-0471223634: John Wiley & Sons, Inc.

Ferraro, Diego, Manuel Garcia, Ville Valtavirta, Uwe Imke, Riku Tuominen, and Jaakko Leppanen. 2019. 'Serpent / SUBCHANFLOW pin-by-pin coupled transient calculations for a PWR minicore', *Annals of Nuclear Energy*, Vol. 137,(Accepted/In press). doi: 10.1016/j.anucene.2019.107090.

Finnemann, Hebert, and Aldo Galati. 1991. *NEACRP 3-D LWR Transient Benchmark. Final Specifications*. Erlangen. NEACRP-L-335 (Rev. 1). Available at: <https://www.oecd-neo.org/science/docs/1991/neacrp-l-1991-335.pdf> (Accessed: 21 October 2019).

García-Herranz, N., D. Cuervo, A. Sabater, G. Rucabado, S. Sánchez-Cervera, and E. Castro. 2017. 'Multiscale neutronics/thermal-hydraulics coupling with COBAYA4 code for pin-by-pin PWR transient analysis', *Nuclear Engineering and Design*, Vol. 321, pp. 38–47. doi: 10.1016/j.nucengdes.2017.03.017.

Geelhood, K. J., W. G. Luscher, and C. E. Beyer. 2011. *FRAPCON-3.4: A Computer Code for the Calculation of Steady-State, Thermal-Mechanical Behavior of Oxide Fuel Rods for High Burnup*, NUREG/CR-7022. Available at: <https://www.nrc.gov/docs/ML1110/ML11101A005.pdf> (Accessed: 21 October 2019).

Gomez-Torres, Armando Miguel, Victor Hugo Sanchez-Espinoza, Kostadin Ivanov, and Rafael Macian-Juan. 2012. 'DYN SUB: A high fidelity coupled code system for the evaluation of local safety parameters - Part I: Development, implementation and verification', *Annals of Nuclear Energy*, Vol. 48, pp. 123–129. doi: 10.1016/j.anucene.2012.05.011.

Gómez Torres, A. M. 2011. *Further Developments of Multiphysics and Multiscale Methodologies for Coupled Nuclear Reactor Simulations (Doctoral Thesis)*, Fakultät für



*Maschinenwesen*. Technical University of Munich.

Grahn, Alexander, Sören Kliem, and Ulrich Rohde. 2015. 'Coupling of the 3D neutron kinetic core model DYN3D with the CFD software ANSYS-CFX', *Annals of Nuclear Energy*, Vol. 84, pp. 197–203. doi: 10.1016/j.anucene.2014.12.015.

Grgić, Davor, Vesna Benčik, and Siniš Sadek. 2013. 'Coupled code calculation of rod withdrawal at power accident', *Nuclear Engineering and Design*, Vol. 261, pp. 285–305. doi: 10.1016/j.nucengdes.2012.10.026.

Gurecky, William, and Erich Schneider. 2016. 'Development of an MCNP6-ANSYS FLUENT Multiphysics Coupling Capability', *Proceedings paper in ICONE 2016. 26-30 June 2016*, Charlotte, North Carolina, USA. Paper ID: ICONE24-60937. doi: 10.1115/ICONE24-60937.

Hales, J. D., M. R. Tonks, F. N. Gleicher, B. W. Spencer, S. R. Novascone, R. L. Williamson, G. Pastore, and D. M. Perez. 2015. 'Advanced multiphysics coupling for LWR fuel performance analysis', *Annals of Nuclear Energy*, Vol. 84, pp. 98–110. doi: 10.1016/j.anucene.2014.11.003.

Harriague, S., G. Coroli, and E. J. Savino. 1980. 'BACO (Barra Combustible), a computer code for simulating a reactor fuel rod performance', *Nuclear Engineering and Design*, Vol. 56, pp. 91–103. doi: 10.1016/0029-5493(80)90173-9.

Henry, R., I. Tiselj, and L. Snoj. 2017. 'CFD/Monte-Carlo neutron transport coupling scheme, application to TRIGA reactor', *Annals of Nuclear Energy*, Vol. 110, pp. 36–47. doi: 10.1016/j.anucene.2017.06.018.

Holt, L., U. Rohde, M. Seidl, A. Schubert, P. Van Uffelen, and R. Macián-Juan. 2014. 'Development of a general coupling interface for the fuel performance code TRANSURANUS - Tested with the reactor dynamics code DYN3D', *Annals of Nuclear Energy*, Vol. 84, pp. 73–85. doi: 10.1016/j.anucene.2014.10.040.

Holt, L., U. Rohde, S. Kliem, S. Baier, M. Seidl, P. Van Uffelen, and R. Macián-Juan. 2016. 'Investigation of feedback on neutron kinetics and thermal hydraulics from detailed online fuel behavior modeling during a boron dilution transient in a PWR with the two-way coupled code system DYN3D-TRANSURANUS', *Nuclear Engineering and Design*, Vol. 297, pp. 32–43. doi: 10.1016/j.nucengdes.2015.11.005.

Hursin, Mathieu, Thomas J. Downar, and Brendan Kochunas. 2010. 'Consistent Comparison of Full Core PWR Reactivity Initiated Accident with the Method Of Characteristic Code DeCART and the Coarse Mesh Nodal Code PARCS', in *Physor 2010. 9-14 May 2010*, Pittsburgh, PA (United States), ISBN: 9781617820014, pp. 2486-2502.

IAEA-NDS. 2017. *ENDF: Evaluated Nuclear Data File*. (Online Site) Available at: <https://www-nds.iaea.org/exfor/endl.htm> (Accessed: 21 October 2019).

IAEA. 2019. *PRIS (Power Reactor Information System)*. (Online Site) Available at: <https://pris.iaea.org/PRIS/WorldStatistics/OperationalReactorsByType.aspx> (Accessed: 7 February 2020).

IAEA - Safety Assessment Section. 2003. *Safety margins of operating reactors Analysis of uncertainties and implications for decision making - IAEA-TECDOC-1332*. Available at: [http://www-pub.iaea.org/MTCD/publications/PDF/te\\_1332\\_web.pdf](http://www-pub.iaea.org/MTCD/publications/PDF/te_1332_web.pdf) (Accessed: 24 November 2017).

IAPWS. 2007. *Revised Release on the IAPWS Industrial Formulation 1997 for the Thermodynamic Properties of Water and Steam*. Lucerne, Switzerland. IAPWS R7-97(2012). Available at: <http://www.iapws.org/relguide/IF97-Rev.pdf> (Accessed: 27 October 2019).

Imke, Uwe, Victor Sanchez, and Armando Miguel Gomez-Torres. 2010. 'SUBCHANFLOW: A New Empirical Knowledge Based Subchannel Code', Jahrestagung Kerntechnik 2010, Berlin, 4.-6.Mai 2010 Berlin. INFORUM GmbH, 2010 CD-ROM Paper 202.

Imke, Uwe, and Victor Hugo Sanchez. 2012. 'Validation of the Subchannel Code SUBCHANFLOW Using the NUPEC PWR Tests (PSBT)', *Journal of Science and Technology of Nuclear Installations*, Vol. 2012, Article ID 465059. pp. 12. doi: 10.1155/2012/465059.

Ivanov, A., V. Sanchez, R. Stieglitz, and K. Ivanov. 2013. 'High fidelity simulation of conventional and innovative LWR with the coupled Monte-Carlo thermal-hydraulic system MCNP-SUBCHANFLOW', *Nuclear Engineering and Design*, Vol. 262, pp. 264–275. doi: 10.1016/j.nucengdes.2013.05.008.

Ivanov, A., V. Sanchez, and U. Imke. 2011. 'Development of a Coupling Scheme Between MCNP5 and Subchanflow for the Pin- and Fuel Assembly-Wise Simulation of LWR and Innovative Reactors', *M&C*, May 8-12, 2011, Rio de Janeiro, Brasil, Proc.on CD-ROM American Nuclear Society, Latin American Section, 2011. ISBN:9788563688002, INIS report number: INIS-BR--17242.

Ivanov, Kostadin, and Maria Avramova. 2007. 'Challenges in coupled thermal-hydraulics and neutronics simulations for LWR safety analysis', *Annals of Nuclear Energy*, Vol. 34(6), pp. 501–513. doi: 10.1016/j.anucene.2007.02.016.

Ivanov, Konstantin, Tara M. Beam, and Anthony J. Baratta. 1999. *Pressurized Water Reactor Main Steam Line Break (MSLB) Benchmark Volume I: Final Specifications*. Technical report NEA/NSC/DOC(99)8. Available at: [https://www.oecd-nea.org/jcms/pl\\_16766](https://www.oecd-nea.org/jcms/pl_16766) (Accessed: 20 September 2020).

Jareteg, Klas, Paolo Vinai, Srdjan Sasic, and Christophe Demazière. 2015. 'Coupled fine-mesh neutronics and thermal-hydraulics - Modeling and implementation for PWR fuel assemblies', *Annals of Nuclear Energy*, Vol. 84, pp. 244–257. doi: 10.1016/j.anucene.2015.01.037.

Kelly III, Daniel, Ann E. Kelly, Brian N. Aviles, Andrew T. Godfrey, Robert K. Salko, and Benjamin S. Collins. 2017. 'MC21/CTF and VERA multiphysics solutions to VERA core physics benchmark progression problems 6 and 7', *Nuclear Engineering and Technology*, Vol. 49, pp. 1326–1338. doi: 10.1016/j.net.2017.07.016.

Keyes, David E., Lois C McInnes, Carol Woodward, Gropp William, Eric Myra, Michael Pernice, and John Bell. 2013. 'Multiphysics simulations: Challenges and opportunities', *The International Journal of High Performance Computing Applications*, Vol. 27(1), pp. 4–83. doi: 10.1177/1094342012468181.

Koebke, Klaus, and Manfred R. Wagner. 1977. 'The determination of the pin power distribution in a reactor core on the basis of nodal coarse mesh calculations', *Atomkernenergie*, Vol. 30(2), pp. 136–141.

Kozlowski, T., and T. J. Downar. 2003. *OECD/NEA and US NRC PWR MOX/UO<sub>2</sub> Core Transient Benchmark, Final Specifications, Revision 2*. OECD/NEA. Working Party of the Physics of Plutonium Fuels and Innovative Fuel Cycles. NEA/NSC/DOC(2003)20.

Kozlowski, T., and T. J. Downar. 2007. *PWR MOX/UO<sub>2</sub> Core Transient Benchmark - Final Report*. OECD/NEA, Working Party on Scientific Issues of Reactor Systems. NEA/NSC/DOC(2006)20. ISBN 92-64-02330-5.

Lassmann, K. 1987. 'A fast and simple iteration scheme for the temperature calculation in a fuel rod', *Nuclear Engineering and Design*. North-Holland, Vol. 103(2), pp. 211–214. doi: 10.1016/0029-5493(87)90274-3.

- Lassmann, K. 1992. 'TRANSURANUS: a fuel rod analysis code ready for use', *Journal of Nuclear Materials*, Vol. 188, pp. 295–302. doi: 10.1016/0022-3115(92)90487-6.
- Lassmann, K., Shubert, A., Van Uffelen, P., Gyori, Cs., van de Laar, J.. 2015. 'Transuranus handbook', Institute for Transuranium Elements, European Commission Joint Research Centre, Karlsruhe.
- Lassmann, K., and F. Hohlefeld. 1987. 'The revised URGAP model to describe the gap conductance between fuel and cladding', *Nuclear Engineering and Design*. North-Holland, Vol. 103, pp. 215–221. doi: 10.1016/0029-5493(87)90275-5.
- Le-Pallec, J.C., K. Mer-Nkonga, and N. Crouzet. 2016. 'Neutronics/Fuel Thermo-Mechanics coupling in the Framework of a REA (Rod Ejection Accident) transient Scenario Calculation', in *Physor 2016*. Sun Valley, Idaho, pp. 2743–2757. ISBN: 978-0-89448-726-2.
- Liponi, Luca, Julien Taforeau, and Alain Hébert. 2017. 'Calculation and Verification of Assembly Discontinuity Factors for the DRAGON/PARCS code sequence', in *International Conference on Mathematics and Computational Methods Applied to Nuclear Science & Engineering Science, Nuclear*. 16 – 20 April 2017, Jeju, Korea. ISBN: 978-1-5108-5645-5. PaperID: P009.
- Liu, Rong, Andrew Prudil, Wenzhong Zhou, and Paul K. Chan. 2016. 'Multiphysics coupled modeling of light water reactor fuel performance', *Progress in Nuclear Energy*, Vol. 91, pp. 38–48. doi: 10.1016/j.pnucene.2016.03.030.
- Lochbaum, Dave. 2014. *Preventing Fuel Damage in Nuclear Reactors*. (Online Site) Available at: <https://allthingsnuclear.org/dlochbaum/preventing-fuel-damage-in-nuclear-reactors> (Accessed: 28 October 2019).
- Magedanz, J., M. Avramova, Y. Perin, and A. K. Velkov. 2015. 'High-fidelity multi-physics system TORT-TD/CTF/FRAPTRAN for light water reactor analysis', *Annals of Nuclear Energy*, Vol. 84, pp. 234–243. doi: 10.1016/j.anucene.2015.01.033.
- Mahadevan, Vijay S., and Jean C. Ragusa. 2007. *Coupling Schemes for Multiphysics Reactor Simulation*. Idaho National Laboratory, Idaho Falls, Report: INL/EXT-07-13490.
- Michel, B., J. Sercombe, G. Thouvenin, and R. Chatelet. 2008. '3D fuel cracking modelling in pellet cladding mechanical interaction', *Engineering Fracture Mechanics*, Vol. 75(11), pp. 3581–3598. doi: 10.1016/j.engfracmech.2006.12.014.
- Mylonakis, A. G., M. Varvayanni, N. Catsaros, P. Savva, and D. G. E. Grigoriadis. 2014. 'Multi-physics and multi-scale methods used in nuclear reactor analysis', *Annals of Nuclear Energy*, Vol. 72, pp. 104–119. doi: 10.1016/j.anucene.2014.05.002.
- Mylonakis, Antonios G., Melina Varvayanni, and Nicos Catsaros. 2016. 'On-the-fly towards Pure Monte-Carlo Transient Reactor Core Analysis', in *Proceedings of the International Conference Nuclear Energy for New Europe*. September 5 - 8, 2016, Portoroz, Slovenia. Paper No. 305, ISBN: 978-961-6207-40-9. Available at: [http://www.nss.si/proc/nene2016/html/pdf/NENE2016\\_304.pdf](http://www.nss.si/proc/nene2016/html/pdf/NENE2016_304.pdf) (Accessed: 21 October 2019).
- Mylonakis, Antonios G., M. Varvayanni, and N. Catsaros. 2017. 'A Newton-based Jacobian-free approach for neutronic-Monte Carlo/thermal-hydraulic static coupled analysis', *Annals of Nuclear Energy*, Vol. 110, pp. 709–725. doi: 10.1016/j.anucene.2017.07.014.
- Nawaz, Amjad, Yoshikawa Hidekazu, Ming Yang, and Anwar Hussain. 2016. 'Comparative analysis of RIA and LOCA with and without fuel rod behavior modeling in THEATRe code', *Progress in Nuclear Energy*, Vol. 93, pp. 133–145. doi: 10.1016/j.pnucene.2016.08.009.

- Noori-Kalkhoran, Omid, Abdolhamid Minuchehr, Amir Saied Shirani, and Mohammad Rahgoshay. 2014. 'Full scope thermal-neutronic analysis of LOFA in a WWER-1000 reactor core by coupling PARCS v2.7 and COBRA-EN', *Progress in Nuclear Energy*, Vol. 74, pp. 193–200. doi: 10.1016/j.pnucene.2014.03.006.
- Novascone, S. R., B. W. Spencer, D. Andrs, R. L. Williamson, J. D. Hales, and D. M. Perez. 2013. 'Results from Tight and Loose Coupled Multiphysics in Nuclear Fuels Performance Simulations Using BISON', in *International Conference on Mathematics and Computational Methods Applied to Nuclear Science & Engineering*. Sun Valley, Idaho, pp. 1285-1296, INL/CON-13-28275.
- nuclear reactor fuel types - Encyclopedia Britannica*. 2013. (Online Site) Available at: <https://www.britannica.com/technology/nuclear-reactor/Fuel-types> (Accessed: 29 July 2019).
- O'Donnell, G. M., H. H. Scott, and R. O. Meyer. 2001. *A New Comparative Analysis of LWR Fuel Designs*. Washington. U.S. NRC, Report: NUREG-1754. Available at: <https://www.nrc.gov/docs/ML0136/ML013650469.pdf> (Accessed: 21 October 2019).
- OECD/NEA. 2004a. *Neutronics/Thermal-hydraulics Coupling in LWR Technology, Vol. 3*. ISBN: 92-64-02085-3. Available at: <https://www.oecd-nea.org/science/docs/pubs/nea5434-crissue-s-vol3.pdf> (Accessed: 21 October 2019).
- OECD/NEA. 2004b. *Neutronics/Thermal-hydraulics Coupling in LWR Technology Vol. 1*. ISBN 92-64-02083-7. Available at: <https://www.oecd-nea.org/science/docs/pubs/nea4452-crissue-s-vol1.pdf> (Accessed: 21 October 2019).
- OECD/NEA. 2010. *Nuclear Fuel Behaviour during Reactivity Initiated Accident (RIA) Conditions*. ISBN 978-92-64-99113-2. Available at: <https://www.oecd-nea.org/nsd/reports/2010/nea6847-behaviour-RIA.pdf> (Accessed: 21 October 2019).
- Olander, D. 2009. 'Nuclear fuels - Present and future', *Engineering Journal*, Vol.13 no.1, pp. 1–28. doi: 10.4186/ej.2009.13.1.1.
- Palmtag, Scott, Kevin Clarno, Greg Davidson, Tom Evans, John Turner, Kenneth Belcourt, Russell Hooper, and Rod Schmidt. 2014. 'Coupled Neutronics and Thermal-Hydraulic Solution of a Full-Core PWR Using VERA-CS', in *Physor 2014*. Kyoto, Japan, Paper No. 1127524. doi: 10.11484/jaea-conf-2014-003.
- Peña, C., F. Pellacani, S. Chiva, R. Miró, and R. Macián Juan. 2011. 'CFD-Neutronic Coupled Calculation of a Quarter of a Simplified PWR Fuel Assembly including spacer pressure drop and trubulence enhancement', in *International Nuclear Atlantic Conference*. Belo Horizonte, Brazil. ISBN: 978-85-99141-04-5. Available at: [https://inis.iaea.org/collection/NCLCollectionStore/\\_Public/43/046/43046438.pdf](https://inis.iaea.org/collection/NCLCollectionStore/_Public/43/046/43046438.pdf) (Accessed: 21 October 2019).
- Perin, Yann, and Kiril Velkov. 2017. 'CTF/DYN3D multi-scale coupled simulation of a rod ejection transient on the NURESIM platform', *Nuclear Engineering and Technology*, Vol. 49, pp. 1339–1345. doi: 10.1016/j.net.2017.07.010.
- Philip, Bobby, Mark A. Berrill, Srikanth Allu, Steven P. Hamilton, Rahul S. Sampath, Kevin T. Clarno, and Gary A. Dilts. 2015. 'A parallel multi-domain solution methodology applied to nonlinear thermal transport problems in nuclear fuel pins', *Journal of Computational Physics*, Vol. 286, pp. 143–171. doi: 10.1016/j.jcp.2015.01.029.
- Ragusa, Jean C., and Vijay S. Mahadevan. 2009. 'Consistent and accurate schemes for coupled neutronics thermal-hydraulics reactor analysis', *Nuclear Engineering and Design*, Vol. 239(3), pp. 566–579. doi: 10.1016/j.nucengdes.2008.11.006.

- Rempe, K. R., Kord S. Smith, and A. F. Henry. 1989. 'SIMULATE-3 Pin Power Reconstruction: Methodology and Benchmarking', *Nuclear Science and Engineering*, Vol. 103(4), pp. 334–342. doi: 10.13182/NSE89-A23686.
- Ronchi, C., M. Sheindlin, D. Staicu, and M. Kinoshita. 2004. 'Effect of burn-up on the thermal conductivity of uranium dioxide up to 100.000 MWdt-1', *Journal of Nuclear Materials*, Vol. 327(1), pp. 58–76. doi: 10.1016/j.jnucmat.2004.01.018.
- Rossiter, Glyn, Ian Palmer, and Robert Gregg. 2011. 'Development of the ENIGMA fuel performance code for whole core analysis and dry storage assessment', *Nuclear Engineering and Technology*, Vol. 43, pp. 489–498. doi: 10.5516/NET.2011.43.6.489.
- RSK. 2005. 'Safety aspects of the use of high burn-up fuel elements under reactivity accident conditions (RSK Statement 27.01.2005 - 379. Sitzung)'. Germany. Available at: <http://www.rskonline.de/sites/default/files/reports/epanlage2rsk379hpen.pdf> (Accessed: 15 October 2019).
- Rudling, Peter, Lars Olof Jernkvist, Friedrich Garzarolli, Ron Adamson, Tahir Mahmood, Alfred Strasser, and Charles Patterson. 2016. *Nuclear Fuel Behaviour under RIA Conditions*. (A.N.T. International Report), ReportID: ZIRAT21/IZNA16. Mölnlycke, Sweden. Available at: [https://www.antinternational.com/docs/samples/FM/06/IZNA16-ZIRAT21\\_RIA\\_Sample.pdf](https://www.antinternational.com/docs/samples/FM/06/IZNA16-ZIRAT21_RIA_Sample.pdf) (Accessed: 21 October 2019).
- Sjenitzer, Bart L., and J. Eduard Hoogenboom. 2011. 'A Monte Carlo Method for Calculation of the Dynamic Behaviour of Nuclear Reactors', *Progress in nuclear Science and Technology*, Vol. 2, pp. 716–721. doi: 10.15669/pnst.2.716.
- Smith, Kord, and Benoit Forget. 2013. 'Challenges in the development of high-fidelity LWR core neutronics tools', in *International Conference on Mathematics and Computational Methods Applied to Nuclear Science and Engineering, M and C 2013*. Sun Valley, Idaho, pp. 1809–1825.
- Smith, K. S. 1986. 'Assembly Homogenization Techniques for Light Water Reactor Analysis', *Progress in Nuclear Energy*, Vol. 17(3), pp. 303–335. doi: 10.1016/0149-1970(86)90035-1.
- Snell, Victor G. 2015. 'The Essential CANDU, A Textbook on the CANDU Nuclear Power Plant Technology - Chapter 13 - Reactor Safety Design and Safety Analysis', (Web-based textbook) University Network of Excellence in Nuclear Engineering (UNENE). ISBN 0-9730040. Available at: <http://www.nuceng.ca/candu/pdf/13 - Reactor Safety Design and Safety Analysis.pdf> (Accessed: 21 October 2019).
- Staicu, D., C. Cozzo, G. Pagliosa, D. Papaioannou, S. Bremier, V. V. Rondinella, C. T. Walker, and A. Sasahara. 2011. 'Thermal conductivity of homogeneous and heterogeneous MOX fuel with up to 44 MWd/kgHM burn-up', *Journal of Nuclear Materials*, Vol. 412, pp. 129–137. doi: 10.1016/j.jnucmat.2011.02.042.
- Targa, A., J.-C. Le Pallec, P. Le Tallec, K. Nkonga, N. Crouzet, and S. Chemin. 2016. 'Thermohydraulics - Thermomechanics Best Estimate coupled approach in a Rod Ejection Accident core calculation', in *Proceedings of ICAPP 2016*. April 17-20, 2016, San Francisco, CA, USA. ISBN: 978-0-89448-725-5. PaperID: 16405. pp. 1926-1935.
- Thomas, J. W., H. C. Lee, T. J. Downar, T. Sofu, D. P. Weber, H. G. Joo, and J. Y. Cho. 2003. 'The Coupling of the STAR-CD Software to a Whole-Core Neutron Transport Code DECART for PWR Applications', in *International Conference on Supercomputing in Nuclear Applications*. 22-24 September 2003, Paris. INIS report number: INIS-FR--2660. Available at: [http://www.iaea.org/inis/collection/NCLCollectionStore/\\_Public/35/106/35106298.pdf?r=1](http://www.iaea.org/inis/collection/NCLCollectionStore/_Public/35/106/35106298.pdf?r=1) (Accessed: 21 October 2019).

- Tong, L. S. 1967. 'Heat transfer in water-cooled nuclear reactors', *Nuclear Engineering and Design*. Vol. 6(4), pp. 301–324. doi: 10.1016/0029-5493(67)90111-2.
- U.S. NRC. 2007. *Reactor Concepts Manual Pressurized Water Reactor Systems*. (Online Site) Available at: <https://www.nrc.gov/reading-rm/basic-ref/students/for-educators/04.pdf> (Accessed: 21 October 2019).
- Valtavirta, Ville, Jaakko Leppänen, and Tuomas Viitanen. 2017. 'Coupled neutronics-fuel behavior calculations in steady state using the Serpent 2 Monte Carlo code', *Annals of Nuclear Energy*, Vol. 100, pp. 50–64. doi: 10.1016/j.anucene.2016.10.015.
- Van Brutzel, L., R. Dingreville, and T. J. Bartel. 2015 'State-of-the-Art Report on Multi-scale Modelling of Nuclear Fuels - Chapter 2. Nuclear fuel deformation phenomena.' *NEA Report: NEA/NSC/R(2015)5*. Available at: [http://www.iaea.org/inis/collection/NCLCollectionStore/\\_Public/47/032/47032408.pdf](http://www.iaea.org/inis/collection/NCLCollectionStore/_Public/47/032/47032408.pdf) (Accessed: 18 August 2019).
- Vazquez, Miriam, Haileyesus Tsige-Tamirat, Luca Ammirabile, and Francisco Martin-Fuertes. 2012. 'Coupled neutronics thermal-hydraulics analysis using Monte Carlo and sub-channel codes', *Nuclear Engineering and Design*, Vol. 250, pp. 403–411. doi: 10.1016/j.nucengdes.2012.06.007.
- Vitkova, M., B. Kalchev, and S. Stefanova. 2005. 'Regulatory requirements to the thermal-hydraulic and thermal-mechanical computer codes', in *International conference on WWER fuel performance, modelling and experimental support*. 19 – 23 September 2005 Albena, Bulgaria. INIS reference number: INIS-BG--1107: Available at: [http://www.iaea.org/inis/collection/NCLCollectionStore/\\_Public/37/098/37098345.pdf](http://www.iaea.org/inis/collection/NCLCollectionStore/_Public/37/098/37098345.pdf) (Accessed: 24 October 2017).
- Ward, A., Y. Xu, and T. Downar. 2013. *GenPMAXS-v6.1.1, Code for Generating the PARCS Cross Section Interface File PMAXS*. University of Michigan, Nuclear Engineering and Radiological Sciences Department, Ann Arbor, Michigan.
- Whittle, Karl. 2016. 'Nuclear materials science, Nuclear Fuel, part 2: Operational effects.' (E-Book) IOP Publishing Ltd. doi: 10.1088/978-0-7503-1104-5. Print ISBN: 978-0-7503-1105-2
- Williamson, R. L., J. D. Hales, S. R. Novascone, G. Pastore, D. M. Perez, B. W. Spencer, and R. C. Martineau. 2013. 'Overview of the BISON Multidimensional Fuel Performance Code', in *IAEA Technical Meeting on Modeling of Water-Cooled Fuel Including Design Basis and Severe Accidents*. 28 Oct - 1 Nov 2013, Chengdu China. INL/CON-13-29588. Available at: <https://inldigitallibrary.inl.gov/sites/sti/sti/5883302.pdf> (Accessed: 21 October 2019).
- Wu, Xu, and Tomasz Kozłowski. 2015. 'Coupling of system thermal-hydraulics and Monte-Carlo code: Convergence criteria and quantification of correlation between statistical uncertainty and coupled error', *Annals of Nuclear Energy*, Vol. 75, pp. 377–387. doi: 10.1016/j.anucene.2014.08.016.
- Yilmaz, Mine O., Maria N. Avramova, and Jens G. M. Andersen. 2017. 'Multi-physics code system with improved feedback modeling', *Progress in Nuclear Energy*, Vol. 98, pp. 94–108. doi: 10.1016/j.pnucene.2017.03.007.

# Appendices

## A. Neutronics/thermal-hydraulics coupling

### A.1 PARCS-SCF coupling extra results

Extra results are presented to further support the validation of the PARCS-SCF coupling.

#### *HFP steady state simulation*

Part II of the benchmark is the steady state critical boron concentration calculation at hot full power (HFP) conditions. In this part the TH feedback at full power condition is tested and the correct variable transfer and convergence is proved.

The HFP steady state simulation corresponds to a case with all the CR out. The results for PARCS standalone are compared to PARCS-SCF with crossflow. The axially integrated power distribution is shown in Figure A-1 for PARCS standalone (a) and the relative difference with the PARCS-SCF solution. The relative difference in the power presents a maximum difference of 0.7 % showing a good agreement between the solutions.

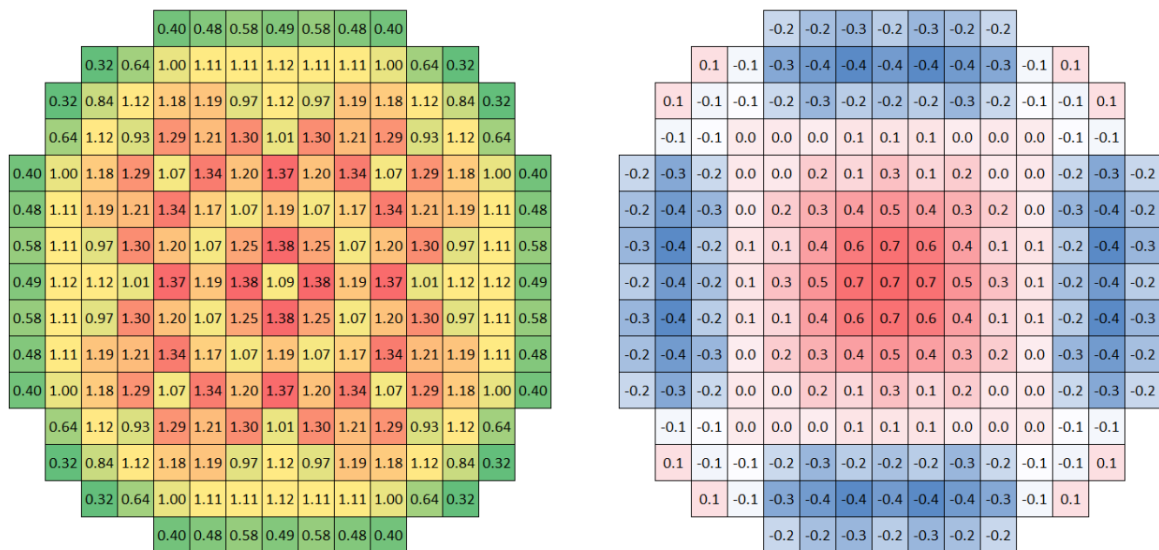


Figure A-1. Axially integrated power distribution predicted by PARCS Standalone (left) and relative difference with PARCS-SCF  $\frac{(P_{PARCS-SCF} - P_{PARCS stdl}) \cdot 100}{P_{PARCS stdl}}$  (right).

In Figure A-2, the outlet moderator temperature distribution predicted by PARCS standalone (a) and the absolute temperature difference between the standalone and the

PARCS-SCF solution is exhibited (b). A maximum difference of 1 K is found for the central channel which is due to the crossflow in the solution.

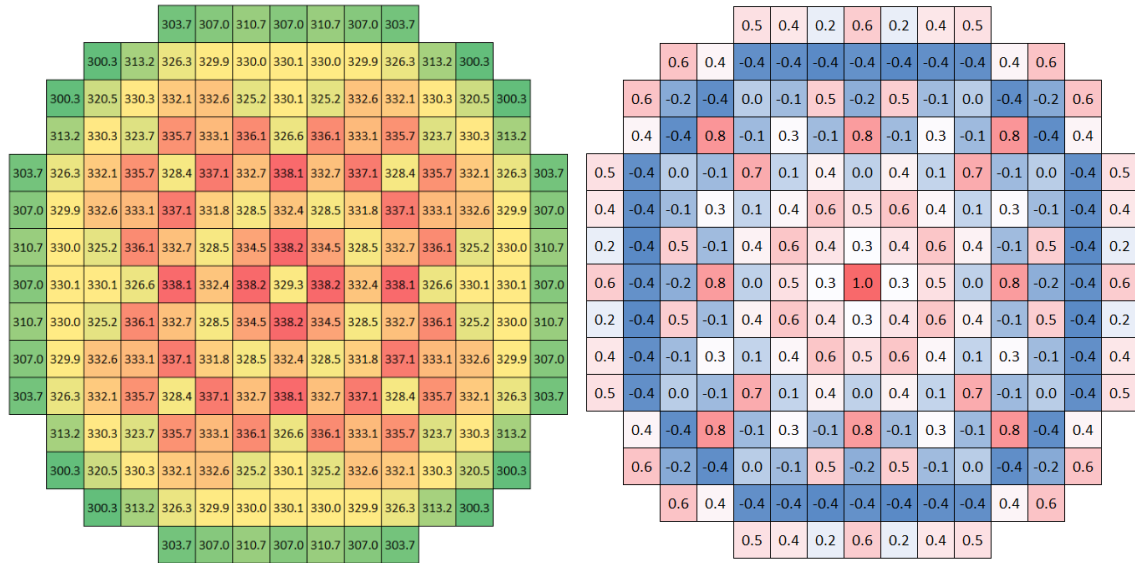


Figure A-2. Predicted outlet moderator temperature (°C) distribution (left) predicted by PARCS, and temperature difference between the PARCS and PARCS-SCF predictions ( $P_{PARCS-SCF} - P_{PARCS\ std}$ ).



### Subchannel level coupling: Comparison with channel level simulation

A 3x3 minicore is calculated at nodal level and subchannel level with PARCS-SCF and a comparison for the solutions is presented. This comparison is a first step in the verification process and the goal is to demonstrate the correct energy balance and the impact in the local solution. Therefore, the outlet coolant temperature of the nodal solution is compared with the bundle average outlet coolant temperature solution at subchannel level. The average temperature is calculated using the enthalpy values as described in Chapter 4.

The minicore configuration is the same in the dimensions to the presented in Appendix C.1. In this case, only the UO<sub>2</sub> FA type is in the core and no control rod is considered, as shown in Figure A-3. The TH conditions for the simulation are the same that presented in Table C-1.

For the comparison, the subchannel level solution was averaged into channels (average fuel assembly) to compare it against the channel level solution. Figure A-4 shows the moderator temperature distribution for PARCS-SCF at nodal level and a comparison with the bundle average subchannel level solution. The difference between both models is less than 0.15 K for the outlet temperature showing the correct energy balance in the subchannel level solution.

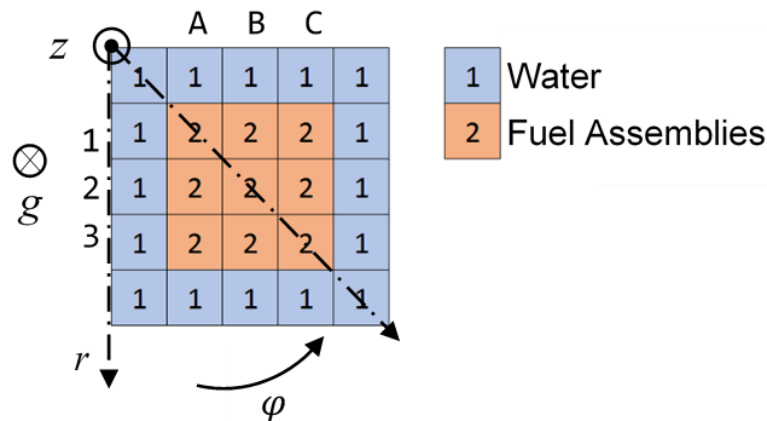


Figure A-3. 3x3 Minicore layout, representation of an axial slice. The core consists of nine UO<sub>2</sub> FA, surrounded on the sides and top and bottom by a water reflector. The neutronic boundary conditions are zero incoming flux.

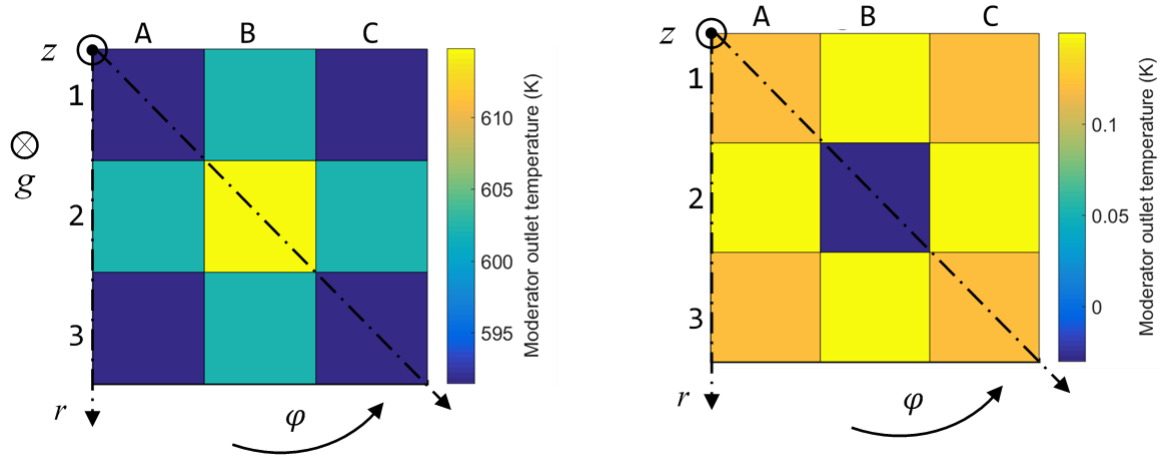


Figure A-4. Predicted PARCS-SCF nodal coolant outlet temperature (K) (left) and difference between the nodal solution against the bundle average full subchannel level solution (right).

The maximum temperature occurs in the central channel where the moderator temperature distribution at subchannel level can be observed in Figure A-5 and the temperature ranges from 612.5 K to 616.5 K. The highest temperatures are in the centre of the FA where the power is higher, and the lower temperatures in the surroundings.

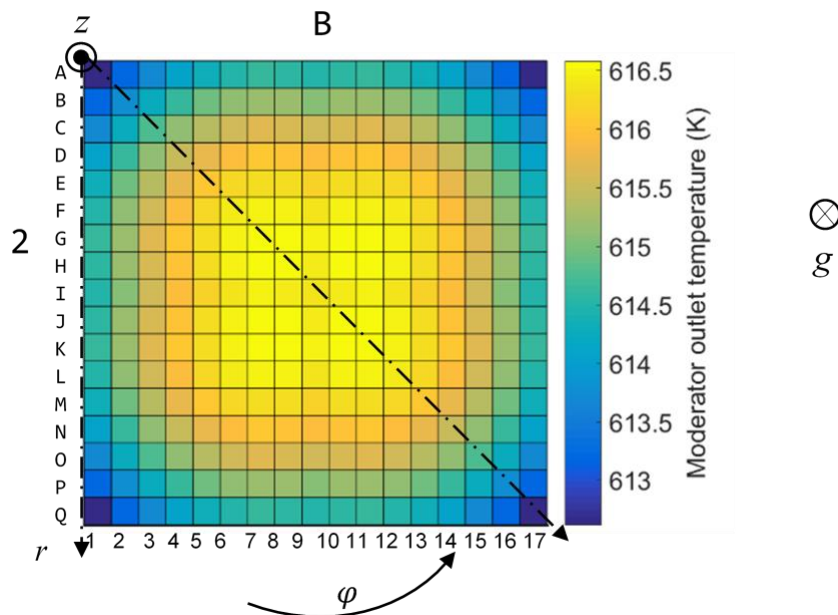


Figure A-5. Subchannel level solution for the channel B2 (central). The average moderator temperature is 614 K, however, the local temperatures present 4 K of variation.

The solutions for the axial moderator temperature distribution in channel B2 is shown in Figure A-6 for the subchannel with highest and the lower temperatures, and for the channel nodal solution and the subchannel-averaged solution.

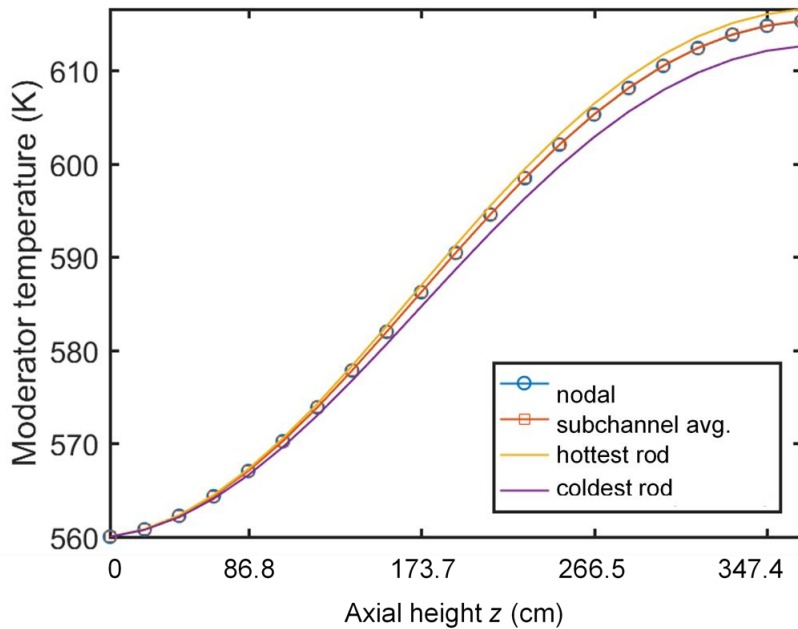


Figure A-6. Axial moderator temperature (K) for the hottest and coldest subchannels located in the central FA, and the nodal and bundle average solution.

The minicore has been also calculated for a hybrid configuration, where the central channel is resolved at subchannel level and the surrounding channels at channel level. In Figure A-7 the location for the MDNB is depicted for the three cases, nodal, hybrid, and full subchannel. In all cases the axial position is the same and, in all cases, it occurs in the central channel. With the subchannel solution local information is found, pointing the location of the pin where it occurs and the values for the local parameters. The found values for the three cases are presented in Table A-1. For the subchannel calculations the MDNB is 3% higher than for the nodal case.

Table A-1. MDNB value and location for the nodal, hybrid and full subchannel solutions.

	Nodalization		
	Nodal	Hybrid	Full Subchannel
rod position in channel, (channel)	(B2)	L13, (B2)	L13, (B2)
mid axial height of node from bottom (cm)	282.9	282.9	282.6
MDNB	3.4115	3.5138	3.5140

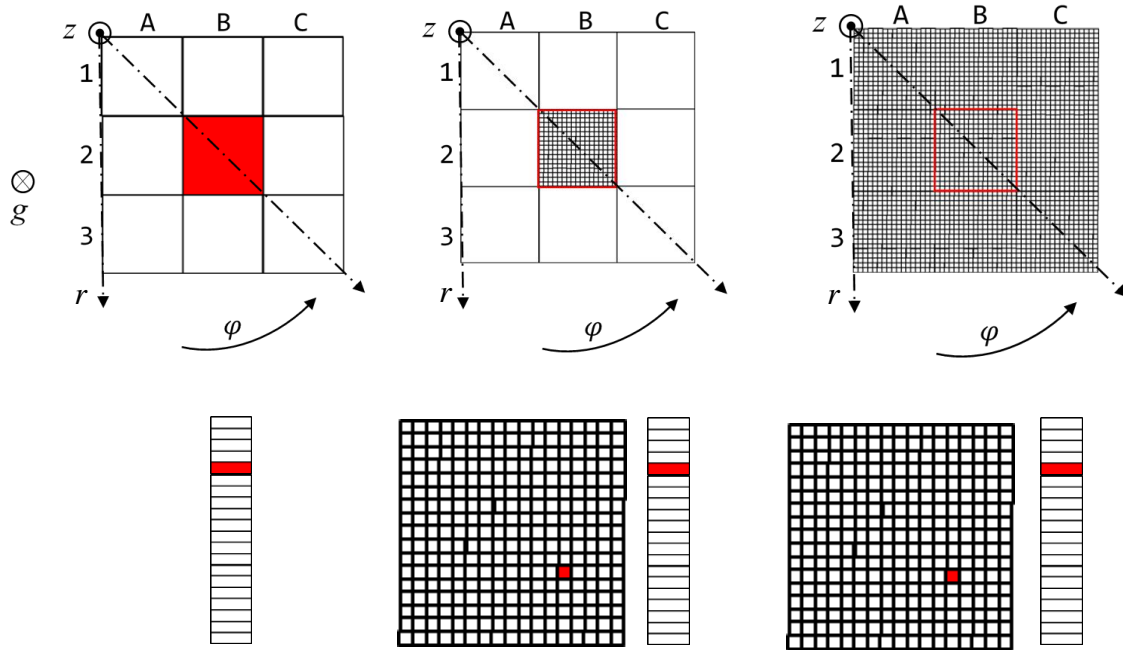


Figure A-7. Location of maximum MDNB. (top) Discretization and channel view. (bottom) zoom in channel and axial position location.

## A.2 Sensitivity analysis for selection of the time step

A sensitivity analysis has been executed on the time-step to be select the time-step size. In Figure A-8 it can be seen the solution of PARCS-SCF using different time-steps sizes for the REA transient presented in chapter 4.3.3.

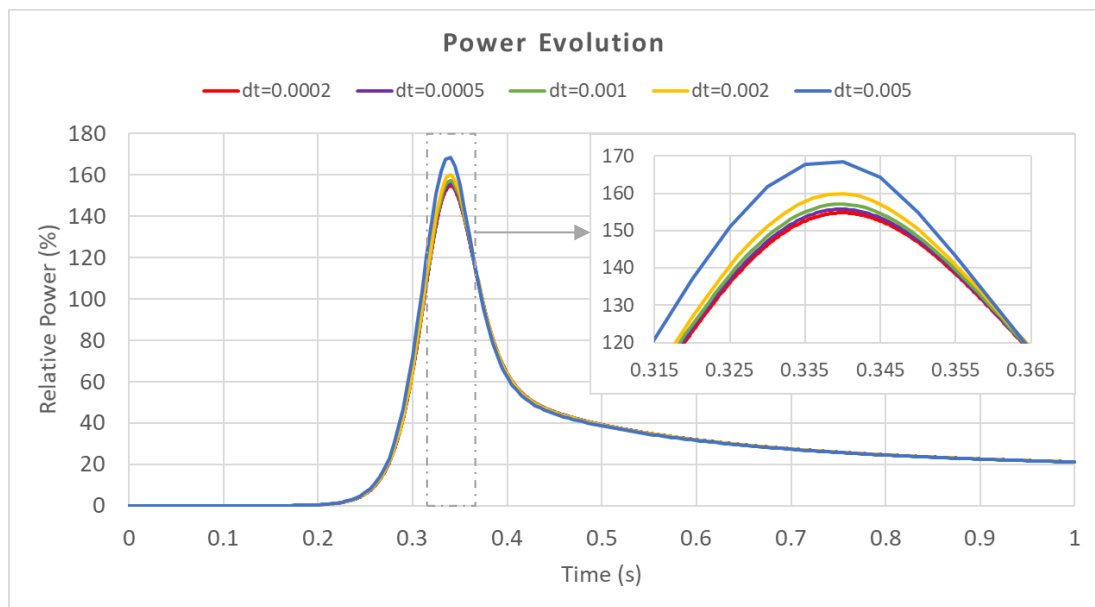


Figure A-8. Time-step sensitivity analysis varying the time step size from 5ms to 0.2 ms. The figure shows the predicted PARCS-SCF power evolution for the REA transient.

Table A-2 shows the predicted power peak for different sizes of time-steps and shows the percentual variation of the power peak between every time the time step is reduced (by a factor of 2 or 2.5). The variation shown in the right column is the percentual variation between successive reductions.

Table A-2. Time step sensitivity analysis. Power peak convergence with increasing smaller times-steps sizes.

Time-step size (ms)	Peak Power (%)	Power peak variation (%)
5	168.5	-
2	159.9	5.09
1	157.1	1.75
0.5	155.7	0.9
0.2	154.7	0.6

In the table, it can be seen that decreasing the time step from 2 ms to 1 ms produces a variation in the power peak of 1.75% and changing it from 1 ms to 0.5 ms varies 0.9% the power peak. The percentual variation every time the time step is reduced to a half decrease with each successive time-step reduction, thus every time the variation is more marginal. A trade-off between computation time and accuracy is a criterion to select the time step size. A criterion of a at least 1% variation in the power peak with half the time step and a time-step of 1 ms is adopted for the calculation with PARCS-SCF.

### A.3 SERPENT/SCF 3x3 Minicore XS generation

The XS sets for the subchannel level calculation are generated with SERPENT-SCF and converted to the PMAX format using the GenPMAXS code. Some modifications were done in the GenPMAXS code for the correct generation of the ADF in the PMAX file. The minicore used in Chapter 4.4.2 is shown in Figure 4-17.

Due to the small core size a correct modelling of the XS and ADFs is of main importance. The cross sections are generated from a colorset which is the minicore itself. In Figure A-9 the meshing used in Serpent is shown to the left, as well as a solution for the flux and a description of the domains, where the XS are condensed for each fuel assembly. Even when the fuel assembly types are the same, e.g. XS3 and XS4, the fluxes are not, thus the need to have a colorset to have a good description of the cross sections and ADFs.

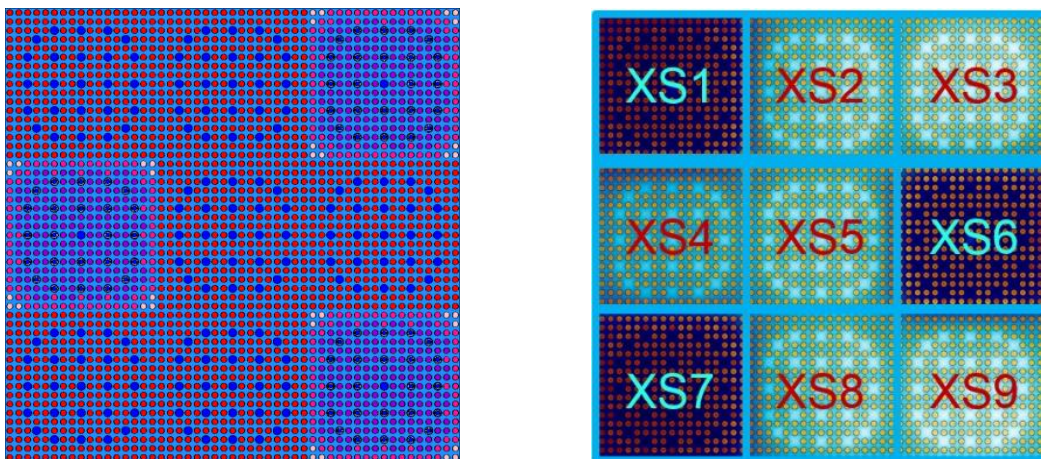


Figure A-9. (left) minicore Serpent meshing, (right) XS generation for each fuel assembly, as it can be seen from the figure on the background, the flux levels are different for same fuel types, thus the need for a colorset to have a better representation of the XS.

#### A.4 Verification of the methodology for prediction of TH safety parameters transient capabilities

For the transient capability of the implemented method a comparison with a higher order solution is currently not feasible, although transient high fidelity research is advancing in the last years (Ferraro *et al.*, 2019), results are not yet mature to be considered as a benchmark. For this reason, a demonstration of the method performance is presented here and a consistent comparison against a nodal a subchannel level solution is done. The purpose of the analysis is to demonstrate the implemented transient solution.

A rod ejection analysis of a 3x3 minicore is presented. The minicore has similar characteristics to the minicore presented in Chapter 4. In this case the control rod in the corner is fully inserted in the beginning, is ejected to 50% in 0.1sec and reintroduced in 0.1sec (see Figure A-10). The focus in this analysis is to show the behaviour at subchannel level, for which the coolant temperature evolution is chosen as an analysis parameter. This generates a large power peak of a very short duration, as shown in Figure A-10. Thus, a big amount of energy is accumulated in the fuels which is then liberated to the coolant.

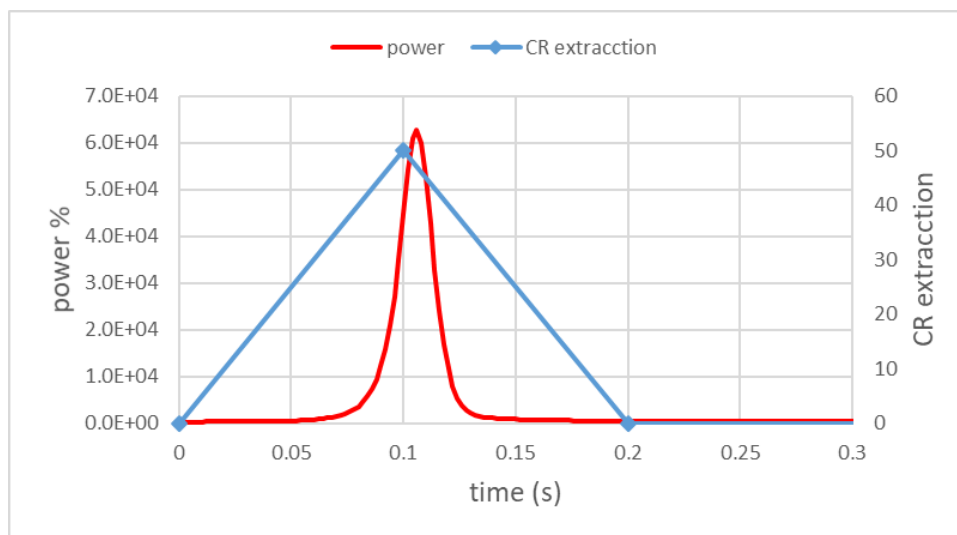


Figure A-10. Rod extraction position in % (blue), and power evolution due to the control rod ejection (red).

In Figure A-11 the outlet temperature distribution at the beginning of the transient is observed and also the difference between the nodal level calculation and the subchannel level average solution, showing a good agreement, with a maximum difference of less than 0.02 K.



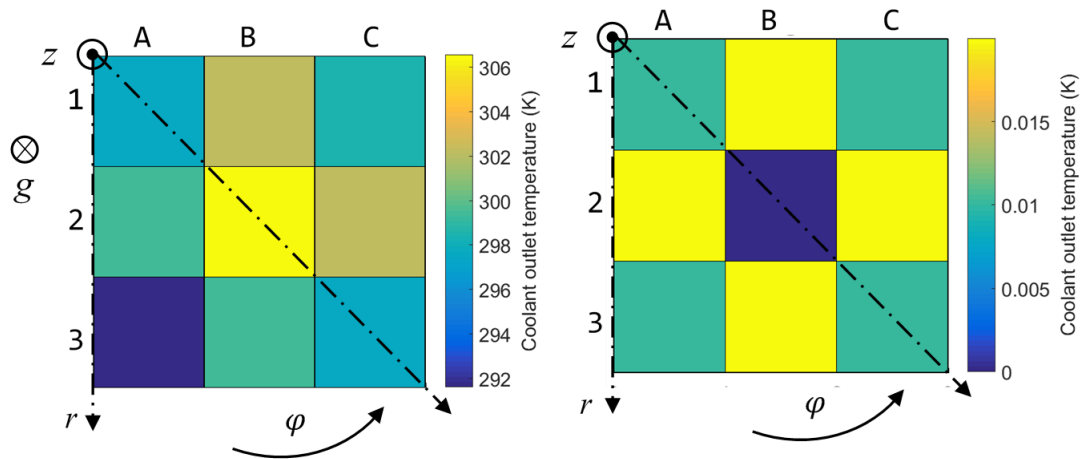


Figure A-11. Coolant outlet temperature distribution (left), and difference between the nodal and subchannel level solution at  $t=0$ .

To analyse the performance of the method, we compare the solutions for the coldest (A3) and hottest channel (B2). In Figure A-12 and Figure A-13 the channel average temperature as well as the hottest and coldest subchannel temperature (of the correspondent channel) are shown.

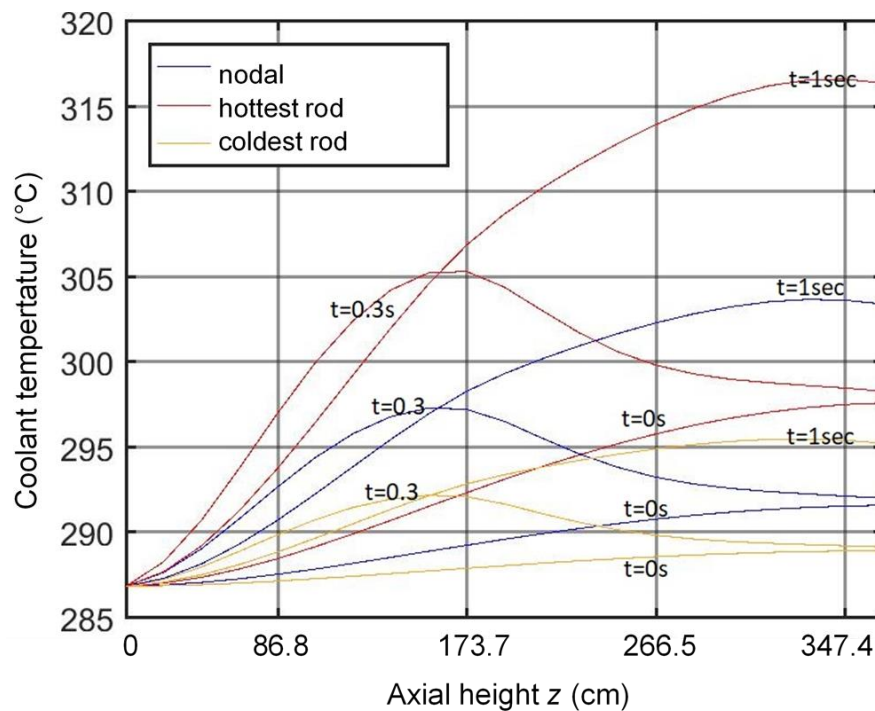


Figure A-12. Evolution of the coolant temperature for the channel A3 average and the hottest and coldest rods in channel A3.



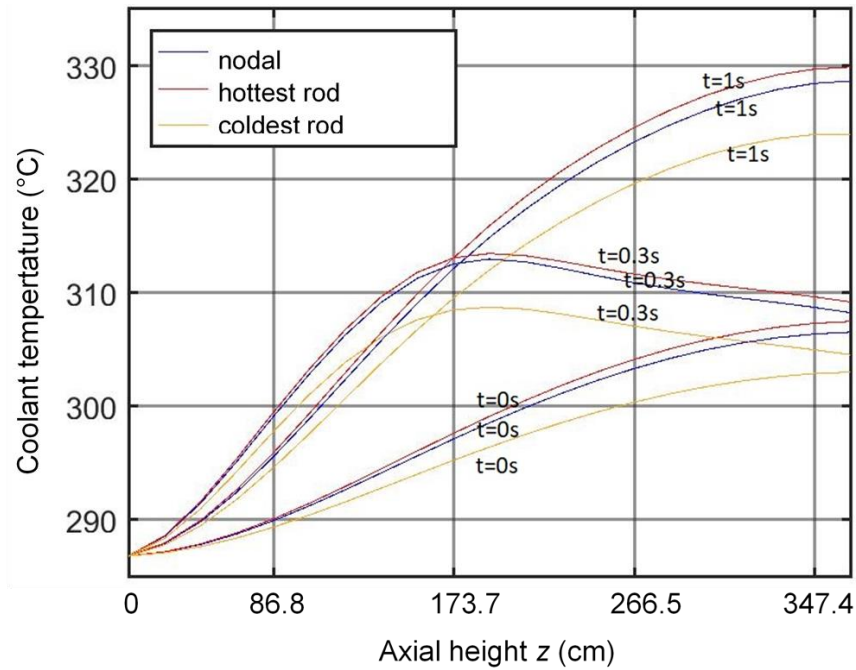


Figure A-13. Evolution of the coolant temperature for the channel B2 average and the hottest and coldest rods in channel B2.

As a verification of the method implementation it has been observed that the subchannel average temperature evolution is almost the same as the nodal level solution. The hottest subchannel coolant temperature evolution remains over the channel average solution during the transient, and the coldest remains significantly below the nodal average. This happens in both cases. In B2, the central channel, there is a lower dispersion of the temperatures, being the difference between the hottest and coldest channel less than 7 K at  $t=1$  sec. However, for channel A3, given the asymmetry of the core power and the gradient in the corner channel there is a difference in temperatures for the coldest and hottest channels of  $\sim 22$  K.

## **B. Neutronics/Thermal-Hydraulics/Thermo-Mechanics coupling**

### **B.1 Description of TRANSURANUS restart file generation**

In the PARCS-SCF-TU calculation, for the generation of the TU restart a base input must be given for each FA type. This base input consists of a regular TU input with the only difference that keywords replace the power and flux information. MATLAB uses these keywords to identify where the computed power and flux must be replaced to generate the working inputs.

To simulate a realistic case, the irradiation conditions of each fuel assembly must be taken into account, meaning that a restart file containing the irradiation history must be generated for each FA with the TU model. Each restart file will depend on:

- the fuel type, burnup, and burnup cycles → Generate linear power over time
- 1 cycle = e.g. 18 months (Cycle = 0 corresponds to 1 month of irradiation)
  - A stop is considered between cycles, e.g. 1 month.
  - A constant linear power is assumed during the cycles in a first approach case.
- The axial power profile used in the burnup corresponds to the axial profile of the power calculated with PARCS-SCF for HFP conditions

An example of the linear heat rating for a fuel rod is given in Figure 6-2. In Figure 6-1 and Figure 5-9 are examples of the maps of fuel type, burnup and cycles in core, which are used for the TRANSURANUS restart files generation. The inputs are then run by a script and the outputs of these runs are organized automatically into folders to be used by the coupled calculation.

### **B.2 OECD/NEA PWR RIA transient benchmark extra results**

The information presented in the following figures should be interpreted as it was explained in Chapter 6, this is a completion of the information for different fuel types and burnups. Figure B-1 to Figure B-4 show the centreline, surface and cladding temperature axial distribution and the axial gap width for low, medium and high burnup fuel. Figure B-5 and Figure B-6 show the temperature evolution at different time steps for fuel assembly L12 (UO<sub>2</sub> 4.2% enrichment, 37.5 GWd/tHM burn-up), where the CR is ejected.

Moreover, Figure B-7 to Figure B-9 show the fuel centreline, fuel surface, cladding and coolant temperature evolution for fuel assembly M12 (UO<sub>2</sub> 4.2% enrichment, 0.15 GWd/tHM burn-up) where the maximum added enthalpy occurs. For this low burnup fuel, it can be seen how even when it is a neighbour of the fuel where the CR is ejected, the temperature evolution has a different behaviour to what it was described for high burnup fuel. Since this is a low burnup fuel, the gap is still open, the temperature evolution is much closer in both modes, with and without pre-irradiation. However there is still a difference, since as seen in Figure B-1 there is a gap width difference, which as explained in Chapter 6 will cause higher centreline and surface temperatures.

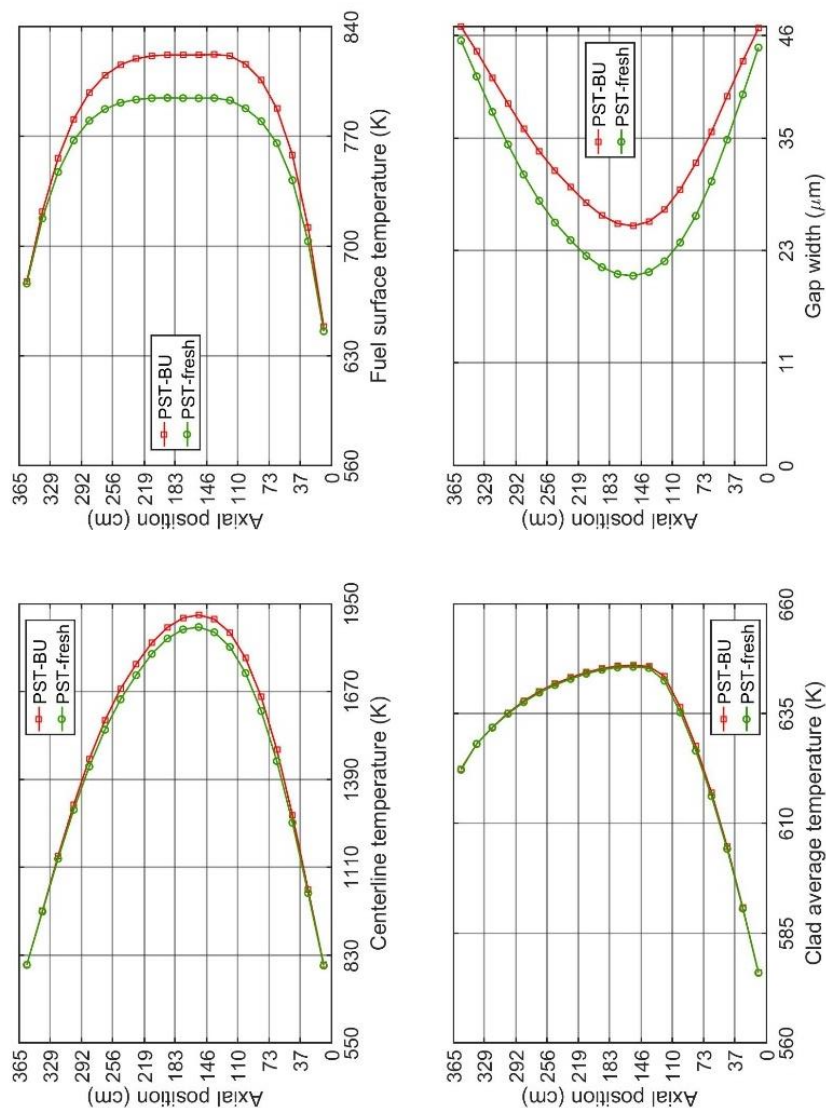


Figure B-1. Centreline, fuel, clad average and coolant axial temperatures distribution for FA H7 UO<sub>2</sub> 4.2 – 0.15 GWd/tHM.

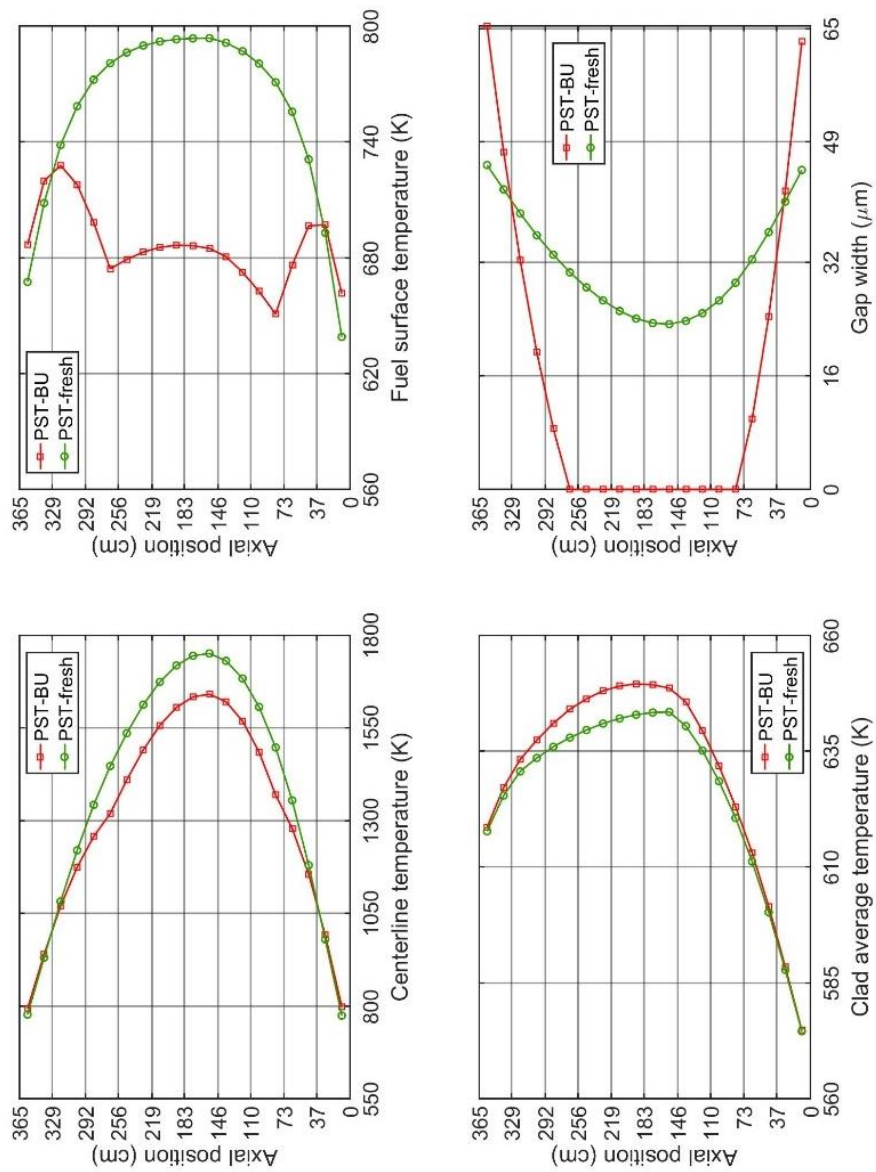


Figure B-2. Centreline, fuel, clad average and coolant axial temperatures distribution for FA G7 UO<sub>2</sub> 4.2% – 17.5 GWd/tHM.

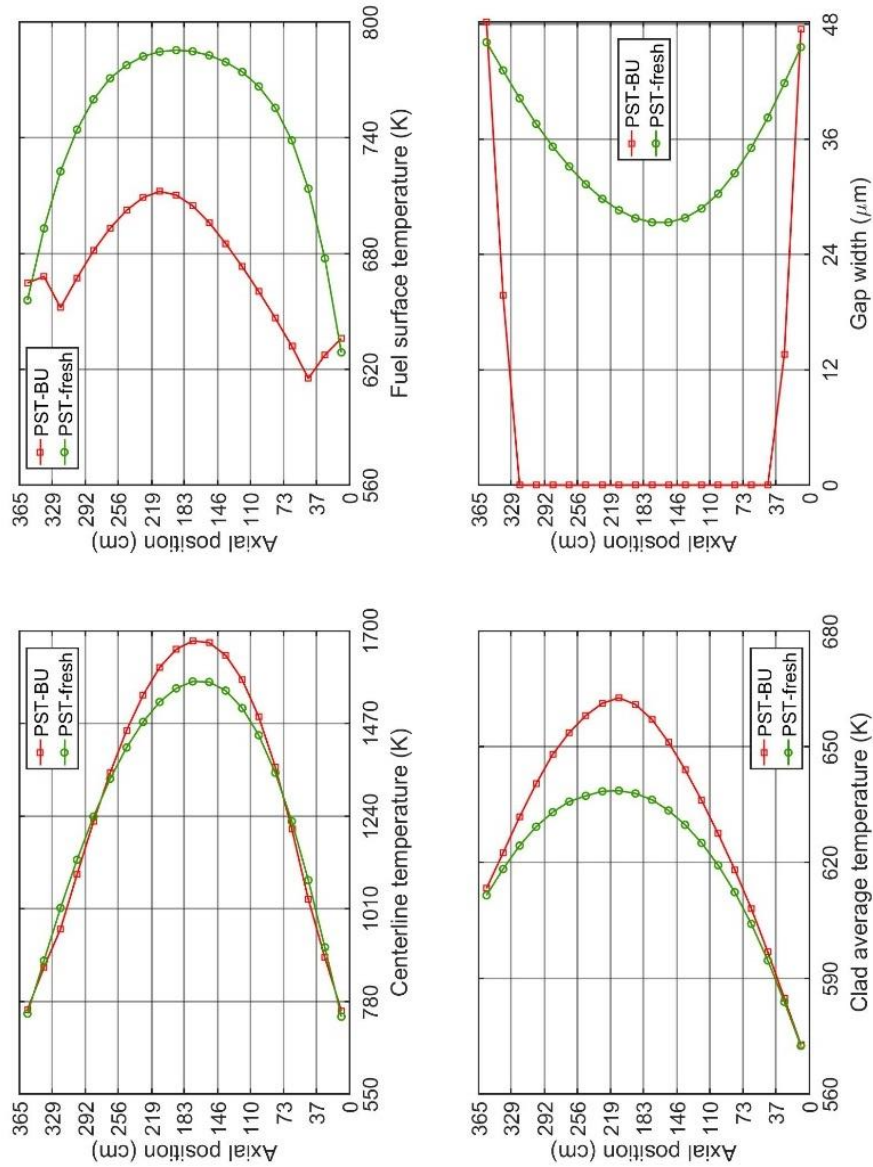


Figure B-3. Centreline, fuel, clad average and coolant axial temperatures distribution for FA H8 UO<sub>2</sub> 4.2% – 35.0 GWd/tHM.

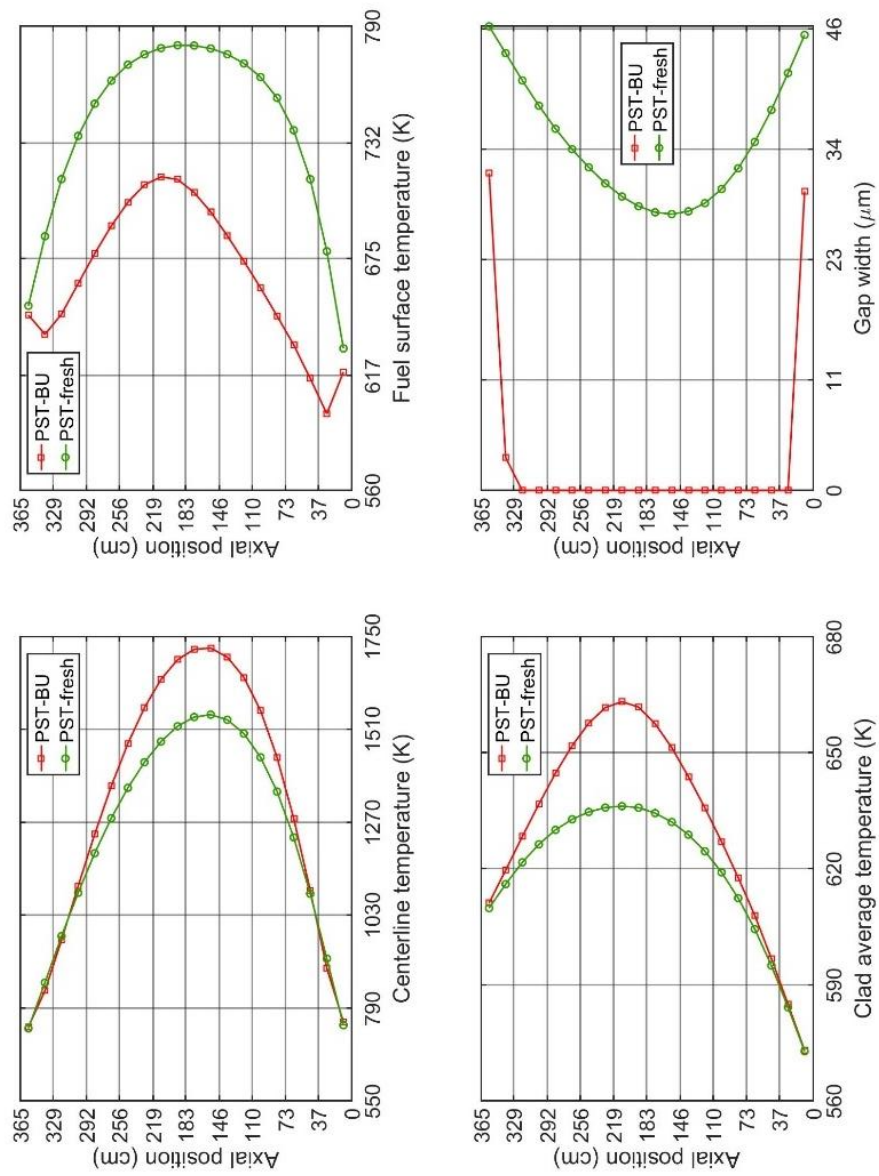


Figure B-4. Centreline, fuel, clad average and coolant axial temperatures distribution for FA E5 MOX 4.0 – 37.5 GWd/tHM - (maximum centerline temperature difference).

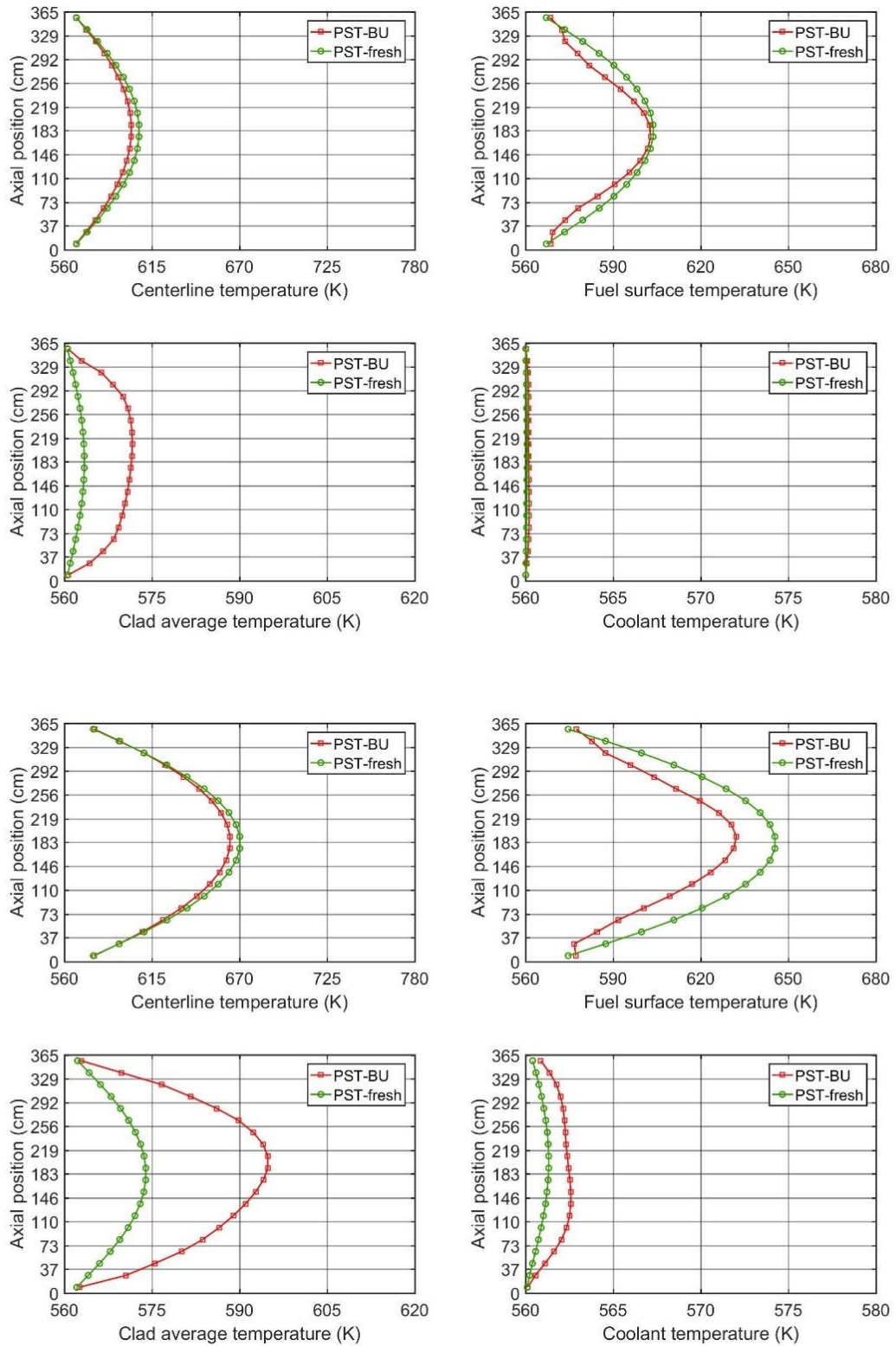


Figure B-5. Temperatures axial distribution for FA L12 (UO<sub>2</sub> 4.2% enrichment, 37.5 GWd/tHM burn-up). Upper:  $t=0.34$  sec. Lower:  $t=0.45$  sec.



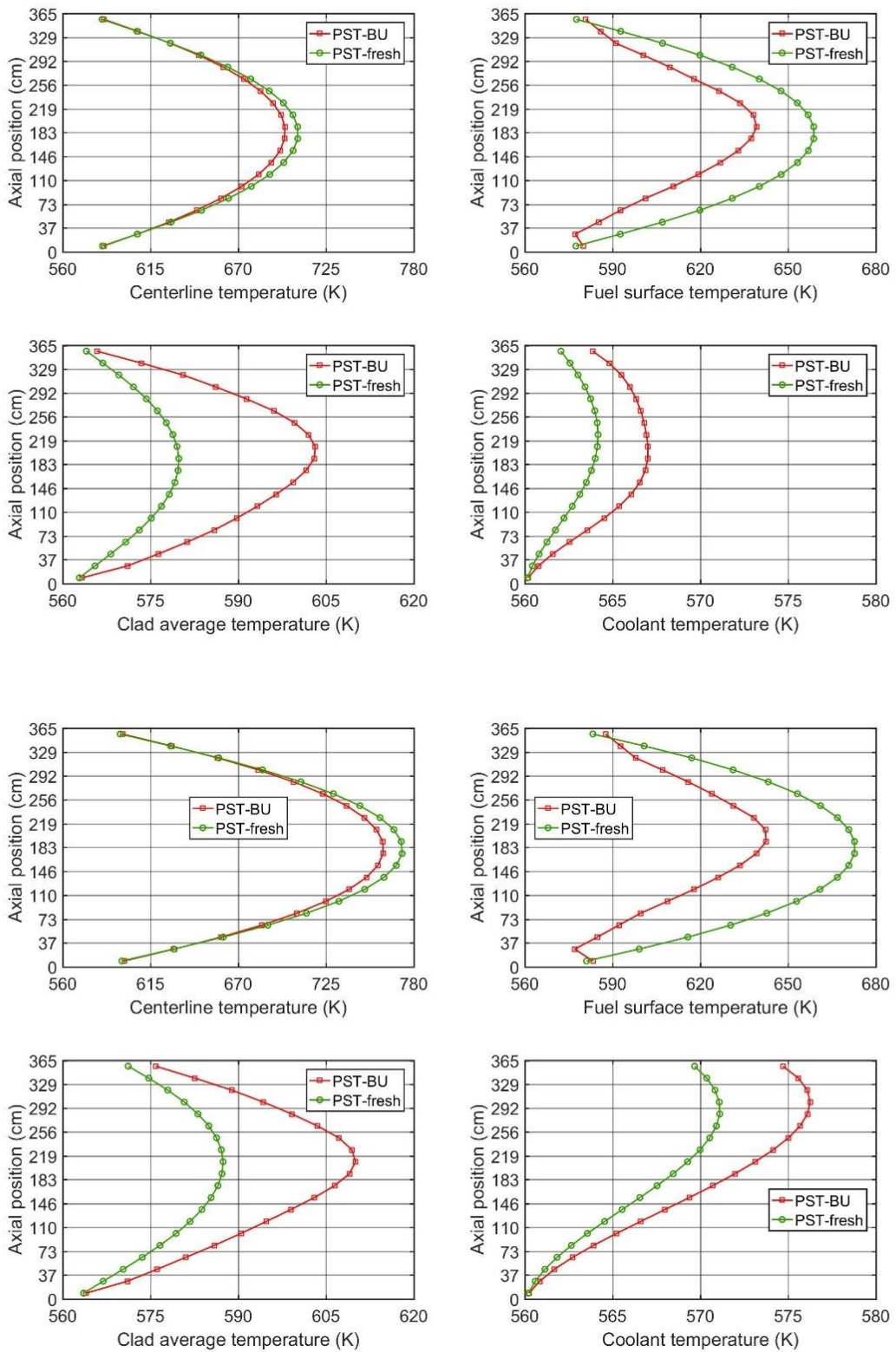


Figure B-6. Temperatures axial distribution for FA L12 (UO<sub>2</sub> 4.2% enrichment, 37.5 GWd/tHM burn-up). Upper: t=0.60 sec. Lower: t=1.00 sec.



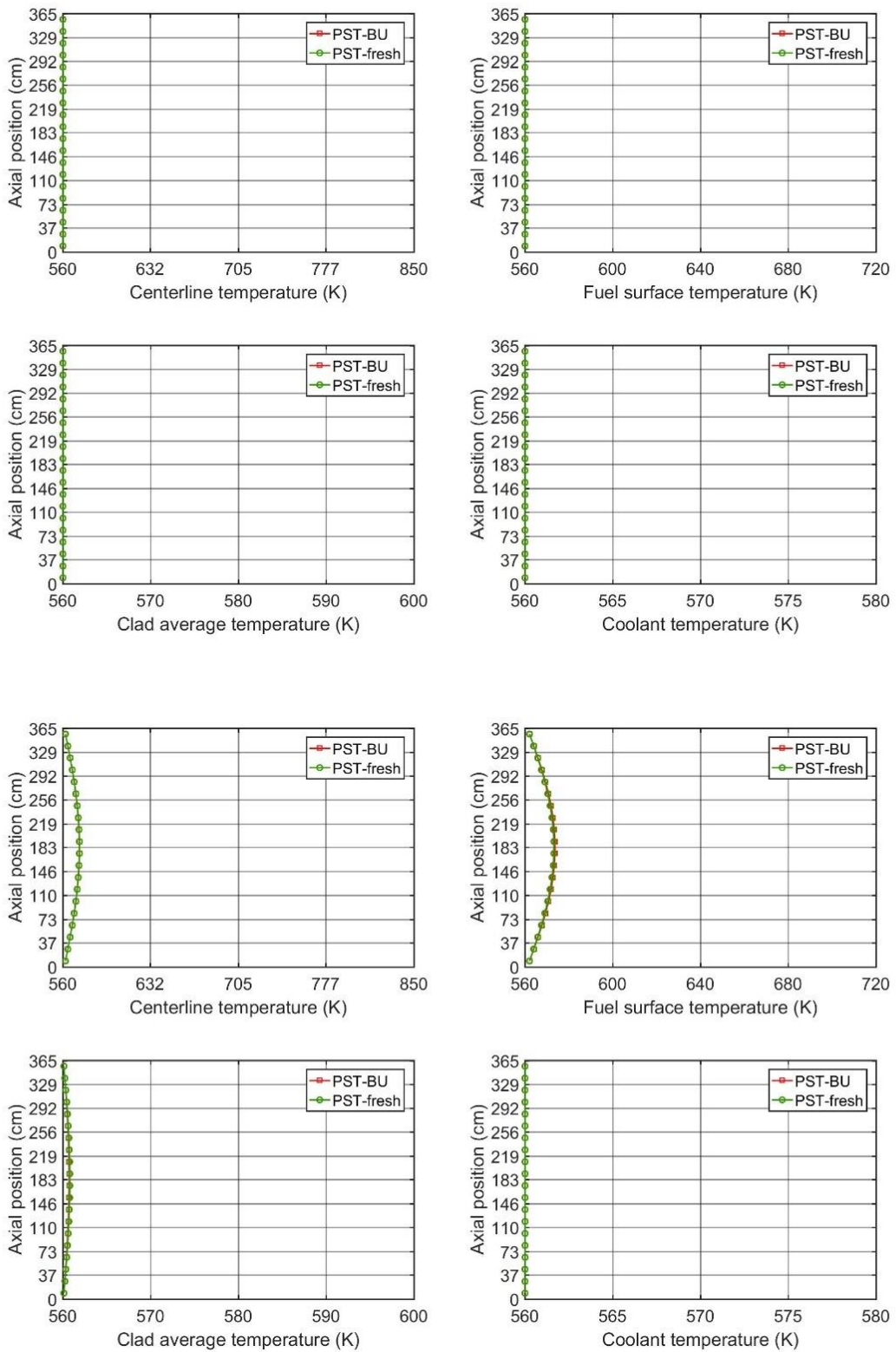


Figure B-7. Temperatures axial distribution for FA M12 (UO<sub>2</sub> 4.5% enrichment, 0.15 GWd/tHM burn-up). Upper: t=0.00 sec. Lower: t=0.30 sec.

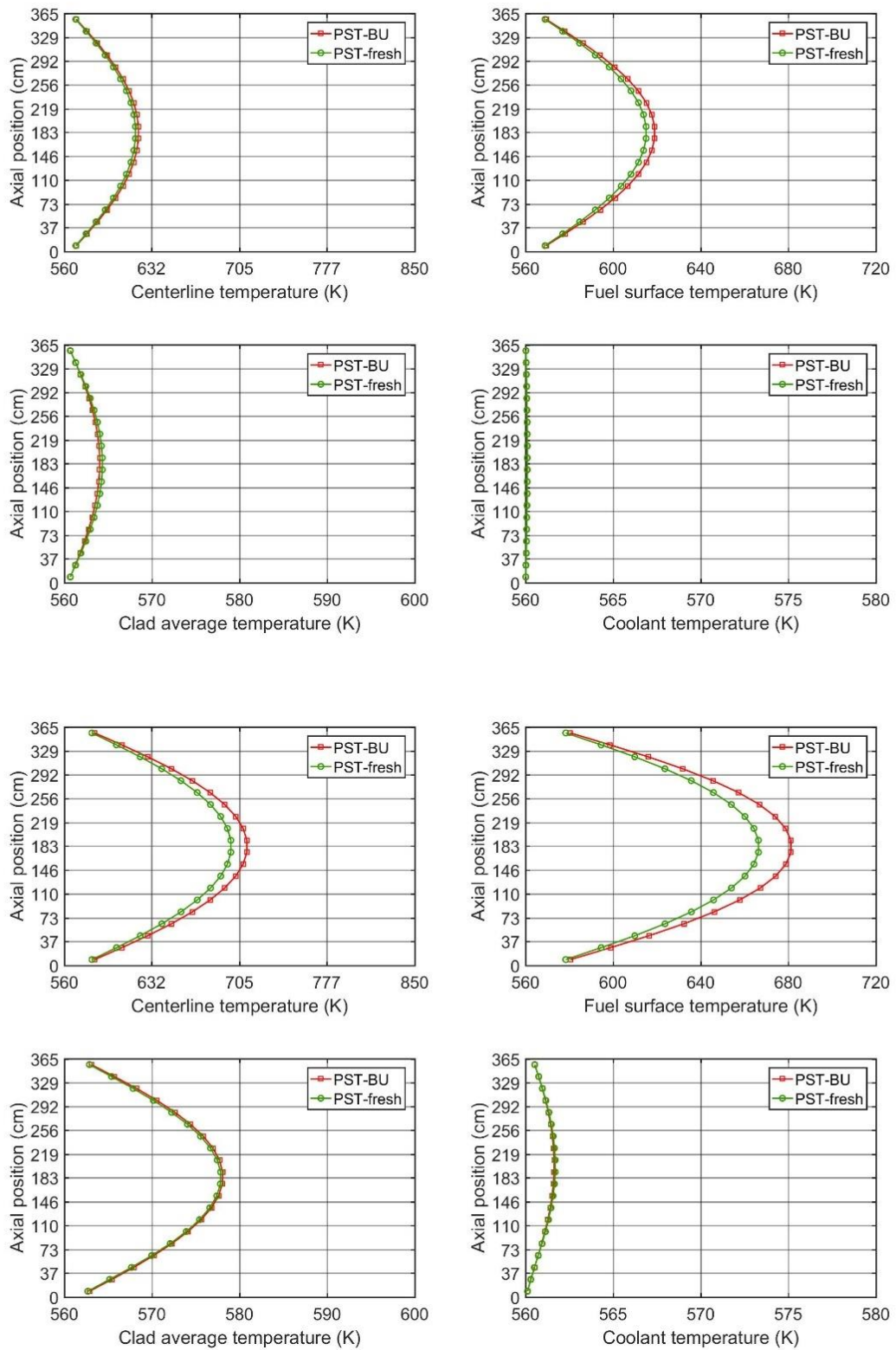


Figure B-8. Temperatures axial distribution for FA M12 (UO<sub>2</sub> 4.5% enrichment, 0.15 GWd/tHM burn-up). Upper: t=0.34 sec. Lower: t=0.45 sec.

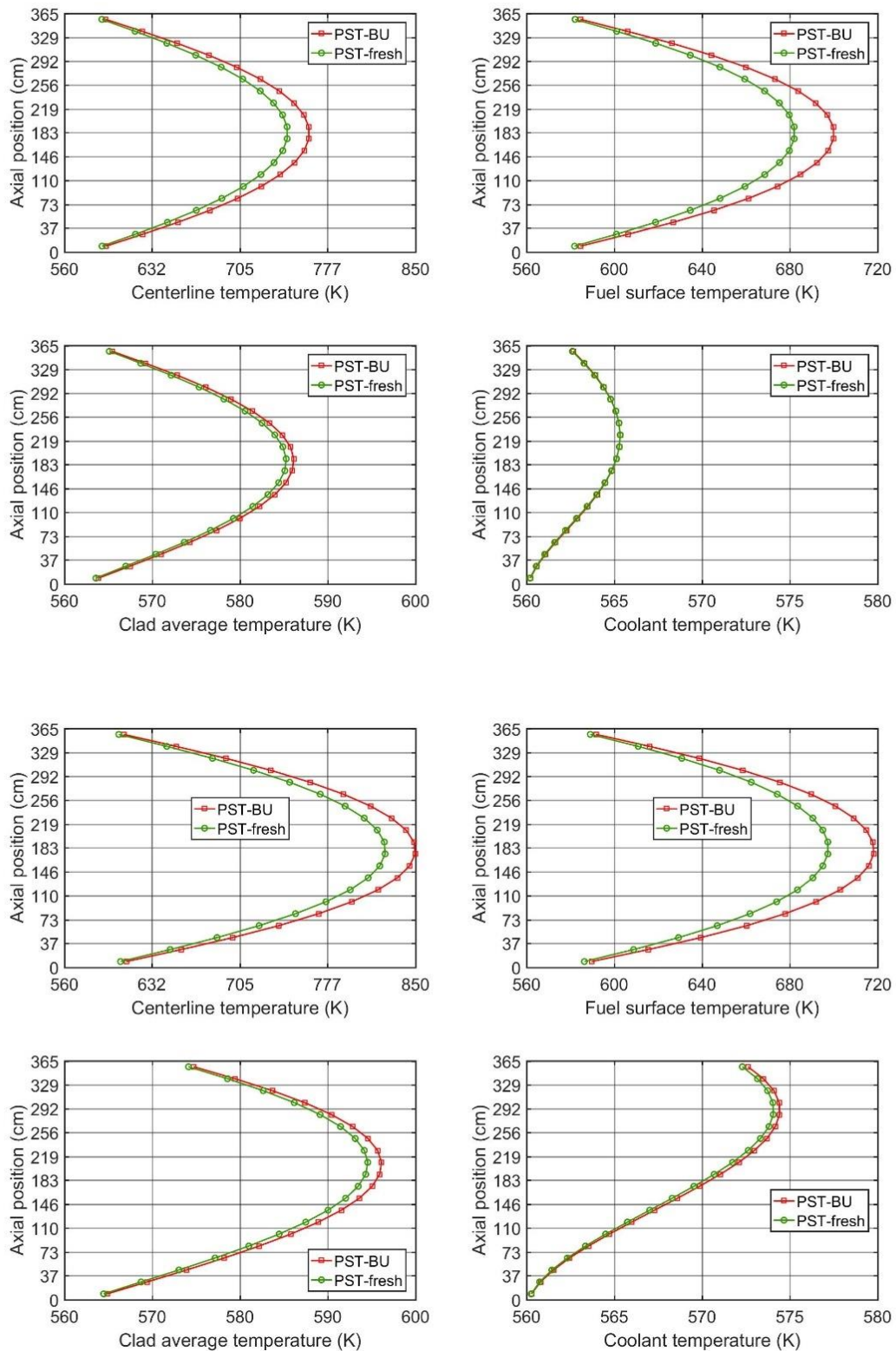


Figure B-9. Temperatures axial distribution for FA M12 ( $\text{UO}_2$  4.5% enrichment, 0.15 GWd/tHM burn-up). Upper:  $t=0.60$  sec. Lower:  $t=1.00$  sec.

### B.3 TRANSURANUS input data for the PWR model

In the TU model the values given in Table B-1 are used. These values were extracted from reports on fuel thermo-mechanics models (O'Donnell, Scott and Meyer, 2001).

Table B-1. Fuel pin data used for the TU model.

Outer fuel radius [mm]	3.922
Inner cladding radius [mm]	3.998
Outer cladding radius [mm]	4.570
Fuel surface roughness [mm]	0.00076
Clad surface roughness [mm]	0.00051
Averaged grain diameter (DKORN)	0.01 mm
Fraction of dish volume	0.02
Total fabrication porosity	0.0521284
Fill gas pressure [MPa]	2.41
Fill gas temperature [°C]	20
Volume fraction factor in gap	0.92061
Corrosion model (ICPRRO)	13
Initial fill gas concentration	100% He

## C. Benchmarks description

### C.1 3x3 PWR minicore description

The 3x3 PWR minicore consists of nine fuel assemblies with a control rod in the top left corner position (A1, see Figure C-1). This is to have an asymmetrical power profile that enhances the crossflow between the channels.

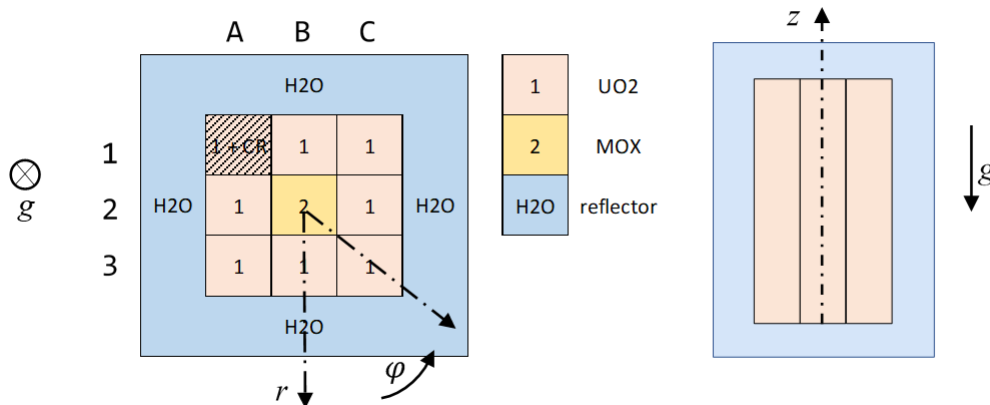


Figure C-1. 3x3 Minicore layout, representation of an axial slice (left) and a side view (right) showing a top and bottom reflector. The core consists of eight UO<sub>2</sub> fuel assemblies and a central MOX fuel assembly. The control rod is inserted in the upper left corner. The core is surrounded on the sides and top and bottom by a water reflector. The neutronic boundary conditions are zero incoming neutron flux.

The fuel assembly (FA) geometry and the material composition are taken from the OECD/NEA U.S. NRC PWR MOX/UO<sub>2</sub> benchmark specifications (Kozlowski and Downar, 2003). The UO<sub>2</sub> FAs correspond to the UO<sub>2</sub> 4.5% and the MOX FA to the MOX 4.3% described in the benchmark specifications, both with 0.15 GWd/tHM burnup. The fuel assembly has a 17x17 cartesian geometry as shown in Figure C-2 for the case of the UO<sub>2</sub> fuel.

The axial active length of the fuels is 365.76 cm discretized in 20 equidistant axial meshes. The reflector surrounding the active core has a width equivalent to one FA (21.42 cm) on the sides and the same at top and bottom. All the boundary conditions for the core are set to zero incoming flux.

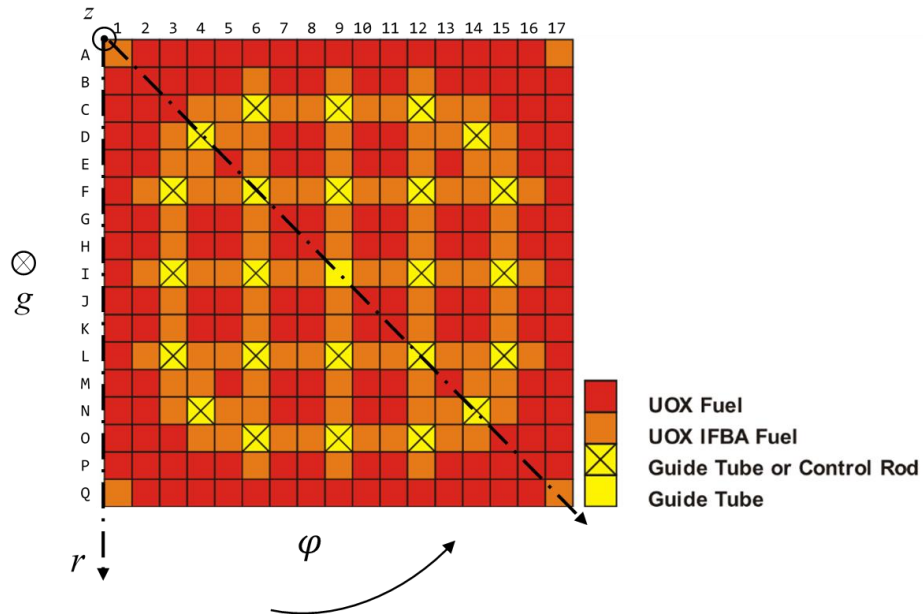


Figure C-2.  $UO_2$  Fuel assembly with a 17x17 Cartesian geometry. UOX = Uranium Oxide, IFBA = Integrated Fuel Burnable Absorber. (modified from (Kozlowski and Downar, 2007)).

The nuclear cross sections are parametrized with the thermal-hydraulics state variables and the boron concentration. The coolant mass flow rate per FA is the same as the OECD/NEA PWR benchmark core. The core nominal power (99.75MW) is chosen to have a heat up of  $\sim 40K$  in the central channel. The main parameters for the model are listed in Table C-1. To achieve a  $k_{eff}$  equal to 1, a critical boron concentration search calculation has been performed with the PARCS, and the obtained critical boron concentration (96.34 ppm) is used.

Table C-1. 3x3 PWR minicore relevant parameters.

Nominal power (at HFP) (MW)	99.75MW
Mass flow rate (kg/sec)	739.08
Coolant inlet temperature $T_{in}$ (K)	560
Inlet pressure [MPa]	15.5
Boron concentration [ppm]	96.34
Core active height (cm)	365.76
Gap heat transfer coefficient (W/(m <sup>2</sup> K))	10000
Top/bottom reflector high (cm)	21.24



PARCS thermo-physical properties for the fuel, necessary for the fuel temperature calculation use a simplified model described in (Finnemann and Galati, 1991). To reduce the origin of differences between the models and perform a code to code comparison, the same thermo-physical properties are used in the SCF and in the internal TH model of PARCS.

### C.2 OECD-NEA UO<sub>2</sub>/MOX PWR benchmark description

The benchmark is based on a four loop Westinghouse PWR with 193 fuel assemblies arranged in a Cartesian geometry with a quarter core rotational symmetry. The fuel rods are composed of UO<sub>2</sub> fuel with 4.2% and 4.5% enrichment and MOX fuel with 4.0% and 4.3% enrichment. The core configuration for a quarter of the core, and its burnup distribution is shown in Figure C-3.

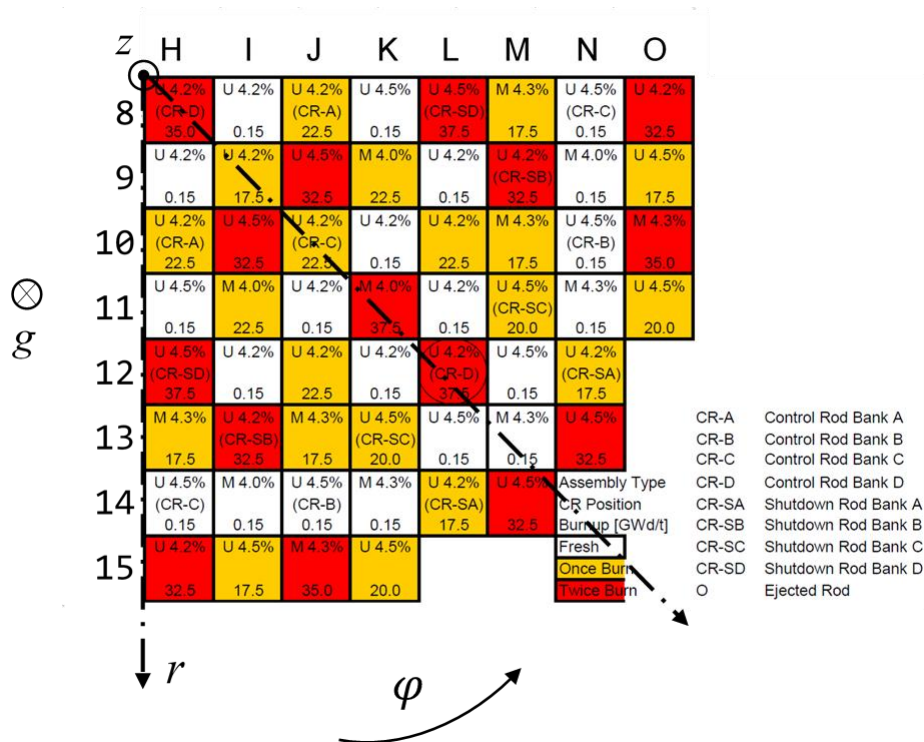


Figure C-3. Benchmark PWR quarter-core loading pattern (modified from (Kozlowski and Downar, 2007)).

The benchmark problem consists of four parts. Part II of the benchmark corresponds to a HPF steady state calculation with TH feedback, which has been calculated for verification purpose and the results for this case are found in Appendix A.1.

Part IV deals with the analysis of a control rod ejection accident at hot zero power (HZP) conditions. The design parameters relevant for the simulation are listed in Table C-2. The

nuclear cross sections used in the calculation are taken from the benchmark database. Cross sections, parametrized with TH parameters, are homogenized in two energy groups, and given for seven burnup points.

Table C-2. Core design parameters.

Number of fuel assemblies	193
Power level (MWth)	3565
Core inlet pressure (MPa)	15.5
HZP core average moderator temperature (K)	560
Fuel lattice / rods per fuel assembly	17x17 / 264
Total active core flow (kg/sec)	15849.4
Assembly fuel length (cm)	365.76
Distance between neighbouring FAs centres (cm)	21.42
Gap heat transfer coefficient (W/(m <sup>2</sup> K))	10000

The core consists of fuel assemblies with a 17x17 geometry containing 264 fuel pins and 25 guide tube positions. There are two fuel assembly types present in the core: UO<sub>2</sub> and MOX types (see Figure C-4). Each type has two different enrichments: UO<sub>2</sub> 4.2%, UO<sub>2</sub> 4.5%, MOX 4.0% and MOX 4.3%.

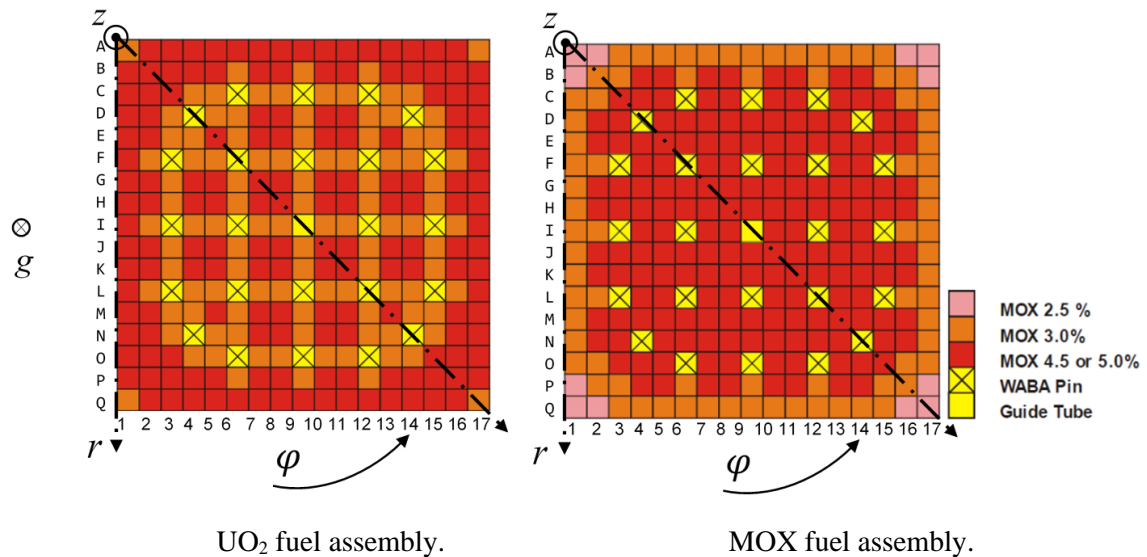


Figure C-4. UO<sub>2</sub> and MOX fuel assembly configuration. Both fuel types contain 264 fuel pins. IFBA: UO<sub>2</sub> fuel with ZrB<sub>2</sub> coating to provide reactivity control (fuel pin). WABA: Annular pellet of Al<sub>2</sub>O<sub>3</sub>-B<sub>4</sub>C with zircalloy cladding water filled for reactivity control (treated as in SCF).